Holographic Correspondence and Exploring New Regimes of AdS/CFT Duality

by

Miok Park

A thesis
presented to the University of Waterloo
in fulfillment of the
thesis requirement for the degree of
Doctor of Philosophy
in
Physics

Waterloo, Ontario, Canada, 2013

I hereby declare that I am the sole author of this thesis. This is a true copy of the thesis, including any required final revisions, as accepted by my examiners.

I understand that my thesis may be made electronically available to the public.

Abstract

We aim to have a comprehensive understanding of holographic correspondence and to demonstrate how the holographic correspondence (or renormalization) can be applied. Thus this thesis is divided into two parts. The first part is devoted to the former purpose (chapters 1 to 4 including appendix A,B, and C), and the second part is dedicated for the latter purpose (chapter 5 to 7).

In Part I, the structure of the AdS/CFT correspondence is analyzed, and the properties of the AdS spacetime is studied in the context of the AdS/CFT correspondence; Here, we investigate the isometry group, the conformal structure, and generation of asymptotic solution near the conformal boundary. This solution yields significant convenience for the process of holographic renormalization. Moreover the properties of the Minkowski spacetime are compared to those of the AdS spacetime. To develop a greater understanding of the Lifshitz/quantum critical theory correspondence, the quantum phase transition is studied. Furthermore The holographic renormalization is briefly reviewed.

In part II, the holographic renormalization associated with the Mann-Marolf (MM) counterterm is investigated for the asymptotically Minkowski spacetime in (n+3) dimensions. As a boundary condition, the cylindrical coordinate is considered. The solution of the MM-counterterm is obtained by solving the given algebraic equation, and from the counterterm solution, the boundary stress tensor is calculated. It is proven that the formula for conserved quantities via the boundary stress tensor holds.

Next, we investigate deformations of Lifshitz holography with the Gauss-Bonnet term in (n+1) dimensional spacetime. To admit the non-trivial solution of the sub-leading orders, a value of the dynamical critical exponent, z, is restricted by $z = n - 1 - 2(n-2)\tilde{\alpha}$, where $\tilde{\alpha}$ is the (redefined) Gauss-Bonnet coupling constant. Such solution of sub-leading orders correspond to the marginally relevant modes for the massive vector field and are generated by U+039B ~ 0, at the asymptotic region. A generic black hole solution, which is characterized by the horizon flux of the vector field and $\tilde{\alpha}$, is considered in the bulk. We explore its thermodynamic properties, which depend on temperature, by varying n and $\tilde{\alpha}$. As a result, the contribution of the marginally relevant mode is found in a function of $\frac{\Lambda^z}{T}$, and the relation between the free energy density and the energy density is numerically recovered when the marginally relevant mode is turned off ($\Lambda = 0$), is obtained.

Acknowledgements

Dedication

This is dedicated to my parents, sister, brother-in-law, and two nephews I love.

Table of Contents

List of Tables

List of Figures

Chapter 1

Introduction

This thesis is concerned with the holographic correspondence principle, constructing the foundations for exploring new regimes of the AdS/CFT correspondence. Applications of the holographic correspondence are demonstrated for holographic renormalization in asymptotically Minkowski spacetime and for Lifshitz spacetime involving a study of quantum criticality. Here we introduce the original AdS/CFT correspondence conjecture and discuss its interpretation as a UV/IR connection. Then we give an overview of this thesis.

1.1 The AdS/CFT Correspondence

In string theory, a new form of "duality" was conjectured by Maldacena [60], which is that

> **Type IIB string theory on $(\mathbf{AdS}_5 \times \mathbf{S}^5)_N$ plus some appropriate boundary conditions (and possibly also some boundary degrees of freedom) is dual to $\mathcal{N} = 4$, $d = 3 + 1$ $U(N)$ super-Yang-Mills.**

To show this, consider N parallel $D3$ branes, which have a Higgsed configuration and are separated by some distance r. Then take the low energy limit, where the theory on the $D3$ brane decouples from the bulk. This condition is written as

$$\alpha' \to 0, \qquad U \equiv \frac{r}{\alpha'} = \text{fixed} \qquad (1.1)$$

where the second is the Higgs expectation value corresponding to this separation, which remains fixed so that the mass of the stretched string is fixed. Thus U has dimensions of mass, and is considered to be the energy scale at which the mass of a string state is translated from the $D3$ brane (AdS description) to open strings (Yang-Mills description) by the Higgs field that breaks the symmetry.

In this limit, the superconformal $\mathcal{N} = 4 \, U(N)$ super-Yang-Mills theory has a symmetry described by the conformal group $SO(2,4)$, and the supergravity solution carrying $D3$ brane charge yields five dimensional Anti-de Sitter (AdS$_5$) space times a five sphere, where the supergravity solution can be trusted in the limit $gN \gg 1$, that is, when N is large. Since it was known that the supersymmetry group of AdS$_5 \times$ S^5 is the same as the superconformal group in $3 + 1$ spacetimes [44], Maldacena's new duality conjecture is established.

Subsequent to this conjecture, Witten proposed a precise correspondence of observables between the conformal field theory and the supergravity [90]. First, the ansatz for the supergravity partition function computed at the boundary of spacetime was suggested to be

$$Z_{\mathrm{S}}(\Phi_0) = \exp(-I_{\mathrm{S}}(\Phi)) \tag{1.2}$$

where Φ is a field on AdS$_{n+1}$ and approaches Φ_0 at infinity. The generating functional for the conformal field on the boundary of AdS$_{n+1}$ spacetime is then constructed so that Φ_0 couples to a conformal field $\mathcal{O}$, i.e.

$$Z_{\mathrm{CFT}} = \left\langle \exp \int_{\mathrm{S}^n} \Phi_0 \, \mathcal{O} \right\rangle_{\mathrm{CFT}}. \tag{1.3}$$

Then the AdS/CFT correspondence is interpreted to be

$$Z_{\mathrm{CFT}}(h) = Z_{\mathrm{S}}(h) \tag{1.4}$$

for a given conformal structure h. Based on this, the equation of the motion for Φ_0 is calculated at the boundary of the spacetime, and the singularity of the solution is identified with the Green's function under an SO$(1, n + 1)$ transformation. As a result, it can be shown that correlation functions in conformal field theory are derived by using the Green's function, and the dimension of the operator O in conformal field theory is influenced by masses of particles in supergravity. Inspired by this idea, for AdS spacetime, the process of obtaining well-defined holographic correlation functions, which is called holographic renormalization, is more precisely constructed and is discussed in detail by [11, 81].

1.2 Introduction of Renormalization

The holographic correspondence can be interpreted as a "UV/IR connection"

$$\text{Gauge/Gravity correspondence} \Leftrightarrow \text{UV/IR connection}$$

i.e. the UV divergence in the field theory is related to the IR divergence in the gravity theory [85]. As this interpretation is an important part of the holographic correspondence, before proceeding to our study of holographic correspondence, we need to clarify what causes divergences in the field theory and in the gravity theory. Also we must study the remedy for those divergent problems, which is known as the field theoretical/holographic renormalization method (or counterterm method). Here we briefly introduce the UV divergence in the field theory, the renormalization method, the renormalization group, and the IR divergence in the gravity theory. The details of the UV divergence, the field theoretical renormalization, and the renormalization group are presented in appendix B. The Wilsonian renormalization is also reviewed in appendix C. The statistical renormalization group is introduced in chapter 3.

Perturbative quantum field theory involves radiative corrections, which form loops that carry large momenta k and yield infinity as $k \to \infty$ in the calculation of correlation functions. This ultraviolet divergence was first discovered in quantum electrodynamics in the 1930's. In order to resolve this divergence problem, Bethe, Feynman, Schwinger, Tomonaga, and Dyson proposed the renormalization method in the late 1940's. The main idea of the renormalization method is to obtain finite values by separating fields and physical variables into the bare quantities (i.e. the infinite part) and renormalized quantities (i.e. the finite part) via some regularization method, which provides a way to subtract the infinity. As there is no restriction that the finite parts should be physical quantities, an ambiguity occurs in the process of separating the infinite part and the finite part. This ambiguity can be fixed by choosing a proper renormalization scheme, which works in a way so as not to change the physical results. That is, the final physical result is required to be independent of the renormalization scheme. This idea became a motivation for the renormalization group later.

In the 1970s the renormalization group was developed in condensed matter physics by Wilson in order to understand a certain property, which is known as universality. The idea is based on the scale-dependent effective action, which is obtained by eliminating the high energy degrees of freedom. The renormalization is performed by integrating over momentum in the range $\Lambda < k < \Lambda_0$ where Λ_0 is a UV cutoff, or by decimating suitably chosen subsets of fields until the sequence reaches a fixed point. This process does not

require any strong assumptions about the structure of the theory like renormalizability in the field theoretic sense, and does not yield any divergence problems since the lattice spacing itself plays the role of a natural cutoff. As a result, this process gives a bridge from the microscopic state to the macroscopic state.

On the other hand, in gravity theory, the variation of the Einstein-Hilbert action yields the Einstein equations and additional terms, which are associated with the variation of metric derivatives at the boundary of the spacetime. Gibbons and Hawking pointed out that the additional terms at the boundary must not be ignored but instead must cancel. They introduced the Gibbons-Hawking boundary term to fix this problem,

$$ S = \frac{1}{16\pi G} \int_{\mathcal{M}} \sqrt{-g} R - \frac{1}{8\pi G} \int_{\partial \mathcal{M}} \sqrt{-h} K \qquad (1.5) $$

where g is the determinant of the metric on the spacetime, R is a Ricci scalar with respect to g_{ab}, h is the determinant of the induced metric on the boundary, and K is the trace of its extrinsic curvature. While this new boundary term is well defined for spatially compact spacetimes, it diverges for noncompact ones as r goes to ∞. That is, in gravity theory, an IR divergence occurs by having infinite volume of the spacetime at the level of the action. As a remedy for the IR divergent problem of the gravitational action, counterterms, which are locally defined and covariant, are added into the action. In other contexts, counterterms also play an important role by making a contribution to the conserved charges of the spacetime. From a holographic correspondence perspective, counterterms are required not only to make the action finite, but also to produce well-defined holographic correlation functions. This process is called holographic renormalization.

1.3 Overview of Thesis

One of main objectives of this thesis is to get a more comprehensive idea of holographic correspondence. To do so, we shall consider the basic structure of spacetime, field theory, and holographic renormalization, with the aim of setting foundations for exploring new regimes, such as AdS/QCD duality [38, 43, 53], gravity/condensed matter theory duality [15, 18, 46, 51, 56, 65, 78] or gravity/fluid duality [19, 55, 77]. The other objective is to apply this understanding to demonstrate how holographic renormalization can be performed in non-asymptotically AdS spacetimes and how gravitational information is delivered to a field theory via the holographic correspondence. To clarify these objectives, we divide our approach for exploring the holographic correspondence into four steps and describe our work for each step as follows.

4

The first step is to understand the basic properties of spacetime and the field theory. AdS spacetime and conformal field theory possess the same isometry group, and this fact makes it possible to establish the AdS/CFT correspondence as mentioned above. Thus it is crucial to investigate symmetries for describing a spacetime and a field theory in order to expand the breadth of the holographic correspondence. Another factor we should consider is the properties of an asymptotic boundary of spacetime. The asymptotic boundary is a place in which matter fields from the conformal theory reside, and where the gravitational information is transferred to matter fields. Thus it is also important to find a physically well defined boundary at an asymptotic region of a spacetime. With these factors in mind, we analyze AdS spacetime comparing it to Minkowski spacetime, and briefly mention Lifshitz spacetime in chapter 2. Conformal field theory is not covered in this thesis, but an introduction to quantum critical theory is in chapter 3.1.

The second step is to find a method for holographic renormalization. Holographic renormalization is the key process for constructing holographic correlation functions and to accomplish the holographic correspondence. While field theoretical renormalization methods (including the statistical renormalization) are well established, a standard method for holographic renormalization has not been found (except for AdS spacetime, whose general algorithm of generating counterterms is known [11, 61, 36]). Of course the method of holographic renormalization could differ from field theoretical renormalization. However it is important to study the field theoretic renormalization process from a holographic perspective. One of the reasons is that holographic renormalization for asymptotically AdS spacetimes is inspired by field theoretic renormalization methods, and so we should not disregard a chance to apply it to other spacetimes. The other is that we could expect that related phenomena such as renormalization flow could be reproduced via a holographic dual description. In order to gain an understanding of renormalization, standard field theoretic renormalization is reviewed in appendix B, and statistical renormalization is reviewed in chapter 3.2 and 3.3 (the Wilsonian renormalization is also reviewed in chapter C). The holographic renormalization for the AdS case is reviewed in chapter 4. Indeed, holographic renormalization is a fundamental problem that should be resolved in gravity theory, even apart from the holographic correspondence. The reason is that it involves the gravitational action principle at the boundary of spacetime and provides a way of yielding conserved quantities. With this motivation, the holographic renormalization for the Minkowski spacetime is studied in chapter 5.

The third step is to apply the holographic correspondence. One way of approaching this is to choose the spacetime and then find an applicable field theory to be its dual. Such is the case for the Minkowski spacetime: it is relatively well understood, but its dual field theory has not been found yet. Furthermore, if we assume a conformal field

theory is its dual, we do not know how the isometry group of conformal field theory is to be connected to the isometry group of the Minkowski spacetime. An alternative approach is to go from field theory to gravity theory, which is the case for the study of high temperature superconductors or Lifshitz-like field theories. In this case, we should configure the gravitational action so that it asymptotically shares the same symmetries as the field theory. As an example of such a realization for the holographic correspondence, the deformation of Lifshitz holography in $(n+1)$ dimensions is investigated in chapter 6.

The fourth step is to seek richer corresponding structures between the gravity theory and the field theory. For example, in condensed matter theory, the idea of renormalization group flow is implemented in the context of the holographic correspondence. This yields interesting phenomena by inducing transitions of spacetime according to the energy scale. For example, holographic renormalization group flow from UV Lifshitz spacetime to IR AdS spacetime has been found [56, 18]. Or we can apply a modified gravitational action by adding higher curvature terms, and see what new effects to emerge. In this regard, the deformation of the Lifshitz spacetime with a Gauss-Bonnet term in $(n+1)$ dimensions is studied in chapter 7.

Chapter 2

Anti-de Sitter Spacetime

Anti-de Sitter (henceforth AdS) spacetime is defined by the vacuum solution to the Einstein equations with the negative cosmological constant. AdS spacetime is a somewhat unrealistic spacetime for describing our universe due to the negative cosmological constant Λ, which is contrary to the modern cosmological observations consistent with the so-called Lambda-Cold Dark Matter (Λ-CDM) description as determined from the observed data of Cosmic Microwave Background Radiation (CMBR). Nevertheless, it has been actively studied since some interesting features are shown in its theoretical aspects, and moreover specific properties of this spacetime are essential in formulating the AdS/CFT correspondence.

The purposes of this chapter are to illustrate the general properties of AdS spacetime comparing it with Minkowski spacetime, and to understand distinguished characteristics that make it possible to establish the AdS/CFT correspondence.

2.1   General Properties

The Einstein equations with cosmological constant in $(n + 1)$ dimensions is

$$G_{\mu\nu} \equiv R_{\mu\nu} - \frac{1}{2}g_{\mu\nu}R = 8\pi G T_{\mu\nu} - \Lambda g_{\mu\nu} \tag{2.1}$$

where $T_{\mu\nu}$ is energy-momentum tensor and is determined by the matter content in spacetime. In the absence of matter ($T_{\mu\nu} = 0$), this simply becomes

$$R = \frac{2(n+1)}{(n-1)}\Lambda \tag{2.2}$$

where for $\Lambda = 0$ the scalar curvature is zero and becomes flat-Minkowski spacetime, for $\Lambda > 0$ the spacetime is positively curved and is called de Sitter spacetime (henceforth dS), and for $\Lambda < 0$ the spacetime is negatively curved and is known as Anti-de Sitter spacetime. That is, those three spacetimes are vacuum solutions derived from the Einstein equations, but different from the Minkowski spacetime, the de Sitter and the Anti-de Sitter spacetime intrinsically (i.e. without matters) curved spacetimes.

One common feature of these three spacetimes is their maximal symmetry: they possess the maximal number of independent Killing vectors. This is an intrinsic property of space-time regardless of coordinates chosen and is given by $n+1+n(n+1)/2 = (n+1)(n+2)/2$ in $(n+1)$ dimensional spacetime. Then the Riemann curvature tensor for any maximally symmetric spacetime with $(n+1)$ dimensions at any point and in any coordinates becomes

$$R_{\rho\sigma\mu\nu} = \frac{R}{n(n+1)}(g_{\rho\mu}g_{\sigma\nu} - g_{\rho\nu}g_{\sigma\mu}). \tag{2.3}$$

For the **Minkowski space** $\mathbb{M}^{n+1}$, the Killing vectors as generators of symmetry hold both for Lorentz transformations, which has isometry group $SO(1,n)$ with $n(n+1)/2$ generators, and for translations with $n+1$ generators, and so the Minkowski spacetime is represented by the **Poincarè group** with $(n+1)(n+2)/2$ generators. On the other hand, the isometry groups of the **dS**$_{n+1}$ and the **AdS**$_{n+1}$ become **SO(1,n+1)** and **SO(2,n)** respectively with $(n+1)(n+2)/2$ generators.

In addition, for the non-zero cosmological constant cases, when matter is present with energy density ρ and pressure p we have

$$T^{\mu}_{\nu} = \begin{pmatrix} \rho & 0 & \cdots \\ 0 & p & \cdots \\ & \vdots & \end{pmatrix}, \tag{2.4}$$

the positive cosmological constant Λ (negative Λ) contributes positively (negatively) to the energy, but negatively (positively) to the pressure.

2.2 Conformal Structure

2.2.1 Conformal Diagram

Let us consider the global coordinates of AdS spacetime

$$ds^2 = \frac{l^2}{\cos^2\theta}\big(- dt^2 + d\theta^2 + \sin^2\theta d\Omega^2_{n-1}\big).$$

This coordinate makes the spacelike infinity finite, but it introduces a singularity at $\theta = \frac{\pi}{2}$. To obtain a spacetime smoothly extending to the boundary, we follow the general process of compactification as follows.

Let us consider a manifold $\mathcal{M}$ with its boundary $\partial\mathcal{M}$ and introduce a function f, which is called a *defining function* that satisfies some conditions (i.e. $f|_{\partial\mathcal{M}} = 0$, $f'|_{\partial\mathcal{M}} \neq 0$, and $f|_{\mathcal{M}} > 0$), and plays the role of adding points at the boundary of the original manifold so that the manifold becomes conformally compact. If $d\tilde{s}^2$ is a metric for the compactified manifold and ds^2 is a metric for the original manifold, then

$$d\tilde{s}^2 = f^2 ds^2, \tag{2.5}$$

and to be general f can be replaced by

$$f \to f e^w \tag{2.6}$$

where w is a function without poles at the boundary.

By going through this process, we can work with the conformally compactified spacetime and draw conformal diagrams. One for the AdS spacetime is depicted in Fig.2.1 and one for Minkowski spacetime is also inserted in Fig.2.2 for comparison.

For the AdS case in Fig.2.1 (a), as we illustrated in (A.5), the compactification only applies to the spatial coordinate θ; there is no way to compactify the time direction, and so the range of time still remains $|t| < \infty$. Thus in the diagram spatial infinity is at the finite length $\frac{\pi}{2}$ denoted as i^0, but the future and past-timelike infinities, which are i^+ and i^- respectively, are just denoted at the top and bottom of the diagram.

Regarding spatial infinity, this conformal structure of AdS spacetime has a uniquely well-defined boundary at spacelike infinity that provides an opportunity to formulate the AdS/CFT correspondence.

The consequence of the timelike infinity is very interesting. That fact indicates that AdS spacetime is not globally hyperbolic, and so a Cauchy surface does not exist; however, a Cauchy surface can be formulated for the diamond shaped region in Fig.A.2 (b) and so one can make predictions only in this region. Another feature is found by considering geodesics as shown in Fig.2.1 (b). The geodesics normal to $t = 0$ converge at p and q, and all other timelike geodesics from p expand out and converge to q. This process keeps being continued as timelike geodesics from the converged point q re-expand out and reconverge to another p and on and on. This fact implies that the timelike geodesic from p can never reach the boundary i^0. In contrast, a null geodesic from p can reach the boundary. This property yields interesting physical results involving superradiance [35, 84].

9

(a) Conformal Diagram of AdS spacetime

(b) Geodesics from p
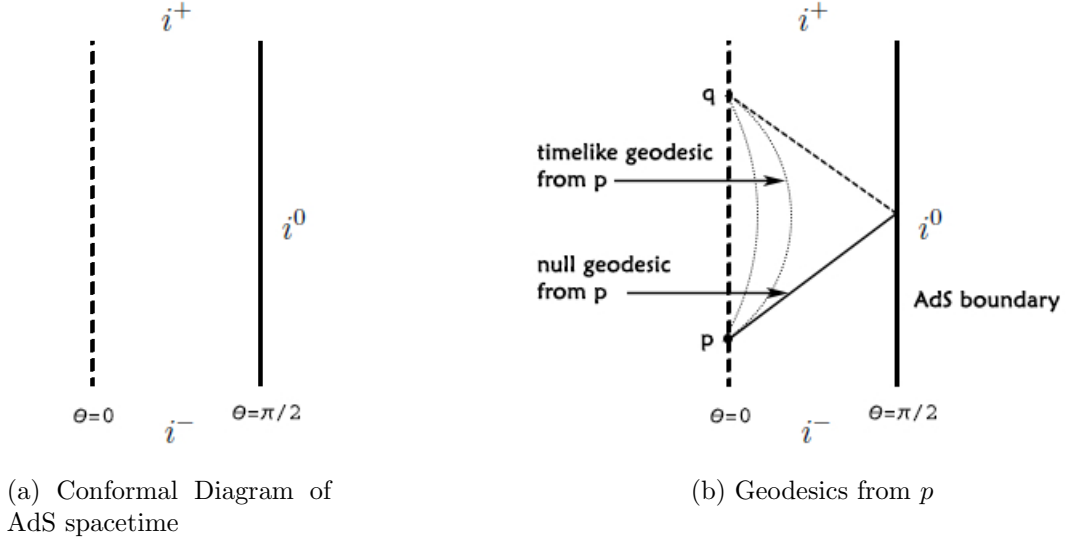
Figure 2.1: Conformal Diagrams and geodesics of the AdS spacetime

Now let us compare the conformal diagrams for the AdS in Fig.2.1 (a) and Minkowski spacetimes in Fig.2.2. As seen in the diagrams, the big distinction is that the conformal structure of the Minkowski spacetime has two kinds of infinities (disregarding timelike infinity), which are the null infinities $\Im^{\pm}$ and the spatial infinity i^0, represented by two lines and a point. This means that from the perspective of formulating a dual theory like AdS/CFT the conformal boundary of Minkowski spacetime is not uniquely determined, which is different from the AdS/CFT. It can be either the null infinity or the spatial infinity. Considering the conformal boundary to be a promising place for the gauge theory to reside, null infinity might be not eligible. For the spacelike infinity, it is depicted as a point not a line, and so it is hard to expect that physical fields admit smooth limit at the point i^0. These aspects of the conformal structure of Minkowski spacetimes make it difficult to establish a dual theory.

2.3 Asymptotic Solution Near Conformal Boundary

For the AdS spacetime, it is known how to formulate gravitational solutions at the conformal boundary in general [33], [81]. In this section, we study the construction of gravita-
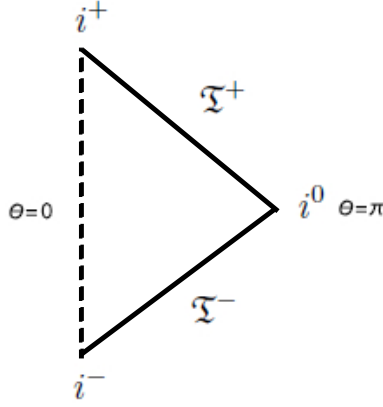
Figure 2.2: Conformal diagram for Minkowski spacetime

tional solutions in the AdS spacetime by following [33, 81], and investigate the possibility of applying the same method to the Minkowski spacetime.

Let us start with the gravitational action in $(n+1)$-dimensional AdS spacetime

$$S_{\text{gravity}} = \frac{1}{16\pi G_N} \int_{\mathcal{M}} d^{n+1}x \sqrt{G}(R[G] + 2\Lambda) - \frac{1}{8\pi G} \int_{\partial \mathcal{M}} d^d x \sqrt{\gamma} K \tag{2.7}$$

where $G_{\mu\nu}$ is the bulk gravitational field and K is the extrinsic curvature. The equation of motion is

$$R_{\mu\nu} - \frac{1}{2} R G_{\mu\nu} = -\Lambda G_{\mu\nu}. \tag{2.8}$$

and the curvature tensor is given by

$$R_{\kappa\lambda\mu\nu} = \frac{1}{l^2}(G_{\kappa\mu}G_{\nu\lambda} - G_{\mu\lambda}G_{\nu\kappa}) \tag{2.9}$$

where l is the AdS radius which is $\Lambda = n(n-1)/2l^2$. The equation is satisfied with

$$ds^2 = G_{\mu\nu}dx^\mu dx^\nu = \frac{l^2}{\cos^2 r}\big(-dt^2 + dr^2 + \sin^2\theta d\Omega_{n-1}^2\big) \tag{2.10}$$

which is obtained in (A.6), but in this coordinate the metric becomes singular at $r = \frac{\pi}{2}$ and is not defined at the conformal boundary $r = \frac{\pi}{2}$. Thus we need to find a well-defined

11

solution at the conformal boundary. This can be achieved by determining the defining function f, which is defined in (2.5) and, at the conformal boundary, f is additionally restricted by

$$|df|^2 = \tilde{G}^{\mu\nu}\partial_\mu f \partial_\nu f. \tag{2.11}$$

where $\tilde{G} = f^2 G$ and which is related to

$$R_{\kappa\lambda\mu\nu}[G] = |df|^2(G_{\kappa\mu}G_{\nu\lambda} - G_{\mu\lambda}G_{\nu\kappa}) + \mathcal{O}(r^{-3}). \tag{2.12}$$

This quantity describes the curvature tensor near the boundary and the order r^{-4} becomes the leading order as the boundary is $r = 0$. The $|df|^2$ is obtained by solving the Einstein equations with (2.12), and it becomes

$$|df|^2 = \frac{1}{l^2}. \tag{2.13}$$

Here we take the defining function f to be the radial coordinate r, and then the bulk metric expanding near the boundary becomes

$$ds^2 = G_{\mu\nu}dx^\mu dx^\nu = \frac{l^2}{r^2}(dr^2 + g_{ij}(x,r)dx^i dx^j) \tag{2.14}$$

which is known as the Graham-Fefferman coordinate system [37]. Expanding $g_{ij}(x,r)$ in powers of r, its general form is given by

$$g_{ij}(x,r) = g_{(0)ij} + r g_{(1)ij} + r^2 g_{(2)ij} + \cdots + r^n g_{(n)} + h_{(n)} r^n \log r^2 + \mathcal{O}(r^{(n+1)}) \tag{2.15}$$

where n is from the $(n + 1)$-dimensions and the logarithmic term with $h_{(n)}$ enters only for even n. As the terms associated with odd powers of r vanish by the Einstein equations, for convenience, we replace the parameter r with ρ by $\rho = r^2$ and then the metric is rewritten as

$$ds^2 = G_{\mu\nu}dx^\mu dx^\nu = l^2\left(\frac{d\rho^2}{4\rho^2} + \frac{1}{\rho}g_{i,j}dx^i dx^j\right) \tag{2.16}$$

where

$$g(x,\rho) = g_{(0)} + \cdots + \rho^{n/2}g_{(n)} + h_{(n)}\rho^{n/2}\log\rho + \cdots . \tag{2.17}$$

Plugging (2.16) into the Einstein equations, it yields

$$\rho(2g'' - 2g'g^{-1}g' + \text{Tr}(g^{-1}g')g') + \mathcal{R}(g) - (n-2)g' - \text{Tr}(g^{-1}g')g = 0, \tag{2.18}$$

$$D_i\text{Tr}(g^{-1}g') - D^j g'_{ij} = 0, \tag{2.19}$$

$$\text{Tr}(g^{-1}g'') - \frac{1}{2}\text{Tr}(g^{-1}g'g^{-1}g') = 0 \tag{2.20}$$

12

where the prime denotes the derivative with respect to ρ, and D_i is the covariant derivative with associated with g, and $\mathcal{R}$ is the Ricci tensor of g. Expanding equations (2.18)-(2.20) order by order in ρ with (2.17) and setting $\rho = 0$, the relations between coefficients in (2.17) are obtained. In this process, cases of even n break down at order $\rho^{n/2}$ unless the logarithmic term is present. This is the reason that $h_{(n)}$ is present in (2.17) where $h_{(n)}$ is restricted by

$$\mathrm{Tr}(g_0)^{-1}h_{(n)} = 0, \qquad D^i h_{(n)ij} = 0. \tag{2.21}$$

Solving (2.18) for $n = 2$ and $n = 4$ cases, the $g_{(k)}$ for $k < n$ and the $h_{(n)}$ are expressed in terms of $g_{(0)}$,

$$g_{(2)ij} = \frac{1}{n-2}\left(R_{ij} - \frac{1}{2(n-1)}\mathcal{R}g_{(0)ij}\right),$$

$$\begin{aligned}
g_{(4)ij} = \frac{1}{n-4}\Bigg(&\frac{1}{4(n-2)}D_k D^k \mathcal{R}_{ij} - \frac{1}{8(n-1)}D_i D_j \mathcal{R} - \frac{1}{8(n-1)(n-2)}D_k D^k \mathcal{R}g_{(0)ij} \\
&- \frac{1}{2(n-2)}\mathcal{R}^{kl}\mathcal{R}_{ikjl} + \frac{n-4}{2(d-2)^2}\mathcal{R}_i{}^k\mathcal{R}_{kj} + \frac{1}{(n-1)(n-2)^2}\mathcal{R}\mathcal{R}_{ij} \\
&+ \frac{1}{4(d-2)^2}\mathcal{R}^{kl}\mathcal{R}_{kl}g_{(0)ij} - \frac{3n}{16(n-1)^2(n-2)^2}\mathcal{R}^2 g_{(0)ij}\Bigg)
\end{aligned} \tag{2.22}$$

and these obviously become singular for $n = 2$ and $n = 4$. Thus, we instead obtain the trace and divergence of $g_{(n)}$ from (2.19) and (2.20), and then $g_{(n)}$ takes the form

$$\nabla^i g_{(n)ij} = \nabla^i A_{(n)ij}, \qquad n = 2, 4 \tag{2.23}$$

where

$$\begin{aligned}
A_{(2)ij} &= g_{(0)ij}\mathrm{Tr}g_{(2)}, \\
A_{(4)ij} &= -\frac{1}{8}\left(\mathrm{Tr}\, g_{(2)}^2 - (\mathrm{Tr}\, g_{(2)})^2\right)g_{(0)ij} + \frac{1}{2}g_{(2)j}{}^k g_{(2)kj} - \frac{1}{4}g_{(2)ij}\mathrm{Tr}\, g_{(2)}
\end{aligned} \tag{2.24}$$

Integrating (2.23), it involves an integration constant t_{ij}, which is not determined by the Einstein equations, and as g_{ij} and A_{ij} are symmetric, t_{ij} also becomes a symmetric tensor. For $n = 2$, the integration of (2.23) yields

$$g_{(2)ij} = \frac{1}{2}(\mathcal{R}g_{(0)ij} + t_{ij}) \tag{2.25}$$

where the t_{ij} satisfy

$$D^i t_{ij} = 0, \qquad \mathrm{Tr}\, t = -R, \tag{2.26}$$

13

and for $n = 4$, the integration of (2.23) has the solution

$$g_{(4)ij} = \frac{1}{8}g_{(0)ij}\left((\mathrm{Tr}g_{(2)})^2 - \mathrm{Tr}g_{(2)}^2\right) + \frac{1}{2}g_{(2)i}{}^k g_{(2)kj} - \frac{1}{4}g_{(2)ij}\mathrm{Tr}g_{(2)} + t_{ij} \tag{2.27}$$

where the t_{ij} satisfy

$$D^i t_{ij} = 0, \quad \mathrm{Tr}\, t = -\frac{1}{4}\left(\mathrm{Tr}(g_{(2)})^2 - \mathrm{Tr}g_{(2)}^2\right). \tag{2.28}$$

For odd n, the $g_{(d)ij}$ is only restricted by

$$D^i g_{(d)ij} = 0, \qquad \mathrm{Tr}g_{(d)} = 0, \tag{2.29}$$

and so becomes

$$g_{(d)ij} = t_{ij}. \tag{2.30}$$

In summary, in the AdS_{n+1} spacetime we can take the metric, which is well-defined near the boundary, in the form of (2.16) with (2.17), where the $h_{(d)}$ only appears for even n. Then we find the relations between the coefficients $g_{(0)}, g_{(k)}, h_{(n)}$ and $g_{(n)}$ by solving the Einstein equations order by order in ρ. The $g_{(k)}$ for $k < n$ and $h_{(n)}$ are explicitly expressed in terms of $g_{(0)}$ from (2.18), and those coefficients are determined if $g_{(0)}$ is provided from the boundary conditions of the spacetime. On the other hand, the $g_{(n)}$ should be obtained by integrating (2.23), which is derived from (2.19) and (2.20), and so are accompanied with the integration constant, which is the undetermined symmetric tensor t_{ij}.

In the holographic renormalization procedure, which will be discussed in Chapter 5, the divergences of the action are shown as functions of $g_{(0)}$, and so the counter terms, which remove the divergence of the action, are automatically generated as a function of $g_{(0)}$. The $h_{(n)}$ for even n is connected to the conformal anomaly, and the $g_{(n)ij}$ and t_{ij} are related to the expectation value of the boundary stress energy tensor by

$$\langle T_{ij}(x)\rangle_s = \frac{2}{\sqrt{g_{(0)}(x)}}\frac{\delta S_{\mathrm{ren}}}{\delta g_{(0)}^{ij}(x)} = \frac{nl^{n-1}}{16\pi G_N}g_{(n)ij} + X_{ij}[g_{(k)}]$$

where S_{ren} is the renormalized bulk action and $X_{ij}[g_{(k)}]$ is a function of $g_{(k)}$ for $k < n$.

Considering the possibility of applying this process to the Minkowski spacetime, it is known that the relations of the coefficients of the metric are given in the form of differential equation (not by the algebraic relations, which works for the AdS case), and moreover the Einstein equations require some restrictions on $g_{(0)}$ [81]. Thus it is hard to expect to obtain

14

the general set (i.e $\{g_{(0)}, g_{(2)}, \cdots, g_{(n)}\}$) of metric solutions near the conformal boundary with this method. In the holographic renormalization picture, this fact makes it difficult to generate the universal set of the local counterterms and explains the reason that the general algorithm to generate the counterterms is barely known for Minkowski spacetime. Nevertheless, there was a remarkable try to generate local counterterms, in which the counterterms do not take an explicit form, but are provided as solutions derived by the given differential equation in [63, 64, 75]. This method is investigated in detail in Chapter 6.

2.4 Discussion

Some essential points are found in order to establish the gravity/gauge duality theory on investigating the structure of the AdS/CFT correspondence. One is that the symmetries of spacetime are equivalent to the symmetries of gauge theory. The other is that the space-time has a well-defined boundary, which does not include any singularity at the infinity and becomes a suitable place for the dual gauge fields to reside. In this section, we understood what properties of the AdS spacetime make it suitable under these conditions by investigating the isometry group of the spacetime and its conformal structure. Related to these points, we also found some distinctions between the AdS spacetime and the Minkowski spacetime by comparison. In addition, based on [33, 81], we showed a general derivation of the metric solution near the boundary in the AdS_{n+1} spacetime by solving the Einstein equations, which is convenient for the process of holographic renormalization.

In section 2.1, general properties gleaned from general relativity theory are illustrated for the AdS spacetime. The important note is that the AdS_{n+1} spacetime is the maximally symmetric spacetime having the maximal number of independent Killing vectors $(n + 1)(n + 2)/2$. This symmetry of the spacetime is represented by the isometry group $SO(2, n)$, which is $(n+2)$ Lorentz group and is identical with the group structure of conformal field theory. On the other hand, the Minkowski spacetime $\mathbb{M}^{n+1}$ is also a maximally symmetric spacetime possessing $(n + 1)(n + 2)/2$ independent Killing vectors. However the isometry group of the Minkowski spacetime is the Poincarè group, which has the Lorentz symmetry $SO(1, n)$ plus the translation symmetry. Note that the symmetries of asymptotically Minkowski spacetime are different from those of Minkowski spacetime. In asymptotically Minkowski space-time, as null infinity is approached, the group of asymptotic symmetries is known as the BMS group; approaching spatial infinity, the group of asymptotic symmetries is known as the SPI group [88]. It is not yet known what connection the $SO(2, n)$ group has with the Poincarè group (or BMS or SPI group), making it

difficult to build a (asymptotically) Minkowski/CFT correspondence.

In section 2.2, the conformal structure of AdS spacetime was studied and compared with Minkowski spacetime. As shown in Fig.2.1, the AdS spacetime has a uniquely determined conformal boundary at spacelike infinity, but as the timelike direction is not associated with compactification, its conformal boundary at $\theta = \frac{\pi}{2}$ is stretched out. This conformal feature gives an opportunity to establish AdS/CFT correspondence on AdS spacetime.

The conformal diagram for the (asymptotically) Minkowski spacetime has a spacelike infinity and null infinities denoted as the point and the lines respectively at the boundaries as shown in Fig.2.2. This indicates that if the boundary of spacetime, where dual gauge fields will be placed, is chosen to be the conformal boundary, it is not uniquely determined, but could either be null infinity or spacelike infinity. From the holographic duality perspective, it is difficult to consider null infinity as a place where the dual gauge fields reside, but there have been several attempts for this case [32, 82] (for asymptotically flat spacetime see [1, 2, 4, 30, 69, 70]). Conversely the spacelike infinity is represented as one point, and so it is hard to expect a smooth limit of physical fields to that point. These properties of the conformal structure make it hard to formulate the duality theory of the (asymptotically) Minkowski spacetime. However it is known that it is not necessary for the spacetime of the dual gauge fields to be the conformal boundary, and so as an alternative for an asymptotically flat spacetime, one considers the asymptotic boundary to be an n-dimensional hyperboloid $\mathcal{H}$, which agrees with the boundary conditions [6, 8, 63, 64, 67, 75].

In section 2.3, we demonstrated how to derive the general solution of the metric near the conformal boundary of the AdS_{n+1} spacetime, which plays an important role in building counterterms, by following [81]: set up the general form of the metric induced at infinity and plug the metric into the Einstein equations. The coefficients in the metric are given by algebraic relations, and this property enables one to automatically construct counterterms in the holographic renormalization process. On the other hand, when applying this method to Minkowski spacetime, the relations amongst coefficients in the metric take the form of differential equations, and the Einstein equations require more restrictions on those coefficients. Thus this algorithm does not produce big benefits for Minkowski spacetime in the holographic renormalization process. Distinct from this method, a remarkable way to generate counterterms was suggested by Mann and Marolf for the asymptotically Minkowski spacetime. This method is studied in chapter 5, where we set up the asymptotically flat metric for cylindrical coordinates in $(n + 3)$ dimensional spacetime and test the new counterterm method, where the counterterms are produced by solving a given differential equation called the Mann-Marolf relation.

The Lifshitz spacetime, which will be introduced in Chapter 6 and 7, has recently drawn

a lot of attention in terms of strongly correlated systems via the holographic correspondence formulation. Lifshitz spacetime is basically constructed by breaking Lorentz symmetry but conserving scaling symmetry, and so it becomes anisotropic and non-relativistic. Thus Lifshitz spacetime is invariant under spatial and temporal translations, spatial rotation, and P and T symmetry, which is a fewer number of symmetries than AdS or Minkowski spacetime [56]. This property suggests Lifshitz spacetime is dual to a Lifshitz-like field theory in condensed matter physics. In term of the properties of the Lifshitz spacetime, it is known that this spacetime yields nonzero components of the Riemann tensor, which diverge as $r \to 0$ if $z \neq 1$, in a parallel-propagated orthonormal frame, and possesses a naked singularity, which is a null curvature singularity [27, 45, 52]. More properties of these spacetimes are been being studied.

Chapter 3

Quantum Phase Transition and Statistical RG

In quantum critical phenomena associated with continuous (or second order) phase transitions, it is experimentally observed that different microscopic systems are characterized by the same set of critical exponents, which determine the vanishing characteristic energy scale and the diverging correlation length scale at the quantum critical point $g = g_c$. This is known as universality (or universal class), and later it is understood in the sense that when different microscopic systems described by many parameters approach the critical point, the scale-dependent parameters (or properties) of the system become much less important, and a few scale-independent parameters (or properties) survive. Thus systems sharing the same (critical) parameter at the critical point are classified in the same universal class. In this chapter, we first study the quantum phase transition [80] in section 3.1, and understand the renormalization method in the statistical context [58, 68] in section 3.2 and 3.3.

3.1   Basic Concepts of Quantum Phase Transition

As mentioned in the introduction, the Wilsonian RG was developed for explaining unusual physical phenomena called quantum critical phenomena. Here we understand physical properties revealed in the quantum critical point at zero temperature and in the vicinity of it at finite temperature. In the first subsection, we classify phase transitions and then focus on the second order phase transitions. In the following subsection, the nonzero temperature phase transition is discussed.

3.1.1   Quantum Phase Transition

The thermodynamic state of a macroscopic system in thermal equilibrium is calculated from the relevant thermodynamic potential Ω by using the partition function $\mathcal{Z}$

$$\mathcal{Z} = e^{-\Omega/T} \tag{3.1}$$

where T is temperature. In the thermodynamic limit where the number of particles and the volume go to infinity while their ratio remains constant, the (generalized) free energy $f = \Omega/V$ approaches a constant independent of V. Considering a system characterized by a set of coupling constant $g_1, \cdots, g_k$, the partition function in the thermodynamic limit takes the form

$$\mathcal{Z}(g_1, \cdots, g_K) = e^{-Vf(g_1, \cdots, g_k)/T}. \tag{3.2}$$

As the information of the system in the thermodynamic limit is derived from the free energy above, we can discern some distinct physical properties by analyzing a function of the free energy with respect to the coupling constants.

For this purpose, let us consider the free energy $f(g_1, \cdots, g_k)$ in the k-dimensional coupling space. In general, the free energy is almost analytic everywhere, but in the thermodynamic limit, $f(g_1, \cdots, g_k)$ shows nonanalyticity at points, lines, or other manifolds whose dimension is smaller than k. This nonanalyticity becomes the phase boundaries separating different phases of system, and the region where $f(g_1, \cdots, g_k)$ is analytic in coupling space defines the phase. Different types of nonanalyticity classify different types of phase transition, and it is largely distinguished by the discontinuous (or first order) phase transition and the continuous (or second order) phase transition. The former is characterized by $f(g_1, \cdots, g_k)$ being continuous but at least one of its derivatives with respect to g_i, $\partial f/\partial g_i$, is discontinuous at the phase boundary. The latter is confined to cases for which the $f(g_1, \cdots, g_k)$ and all its partial derivatives $\partial f/\partial g_i, i = 1, \cdots, k$ are continuous, but it exhibits a discontinuity in the second derivative of the free energy at the phase boundary. In the discontinuous transition, a system is characterized by thermodynamic variables such as the chemical potential or pressures. However in the continuous phase transition, its properties can usually be characterized by an order parameter, which in general is a quantity that becomes zero (i.e. complete disorder) in one phase and non-zero in the other, and so measures the degree of order in a system by varying from zero to the saturation value. Here we focus on the second order phase transition, especially the quantum critical region.

The quantum phase transitions belonging to the second order phase transition are accompanied by a quantum critical point leading to a nonanalyticity at the dimensionless

coupling constant $g = g_c$, and mostly happen when Δ, which is the characteristic energy scale of the lowest excitation above the ground state, vanishes as g approaches g_c at zero temperature. That is at the critical point the degrees of freedom of the system are coupled to each other and act like a single entity. In most cases Δ can be written roughly as

$$\Delta \sim J|g - g_c|^{z\nu} \tag{3.3}$$

where J is the energy scale of a characteristic microscopic coupling, and $z\nu$ is a critical exponent. In general the quantum critical states are characterized by critical exponents that characterize power law behaviour of various quantities. Besides ν, there is α (for specific heat), β (for order parameter), γ (for susceptibility), δ (for critical isotherm) and η (for correlation function); these six exponents are not independent of each other but are related by scaling and sometimes by hyperscaling, and so two of them become independent. An important note is that even though two systems may have different microscopic details they are characterized by the same set of exponents. This peculiar property of the exponents is said to be universal, and the same set of exponents are classified to the same universality class. It is known that all materials can be sorted into universality classes having the same critical exponents.

As having the vanishing characteristic energy scale at $g = g_c$, the same kind of singular property of the continuous phase transition appears as a divergence of characteristic length scale ξ, which indicates the typical length scale of the regions where the degrees of freedom are strongly coupled, and the diverging characteristic length scale obeys

$$\xi^{-1} \sim \Lambda|g - g_c|^{\nu} \tag{3.4}$$

where ν is a critical exponent and Λ is a momentum cutoff or an inverse length scale of order the inverse lattice spacing. Comparing the rates of the vanishing characteristic energy scale (3.3) and the diverging characteristic length scale (3.4), we see that

$$\Delta \sim \xi^{-z} \tag{3.5}$$

where z is a dynamical critical exponent, and so the characteristic energy vanishes the inverse of the correlation length with power of z.

Besides static phenomena, one interesting feature is shown in dynamic phenomena in the vicinity of a critical point. This is known as *critical slowing down*, and it is observed that when one approaches the critical point, temporal correlations of the order parameter decay slower and slower. Defining the correlation time τ_c to be the typical decay time of a temporal order-parameter fluctuation, τ_c diverges as

$$\tau_c = \xi^z \tag{3.6}$$

where z is also the dynamical critical exponent.

Now let us consider the free energy f in the vicinity of the critical point. Considering a magnet with free energy $f(t, h)$, where t is called reduced temperature and is defined as $t = (T - T_c)/T_c$ and h is the magnetic field, we can expect the $f(t, h)$ to be decomposed into a singular part and a regular part

$$f(t, h) = f_{\text{sng}}(t, h) + f_{\text{reg}}(t, h) \tag{3.7}$$

where the $f_{\text{sng}}(t, h)$ becomes dominant in the vicinity of the quantum critical point. As physical properties should be unchanged under rescaling through the renormalization group procedure (which will be discussed in section 3.2), in a continuous phase transition the singular part $f_{\text{sng}}(t, h)$ of the free energy should be homogenous as

$$f_{\text{sig}}(t, h) = b^{-D} f_{\text{sig}}(b^{y_t} t, b^{y_h} h) \tag{3.8}$$

where y_t and y_h are expressions standing for relevant critical exponents. However, since time scales as $(\text{length})^z$ in (3.6), at zero temperature the singular part of the free energy should be modified as

$$f_{\text{sng}}(g, h) = b^{-(D+z)} f_{\text{sng}}(b^{y_g} g, b^{y_h} h). \tag{3.9}$$

Thus in a quantum critical system, the time in some sense acts as an extra dimension z by increasing the effective dimensionality of the system from D which is a spatial dimension of the system to $D + z$ in the vicinity of a quantum critical point, and so the system is described by having different scalings of time and space in the continuous phase transition. At finite temperature, the singular part of the free energy (3.9) is generalized to

$$f_{\text{sng}}(g, h, T) = b^{-(D+z)} f_{\text{sng}}(b^{y_g} g, b^{y_h} h, b^z T). \tag{3.10}$$

Note that the quantum phase transition is a continuous phase transition. It happens only at zero temperature and exhibits its diverging and vanishing properties for Δ and ξ respectively, which refer to singularities of the ground state of the system. Since there is no thermal fluctuation at zero temperature, the quantum phase transition is driven by quantum fluctuations, and it occurs by controlling order parameters such as pressure, magnetic field, or chemical doping.

3.1.2 Finite Temperature Transition and Crossovers

Strictly speaking, the quantum phase transition occurs only at $g = g_c$ and absolute zero temperature $T = 0$. However it has been found that the quantum critical point can fan
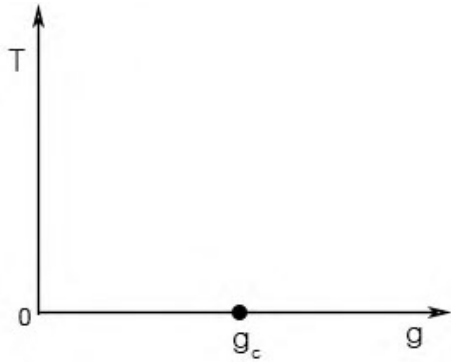
(a) quantum critical point exists at $g = g_c$ and zero. temperature
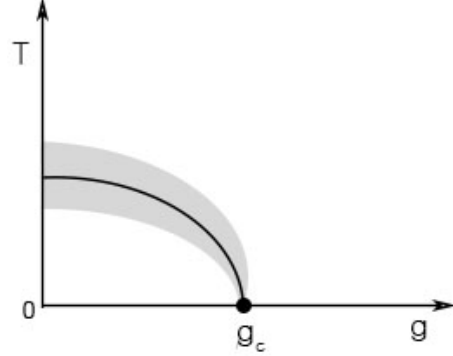
(b) second order phase transition occurs along the solid line at $T > 0$ and terminates at quantum critical point $g = g_c$ and zero temperature.

Figure 3.1: Two Possible Phase Diagrams

out to a wide quantum critical region over a broad range of values of $|g - g_c|$ at nonzero temperature $T > 0$. Thus in describing the second phase transition, two possible phase diagrams [80] can be considered as shown in Fig.3.1. For the first, the quantum phase transition happens only at zero temperature; it does not have any phase transition (i.e. the free energy is analytic) at any $T > 0$ as shown in Fig 3.1 (a). For the second, the free energy is not analytic along the solid line terminating at the quantum critical point at $g = g_c$ and $T = 0$ as shown in Fig.3.1 (b), and so the solid line becomes a locus of second-order phase transitions at finite temperature. The shaded region indicates that the theory of phase transitions in classical system driven by thermal fluctuation can be applied. Based on the case of Fig.3.1 (b), we investigate dominant effects for each states of the phase diagrams in the vicinity of a quantum critical point at nonzero temperature regime.

So far the energy scale Δ, which characterizes the ground state of a system, is used for our discussions, and now due to non-zero temperature, a second energy scale $k_B T$ is included in our consideration. To characterize the dynamics at $T > 0$ we define the thermal equilibration time τ_{eq}, which is characteristic time taken for achieving local thermal equilibrium after a weak external perturbation. We also roughly divide the phase diagram into three regions as shown in Fig.3.2, which separates the quantum critical region from the others.

In region I in Fig.3.2, it is found that the equilibration time τ_{eq} scale has a large value
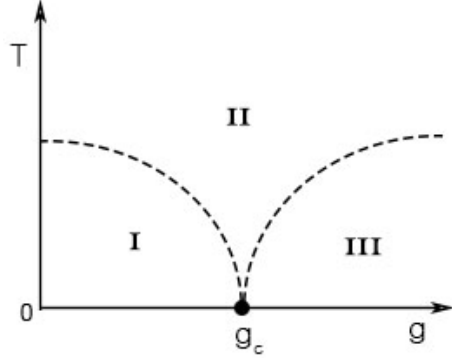
Figure 3.2: Separation of phase diagram into three regimes. The dashed line are smooth crossovers at T.

and so the dynamics of a (quantum) system is classically dealt with. Specifically, the solid line of second-order phase transitions in Fig.3.1 (b) lies in this region, and the region above the phase transition line describes the disordered phase in which the thermodynamic average of the order parameter is zero but fluctuations are non-zero as the order is short range. In the region below the phase transition line, the ordered (i.e. long range order) state is placed, where correlation function decays to a constant at large distance.

In the regions II and III in Fig.3.2, the equilibration time τ_{eq} scale is short, and so there is a competition between quantum fluctuations with energy scale Δ and thermal fluctuations with energy scale $k_B T$. In the region II, thermal excitation of quantum critical ground state is dominant by $\Delta < k_B T$, and in the region III, quantum fluctuation is controlling a system by $\Delta > k_B T$. The dashed line between I and II, and II and III are smooth crossovers at $T \sim |g - g_c|^{z\nu}$.

The detailed phase diagrams are depicted in Fig.3.3, where the left is for a system having no long range order at finite temperature, but the right is for a system for exhibiting long-range order at finite temperature, and which is referred from [58].
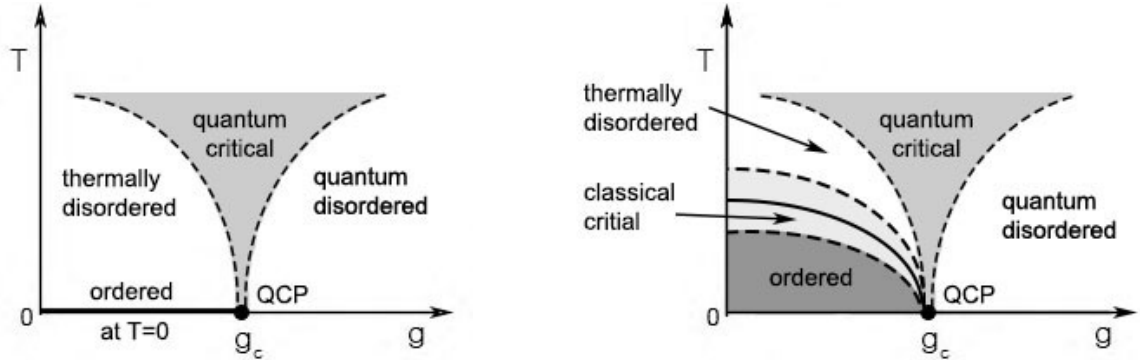
(a) phase diagram with no long-range order at $T \neq 0$

(b) phase diagram having long-range order at $T \neq 0$

Figure 3.3: Two Possible Phase Diagrams

3.2 The Basic Idea of the RG Transformation

The statistical renormalization process consists of two steps

1. Mode Elimination (Decimation)

2. Rescaling

The first step is basically to reduce the information to the level just necessary for describing the system, and this idea is performed by a coarse-graining operation. The operation proceeds by integrating over momenta in the shell $\Lambda \leq k \leq \Lambda_0$, where Λ_0 is UV cutoff. Or in lattice theory, it is performed by blocking lattices (there are various ways to form block variables) and by averaging over the block variables, and this process is repeatedly carried out to a new lattice until the same process or the same blocking is not applicable. As this process is carried out based on the scale invariance of a system in a certain range, a final lattice has the similar properties with the original lattice. The second step applies to the physical quantities such as length of a lattice, wave vectors, or fields (e.g. in a form of $\Lambda = \Lambda_0/b$, where b is the step size of renormalization group transformation) to restore the same form before the mode elimination. The combined process is illustrated in Fig.3.4, which is referred from [58].

The effect of conducting two steps should be explained by the modification of the coupling constant g in a way that the initial couplings $g = (g_1, g_2, g_3, \cdots)$ with the initial
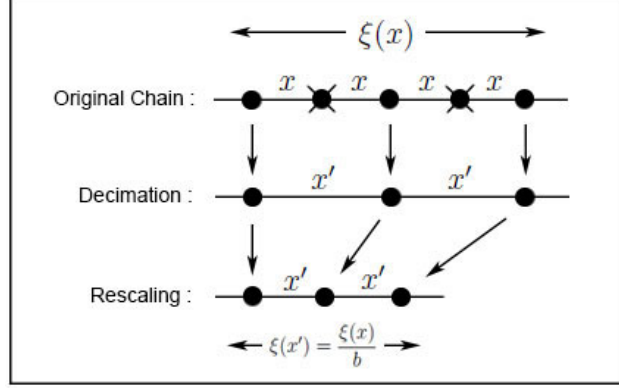
Figure 3.4: Pictorial Representation of RG Transformation

action $S[\Phi, g]$ replaced by the modified couplings $g' = (g'_1, g'_2, g'_3, \cdots)$ with the modified action $S'[\Phi', g']$. Then this combined procedure makes a map between the initial set of coupling and the final set of couplings such as

$$g' = \mathcal{R}(b; g) \tag{3.11}$$

where g' and g are sets of coupling constants, and the function $\mathcal{R}(b; g)$ transforms g to g' and is called renormalization group (RG) transformation, where b is the step size of RG transformation. The form of $\mathcal{R}(b; g)$ takes a complicated nonlinear function of the coupling constant, and also depends on a scaling factor b. The set of $\mathcal{R}(b; g)$ becomes a semigroup, which possesses the same composition law as a group, but the inverse of each transformation is not required; this group is labeled by a continuous parameter b. That is, two successive transformation with scale factor b and b' is equivalent to a single transformation with the scale factor $b'' = b'b$. Assuming that

$$g' = \mathcal{R}(b; g), \qquad g'' = \mathcal{R}(b'; g'), \tag{3.12}$$

the composition law allows

$$g'' = \mathcal{R}(b'; \mathcal{R}(b; g)) = \mathcal{R}(b'b; g) = \mathcal{R}(b''; g), \tag{3.13}$$

and then for given initial coupling $g^{(0)} = g$, the complete RG procedure yields a chain of renormalized couplings $g^{(n)}$

$$g^{(n)} = \mathcal{R}(b; g^{(n-1)}) = \mathcal{R}(b^n; g). \tag{3.14}$$

25

(a) perfectly ordered ($\xi = \infty$)   (b) completely disordered ($\xi = 0$)   (c) correlated in a finite region
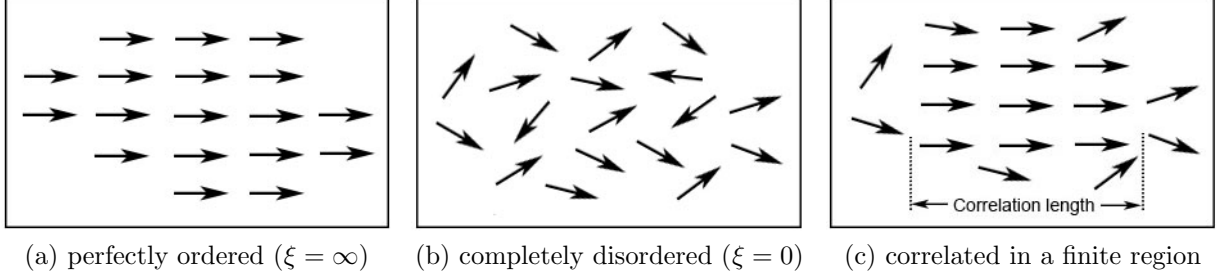
Figure 3.5: pictorial representation of correlation length

Iterating the RG transformation $\mathcal{R}(b; g)$ on the (possibly infinite) set of couplings $g = (g_1, g_2, g_3, \cdots)$, at a special point $g^* = (g_1^*, g_2^*, g_3^*, \cdots)$, it reaches a fixed point of the RG satisfying

$$g^* = \mathcal{R}(b; g^*) \tag{3.15}$$

and these points are called RG fixed points.

Now let us consider what happens to correlation length at fixed points. The correlation length is defined by regions where spins on lattices are strongly correlated, and so largely three states are possible: perfectly ordered, completely disordered, and correlated finite region as shown in Fig.3.5, which is referred from [68]. By the RG procedure, the correlation length is rescaled by

$$\xi(g') = \frac{\xi(g)}{b} \tag{3.16}$$

with arbitrary $b > 1$, and at any fixed point $g = g' = g^*$ it yields

$$\xi(g^*) = \frac{\xi(g^*)}{b}. \tag{3.17}$$

As b is finite and positive, the above relation is satisfied with either $\xi = \infty$ or $\xi = 0$. That is, at any RG fixed points a correlation length becomes infinity (strongly coupled) as shown in Fig.3.5 (a) or vanishes (completely decoupled) as shown in Fig.3.5 (b). For the infinite correlation length the fixed points are considered as critical points with continuous phase transitions and are called *critical fixed points*, and for the zero correlation length the fixed points are called *trivial fixed points*. In general, the RG transformation has more than two fixed points or even a continuum of fixed points forming a certain manifold in coupling space.

3.3   General Properties of RG Flow

As we are interested in fixed points, let us consider an infinitesimal variation near the fixed point g^* such as

$$\delta g' \equiv g' - g^* = \mathcal{R}(b; g) - \mathcal{R}(b; g^*), \tag{3.18}$$

for linear order in δg we can express it in the linearized differential form

$$\delta g_i' = \left. \frac{\partial \mathcal{R}_i(b; g)}{\partial g_j} \right|_{g^*} \delta g_j = \mathbf{R}_{ij}(b; g^*)\delta g_j \tag{3.19}$$

which is called the linearized RG flow in the vicinity of the RG fixed point g^*, and where $\mathbf{R}(b; g^*)$ is a matrix in coupling space and takes a different form for each fixed points. Local behaviour of the RG flow in the vicinity of a fixed point can be roughly predicted or classified by determining the eigenvalues of the matrix $\mathbf{R}(b; g)$. In general we do not have any constraints on the $\mathbf{R}(b; g)$ to be diagonalized, so we consider the matrix $\mathbf{R}(b; g)$ with left and right eigenvectors. For our purpose let us take only the left eigenvectors v_α^T and the corresponding eigenvalues $\lambda_\alpha(b)$. By definition we obtain

$$v_\alpha^T \mathbf{R}(b; g^*) = v_\alpha^T \lambda_\alpha(b), \tag{3.20}$$

and by projecting the coupling constant δg onto the left eigenvector v_α^T of the matrix $\mathbf{R}(b; g^*)$ we take

$$u_\alpha = v_\alpha^T \delta g = \sum_i v_{\alpha,i} \delta g_i \tag{3.21}$$

where u_α are special linear combination of the coupling constants and called scaling variables, and under the RG transformation, we have

$$u_\alpha' = u_\alpha^T \delta g' = v_\alpha^T \mathbf{R}(b; g^*)\delta g = \lambda_\alpha(b) v_\alpha^T \delta g = \lambda_\alpha(b) u_\alpha. \tag{3.22}$$

As mentioned the RG transformation $\mathcal{R}(b; g)$ holds semigroup properties and so two RG transformations yield

$$\mathcal{R}(b'; \mathcal{R}(b; g)) = \mathcal{R}(b'b; g) = \mathcal{R}(bb'; g) = \mathcal{R}(b; \mathcal{R}(b'; g)). \tag{3.23}$$

This implies that the transformation matrices associated with the linearized RG flow near a given fixed point satisfy

$$\mathbf{R}(b; g^*)\mathbf{R}(b'; g^*) = \mathbf{R}(bb'; g^*) = \mathbf{R}(b'; g^*)\mathbf{R}(b; g^*). \tag{3.24}$$

Since the matrices $R(b; g^*)$ and $R(b'; g^*)$, which have different values b commute in (3.24), the eigenvectors v_α^T are independent of b and then (3.24) is expressed in terms of eigenvalues

$$\lambda_\alpha(b)\lambda_\alpha(b') = \lambda_\alpha(bb'). \tag{3.25}$$

This has the solution as follows

$$\lambda_\alpha(b) = b^{y_\alpha} \tag{3.26}$$

where the exponent y_α is independent of b and is called the renormalization group eigenvalues associated with the scaling variables u_α. Then (3.22) can be rewritten as

$$u'_\alpha = b^{y_\alpha} u_\alpha \tag{3.27}$$

or be expressed in the differential form as

$$\frac{du_\alpha}{dl} = y_\alpha u_\alpha. \tag{3.28}$$

where $u^*_\alpha = 0$ from $u_\alpha = \sum_i v_{\alpha,i}(g_i - g^*_i)$. As we started by obtaining the linearized RG flow (3.19) in the vicinity of the fixed point, the subsequent results (3.27) or (3.28) are taken into account for the linear level, and so they give the linear level predictions about growing or decaying properties of the scaling variables of u_α. Then the local behaviours of u_α in the vicinity of a fixed point g^* can be classified into three cases due to a sign of the y_α as follows

- $y_\alpha > 0$: **scaling variables u_α are called *relevant***
  the small initial deviation of u_α from the fixed point grows exponentially upon iterating the RG so that the RG flow is repelled from the fixed point

- $y_\alpha < 0$: **scaling variables u_α are called *irrelevant***
  the small initial deviation of u_α from the fixed point decays upon iterating the RG

- $y_\alpha = 0$: **scaling variables u_α are called *marginal***
  the RG flow in coupling space can approach (*marginally irrelevant*) a fixed point or flow away (*marginally relevant*) from a fixed point; the local behaviour of the RG flow is determined by considering higher orders in the coupling constants

Chapter 4

Review of Holographic Renormalization

In this chapter, we seek a comprehensive understanding by reviewing holographic renormalization for the AdS spacetime constructed in [81]. From a holographic perspective, we might expect that the two-point correlation function at the boundary of the spacetime can be written as

$$\langle O(x)O(0)\rangle = -\frac{\delta^2 S_{\text{on-shell}}}{\delta\Phi_{(0)}(x)\delta\Phi_{(0)}(0)}\bigg|_{\Phi_{(0)}=0}, \tag{4.1}$$

but this yields infinite answers due to the diverging on-shell action as r goes to infinity. Thus the purpose of holographic renormalization is to formulate well-defined holographic correlation functions. Inspired by field theoretical renormalization, holographic renormalization follows the procedure:

1. To compute the most general asymptotic solutions

2. To regulate the divergence by restricting the radial coordinate to have a finite range

3. To add suitable covariant counterterms

4. To get renormalized on-shell action

Here we investigate each steps and briefly demonstrate the results for the one point function.

General Asymptotic Solutions

As discussed in chapter 2, the general form of the asymptotic solution for AdS spacetime, which is expanded near conformal boundary, becomes

$$ds^2 = G_{\mu\nu}dx^\mu dx^\nu = \frac{d\rho^2}{4\rho^2} + \frac{1}{\rho}g_{ij}(x, \rho)dx^i dx^j,$$

$$g(x, \rho) = g_{(0)} + \cdots + \rho^{d/2}g_{(d)} + h_{(d)}\rho^{d/2}\log\rho + \cdots \tag{4.2}$$

where $l^2 = 1$ is taken. For matter fields in the bulk of spacetime, the equation of motions takes the second order differential equation, and two independent solutions associated with ρ^m and ρ^{m+n} are yielded in asymptotic region. Then the general form of the bulk fields can be written as

$$\mathcal{F}(x, \rho) = \rho^m \big(f_{(0)}(x) + f_{(2)}(x)\rho + \cdots + \rho^n(f_{(2n)}(x) + \log\rho\tilde{f}_{(2n)}(x)) + \ldots\big) \tag{4.3}$$

where n and $2m$ are non-negative integers. With this ansatz, solving the equation of motions iterately for a small value of ρ (i.e. the boundary is at $\rho = 0$), $f_{(2k)}(x)$, where $k < n$, and $\tilde{f}_{(2n)}(x)$ are uniquely determined by $f_{(0)}(x)$. While $f_{(2n)}(x)$ is not determined by the near-boundary analysis, but is given by the Dirichlet boundary condition. Later, $f_{(0)}(x)$ is interpreted as the source for field theory, and $\tilde{f}_{(2n)}$ is related to conformal anomalies [81].

Regularization

Here we compute the on-shell action with these asymptotic solutions. We first set up the boundary of the spacetime in a range $\rho \geq \epsilon$, where ϵ is very small, and compute the boundary term at $\rho = \epsilon$. Then as $\epsilon \to 0$, a finite number of diverging terms are isolated, and the on-shell action takes the form

$$S_{reg}[f_{(0)}; \epsilon] = \int_{\rho=\epsilon} d^4x\sqrt{g_{(0)}}\big[\epsilon^{-\nu}a_{(0)} + \epsilon^{-(\nu+1)}\,a_{(2)} + \ldots - \log\epsilon\,a_{(2\nu)} + \mathcal{O}(\epsilon^0)\big] \tag{4.4}$$

where ν is a positive number and only depends on the scale dimension of the dual operator, and $a_{(2k)}$ becomes a function of $f_{(0)}$.

Constructing Counterterms

To remove the divergence in the on-shell action, the counterterm can be constructed as

$$S_{\text{ct}}[\mathcal{F}(x,\epsilon);\epsilon] = -\text{divergent terms of } S_{\text{reg}}[f_{(0)};\epsilon] \tag{4.5}$$

where $f_{(0)}$ is reexpressed by $\mathcal{F}(x,\epsilon)$, which is evaluated at the regulated surface $\rho = \epsilon$, via $f_{(0)} = f_{(0)}(\mathcal{F}(x,\epsilon);\epsilon)$ in (4.3). That is, the coefficients $a_{(2k)}$ are inverted to $a_{(2k)}(f_{(0)}(x)) = a_{(2k)}(\mathcal{F}(x,\epsilon),\epsilon)$.

Renormalized On-Shell Action

By adding the counterterms, the subtraction action is defined as

$$S_{\text{sub}}[\mathcal{F}(x,\epsilon);\epsilon] = S_{\text{reg}}[f_{(0)};\epsilon] + S_{\text{ct}}[\mathcal{F}(x,\epsilon);\epsilon], \tag{4.6}$$

and by taking the limit $\epsilon \to 0$, the renormalized action is obtained

$$S_{\text{ren}}[f_{(0)}] = \lim_{\epsilon \to 0} S_{\text{sub}}[\mathcal{F};\epsilon]. \tag{4.7}$$

From this renormalization process, the one point function of the operator $\mathcal{O}_F$ is defined by the renormalized action

$$\langle \mathcal{O}_F \rangle_s = \frac{1}{\sqrt{g_0}} \frac{\delta S_{\text{ren}}}{\delta f_{(0)}} = \lim_{\epsilon \to 0} \left(\frac{1}{\epsilon^{d/2-m}} \frac{1}{\sqrt{\gamma}} \frac{\delta S_{\text{sub}}}{\delta \mathcal{F}(x,\epsilon)} \right) \tag{4.8}$$

where the second term indicates that its calculation is performed by using the subtraction action and is taken to the limit of $\epsilon \to 0$.

One Point functions

Supposing the gravitational action $S[\Phi, A_\mu, G_{\mu\nu}, \ldots]$, the one point function is defined by using the renormalized action S_{ren}, and each of them are expressed as

$$\Phi \to \langle \mathcal{O}(x) \rangle_s = \frac{1}{\sqrt{g_{(0)(x)}}} \frac{\delta S_{\text{ren}}}{\delta \Phi_{(0)}(x)} \sim \phi_{(2\Delta-d)}(x), \tag{4.9}$$

$$A_\mu \to \langle J_i(x) \rangle_s = \frac{1}{\sqrt{g_{(0)(x)}}} \frac{\delta S_{\text{ren}}}{\delta A^i_{(0)}(x)} \sim A_i(x), \tag{4.10}$$

$$G_{\mu\nu} \to \langle T_{ij}(x) \rangle_s = \frac{2}{\sqrt{g_{(0)(x)}}} \frac{\delta S_{\text{ren}}}{\delta g^{ij}_{(0)}(x)} \sim g_{(d)ij}(x) \tag{4.11}$$

31

where $\mathcal{O}$ is the operator of the field theory, J_i is the boundary symmetry current which couples to the bulk gauge field A_μ, and T_{ij} is the boundary stress energy tensor that couples to the boundary metric $g_{(0)ij}$. Here ϕ, A_{mi}, and $g_{(d)ij}$ are the asymptotic solutions of Φ, A_μ, and G_μ calculated at the boundary of the spacetime, and are dual to $\langle \mathcal{O}(x) \rangle_s$, $\langle J_i(x) \rangle_s$, and $\langle T_{ij}(x) \rangle_s$ in field theory respectively.

Chapter 5

Holographic Renormalization in Asymptotically Flat Spacetime

5.1 Introduction

As mentioned in the introduction, the holographic correspondence (gauge/gravity correspondence) can be interpreted as a UV/IR connection, which means that a UV divergence of the correlation function in field theory corresponds to an IR divergence of the gravitational action at the boundary of the spacetime. In field theory, the way to remove the divergence is known as the renormalization method, which is studied in detail in appendix B. On the other hand, in gravity theory, for asymptotically AdS spacetimes an algorithm to generate counterterms removing the divergence of the action had been found [11, 61, 36], but for asymptotically Minkowski spacetimes a unique way to construct the counterterms was not known. The reason can be found in different asymptotic behaviours of those spacetimes. As seen in previous chapters, for the AdS spacetime the general asymptotic solutions, expanded near the conformal boundary, are obtained by solving the decomposed Einstein equations at the boundary of a spacetime (in chapter 2), and the counterterms are automatically formulated from these asymptotic solutions (in chapter 4). However, this method, i.e. boundary analysis of spacetime, is of little benefit to asymptotically Minkowski spacetimes, because their asymptotic solutions are not fixed by the Einstein equations. This makes it difficult to construct counterterms, as discussed in chapter 2. Instead, it seems to be more relevant for asymptotically Minkowski spacetimes to obtain the counterterms by solving the differential equations for each boundary condition.

Furthermore, in the process of the holographic renormalization, it is expected that the

holographic correlation function is obtained from the gravitational action, and so building counterterms becomes a crucial factor[81]. The importance of the counterterm is also revealed in gravity theory by involving conserved charges of a spacetime. From the boundary stress tensor formula, which will be discussed below, the counterterms participate in yielding conserved quantities associated with the boundary action, which includes a Gibbons-Hawking term. This chapter is concerned with both of these rationales for counterterms, but since the dual field theory of the Minkowski spacetime has not been found yet, we focus on checking our counterterm solution associated with the conserved quantities. That is, we obtain the counterterm solution for the given differential equations, which is the procedure expected to be the basis for yielding well-defined correlation functions in the future, and continue to check if our counterterm solution yields well-defined conserved quantities via the boundary stress tensor.

Mann and Marolf [63] suggested an algebraic equation in the components of $\hat{K}_{ab}$ such as

$$\mathcal{R}_{ab} = \hat{K}_{ab}\hat{K} - \hat{K}_a{}^c\hat{K}_{cb} \tag{5.1}$$

where $\mathcal{R}_{ab}$ is the Ricci tensor of h_{ab} induced on $\partial\mathcal{M}$, where h_{ab} is the induced metric defined at the boundary of the spacetime, and $\hat{K}$ is the trace of $\hat{K}_{ab}$ contracted with h^{ab}. The motivation behind Eq. (5.1) comes from the Gauss-Codazzi relation

$$\mathcal{R}_{abcd} = R_{abcd}^{Ref} + K_{ac}K_{bd} - K_{ad}K_{bc} \tag{5.2}$$

where $\mathcal{R}_{abcd}$ and R_{abcd}^{Ref} are respectively the Riemann tensor on $\partial\mathcal{M}$ and on the bulk spacetime $\mathcal{M}$. For an asymptotically flat spacetime R_{abcd}^{Ref} obviously vanishes. Replacing K_{ab} with a tensor $\hat{K}_{ab}$ and contracting (5.2) with h^{cd} yields (5.1). The counterterm $\hat{K}_{ab}$ is inserted into the action

$$S = \frac{1}{16\pi G}\int_{\mathcal{M}}\sqrt{-g}R - \frac{1}{8\pi G}\int_{\partial\mathcal{M}}\sqrt{-h}K + \frac{1}{8\pi G}\int_{\partial\mathcal{M}}\sqrt{-h}\hat{K} \tag{5.3}$$

where the first two terms are the Einstein-Hilbert and the Gibbons-Hawking terms respectively. It has been proven [63] that this counter term renders the action finite on asymptotically flat spacetimes and is stationary under metric variations for two standard asymptotic hypersurfaces, respectively referred to as "cylindrical" and "hyperbolic" boundary spacetimes $(\partial\mathcal{M}, h)$.

The boundary stress tensor is defined as the functional derivative of the on-shell action with respect to h_{ab}, which takes the form

$$T_{ab}^\pi = \frac{2}{\sqrt{-h}}\frac{\delta S}{\delta h^{ab}} = \frac{1}{8\pi G}\left(\pi_{ab} - \hat{\pi}_{ab}\right) \tag{5.4}$$

34

where h_{ab} is the induced metric on the asymptotic boundary, $\pi_{ab} = K_{ab} - K h_{ab}$ is the conjugate momentum of the gravitational field, and $\hat{\pi}_{ab}$ is an analogous contribution from the counterterm $\hat{K}$. Then the conserved charge associated with the Killing vector ξ^a via (5.4) in cylindrical coordinates is

$$Q[\xi] = \oint_{C_r} d^{n+1}x \sqrt{\gamma_{C_r}} u^a_{C_r} T^\pi_{ab} \xi^a \tag{5.5}$$

in $(n+3)$ dimensions, where γ is the trace of the induced metric on the $r = const.$ boundary at $t = const.$, and C_r is a Cauchy surface within a constant r hypersurface $\mathcal{H}_r$ such that $C = \lim_{r\to\infty} C_r$ is a Cauchy surface in the cylindrical boundary $\mathcal{H}$, and u^a is a timelike unit vector normal to C in $\mathcal{H}_r$.

In practice, however, the variation of the action has additional terms as a consequence of the definition (5.1); these are represented by Δ^{ab} and must be added to eq. (5.4). Despite this, we shall demonstrate that the quantities Δ^{ab} do not modify either conserved quantities as given by (5.5) or the conservation of the boundary stress-energy for cylindrical boundary conditions. Investigation of the connection between the boundary stress energy in (5.4) with the counter term definition (5.1) indicated that the extra term Δ^{ab} vanishes for higher than 4-dimensional spacetime and makes no contribution to the conserved charge for 4-dimensional spacetime [64]. These computations were carried out using hyperboloid coordinates for the boundary of the asymptotically flat spacetime, compatible with previous studies [13, 12, 6]. Specifically the conserved charges were shown to agree [64] with those defined by Ashtekar and Hansen [6].

Our concrete objective in this chapter is to investigate the boundary stress tensor (5.4) associated with the Mann-Marolf counterterm for cylindrical boundary conditions. As the structure of the boundary and the falloff rates of the metric components differ from those in the hyperbolic case, our aim is to understand the role played by Δ^{ab} in the context of defining a boundary stress-energy and conserved charges. As many spacetimes are commonly described in coordinates that asymptote to cylindrical ones, using the cylindrical boundary condition thus has great practical advantages for computation. By contrast, hyperboloid coordinates are rather impractical insofar as they require a non-trivial transformation of the coordinates of most asymptotically flat metrics.

With the same purpose, Astefanesei, Mann, and Stelea made some preliminary investigations using cylindrical coordinates, but considered only leading order fall-off conditions on components of the metric [9]. This is not sufficient for understanding the role played by Δ^{ab} in the asymptotically flat boundary counterterm approach using (5.1).

We begin with defining an $(n+3)$-dimensional asymptotically flat and static spacetime in cylindrical coordinates, whose metric functions fall off at least as fast as $r^{-(n+2)}$. We then

35

compute Δ^{ab} as a power series in $1/r$ up to the relevant fall off levels that could potentially affect the conserved charges. We find that i) to leading order, Δ^{ab} is manifestly zero for arbitrary dimensions, ii) the first sub-leading order of Δ^{ab} for $n = 1$ is zero, iii) Δ^{ab} does not vanish for $n > 1$, but iv) its non-vanishing does not affect conserved quantities. In addition, we find that for $n \geq 2$ manifestly $\mathcal{D}^a T_{ab} = 0$, but for $n = 1$ satisfying $\mathcal{D}^a T_{ab} = 0$ requires a condition between higher-order coefficients in the metric. Finally, we show explicitly how the conserved quantity formula (5.5) associated with the counterterm (5.1) works in $(n + 3)$-dimensional static spacetime.

This chapter proceeds as follows. In section 5.2, we review a variation of the action and the boundary stress tensor demonstrated already in [63, 64], and introduce our definition of asymptotic flatness in the cylindrical coordinates. In section 5.3, we obtain the solution for MM-counterterm by solving decomposed Einstein equations, and then in section 5.4, with the counterterm solution we find Δ^{ab} and investigate how the non-zero value of Δ^{ab} modifies the conserved quantity formula (5.5). Also in section 5.5 we check the conservation of the boundary stress tensor T^{ab} in a sense that $\mathcal{D}_a T^{ab} = 0$. In section 5.6, we provide explicit examples of how to compute conserved charges in $(n+3)$-dimensional static spacetime. In section 5.7, we discuss the results.

5.2   Preliminaries

5.2.1   A Variation of the action and the Boundary Stress Tensor

In this section, we start with the action (5.3). We compute the variation of the action with respect to h_{ab} and find the form of the boundary stress tensor.

Taking a variation of the action with respect to the metric and eliminating the equation of the motion, we get

$$\delta S = \frac{1}{16\pi G} \int_{\partial \mathcal{M}} \sqrt{-h} \left[\left(\pi^{ab} + h^{ab}\hat{K} - 2\hat{K}^{ab} \right) \delta h_{ab} + 2h^{ab}\delta\hat{K}_{ab} \right] \tag{5.6}$$

where $\pi^{ab} = K^{ab} - Kh^{ab}$, $\hat{\pi}^{ab} = \hat{K}^{ab} - \hat{K}h^{ab}$. To express $\delta\hat{K}_{ab}$ in terms of δh_{ab}, we take the derivation of (5.1) with respect to h_{ab}

$$\delta\mathcal{R}_{cd} = \delta\hat{K}_{ab}L_{cd}{}^{ab} + \left(\hat{K}_{cd}\hat{K}_{mn} - \hat{K}_{cm}\hat{K}_{nd} \right)\delta h^{mn} \tag{5.7}$$

where $L_{cd}{}^{ab}$ implies

$$L_{cd}{}^{ab} = h^{ab}\hat{K}_{cd} + \delta_c^a\delta_d^b\hat{K} - \delta_c^a\hat{K}_d^b - \delta_c^b\hat{K}_d^a. \tag{5.8}$$

36

Using the identity

$$(L^{-1})_{ab}{}^{mn}(L)_{mn}{}^{cd} = \delta_a^c \delta_b^d, \tag{5.9}$$

(5.7) is changed to

$$\delta \hat{K}_{ab} = (L^{-1})_{ab}{}^{cd}\left[\delta \mathcal{R}_{cd} + \left(\hat{K}_{cd}\hat{K}^{kl} - \hat{K}_c^k \hat{K}_d^l\right)\delta h_{kl}\right], \tag{5.10}$$

and then (5.6) is rearranged to

$$\delta S = \frac{1}{16\pi G}\int_{\partial\mathcal{M}}\sqrt{-h}\left[\left(\pi^{ab} - \hat{\pi}^{ab} - \hat{K}^{ab} + 2\tilde{L}^{cd}\left(\hat{K}_{cd}\hat{K}^{ab} - \hat{K}_c^a \hat{K}_d^b\right)\right)\delta h_{ab} + 2\tilde{L}^{ab}\delta\mathcal{R}_{ab}\right] \tag{5.11}$$

where $\hat{\pi}^{ab} = \hat{K}^{ab} - h^{ab}\hat{K}$, and $\tilde{L}^{ab}$ indicates

$$L_{cd}{}^{ab} = h^{ab}\hat{K}_{cd} + \delta_c^a\delta_d^b\hat{K} - \delta_c^a\hat{K}_d^b - \delta_c^b\hat{K}_d^a, \tag{5.12}$$
$$\tilde{L}^{ab} = h^{cd}(L^{-1})_{cd}{}^{ab}. \tag{5.13}$$

Using the fact that

$$\delta R_{ab} = -\frac{1}{2}h^{kl}D_a D_b \delta h_{kl} - \frac{1}{2}h^{kl}D_k D_l \delta h_{ab} + h^{kl}D_k D_{(a}\delta h_{b)l} \tag{5.14}$$

and doing integration by parts, (5.11) becomes

$$\delta S = \frac{1}{16\pi G}\int_{\partial\mathcal{M}}\sqrt{-h}\left[\pi^{ab} - \hat{\pi}^{ab} - \hat{K}^{ab} + 2\tilde{L}^{cd}\left(\hat{K}_{cd}\hat{K}^{ab} - \hat{K}_c^a \hat{K}_d^b\right)\right.$$
$$\left.-\mathcal{D}^2\tilde{L}^{ab} - h^{ab}\mathcal{D}_k\mathcal{D}_l\tilde{L}^{kl} + \mathcal{D}_k\left(\mathcal{D}^a\tilde{L}^{kb} + \mathcal{D}^b\tilde{L}^{ka}\right)\right]\delta h_{ab}. \tag{5.15}$$

where $\mathcal{D}_a$ is a covariant derivative compatible with h_{ab} defined on an $n+2$ dimensional hypersurface. If we define Δ^{ab} as

$$\Delta^{ab} = \hat{K}^{ab} - 2\tilde{L}^{cd}\left(\hat{K}_{cd}\hat{K}^{ab} - \hat{K}_c^a \hat{K}_d^b\right) + \mathcal{D}^2\tilde{L}^{ab} + h^{ab}\mathcal{D}_k\mathcal{D}_l\tilde{L}^{kl} - \mathcal{D}_k\left(\mathcal{D}^a\tilde{L}^{kb} + \mathcal{D}^b\tilde{L}^{ka}\right), \tag{5.16}$$

(5.15) is written as

$$\delta S = \frac{1}{16\pi G}\int_{\partial\mathcal{M}}\sqrt{-h}\left(\pi^{ab} - \hat{\pi}^{ab} - \Delta^{ab}\right)\delta h_{ab} \tag{5.17}$$

37

and this form of the variation of the action yields the boundary stress tensor, which is defined as the functional derivative of the on-shell action with respect to h_{ab}, associated with MM-counterterm

$$T_{ab} := \frac{2}{\sqrt{-h}} \frac{\delta S}{\delta h^{ab}} = \frac{1}{8\pi G} \left(\pi_{ab} - \hat{\pi}_{ab} - \Delta_{ab} \right) \tag{5.18}$$

where only T_{ab}^π, which indicates the first two terms in the right side, is expected to yield conserved charges. The explicit form of Δ^{ab} will be obtained in section 5.4.

5.2.2 Asymptotic Flatness

Adopting an approach to defining asymptotic flatness similar to that in hyperbolic coordinates [13] [12], we define a spacetime $(\mathcal{M}, g)$ in cylindrical coordinates and confine ourselves to this spacetime throughout this chapter. Assuming that a static spacetime $(\mathcal{M}, g)$ is radially smooth of order m at spatial infinity in $(n + 3)$ dimensions, the components of the metric take the asymptotic form

$$g_{\mu\nu} = \eta_{\mu\nu} + \sum_{k=1}^{m} \frac{l_{\mu\nu}^{(k)}(\eta^A/r)}{r^{n+k-1}} + f_{\mu\nu}^{(m+1)}(r, \eta^A) \tag{5.19}$$

where $n \geq 1$, r is a radial coordinate, and η^A are angular coordinates associated with the metric $\mu_{AB}^{(0)}$ on the unit sphere S^{n+1}, and $l_{\mu\nu}^{(k)}$ is C^∞ in η^A/r and $f^{(k)} = \mathcal{O}(1/r^m)$. Defining functions $w^a(\eta^A)$ at $t = const.$ such that

$$\frac{x^a}{r} = w^a(\eta^A), \qquad dx^a = w^a dr + r w_{,A}^a d\eta^A, \tag{5.20}$$

(5.19) transforms into

$$\eta_{\mu\nu} dx^\mu dx^\nu = -dt^2 + dr^2 + r^2 \mu_{AB}^{(0)} d\eta^A d\eta^B,$$
$$\tilde{\gamma}^{(k)} = -l_{tt}^{(k)}, \quad \tilde{\alpha}^{(k)} = l_{ab}^{(k)} w^a w^b, \quad J_A^{(k)} = l_{ab}^{(k)} w^a w_{,A}^b, \quad \mu_{AB}^{(k)} = l_{ab}^{(k)} w_{,A}^a w_{,B}^b \tag{5.21}$$

in turn yielding the explicit form

$$ds^2 = -\left(1 + \sum_{k=1}^{m} \frac{\tilde{\gamma}^{(k)}(\eta^A)}{r^{n+k-1}} + \mathcal{O}\left(\frac{1}{r^{m+1}}\right) \right) dt^2 + \left(1 + \sum_{k=1}^{m} \frac{\tilde{\alpha}^{(k)}(\eta^A)}{r^{n+k-1}} + \mathcal{O}\left(\frac{1}{r^{m+1}}\right) \right) dr^2$$
$$+ 2\left(\sum_{k=1}^{m} \frac{J_A^{(k)}(\eta^A)}{r^{n+k-1}} + \mathcal{O}\left(\frac{1}{r^{m+1}}\right) \right) r dr d\eta^A + r^2 \left(\mu_{AB}^{(0)} + \sum_{k=1}^{m} \frac{\mu_{AB}^{(k)}(\eta^A)}{r^{n+k-1}} + \mathcal{O}\left(\frac{1}{r^{m+1}}\right) \right) d\eta^A d\eta^B \tag{5.22}$$

where $\tilde{\gamma}^{(k)}$, $\tilde{\alpha}^{(k)}$ are smooth functions, and $J_A^{(k)}$ are smooth vector fields, and $\mu_{AB}^{(1)}$, $\mu_{AB}^{(2)}$ are smooth tensor fields on S^{n+1}. The symbols $\mathcal{O}(r^{-(m+1)})$ refer to terms that fall-off at least as fast as $r^{-(m+1)}$ as one approaches spacelike infinity, i.e., $r \to +\infty$ with fixed η. Without loss of generality, we find it convenient to substitute

$$\left(1 + \sum_{k=1}^{m} \frac{\tilde{\alpha}^{(k)}}{r^{n+k-1}}\right) = \left(1 + \sum_{k=1}^{m} \frac{\alpha^{(k)}}{r^{n+k-1}}\right)^2 + \mathcal{O}\left(\frac{1}{r^{m+1}}\right) \tag{5.23}$$

in (5.22), and likewise for the g_{tt}-component ($\tilde{\gamma}$ changes to γ). In order to simplify the metric, we first try to remove $J_A^{(1)}$ in (5.22) by using a coordinate transformation

$$\eta^A = \bar{\eta}^A + \frac{1}{r^n}G^{(1)A}(\bar{\eta}^B), \qquad r = \bar{r}, \qquad t = t,$$

$$d\eta^A = d\bar{\eta}^A + \frac{1}{r^n}G_{,B}^{(1)A}d\bar{\eta}^B - \frac{n}{r^{n+1}}G^{(1)A}dr. \tag{5.24}$$

Applying (5.24) into (5.22), the leading term of the g_{rA}-component is eliminated by choosing

$$J_A^{(1)} = nG^{(1)B}\mu_{AB}^{(0)}, \tag{5.25}$$

and this allows us to set $J_A^{(1)} = 0$ in (5.22). Subsequently we get rid of $\alpha^{(2)}$ via the additional coordinate transformation :

$$r = \bar{r} + \frac{1}{\bar{r}^n}F^{(2)}(\eta^A),$$

$$dr = d\bar{r} - n\frac{1}{\bar{r}^{n+1}}F^{(2)}d\bar{r} + \frac{1}{\bar{r}^n}F_{,B}^{(2)}d\eta^B. \tag{5.26}$$

Plugging these into (5.22), the $1/\bar{r}^{n+1}$-term in $d\bar{r}^2$ can be set to zero via

$$\alpha^{(2)} = nF^{(2)} \tag{5.27}$$

where the leading term in $rdrd\eta^A$ is not affected. Generalizing these coordinate transformations to include higher orders of $1/r$ yields

$$\eta^A = \bar{\eta}^A + \frac{1}{\bar{r}^{n+k-1}}G^{(k)A}, \qquad r = \bar{r} + \frac{1}{\bar{r}^{n+k-1}}F^{(k+1)} \tag{5.28}$$

where these transformations are sequentially applied to the above to the metric. We can then show that

$$J_A^{(1)} = J_A^{(2)} = \cdots = J_A^{(m)} = 0,$$
$$\alpha^{(2)} = \alpha^{(3)} = \cdots = \alpha^{(m)} = 0. \tag{5.29}$$

39

We finally obtain the simplified form of the metric

$$ds^2 = \left(1 + \frac{\alpha}{r^n}\right)^2 dr^2 - \left(1 + \frac{\gamma^{(1)}}{r^n} + \frac{\gamma^{(2)}}{r^{n+1}} + \mathcal{O}\left(\frac{1}{r^{n+2}}\right)\right)^2 dt^2$$
$$+ r^2 \left(\mu_{AB}^{(0)} + \frac{1}{r^n}\mu_{AB}^{(1)} + \frac{1}{r^{n+1}}\mu_{AB}^{(2)} + \mathcal{O}\left(\frac{1}{r^{n+2}}\right)\right) d\eta^A d\eta^B,$$

which we rewrite as

$$ds^2 = N^2 dr^2 + h_{ab} dx^a dx^b$$
$$= \left(1 + \frac{\alpha}{r^n}\right)^2 dr^2 + \left(h_{ab}^{(0)} + \frac{1}{r^n}h_{ab}^{(1)} + \frac{1}{r^{n+1}}h_{ab}^{(2)} + \cdots\right) dx^a dx^b \qquad (5.30)$$

where $x^a = (t, \eta^A)$ are coordinates on the $(n+2)$-dimensional hypersurface compatible with the metric h_{ab}, whose expansion is

$$h_{ab}dx^a dx^b = -\left(1 + \frac{\gamma^{(1)}}{r^n} + \frac{\gamma^{(2)}}{r^{n+1}} + \mathcal{O}\left(\frac{1}{r^{n+2}}\right)\right)^2 dt^2$$
$$+ r^2 \left(\mu_{AB}^{(0)} + \frac{1}{r^n}\mu_{AB}^{(1)} + \frac{1}{r^{n+1}}\mu_{AB}^{(2)} + \mathcal{O}\left(\frac{1}{r^{n+2}}\right)\right) d\eta^A d\eta^B \qquad (5.31)$$

where $a = t, A$.

The boundary spacetime $(\partial\mathcal{M}, h)$ is actually a one-parameter family $(\mathcal{M}_\Omega, g_\Omega)$ where $\mathcal{M}_\Omega \subset \mathcal{M}$ and $\mathcal{M}_\Omega$ converges to $\mathcal{M}$ with increasing Ω. The boundary of a region $(\mathcal{M}_\Omega, g_\Omega)$ for a certain value of Ω is described by $(\partial\mathcal{M}_\Omega, h_\Omega)$. As Ω is varied, we get a family of boundaries that provide a specific way of 'cutting-off' the space-time $\mathcal{M}$, with the asymptotic boundary obtained as $\Omega \to \infty$. In this chapter, our interest is in the class "cylindrical cut-offs", for which

$$\Omega^{cyl} = r + O(r^0). \qquad (5.32)$$

Note that the metric (5.30) takes the same form as the metric in hyperbolic coordinates [64] except that h_{ab} is further decomposed into a tt-component and angular components. Naively one might expect that our result is easily derived from the hyperbolic case in ref. [64] where Ω is taken to be

$$\Omega^{hyp} = \rho + O(\rho^0). \qquad (5.33)$$

and the coordinate ρ is defined by $\rho^2 = r^2 - t^2$. However this is not true since in hyperbolic coordinates the boundary metric (parametrized by a surface ρ=constant) is manifestly covariant under a variation, whereas in cylindrical coordinates the boundary metric defined

at $r =$constant does not change fully covariantly. In particular, the tt-component and angular components in the induced metric h_{ab} have expansions in different orders of r. For example, taking a variation with respect to each surface parameter, i.e. ρ or r, in hyperbolic coordinates

$$\frac{\partial}{\partial \rho}\left(\rho h_{ab}^{(0)}\right) = h_{ab}^{(0)}, \tag{5.34}$$

whereas in cylindrical coordinates

$$\frac{\partial}{\partial r}\left(r h_{ab}^{(0)}\right) = h_{ab}^{(0)} + 2r^2 \mu_{ab}^{(0)}. \tag{5.35}$$

In (5.35) only the angular components transform covariantly in the $(n+1)$ dimensional subspace, whereas in (5.34), all components transform covariantly. This distinction introduces new features and subtleties in cylindrical coordinate that are rather more complicated than the hyperbolic case.

5.3   The MM-Counterterm Solution

Here we find the MM-counterterm solution $\hat{K}_{ab}$ in (5.1) by solving the decomposed Einstein equations.

5.3.1   Solving Decomposed Einstein Equations

We start by setting up the spacelike normal vector n^α on a cylindrical hypersurface $r =$constant, where asymptotically $r \to \infty$, and calculate its extrinsic curvature K_{ab}. At the boundary the decomposed Einstein equations are

$$\begin{align}
\perp (R_{ab}) &= \mathcal{R}_{ab} + \mathcal{D}_a a_b - a_a a_b - \pounds_n K_{ab} - K K_{ab} + 2K_a^c K_{cb}, \tag{5.36} \\
\perp (R_{ac} n^c) &= \mathcal{D}^b K_{ab} - \mathcal{D}_a K = -\mathcal{D}^b \pi_{ab}, \tag{5.37} \\
R_{ab} n^a n^b &= -\pounds_n K - K^{ab} K_{ab} + (\mathcal{D}_b a^b - a^b a_b), \tag{5.38}
\end{align}$$

where a^b and K_{ab} are defined by

$$a^b = n^a \nabla_a n^b, \quad K_{ab} = \nabla_a n_b - n_a a_b, \tag{5.39}$$

and the last equation can be rewritten as

$$\mathcal{R} - K^2 + K^{ab} K_{ab} = 0. \tag{5.40}$$

For asymptotically flat spacetimes, the left-hand sides of (5.36) − (5.38) become zero as $r \to \infty$. Equation (5.36) yields $\mathcal{R}_{ab}$. The remaining equations yield constraint conditions between the coefficients in the metric, e.g. α, $\gamma^{(1)}$ or $\gamma^{(2)}$. We solve the decomposed Einstein equation in powers of $1/r$, i.e. $\mathcal{R}_{ab} = \mathcal{R}^{(0)}_{ab} + \frac{1}{r^n}\mathcal{R}^{(1)}_{ab} + \frac{1}{r^{n+1}}\mathcal{R}^{(2)}_{ab} + \cdots$, where for $n = 1$ the sub-sub-leading term must be separately dealt with from the $n \geq 2$ cases. This is because when $n = 1$ the product of two sub-leading terms has the same order as the sub-sub-leading term (both of order of $1/r^2$), whereas for $n \geq 2$ this product is of order of $1/r^{2n}$ and falls off faster than the sub-sub-leading term (of order $1/r^{n+1}$) and so does not contribute at that order.

The $n \geq 2$ Case

In the asymptotically flat spacetime, which is described by the metric (5.30), the extrinsic curvature is

$$K_{ab} = r\mu^{(0)}_{ab} + \frac{1}{r^{n-1}}\left(\mu^{(1)}_{ab} - \alpha\mu^{(0)}_{ab} - \frac{n}{2r^2}h^{(1)}_{ab}\right) + \frac{1}{r^n}\left(\mu^{(2)}_{ab} - \frac{(n+1)}{2r^2}h^{(2)}_{ab}\right) + \mathcal{O}\left(\frac{1}{r^{n+3}}\right), \quad (5.41)$$

and taking the trace of it yields

$$K = \frac{(n+1)}{r} - \frac{1}{r^{n+1}}\left(\alpha(n+1) + \frac{n}{2}h^{(1)}\right) - \frac{1}{r^{n+2}}\frac{(n+1)}{2}h^{(2)} + \mathcal{O}\left(\frac{1}{r^{n+3}}\right) \quad (5.42)$$

where $K = K_{ab}h^{ab}$ and $h^{(m)} = h^{(m)}_{ab}h^{(0)ab}$ for $m = 1, 2$. The acceleration becomes

$$a_a = \left(0, -\frac{1}{r^n}D_a\alpha\right). \quad (5.43)$$

The first decomposed Einstein equation (5.36) is

$$0 = \mathcal{R}^{(0)}_{ab} - n\mu^{(0)}_{ab} + \frac{1}{r^n}\left[\mathcal{R}^{(1)}_{ab} - \left(n\mu^{(1)}_{ab} - n\alpha\mu^{(0)}_{ab} - \frac{n}{2}h^{(1)}\mu^{(0)}_{ab} + D_aD_b\alpha\right)\right]$$
$$+ \frac{1}{r^{n+1}}\left[\mathcal{R}^{(2)}_{ab} - \left(n\mu^{(2)}_{ab} - \frac{(n+1)}{2}h^{(2)}\mu^{(0)}_{ab} + \frac{(n+1)}{2r^2}h^{(2)}_{ab}\right)\right] + \mathcal{O}\left(\frac{1}{r^{n+3}}\right), \quad (5.44)$$

the second one (5.37) takes the form

$$0 = \frac{1}{r^{n+1}}\left[D_a\gamma^{(1)} + nD_a\alpha - \frac{n}{2}\left(D^bh^{(1)}_{ab} - D_ah^{(1)}\right)\right]$$
$$+ \frac{1}{r^{n+2}}\left[D_a\gamma^{(2)} - \frac{(n+1)}{2}\left(D^bh^{(2)}_{ab} - D_ah^{(2)}\right)\right] + \mathcal{O}\left(\frac{1}{r^{n+3}}\right), \quad (5.45)$$

42

and the last (5.38) gives

$$0 = \mathcal{R}^{(0)} - \frac{n(n+1)}{r^2} + \frac{1}{r^n}\left[\mathcal{R}^{(1)} - \left(-\frac{2n(n+1)}{r^2}\alpha - \frac{n(n+1)}{r^2}h^{(1)} + \frac{2n}{r^2}\mu^{(1)}\right)\right]$$

$$+ \frac{1}{r^{n+1}}\left[\mathcal{R}^{(2)} - \left(\frac{(2n+1)}{r^2}\mu^{(2)} - \frac{(n+1)^2}{r^2}h^{(2)}\right)\right] + \mathcal{O}\left(\frac{1}{r^{n+3}}\right). \tag{5.46}$$

Note that the asymptotic expansion of $\mathcal{R}_{ab}^{(m)}$ is defined as

$$\mathcal{R}_{ab}^{(m)} = \frac{1}{2}\left(D^c D_a h_{cb}^{(m)} + D^c D_b h_{ac}^{(m)} - D^c D_c h_{ab}^{(m)} - D_a D_b h^{(m)}\right) \tag{5.47}$$

where $m = 1, 2$, and $\mathcal{R}^{(m)}$ is the trace of (5.47)

$$\mathcal{R}^{(m)} = h^{(0)ab}\mathcal{R}_{ab}^{(m)}. \tag{5.48}$$

As the solutions to the decomposed Einstein equations have to be consistent with each other, we first compare the $\mathcal{R}$'s, one from contracting $\mathcal{R}_{ab}$ in (5.44) with $h^{(0)ab}$ and the other from (5.46). We get

$$\mathcal{R}^{(1)} = 2D^2\alpha = \frac{2n}{r^2}\mu^{(1)} - \frac{2n(n+1)}{r^2}\alpha - \frac{n(n+1)}{r^2}h^{(1)}, \tag{5.49}$$

$$\mathcal{R}^{(2)} = \frac{n}{2r^2}h^{(2)} = \frac{n}{(n+2)r^2}\mu^{(2)} = -\frac{2}{r^2}\gamma^{(2)}. \tag{5.50}$$

Now, taking the covariant derivative D^a of (5.45) yields an expression for the Ricci scalar via (5.47) − (5.48); this Ricci scalar agrees with (5.49) − (5.50) provided

$$D^2\gamma^{(1)} = 0, \tag{5.51}$$

$$D^2\gamma^{(2)} = -\frac{(n+1)}{r^2}\gamma^{(2)}, \quad D^2\mu^{(2)} = -\frac{(n+1)}{r^2}\mu^{(2)}, \quad D^2h^{(2)} = -\frac{(n+1)}{r^2}h^{(2)}. \tag{5.52}$$

The $n = 1$ Case

As mentioned, the $n = 1$ case needs to be separately dealt with from the case with general n, because the sub-sub-leading order is expressed not only by the sub-sub-leading order quantities, but also by a combination of the sub-leading order values.

43

Setting $n = 1$ in the metric (5.30), the extrinsic curvature at the boundary of the spacetime is

$$K_{ab} = r\mu_{ab}^{(0)} + \left(\mu_{ab}^{(1)} - \alpha\mu_{ab}^{(0)} - \frac{1}{2r^2}h_{ab}^{(1)}\right) + \frac{1}{r}\left(\mu_{ab}^{(2)} - \alpha\mu_{ab}^{(1)} + \frac{\alpha}{2r^2}h_{ab}^{(1)} - \frac{1}{r^2}h_{ab}^{(2)}\right) + \mathcal{O}\left(\frac{1}{r^2}\right), \quad (5.53)$$

and its trace is

$$K = \frac{2}{r} - \frac{1}{r^2}\left(2\alpha + \frac{1}{2}h^{(1)}\right) + \frac{1}{r^3}\left(-h^{(2)} + \frac{\alpha}{2}h^{(1)} + \frac{1}{2}h_{ab}^{(1)}h^{(1)ab}\right) + \mathcal{O}\left(\frac{1}{r^4}\right). \quad (5.54)$$

The acceleration a_a becomes

$$a_a = \left(0, -\frac{1}{r}D_a\alpha + \frac{1}{r^2}\alpha D_a\alpha\right). \quad (5.55)$$

Solving the decomposed Einstein equations as the previous section, (5.36) yields

$$\begin{aligned}
0 =& \mathcal{R}_{ab}^{(0)} - \mu_{ab}^{(0)} + \frac{1}{r}\left[\mathcal{R}_{ab}^{(1)} - \left(\mu_{ab}^{(1)} - \alpha\mu_{ab}^{(0)} - \frac{1}{2}h^{(1)}\mu_{ab}^{(0)} + D_aD_b\alpha\right)\right] \\
&+ \frac{1}{r^2}\left[\mathcal{R}_{ab}^{(2)} - \left(\mu_{ab}^{(2)} + \frac{1}{r^2}h_{ab}^{(2)} - h^{(2)}\mu_{ab}^{(0)} - \alpha\mu_{ab}^{(1)} - \frac{\alpha}{r^2}h_{ab}^{(1)} + \alpha h^{(1)}\mu_{ab}^{(0)}\right.\right. \\
&\left.\left. - \frac{1}{2}h^{(1)}\mu_{ab}^{(1)} + \frac{1}{4r^2}h^{(1)}h_{ab}^{(1)} + \frac{1}{2}h_{cd}^{(1)}h^{(1)cd}\mu_{ab}^{(0)} - \frac{1}{2r^2}h_a^{(1)e}h_{eb}^{(1)} - \alpha D_aD_b\alpha\right.\right. \\
&\left.\left. - \frac{1}{2}(D_a h_{bd}^{(1)} + D_b h_{ad}^{(1)} - D_d h_{ab}^{(1)})D^d\alpha\right)\right] + \mathcal{O}\left(\frac{1}{r^3}\right),
\end{aligned} \quad (5.56)$$

(5.37) takes the form

$$\begin{aligned}
0 =& \frac{1}{r^2}\left[D_a\gamma^{(1)} + D_a\alpha - \frac{1}{2}\left(D^b h_{ab}^{(1)} - D_a h^{(1)}\right)\right] + \frac{1}{r^3}\left[\left(D_a\gamma^{(2)} + \frac{\alpha}{2}(D^b h_{ab}^{(1)} - D_a h^{(1)})\right.\right. \\
&+ \frac{1}{2}h_a^{(1)c}D_c\alpha - \frac{1}{2}h^{(1)}D_a\alpha - \alpha D_a\gamma^{(1)} - 2\gamma^{(1)}D_a\gamma^{(1)} - \frac{3}{4}h^{(1)cd}D_a h_{cd}^{(1)} + \frac{1}{2}h_{ea}^{(1)}D_b h^{(1)be} \\
&\left.\left. + \frac{1}{2}h^{(1)bc}D_c h_{ab}^{(1)} - \frac{1}{4}h_{ea}^{(1)}D^e h^{(1)}\right) - \left(D^b h_{ab}^{(2)} - D_a h^{(2)}\right)\right] + \mathcal{O}\left(\frac{1}{r^4}\right),
\end{aligned} \quad (5.57)$$

and (5.38) is

$$\begin{aligned}
0 =& \mathcal{R}^{(0)} - \frac{2}{r^2} + \frac{1}{r}\left[\mathcal{R}^{(1)} - \frac{1}{r^2}\left(-4\alpha - 2h^{(1)} + 2\mu^{(1)}\right)\right] \\
&+ \frac{1}{r^2}\left[\mathcal{R}^{(2)} - \frac{1}{r^2}\left(3\mu^{(2)} - 4h^{(2)} - 3\alpha\mu^{(1)} + 4\alpha h^{(1)} + 2\alpha^2 - \frac{1}{2}h^{(1)}\mu^{(1)}\right.\right. \\
&\left.\left. + \frac{1}{4}(h^{(1)})^2 + \frac{7}{4}h_{ab}^{(1)}h^{(1)ab} - r^2\mu_{ab}^{(1)}h^{(1)ab} + r^2 h^{(1)ab}D_a D_b\alpha\right)\right] + \mathcal{O}\left(\frac{1}{r^4}\right).
\end{aligned} \quad (5.58)$$

44

For the sub-leading order, we have the same consistency conditions (5.49) and (5.51) with $n = 1$ from (5.56) $-$ (5.58); specifically (5.49) is

$$\mathcal{R}^{(2)} = 2D^2\alpha = -\frac{4}{r^2}\alpha - \frac{4}{r^2}\gamma^{(1)}, \tag{5.59}$$

and from this, we can infer that

$$D_a D_b \alpha = -\alpha\mu_{ab}^{(0)} - \gamma^{(1)}\mu_{ab}^{(0)} \tag{5.60}$$

which is useful later in calculating Δ^{ab}. In addition, we have

$$\mu_{ab}^{(1)} = -2\alpha\mu_{ab}^{(0)}, \quad D_a\gamma^{(1)} = 0, \tag{5.61}$$

by disposing of the supertranslation which requires the magnetic part of the four dimensional Weyl tensor to be zero

$$k_{ab} = h_{ab}^{(1)} + 2\alpha r^2\mu_{ab}^{(0)} - 2\gamma^{(1)}u_a^{(0)}u_b^{(0)}, \tag{5.62}$$

$$t_{ab} = \epsilon_a{}^{cd}D_c k_{bd} = 0. \tag{5.63}$$

Applying (5.49) and (5.61) to the sub-sub-leading order of (5.56) $-$ (5.58), we obtain

$$-\frac{1}{r^2}\mu^{(2)} - \frac{6}{r^2}\gamma^{(2)} + \frac{2}{r^2}\alpha^2 + \frac{8}{r^2}\alpha\gamma^{(1)} + \frac{2}{r^2}(\gamma^{(1)})^2 = 0, \tag{5.64}$$

$$-\frac{1}{r^2}\mu^{(2)} - \frac{8}{r^2}\gamma^{(2)} + \frac{6}{r^2}\alpha\gamma^{(1)} + \frac{2}{r^2}(\gamma^{(1)})^2 - D^2\gamma^{(2)} + 2D_a\alpha D^a\alpha = 0, \tag{5.65}$$

$$D^2\gamma^{(2)} + \frac{2}{r^2}\gamma^{(2)} + \frac{2}{r^2}\alpha\gamma^{(1)} + \frac{2}{r^2}\alpha^2 - 2D_a\alpha D^a\alpha = 0. \tag{5.66}$$

5.3.2 Solving the MM-relation

For convenience, redefining $\hat{K}_{ab}$ in terms of $\hat{Q}_{ab}$

$$\hat{K}_{ab} = r\hat{Q}_{ab} = r\hat{Q}_{ab}^{(0)} + \frac{1}{r^{n-1}}\hat{Q}_{ab}^{(1)} + \frac{1}{r^n}\hat{Q}_{ab}^{(2)} + \cdots, \tag{5.67}$$

the relation (5.1) is rewritten as

$$r^2(\hat{Q}_{ab}\hat{Q} - h^{cd}\hat{Q}_{ac}\hat{Q}_{bc}) = \mathcal{R}_{ab}. \tag{5.68}$$

45

and this is expanded as

$$\mathcal{R}_{ab}^{(0)} = n\mu_{ab}^{(0)}, \tag{5.69}$$

$$\mathcal{R}_{ab}^{(1)} = r^2\hat{Q}^{(1)}\mu_{ab}^{(0)} + (n-1)\hat{Q}_{ab}^{(1)} - 2u_a^{(0)}u^{(0)c}\hat{Q}_{cb}^{(1)} - \mu^{(1)}\mu_{ab}^{(0)} + \mu_{ab}^{(1)}, \tag{5.70}$$

$$(n \geq 2), \quad \mathcal{R}_{ab}^{(2)} = r^2\hat{Q}^{(2)}\mu_{ab}^{(0)} + (n-1)\hat{Q}_{ab}^{(2)} - 2u_a^{(0)}u^{(0)c}\hat{Q}_{cb}^{(2)} - \mu^{(2)}\mu_{ab}^{(0)} + \mu_{ab}^{(2)}, \tag{5.71}$$

$$(n = 1), \quad \mathcal{R}_{ab}^{(2)} = r^2\hat{Q}^{(2)}\mu_{ab}^{(0)} - \mu^{(2)}\mu_{ab}^{(0)} + \mu_{ab}^{(2)} - 2u_a^{(0)}u^{(0)c}\hat{Q}_{bc}^{(2)} + \frac{r^2}{4}\mathcal{R}^{(1)}\mathcal{R}_{ab}^{(1)}$$

$$+ \frac{r^2}{4}\mathcal{R}^{(1)}\mu_{ab}^{(1)} - \frac{1}{4}\mu^{(1)}\mathcal{R}_{ab}^{(1)} - \frac{r^2}{2}\mathcal{R}_{cd}^{(1)}h^{(1)cd}\mu_{ab}^{(0)} - \frac{r^2}{4}\mathcal{R}_{\ a}^{(1)c}\mathcal{R}_{cb}^{(1)}$$

$$+ \frac{1}{4}\mathcal{R}_{ae}^{(1)}\mu_{\ b}^{(1)e} + \frac{1}{4}\mu_{\ a}^{(1)e}\mathcal{R}_{eb}^{(1)} - \frac{1}{4}\mu^{(1)}\mu_{ab}^{(1)} + \frac{1}{2}\mu_{cd}^{(1)}\mu^{(1)cd}\mu_{ab}^{(0)} - \frac{1}{4}\mu_{\ a}^{(1)c}\mu_{cb}^{(1)} \tag{5.72}$$

where the sub-sub-leading order is separately treated as noted above, and $\hat{Q}^{(i)}$ is the trace of $\hat{Q}_{ab}^{(i)}$.

The $n \geq 2$ Case

In order to solve the MM-relation, we need to solve (5.69) − (5.71) for $\hat{Q}_{ab}$. For $n \geq 2$, $\hat{Q}_{ab}$ is uniquely determined as follows

$$\hat{Q}_{ab}^{(0)} = \mu_{ab}^{(0)}, \tag{5.73}$$

$$\hat{Q}_{ab}^{(1)} = \frac{1}{(n-1)}\left[\mathcal{R}_{ab}^{(1)} - \frac{r^2}{2n}\mathcal{R}^{(1)}\mu_{ab}^{(0)} - \frac{r^2}{n(n+1)}\mathcal{R}_{cd}^{(1)}u^{(0)c}u^{(0)d}\mu_{ab}^{(0)}\right.$$

$$\left. + \frac{2}{(n+1)}u_a^{(0)}u^{(0)c}\mathcal{R}_{cb}^{(1)} + \frac{1}{2}\mu^{(1)}\mu_{ab}^{(0)} - \mu_{ab}^{(1)}\right], \tag{5.74}$$

$$\hat{Q}_{ab}^{(2)} = \frac{1}{(n-1)}\left[\mathcal{R}_{ab}^{(2)} - \frac{r^2}{2n}\mathcal{R}^{(2)}\mu_{ab}^{(0)} - \frac{r^2}{n(n+1)}\mathcal{R}_{cd}^{(2)}u^{(0)c}u^{(0)d}\mu_{ab}^{(0)}\right.$$

$$\left. + \frac{2}{(n+1)}u_a^{(0)}u^{(0)c}\mathcal{R}_{cb}^{(2)} + \frac{1}{2}\mu^{(2)}\mu_{ab}^{(0)} - \mu_{ab}^{(2)}\right] \tag{5.75}$$

where u_a is the timelike normal vector and μ_{ab} is the pull-back metric of μ_{AB} for $A, B = \theta_1, ..., \theta_{n+1}$ on $(n+1)$-dimensional spacelike hypersurface, and $\hat{Q}_{ab}^{(m)}$, $\mathcal{R}_{ab}^{(m)}$, $u_a^{(m)}$ or $\mu_{ab}^{(m)}$ for $m = 0, 1$, and 2 are lowered and raised by $h_{ab}^{(0)}$. As $\mathcal{R}_{ab}^{(1)}$ is constructed in terms of the pull-back metric components $\mu_{ab}^{(0)}$ and $\mu_{ab}^{(1)}$, the first sub-leading order $\hat{Q}_{ab}^{(1)}$ has just angular components, since α is independent of time, t. Since $\mathcal{R}_{ab}^{(2)}$ has tt and angular components,

$\hat{Q}_{ab}^{(2)}$ also is expressed by tt and angular components. Plugging (5.44) and (5.45) into (5.74) and (5.75), we finally obtain

$$\hat{Q}_{ab}^{(0)} = \mu_{ab}^{(0)}, \tag{5.76}$$

$$\hat{Q}_{ab}^{(1)} = \frac{1}{(n-1)}\left[(n-1)\mu_{ab}^{(1)} + \alpha\mu_{ab}^{(0)} + \gamma^{(1)}\mu_{ab}^{(0)} + D_a D_b \alpha\right], \tag{5.77}$$

$$\hat{Q}_{ab}^{(2)} = \frac{1}{(n-1)}\left[\frac{(n-1)}{2r^2}h_{ab}^{(2)} + \frac{(n+2)}{n}\gamma^{(2)}\mu_{ab}^{(0)} + n\mu_{ab}^{(2)}\right]. \tag{5.78}$$

The $n = 1$ Case

As seen in (5.70) and (5.72), when $n = 1$, $\hat{Q}_{ab}$ does not show up in the MM-relation and so is not directly obtainable. However we can still derive the trace, $\hat{Q}^{(i)}$, which is

$$\hat{Q}^{(1)} = \frac{1}{2}\mathcal{R}^{(1)} + \frac{1}{2r^2}\mu^{(1)}, \tag{5.79}$$

$$\hat{Q}^{(2)} = \frac{1}{2}\mathcal{R}^{(2)} + \frac{1}{2}\mathcal{R}_{cd}^{(2)}u^{(0)c}u^{(0)d} + \frac{1}{2r^2}\mu^{(2)} - \frac{r^2}{8}(\mathcal{R}^{(1)})^2 + \frac{1}{2}\mathcal{R}_{cd}^{(1)}h^{(1)cd}$$
$$+ \frac{r^2}{8}\mathcal{R}^{(1)cd}\mathcal{R}_{cd}^{(1)} - \frac{1}{r^2}\mu^{(1)cd}\mathcal{R}_{cd}^{(1)} + \frac{1}{8r^2}(\mu^{(1)})^2 - \frac{3}{8r^2}\mu_{cd}^{(1)}\mu^{(1)cd}, \tag{5.80}$$

where $\hat{Q}^{(i)} = \hat{Q}_{ab}^{(i)}h^{(0)ab}$ for $i = 1, 2$, and the contracted with the timelike normal vectors, $\hat{Q}_{ab}^{(i)}u^{(0)a}u^{(0)b}$, which is

$$\hat{Q}_{tt}^{(1)} = 0, \tag{5.81}$$

$$\hat{Q}_{tt}^{(2)} = \frac{1}{2}\mathcal{R}_{tt}^{(2)} = -\frac{1}{r^2}\gamma^{(2)} + \frac{2}{r^2}\alpha\gamma^{(1)}. \tag{5.82}$$

From these values, we can determine $\hat{Q}_{ab}^{(i)}$ up to certain ambiguities, and the forms of $\hat{Q}_{ab}^{(1)}$ can be inferred as follows

$$\hat{Q}_{ab}^{(1)} = \beta_1\mathcal{R}_{ab}^{(1)} + r^2\beta_2\mathcal{R}^{(1)}\mu_{ab}^{(0)} + \lambda_1\mu_{ab}^{(1)} + \lambda_2\mu^{(1)}\mu_{ab}^{(0)}, \tag{5.83}$$

where β_1, β_2, λ_1 and λ_2 are constants that arise from the ambiguities. They are not fixed from (5.79) and (5.81), but are restricted to obey $\beta_1 + 2\beta_2 = \frac{1}{2}$, and $\lambda_1 + 2\lambda_2 = \frac{1}{2}$. Applying

47

(5.60) and (5.61) into (5.83), we have

$$
\begin{aligned}
\hat{Q}_{ab}^{(1)} &= \beta_1(-\alpha\mu_{ab}^{(0)} - \gamma^{(1)}\mu_{ab}^{(0)} + D_a D_b \alpha) + 2\beta_2(-2\alpha - 2\gamma^{(1)})\mu_{ab}^{(0)} - 2\alpha\lambda_1\mu_{ab}^{(0)} - 4\alpha\lambda_2\mu_{ab}^{(0)}, \\
&= \beta_1(-2\alpha - 2\gamma^{(1)})\mu_{ab}^{(0)} + 2\beta_2(-2\alpha - 2\gamma^{(1)})\mu_{ab}^{(0)} - 2\alpha(\lambda_1 + 2\lambda_2)\mu_{ab}^{(0)}, \\
&= (\beta_1 + 2\beta_2)(-2\alpha - 2\gamma^{(1)})\mu_{ab}^{(0)} - 2\alpha(\lambda_1 + 2\lambda_2)\mu_{ab}^{(0)}, \\
&= -2\alpha\mu_{ab}^{(0)} - \gamma^{(1)}\mu_{ab}^{(0)}.
\end{aligned}
\tag{5.84}
$$

As shown the above, regardless of the ambiguities we obtain a unique expression for $\hat{Q}_{ab}^{(1)}$. Arbitrarily fixing the values $\beta_1 = \frac{1}{2}$, $\beta_2 = 0$, $\lambda_1 = \frac{1}{2}$ and $\lambda_2 = 0$, we can equivalently express (5.84) as

$$
\hat{Q}_{ab}^{(1)} = \frac{1}{2}\mu_{ab}^{(1)} + D_a D_b \alpha.
\tag{5.85}
$$

For the sub-sub-leading term, we guess a general form of $\hat{Q}_{ab}^{(2)}$ from (5.80) and (5.82)

$$
\begin{aligned}
\hat{Q}_{ab}^{(2)} =& \kappa_1 \mathcal{R}_{ab}^{(2)} + r^2 \kappa_2 \mathcal{R}^{(2)}\mu_{ab}^{(0)} + \kappa_3 \mathcal{R}_{cd}^{(2)} u^{(0)c} u^{(0)d} u_a^{(0)} u_b^{(0)} + r^2 \kappa_4 \mathcal{R}_{cd}^{(2)} u^{(0)c} u^{(0)d} \mu_{ab}^{(0)} \\
& + \chi_1 \, \mu_{ab}^{(2)} + \chi_2 \, \mu^{(0)}\mu_{ab}^{(0)} - \frac{r^2}{8}\mathcal{R}^{(1)}\mathcal{R}_{ab}^{(1)} + \frac{r^2}{8}\mathcal{R}_{ac}^{(1)}\mathcal{R}^{(1)c}_{\ \ b} - \frac{1}{2}\mathcal{R}_{ac}^{(1)}\mu^{(1)c}_{\ \ b} \\
& + \frac{1}{8}\mu^{(1)}\mu_{ab}^{(1)} - \frac{3}{8}\mu_{ac}^{(1)}\mu^{(1)c}_{\ \ b}.
\end{aligned}
\tag{5.86}
$$

where κ_i for $i = 1, .., 4$ and χ_j for $j = 1, 2$ are additional ambiguities, related by the equations

$$
\kappa_1 + 2\kappa_2 = \frac{1}{2}, \quad -\kappa_3 + 2\kappa_4 = \frac{1}{2}, \quad \kappa_1 + \kappa_3 = \frac{1}{2}, \quad \chi_1 + 2\chi_2 = \frac{1}{2}.
\tag{5.87}
$$

As we have seen, ambiguities in the multiplication of the first order terms are nullified due to (5.60) and (5.61). Expanding (5.86) we obtain

$$
\hat{Q}_{ab}^{(2)} = \lambda_3 \mu_{ab}^{(2)} + \lambda_4 \mu^{(2)}\mu_{ab}^{(0)} - \frac{3}{2}\gamma^{(2)}\mu_{ab}^{(0)} - \frac{1}{r^2}\gamma^{(2)}u_a^{(0)}u_b^{(0)} - \frac{5}{2}\alpha^2\mu_{ab}^{(0)} + \frac{2}{r^2}\alpha\gamma^{(1)}u_a^{(0)}u_b^{(0)}
\tag{5.88}
$$

where we have redefined $\lambda_3 = 2\kappa_1 + \chi_1$ and $\lambda_4 = \chi_2 - \kappa_1$. The ambiguities λ_3 and λ_4 will be fixed at the end of the calculation of $[\Delta^{ab}]^{(2)}$ so that $[\Delta^{ab}]^{(2)}$ does not contribute to the conserved quantities; it turns out $\lambda_3 = -\frac{1}{2}$ and $\lambda_4 = \frac{1}{2}$. Our solution for $\hat{Q}_{ab}^{(2)}$ then becomes

$$
\hat{Q}_{ab}^{(2)} = -\frac{1}{2}\mu_{ab}^{(2)} + \frac{1}{2}\mu^{(2)}\mu_{ab}^{(0)} - \frac{3}{2}\gamma^{(2)}\mu^{(0)ab} - \frac{1}{r^2}\gamma^{(2)}u_a^{(0)}u_b^{(0)} - \frac{5}{2}\alpha^2\mu_{ab}^{(0)} + \frac{2}{r^2}\alpha\gamma^{(1)}u^{(0)a}u^{(0)b}.
\tag{5.89}
$$

5.4 Explicit Form of Δ_{ab}

With the definition of asymptotic flatness in (5.30), we investigate Δ^{ab} by finding its definite form with the solution of the MM-counterterm. Note that Δ^{ab} is a remnant term, obtained from subtracting $\hat{\pi}^{ab}$ from the variation of the MM-counterterm in the action, and so is totally expressed by the MM-counterterm solution $\hat{K}^{ab}$ and its covariant derivatives. Consequently, we shall see that Δ^{ab} does not vanish entirely. We next consider the role that the non-vanishing Δ^{ab} plays with respect to conserved quantities.

5.4.1 Calculation of $\tilde{L}^{(0)ab}$

$L_{ab}{}^{cd}$ is defined in (5.8) and is a shorthand expression for convenience to deal with terms constituted of $\hat{K}_{ab}$'s. Our interest is to get $\tilde{L}^{ab}$ which is defined in (5.13). First we expand $L_{mn}{}^{cd}$ and $(L^{-1})_{ab}{}^{mn}$ in powers of r

$$L_{mn}{}^{cd} = L^{(0)}{}_{mn}{}^{cd} + \frac{1}{r^n}L^{(1)}{}_{mn}{}^{cd} + \frac{1}{r^{n+1}}L^{(2)}{}_{mn}{}^{cd} + \cdots, \tag{5.90}$$

$$(L^{-1})_{ab}{}^{mn} = (L^{-1})^{(0)}{}_{ab}{}^{mn} + \frac{1}{r^n}(L^{-1})^{(1)}{}_{ab}{}^{mn} + \frac{1}{r^{n+1}}(L^{-1})^{(2)}{}_{ab}{}^{mn} + \cdots. \tag{5.91}$$

Plugging them into the identity relation (5.9), the relation is satisfied if

$$(L^{-1})^{(0)\,kl}_{ij} L^{(0)}{}_{kl}{}^{mn} = \delta_i^m \delta_j^n \tag{5.92}$$

and

$$(L^{-1})^{(1)\,pq}_{ij} = -(L^{-1})^{(0)\,kl}_{ij} L^{(1)}{}_{kl}{}^{mn}(L^{-1})^{(0)\,pq}_{mn}, \tag{5.93}$$

$$(n \geq 2), \quad (L^{-1})^{(2)\,pq}_{ij} = -(L^{-1})^{(0)\,kl}_{ij} L^{(2)}{}_{kl}{}^{mn}(L^{-1})^{(0)\,pq}_{mn}, \tag{5.94}$$

$$(n = 1), \quad (L^{-1})^{(2)\,pq}_{ij} = -(L^{-1})^{(0)\,kl}_{ij} L^{(2)}{}_{kl}{}^{mn}(L^{-1})^{(0)\,pq}_{mn} - (L^{-1})^{(1)\,kl}_{ij} L^{(1)}{}_{kl}{}^{mn}(L^{-1})^{(0)\,pq}_{mn}, \tag{5.95}$$

where $L^{(i)}{}_{kl}{}^{mn}$ can be directly read from (5.8)

$$L^{(0)}{}_{ij}{}^{kl} = r h^{(0)kl}\mu_{ij}^{(0)} + \frac{(n+1)}{r}\delta_i^k \delta_j^l - \frac{2}{r}\delta_{(i}^k \mu_{j)}^{(0)l}, \tag{5.96}$$

$$L^{(1)}{}_{ij}{}^{kl} = r\left(h^{(0)kl}\hat{Q}_{ij}^{(1)} + \hat{Q}^{(1)}\delta_i^k \delta_j^l - 2\delta_{(i}^k \hat{Q}_{j)}^{(1)l} - h^{(1)kl}\mu_{ij}^{(0)} \right)$$
$$+ \frac{1}{r}\left(2\delta_{(i}^k \mu_{j)}^{(1)l} - \mu^{(1)}\delta_i^k \delta_j^l \right), \tag{5.97}$$

and for $n \geq 2$

$$
L^{(2)}{}_{ij}{}^{kl} = r\left(h^{(0)kl}\hat{Q}^{(2)}_{ij} + \hat{Q}^{(2)}\delta^k_i\delta^l_j - 2\delta^k_{(i}\hat{Q}^{(2)l}{}_{j)} - h^{(2)kl}\mu^{(0)}_{ij} \right) + \frac{1}{r}\left(2\delta^k_{(i}\mu^{(2)l}{}_{j)} - \mu^{(2)}\delta^k_i\delta^l_j \right),
$$
(5.98)

and for $n = 1$

$$
\begin{aligned}
L^{(2)}{}_{ij}{}^{kl} = r\bigg(& h^{(0)kl}\hat{Q}^{(2)}_{ij} + \hat{Q}^{(2)}\delta^k_i\delta^l_j - 2\delta^k_{(i}\hat{Q}^{(2)l}{}_{j)} - h^{(2)kl}\mu^{(0)}_{ij} - h^{(1)kl}\hat{Q}^{(1)}_{ij} + 2\delta^k_{(i}\hat{Q}^{(1)}_{j)m}h^{(1)ml} \\
& - \hat{Q}^{(1)}_{ab}h^{(1)ab}\delta^k_i\delta^l_j + h^{(1)km}h^{(1)l}_{\ m}\mu^{(0)}_{ij} \bigg) + \frac{1}{r}\bigg(2\delta^k_{(i}\mu^{(2)l}{}_{j)} - \mu^{(2)}\delta^k_i\delta^l_j + \mu^{(1)ab}\mu^{(1)}_{ab}\delta^k_i\delta^l_j \\
& - 2\delta^k_{(i}\mu^{(1)}_{j)m}\mu^{(1)ml} \bigg).
\end{aligned}
$$
(5.99)

When $n = 1$ the sub-sub-leading order term is separately considered from that of general n, because the combination of the sub-leading order terms contributes to the sub-sub-leading order. From the definition (5.13), $\tilde{L}^{ab}$ expands as

$$
\begin{aligned}
\tilde{L}^{ab} &= \left(h^{(0)mn} - \frac{1}{r^n}h^{(1)mn} - \frac{1}{r^{n+1}}h^{(2)mn} + \cdots \right) \\
&\quad \times \left((L^{-1})^{(0)}{}_{mn}{}^{ab} + \frac{1}{r^n}(L^{-1})^{(1)}{}_{mn}{}^{ab} + \frac{1}{r^{n+1}}(L^{-1})^{(2)}{}_{mn}{}^{ab} + \cdots \right) \\
&= \tilde{L}^{(0)ab} + \frac{1}{r^n}\tilde{L}^{(1)ab} + \frac{1}{r^{n+1}}\tilde{L}^{(2)ab} + \cdots,
\end{aligned}
$$
(5.100)

where each order becomes

$$
\tilde{L}^{(0)ab} = h^{(0)mn}(L^{-1})^{(0)}_{mn}{}^{ab},
$$
(5.101)

$$
\tilde{L}^{(1)ab} = h^{(0)mn}(L^{-1})^{(1)}_{mn}{}^{ab} - h^{(1)mn}(L^{-1})^{(0)}_{mn}{}^{ab},
$$
(5.102)

$$
(n \geq 2),\quad \tilde{L}^{(2)ab} = h^{(0)mn}(L^{-1})^{(2)}_{mn}{}^{ab} - h^{(2)mn}(L^{-1})^{(0)}_{mn}{}^{ab},
$$
(5.103)

$$
\begin{aligned}
(n = 1),\quad \tilde{L}^{(2)ab} = & h^{(0)mn}(L^{-1})^{(2)}_{mn}{}^{ab} - h^{(2)mn}(L^{-1})^{(0)}_{mn}{}^{ab} \\
& - h^{(1)mn}(L^{-1})^{(1)}_{mn}{}^{ab} + h^{(1)ml}h^{(1)n}_l(L^{-1})^{(0)}_{mn}{}^{ab}.
\end{aligned}
$$
(5.104)

The $n \geq 2$ Case

The inverse of $(L)^{(0)}{}_{mn}{}^{cd}$ is

$$
(L^{-1})^{(0)}_{ij}{}^{ab} = \frac{r}{(n+1)} \bigg(\delta^a_i \delta^b_j - \frac{r^2}{2n} \mu^{(0)}_{ij} h^{(0)ab} + \frac{1}{n} \delta^a_i \mu^{(0)b}{}_j + \frac{1}{n} \delta^b_i \mu^{(0)a}{}_j
$$
$$
+ \frac{1}{n(n-1)} \mu^{(0)b}{}_i \mu^{(0)a}{}_j + \frac{1}{n(n-1)} \mu^{(0)a}{}_i \mu^{(0)b}{}_j - \frac{1}{n(n-1)} \mu^{(0)}_{ij} \mu^{(0)ab} \bigg), \quad (5.105)
$$

and contracting $(L)^{(0)}{}_{mn}{}^{cd}$ with $h^{(0)ij}$, we simply get

$$
(L^{-1})^{(0)ab} = \tilde{L}^{(0)ab} = \frac{r}{n(n+1)} \bigg(\frac{(n-1)}{2} h^{(0)ab} + \frac{1}{r^2} \mu^{(0)ab} \bigg). \quad (5.106)
$$

Once $(L^{-1})^{(0)}_{ij}{}^{ab}$ is calculated, we can subsequently obtain $(L^{-1})^{(1)}_{ij}{}^{pq}$ and $(L^{-1})^{(2)}_{ij}{}^{pq}$ from the relation (5.93) $-$ (5.94). Contracting them with $h^{(0)ij}$ and plugging into (5.102) $-$ (5.103), we have

$$
\tilde{L}^{(1)ab} = \frac{r}{n(n-1)} \bigg(r^2 \hat{Q}^{(1)ab} - \frac{r^2}{2} \hat{Q}^{(1)} h^{(0)ab} - \frac{2nr^2}{(n+1)^2} \hat{Q}^{(1)} u^{(0)a} u^{(0)b} + \frac{1}{2} \mu^{(1)} h^{(0)ab}
$$
$$
+ \frac{2n}{(n+1)^2} \mu^{(1)} u^{(0)a} u^{(0)b} - \frac{(n-1)^2}{2(n+1)} h^{(1)ab} - \frac{2n}{(n+1)r^2} \mu^{(1)ab} \bigg), \quad (5.107)
$$

and

$$
\widetilde{L}^{(2)ab} = \frac{r}{n(n-1)} \bigg(r^2 \hat{Q}^{(2)ab} - \frac{r^2}{2} \hat{Q}^{(2)} h^{(0)ab} - \frac{2nr^2}{(n+1)^2} \hat{Q}^{(2)} u^{(0)a} u^{(0)b} - \frac{r^2}{(n+1)} \hat{Q}^{(2)tt} h^{(0)ab}
$$
$$
+ \frac{2r^2}{n(n+1)^2} \hat{Q}^{(2)tt} u^{(0)a} u^{(0)b} - \frac{(2n^2+n+1)r^2}{n(n+1)^2} u^{(0)a} \hat{Q}^{(2)b}{}_t - \frac{(2n^2+n+1)r^2}{n(n+1)^2} \hat{Q}^{(2)a}{}_t u^{(0)b}
$$
$$
+ \frac{1}{2} \mu^{(2)} h^{(0)ab} + \frac{2n}{(n+1)^2} \mu^{(2)} u^{(0)a} u^{(0)b} - \frac{(n-1)^2}{2(n+1)} h^{(2)ab} - \frac{2n}{(n+1)r^2} \mu^{(2)ab} \bigg).
$$
$$
(5.108)
$$

As a result, we find

$$\tilde{L}^{(0)ab} = \frac{r}{n(n+1)}\left[\frac{(n+1)}{2r^2}\mu^{(0)ab} - \frac{(n-1)}{2}u^{(0)a}u^{(0)b}\right], \tag{5.109}$$

$$\tilde{L}^{(1)ab} = \frac{r}{n(n-1)}\left[\frac{r^2}{(n-1)}D^aD^b\alpha - \frac{(n-1)}{2r^2}\mu^{(1)ab} + \frac{(n^2+1)}{2(n-1)r^2}\alpha\mu^{(0)ab}\right.$$
$$+ \frac{(n^2+1)}{2(n-1)r^2}\gamma^{(1)}\mu^{(0)ab} + \frac{n}{4r^2}\mu^{(1)}\mu^{(0)}_{ab} - \frac{(n-1)^2}{2(n+1)}\alpha u^{(0)a}u^{(0)b}$$
$$\left.+ \frac{(n-1)^2}{2(n+1)}\gamma^{(1)}u^{(0)a}u^{(0)b} - \frac{n(n-1)^2}{4(n+1)^2}\mu^{(1)}u^{(0)a}u^{(0)b}\right], \tag{5.110}$$

$$\tilde{L}^{(2)ab} = \frac{r}{n(n-1)}\left[\frac{(2n^2-5n+3)}{2(n+1)}\gamma^{(2)}u^{(0)a}u^{(0)b} - \frac{(n^3-4n^2-5n-4)}{2n(n-1)(n+1)r^2}\gamma^{(2)}\mu^{(0)ab}\right.$$
$$\left.- \frac{n(n-3)}{2(n-1)r^2}\mu^{(2)ab}\right]. \tag{5.111}$$

The $n = 1$ Case

In 4-dimensional spacetime, the identity relation (5.92) with $L^{(0)}{}_{ij}{}^{kl}$ in (5.96) gives

$$(L^{-1})^{(0)ab} = \tilde{L}^{(0)ab} = \frac{1}{2r}\mu^{(0)ab}, \tag{5.112}$$

and from this, we can find

$$(L^{-1})^{(0)ab}_{ij} = \frac{r}{2}\left(\delta^a_i\delta^b_j + \frac{r^2}{2}\mu^{(0)}_{ij}u^{(0)a}u^{(0)b}\right). \tag{5.113}$$

Then, $\tilde{L}^{(i)ab}$ for $i = 1, 2$ are expanded as

$$
\begin{aligned}
\tilde{L}^{(1)ab} =& (L^{-1})^{(1)ab} - h^{(1)mn}(L^{-1})^{(0)ab}_{mn} \\
=& \frac{r}{2}\left(r^2\hat{Q}^{(1)ab} - \hat{Q}^{(1)}\mu^{(0)ab} + \frac{1}{2r^2}\mu^{(1)}\mu^{(0)ab} - \frac{1}{r^2}\mu^{(1)ab} \right),
\end{aligned}
\tag{5.114}
$$

$$
\begin{aligned}
\tilde{L}^{(2)ab} =& (L^{-1})^{(2)ab} - h^{(1)mn}(L^{-1})^{(1)ab}_{mn} - h^{(2)mn}(L^{-1})^{(0)ab}_{mn} + h^{(1)ml}h^{(1)n}_l(L^{-1})^{(0)ab}_{mn} \\
=& -\frac{r}{4}\Bigg(2\hat{Q}^{(2)}\mu^{(0)ab} + r^2\hat{Q}^{(2)}_{tt}h^{(0)ab} - 2r^2\hat{Q}^{(2)ab} + 2r^2 u^{(0)a}\hat{Q}^{(2)b}_{\ t} - \frac{1}{r^2}\mu^{(2)}\mu^{(0)ab} \\
& + \frac{2}{r^2}\mu^{(2)ab} - 2\hat{Q}^{(1)}_{mn}\mu^{(1)mn}h^{(0)ab} - 2r^4(\hat{Q}^{(1)})^2 h^{(0)ab} + r^4\hat{Q}^{(1)mn}\hat{Q}^{(1)}_{mn}h^{(0)ab} \\
& + 2\hat{Q}^{(1)}\mu^{(1)}\mu^{(0)ab} + 3r^4\hat{Q}^{(1)}\hat{Q}^{(1)ab} - 3\hat{Q}^{(1)}\mu^{(1)ab} - 2r^4\hat{Q}^{(1)ac}\hat{Q}^{(1)b}_c + 6\hat{Q}^{(1)a}_{\ c}\mu^{(1)bc} \\
& - 2r^2\mu^{(1)}\hat{Q}^{(1)ab} - \frac{3r^4}{2}(\hat{Q}^{(1)})^2 u^{(0)a}u^{(0)b} - r^2\hat{Q}^{(1)}\mu^{(1)}u^{(0)a}u^{(0)b} + \frac{2}{r^2}\mu^{(1)}\mu^{(1)ab} \\
& - \frac{1}{2}(\mu^{(1)})^2 h^{(0)ab} + \mu^{(1)mn}\mu^{(1)}_{mn}h^{(0)ab} - \frac{4}{r^2}\mu^{(1)ac}\mu^{(1)b}_c \Bigg),
\end{aligned}
\tag{5.115}
$$

and finally it becomes

$$
\tilde{L}^{(0)ab} = \frac{1}{2r}\mu^{(0)ab}, \qquad \tilde{L}^{(1)ab} = \frac{1}{r}\alpha\mu^{(0)ab} + \frac{1}{2r}\gamma^{(1)}\mu^{(0)ab},
\tag{5.116}
$$

$$
\begin{aligned}
\tilde{L}^{(2)ab} =& -\frac{1}{4r}\mu^{(2)ab} + \frac{1}{2r}\gamma^{(2)}\mu^{(0)ab} - \frac{r}{4}\gamma^{(2)}u^{(0)a}u^{(0)b} + \frac{13}{4r}\alpha^2\mu^{(0)ab} \\
& + \frac{5}{2r}\alpha\gamma^{(1)}\mu^{(0)ab} + \frac{1}{2r}(\gamma^{(1)})^2\mu^{(0)ab} + \frac{r}{2}\alpha\gamma^{(1)}u^{(0)a}u^{(0)b}.
\end{aligned}
\tag{5.117}
$$

5.4.2   Calculation of Δ^{ab}

Recalling from (5.16) the form of Δ^{ab} is

$$
\Delta^{ab} = \hat{K}^{ab} - 2\tilde{L}^{cd}\left(\hat{K}_{cd}\hat{K}^{ab} - \hat{K}^a_c\hat{K}^b_d \right) + \mathcal{D}^2\tilde{L}^{ab} + h^{ab}\mathcal{D}_k\mathcal{D}_l\tilde{L}^{kl} - \mathcal{D}_k\left(\mathcal{D}^a\tilde{L}^{kb} + \mathcal{D}^b\tilde{L}^{ka} \right),
$$

and we expand Δ^{ab} in powers of $1/r$

$$
\Delta^{ab} = [\Delta^{ab}]^{(0)} + \frac{1}{r^n}[\Delta^{ab}]^{(1)} + \frac{1}{r^{n+1}}[\Delta^{ab}]^{(2)} + \cdots .
\tag{5.118}
$$

53

In order to calculate Δ^{ab}, we need to expand the covariant derivative as

$$
\mathcal{D}_a \tilde{L}^{kl} = D_a^{(0)} \tilde{L}^{(0)kl} + \frac{1}{r^n}\left(D_a^{(0)} \tilde{L}^{(1)kl} + D_a^{(1)} \tilde{L}^{(0)kl} \right) + \frac{1}{r^{n+1}}\left(D_a^{(0)} \tilde{L}^{(2)kl} + D_a^{(2)} \tilde{L}^{(0)kl} \right)
$$

$$
+ \frac{1}{r^{2n}} D_a^{(1)} \tilde{L}^{(1)kl} + \mathcal{O}\left(\frac{1}{r^{n+2}} \right) \tag{5.119}
$$

where $D_a^{(0)}$ is a covariant derivative compatible with $h_{ab}^{(0)}$, and $D_a^{(0)}$ and $D_a^{(i)}$ for $i = 1, 2$ are denoted as

$$
\begin{aligned}
D_a^{(0)} \tilde{L}^{(i)kl} &= \partial \tilde{L}^{(i)kl} + \Gamma_{am}^{(0)k} \tilde{L}^{(i)ml} + \Gamma_{am}^{(0)l} \tilde{L}^{(i)mk} \tag{5.120}\\
D_a^{(i)} \tilde{L}^{(0)kl} &= \Gamma_{am}^{(i)k} \tilde{L}^{(0)ml} + \Gamma_{am}^{(i)l} \tilde{L}^{(0)mk} \tag{5.121}\\
D_a^{(1)} \tilde{L}^{(1)kl} &= \Gamma_{am}^{(1)k} \tilde{L}^{(1)ml} + \Gamma_{am}^{(1)l} \tilde{L}^{(1)mk}. \tag{5.122}
\end{aligned}
$$

In the above the connection is

$$
\Gamma^{(i)a}{}_{bc} = \frac{1}{2} h^{(0)ae}\left(D_b h_{ce}^{(i)} + D_c h_{be}^{(i)} - D_e h_{bc}^{(i)} \right) \tag{5.123}
$$

where $D_a^{(0)}$ is simply denoted as D_a. To simplify the terms having covariant derivatives in Δ^{ab}, we use the commutation relation in appendix D.

The $n \geq 2$ Case

Then we obtain the following values for each part of Δ^{ab} (5.16). The sub-leading orders become

$$
\left[\hat{K}^{ab} - 2\tilde{L}^{cd}(\hat{K}_{cd}\hat{K}^{ab} - \hat{K}_c^a \hat{K}_d^b) \right]^{(1)} =
$$

$$
\frac{r}{n(n-1)}\left[\frac{n(n+1)}{(n-1)r^4}\alpha\mu^{(0)ab} + \frac{n(n+1)}{(n-1)r^4}\gamma^{(1)}\mu^{(0)ab} + \frac{n}{2r^4}\mu^{(1)}\mu^{(0)ab} + \frac{(n+1)}{(n-1)}D^a D^b \alpha \right], \tag{5.124}
$$

$$
\left[\mathcal{D}^2 \tilde{L}^{ab} + h^{ab}\mathcal{D}_k \mathcal{D}_l \tilde{L}^{kl} - \mathcal{D}_k(\mathcal{D}^a \tilde{L}^{kb} + \mathcal{D}^b \tilde{L}^{ka}) \right]^{(1)} =
$$

$$
\frac{r}{n(n-1)}\left[-\frac{n(n+1)}{(n-1)r^4}\alpha\mu^{(0)ab} - \frac{n(n+1)}{(n-1)r^4}\gamma^{(1)}\mu^{(0)ab} - \frac{n}{2r^4}\mu^{(1)}\mu^{(0)ab} - \frac{(n+1)}{(n-1)}D^a D^b \alpha \right.
$$

$$
\left. + D^a D^b \gamma^{(1)} + \frac{n^2}{(n+1)^2}D^2 \mu^{(1)} u^{(0)a} u^{(0)b} + \frac{2n}{(n+1)}D^2 \alpha u^{(0)a} u^{(0)b} \right]. \tag{5.125}
$$

54

The sub-sub leading orders yield

$$
\left[\hat{K}^{ab} - 2\tilde{L}^{cd}(\hat{K}_{cd}\hat{K}^{ab} - \hat{K}_c^a\hat{K}_d^b) \right]^{(2)} =
$$
$$
\frac{r}{n(n-1)} \left[-\frac{(n-1)}{2r^2}h^{(2)ab} + \frac{(n^2+1)}{(n-1)}\mu^{(2)ab} + \frac{2(n^3+n^2+3n+1)}{n(n-1)(n+1)r^4}\gamma^{(2)}\mu^{(0)ab} \right], \quad (5.126)
$$

$$
\left[\mathcal{D}^2\tilde{L}^{ab} + h^{ab}\mathcal{D}_k\mathcal{D}_l\tilde{L}^{kl} - \mathcal{D}_k(\mathcal{D}^a\tilde{L}^{kb} + \mathcal{D}^b\tilde{L}^{ka}) \right]^{(2)} =
$$
$$
\frac{r}{n(n-1)} \left[\frac{(n-1)}{2r^2}h^{(2)ab} - \frac{(2n^2+n+1)}{(n-1)r^4}\mu^{(2)ab} - \frac{(3r^2+7n+4)}{n(n-1)r^4}\gamma^{(2)}\mu^{(0)ab} \right.
$$
$$
\left. + \frac{(n^3-2n^2-n-2)}{n(n-1)(n+1)}D^aD^b\gamma^{(2)} \right]. \quad (5.127)
$$

As a result, we find the leading order and the sub-leading orders to be

$$
[\Delta^{ab}]^{(0)} = 0, \quad (5.128)
$$
$$
[\Delta^{ab}]^{(1)} = \frac{r}{n(n-1)} \left[D^aD^b\gamma^{(1)} + \frac{n^2}{(n+1)^2}D^2\mu^{(1)}u^{(0)a}u^{(0)b} + \frac{2n}{(n+1)}D^2\alpha u^{(0)a}u^{(0)b} \right]. \quad (5.129)
$$

Indeed, that $[\Delta^{ab}]^{(1)}$ is non-zero is quite obvious, because from (5.16) the indices of the first three terms in Δ^{ab} contain only angular components (note $\hat{K}_{ab}^{(1)} = r\hat{Q}_{ab}^{(1)}$), whereas the last four terms (beginning with $\tilde{L}_{ab}^{(1)}$ in (5.16)) have both angular components and tt-components. The angular parts all cancel out except for $D^aD^b\gamma^{(1)}$, but tt-component terms remain.

At sub-sub-leading order we obtain

$$
[\Delta^{ab}]^{(2)} = \frac{r}{n(n-1)^2} \left[\frac{(n^3-2n^2-n-2)}{n(n+1)}D^aD^b\gamma^{(2)} - \frac{(n^3+8n^2+5n+2)}{n(n+1)r^4}\gamma^{(2)}\mu^{(0)ab} \right.
$$
$$
\left. - \frac{n(n+1)}{r^4}\mu^{(2)ab} \right]. \quad (5.130)
$$

In contrast to the sub-leading case, in the sub-sub-leading term both $\hat{K}_{ab}^{(2)}$ $(= r\hat{Q}_{ab}^{(2)}$, given in (5.78)) and $\tilde{L}_{ab}^{(2)}$ (given in (5.111)) carry both tt and angular components. Here we see similarities with the hyperbolic case [64], for which $\hat{K}_{ab}^{(2)} = \rho h_{ab}^{(2)}$ and $h^{(2)} = 0$ were respectably obtained from the MM-relation and the decomposed Einstein equations. These

55

require $\mathcal{R}^{(2)} = 0$, and yield $[\Delta^{ab}]^{(2)} = 0$. For the cylindrical case we are considering, we find that the terms associated with $h_{ab}^{(2)}$ in $\hat{K}_{ab}^{(2)}$ and in $\tilde{L}_{ab}^{(2)}$ cancel out in $[\Delta^{ab}]^{(2)}$, as shown in appendix E. However, unlike the hyperbolic case, in the cylindrical case, $h^{(2)}$ breaks up into $\mu^{(2)}$ and $\gamma^{(2)}$ (explicitly $h^{(2)} = \mu^{(2)} + 2\gamma^{(2)}$); consequently the decomposed Einstein equations imply $\mathcal{R}^{(2)}$ is non-vanishing and contributes to $\hat{K}_{ab}^{(2)}$. Indeed from eq. (5.50) we see that $\mathcal{R}^{(2)}$ can be expressed in terms of any one of $h^{(2)}$, $\mu^{(2)}$, or $\gamma^{(2)}$; we have expressed the result in terms of $\gamma^{(2)}$ in (5.78). The quantity $\gamma^{(2)}$ does not vanish, but remains in (5.130).

The $n = 1$ Case

We also obtain each part of Δ^{ab} (5.16), where for the sub-leading order it becomes

$$\left[\hat{K}^{ab} - 2\tilde{L}^{cd}(\hat{K}_{cd}\hat{K}^{ab} - \hat{K}_c^a\hat{K}_d^b)\right]^{(1)} = 2r\left(\frac{1}{r^4}\alpha\mu^{(0)ab} + \frac{1}{r^4}\gamma^{(1)}\mu^{(0)ab} + D^aD^b\alpha\right), \quad (5.131)$$

$$\left[\mathcal{D}^2\tilde{L}^{ab} + h^{ab}\mathcal{D}_k\mathcal{D}_l\tilde{L}^{kl} - \mathcal{D}_k(\mathcal{D}^a\tilde{L}^{kb} + \mathcal{D}^b\tilde{L}^{ka})\right]^{(1)} =$$
$$\frac{3r}{2}\left(-\frac{1}{r^4}\alpha\mu^{(0)ab} - \frac{1}{r^4}\gamma^{(1)}\mu^{(0)ab} - D^aD^b\alpha\right), \quad (5.132)$$

and for the sub-sub-leading order it is

$$\left[\hat{K}^{ab} - 2\tilde{L}^{cd}(\hat{K}_{cd}\hat{K}^{ab} - \hat{K}_c^a\hat{K}_d^b)\right]^{(2)} = \frac{1}{r}\left(\gamma^{(2)}u^{(0)a}u^{(0)a} - 2\alpha\gamma^{(1)}u^{(0)a}u^{(0)b} - \frac{3}{r^4}\mu^{(2)ab}\right.$$
$$\left. + \frac{1}{r^4}\mu^{(2)}\mu^{(0)ab} + \frac{1}{2r^4}\gamma^{(2)}\mu^{(0)ab} - \frac{1}{r^4}\alpha\gamma^{(1)}\mu^{(0)ab}\right), \quad (5.133)$$

$$\left[\mathcal{D}^2\tilde{L}^{ab} + h^{ab}\mathcal{D}_k\mathcal{D}_l\tilde{L}^{kl} - \mathcal{D}_k(\mathcal{D}^a\tilde{L}^{kb} + \mathcal{D}^b\tilde{L}^{ka})\right]^{(2)} = \frac{1}{r}\left(-\gamma^{(2)}u^{(0)a}u^{(0)a} + 2\alpha\gamma^{(1)}u^{(0)a}u^{(0)b}\right.$$
$$+ \frac{1}{r^4}\mu^{(2)ab} - \frac{1}{2r^4}\mu^{(2)}\mu^{(0)ab} - \frac{1}{r^4}\gamma^{(2)}\mu^{(0)ab} + \frac{2}{r^4}\alpha\gamma^{(1)}\mu^{(0)ab} + \frac{1}{2r^4}\alpha^2\mu^{(0)ab} + \frac{1}{2r^4}(\gamma^{(1)})^2\mu^{(0)ab}$$
$$- \frac{r^2}{4}D^aD^b\mu^{(2)} - \frac{r^2}{2}D^aD^b\gamma^{(2)} + \frac{1}{4}D^2\mu^{(2)}\mu^{(0)ab} + \frac{3}{4}D^2\gamma^{(2)}\mu^{(0)ab} - 4r^2D^a\alpha D^b\alpha - 5r^2\alpha D^aD^b\alpha$$
$$- 3r^2\gamma^{(1)}D^aD^b\alpha - \frac{1}{2}D^e\alpha D_e\alpha\mu^{(0)ab} + \frac{11}{4}D^2\alpha^2\mu^{(0)ab} + \frac{13}{4}D^2(\alpha\gamma^{(1)})\mu^{(0)ab}$$
$$- \frac{3r^2}{2}D^2\alpha^2u^{(0)a}u^{(0)b} - \frac{5r^2}{4}\gamma^{(1)}D^2\alpha u^{(0)a}u^{(0)b}\right). \quad (5.134)$$

Up to sub-leading order we find

$$[\Delta^{ab}]^{(0)} = 0, \quad \text{and} \quad [\Delta^{ab}]^{(1)} = 0, \tag{5.135}$$

where we have used $D_a D_b \alpha = -\alpha \mu_{ab}^{(0)} - \gamma^{(1)} \mu_{ab}^{(0)}$, which can be inferred from $D^2 \alpha = -\frac{2}{r^2}\alpha - \frac{2}{r^2}\gamma^{(1)}$. The sub-sub-leading term is

$$
\begin{aligned}
[\Delta^{ab}]^{(2)} &= -\frac{2}{r^3}\mu^{(2)ab} - \frac{2}{r^3}\gamma^{(2)}\mu^{(0)ab} - \frac{4}{r^3}\alpha^2\mu^{(0)ab} - \frac{6}{r^3}\alpha\gamma^{(1)}\mu^{(0)ab} - \frac{4}{r^3}(\gamma^{(1)})^2\mu^{(0)ab} \\
&\quad + \frac{9}{2r}D^e\alpha D_e\alpha\mu^{(0)ab} + rD^aD^b\gamma^{(2)} - 5rD^a\alpha D^b\alpha - \frac{3r}{2}D^2\alpha^2 u^{(0)a}u^{(0)a} - \frac{5r}{4}D^2(\alpha\gamma^{(1)})u^{(0)a}u^{(0)b}.
\end{aligned} \tag{5.136}
$$

These results for $n = 1$ are commensurate with the hyperbolic case [64], which has manifestly vanishing $[\Delta^{ab}]^{(0)}$ and $[\Delta^{ab}]^{(1)}$, but non-vanishing $[\Delta^{ab}]^{(2)}$.

That we find Δ^{ab} non-vanishing implies that the boundary stress tensor in cylindrical coordinates generally takes the form T_{ab} in (5.18) and not T_{ab}^π in (5.4).

5.4.3 Conserved Quantities and Δ^{ab}

Since the boundary stress tensor is described not by T_{ab}^π but by T_{ab} (due $\Delta^{ab} \neq 0$), we now consider how Δ^{ab} is related to conserved quantities as given in equation (5.5). Plugging $T_{ab} = T_{ab}^\pi - \Delta_{ab}$ into (5.5), we see that Δ^{ab} will contribute to conserved quantities via

$$Q^\Delta[\xi] = -\frac{1}{8\pi G}\oint d^{n+1}x\sqrt{\gamma}u^a\Delta_{ab}\xi^b. \tag{5.137}$$

For $n \geq 2$ we find that $Q^\Delta[\xi] = 0$. The sub-leading term contributes

$$
\begin{aligned}
[Q^\Delta]^{(1)} &= -\frac{1}{8\pi G}\oint d^{n+1}x\sqrt{\gamma}u^{(0)a}[\Delta_{ab}]^{(1)}\xi^{(0)b}, \\
&= \frac{r}{8\pi G}\frac{1}{(n-1)(n+1)}\oint d^{n+1}x\sqrt{\gamma}\left(\frac{n}{(n+1)}D^2\mu^{(1)} + 2D^2\alpha\right), \\
&= 0, \tag{5.138}
\end{aligned}
$$

where $u^{(0)a} = -\delta_t^a$ and $\xi^{(0)t} = 1$ has been used, and the total derivative on the closed surface becomes zero. The sub-sub-leading order also makes no contribution, since from

57

(5.130) we see that $[\Delta_{ab}]^{(2)}$ contracted with the timelike normal vector $u^{(0)a}$ vanishes, and so $[Q^\Delta]^{(2)}$ obviously becomes zero.

For $n = 1$ $[\Delta^{ab}]^{(1)} = 0$ and so only the sub-sub-leading term could possibly contribute. Carrying out similar manipulations to the previous case, we get

$$
\begin{aligned}
[Q^\Delta]^{(2)} &= -\frac{1}{8\pi G} \oint d^2x \sqrt{\gamma} u^{(0)a} [\Delta_{ab}]^{(2)} \xi^{(0)b}, \\
&= -\frac{1}{8\pi G} \oint d^2x \sqrt{\gamma} \left(\frac{3r}{2} D^2 \alpha^2 + \frac{5r}{4} D^2 (\alpha \gamma^{(1)}) \right), \\
&= 0,
\end{aligned}
\tag{5.139}
$$

where $u^{(0)a} = -\delta_t^a$ and $\xi^{(0)t} = 1$ has been used, and the total derivative on the closed surface becomes zero at the end. Indeed, this result is expected, because we required that $\hat{Q}_{ab}^{(2)}$ not contribute to conserved charges.

Hence $Q^\Delta = 0$ even though $\Delta^{ab} \neq 0$. As a result the conserved quantity formula is of the form (5.5) and is given only in terms of T_{ab}^π.

5.5 Divergence of the Boundary Stress Tensor, $\mathcal{D}^a T_{ab}$

In [63], it was argued that the full boundary stress tensor is conserved in that $\mathcal{D}^a T_{ab} = 0$. We reconsider this relation in view of the fact that $\Delta^{ab} \neq 0$.

Recall that the full boundary stress tensor, T_{ab}, is

$$
T_{ab} = T_{ab}^\pi - \frac{1}{8\pi G} \Delta_{ab}.
\tag{5.140}
$$

Expanding its divergence in a power series yields

$$
\begin{aligned}
\mathcal{D}^a T_{ab} =& [\mathcal{D}^a T_{ab}]^{(0)} + \frac{1}{r^n} [\mathcal{D}^a T_{ab}]^{(1)} + \frac{1}{r^{n+1}} [\mathcal{D}^a T_{ab}]^{(2)} + \cdots \\
=& \left([\mathcal{D}^a T_{ab}^\pi]^{(0)} - \frac{1}{8\pi G} [\mathcal{D}^a \Delta_{ab}]^{(0)} \right) + \frac{1}{r^n} \left([\mathcal{D}^a T_{ab}^\pi]^{(1)} - \frac{1}{8\pi G} [\mathcal{D}^a \Delta_{ab}]^{(1)} \right) \\
&+ \frac{1}{r^{n+1}} \left([\mathcal{D}^a T_{ab}^\pi]^{(2)} - \frac{1}{8\pi G} [\mathcal{D}^a \Delta_{ab}]^{(2)} \right) + \cdots
\end{aligned}
\tag{5.141}
$$

where $\mathcal{D}^a$ is the covariant derivative associated with h_{ab}.

For $n \geq 2$, we have

$$T_{ab}^{\pi} = -\frac{r}{8\pi G}\left[\frac{1}{r^n}\left(\frac{n}{2r^2}h_{ab}^{(1)} + \frac{1}{r^2}\gamma^{(1)}h_{ab}^{(0)} + \frac{n}{(n-1)}\alpha^{(1)}\mu_{ab}^{(0)} + \frac{1}{(n-1)}\gamma^{(1)}\mu_{ab}^{(0)} + \frac{1}{(n-1)}D_aD_b\alpha\right)\right.$$
$$\left. + \frac{1}{r^{n+1}}\left(\frac{n(n+1)}{2(n-1)r^2}h_{ab}^{(2)} + \frac{(n+1)(n+2)}{n(n-1)}\gamma^{(2)}\mu_{ab}^{(0)} - \frac{(n+1)}{(n-1)r^2}\gamma^{(2)}u_a^{(0)}u_b^{(0)}\right) + \cdots\right],$$
$$(5.142)$$

and plugging this and $(5.128) - (5.130)$ into (5.141), we get

$$\mathcal{D}^a T_{ab} = \frac{1}{r^n}\left(\frac{1}{8\pi G}\frac{1}{(n-1)r}D_b\gamma^{(1)} - \frac{1}{8\pi G}\frac{1}{(n-1)r}D_b\gamma^{(1)}\right) + \frac{1}{r^{n+1}}\left(0 - 0\right) + \cdots ,$$
$$= 0. \qquad (5.143)$$

where D^a is associated with $h_{ab}^{(0)}$. This verifies that the full boundary stress tensor, T_{ab}, is conserved.

For $n = 1$, we take

$$T_{ab}^{\pi} = -\frac{r}{8\pi G}\left[\frac{1}{r}\left(-\frac{2}{r^2}\gamma^{(1)}u_a^{(0)}u_b^{(0)}\right) + \frac{1}{r^2}\left(\frac{1}{2}\mu_{ab}^{(2)} + \frac{3}{2}\gamma^{(2)}\mu_{ab}^{(0)} - \frac{23}{2}\alpha^2\mu_{ab}^{(0)}\right.\right.$$
$$- 5\alpha\gamma^{(1)}\mu_{ab}^{(0)} - (\gamma^{(1)})^2\mu_{ab}^{(0)} - \frac{1}{2r^2}\mu^{(2)}u^{(0)a}u^{(0)b} + \frac{3}{r^2}\gamma^{(2)}u^{(0)a}u^{(0)b}$$
$$\left.\left. + \frac{4}{r^2}\alpha\gamma^{(1)}u^{(0)a}u^{(0)b} + \frac{15}{r^2}\alpha^2u^{(0)a}u^{(0)b} + \frac{4}{r^2}(\gamma^{(1)})^2u^{(0)a}u^{(0)b}\right) + \cdots\right]. \qquad (5.144)$$

and substituting this with (5.136) into (5.141), it yields

$$\mathcal{D}^a T_{ab} = \frac{1}{r}\left(0 - 0\right) + \frac{1}{r^2}\left[\frac{1}{8\pi G}\left(-\frac{22}{r}\alpha D_b\alpha - \frac{3}{2r}\gamma^{(1)}D_b\alpha\right)\right.$$
$$\left. - \frac{1}{8\pi G}\left(\frac{3}{r}D_b\gamma^{(2)} - \frac{14}{r}\alpha D_b\alpha - \frac{20}{r}\gamma^{(1)}D_b\alpha\right)\right] + \cdots ,$$
$$= \frac{1}{8\pi G}\frac{1}{r^2}\left(-\frac{3}{r}D_b\gamma^{(2)} - \frac{8}{r}\alpha D_b\alpha + \frac{37}{2r}\gamma^{(1)}D_b\alpha\right) \qquad (5.145)$$

where the second sub-leading order does not vanish. To be conserved, we require

$$D_b\left(3\gamma^{(2)} + 4\alpha^2 - \frac{37}{2}\alpha\gamma^{(1)}\right) = 0 \qquad (5.146)$$

and this relation can be satisfied by applying $(5.64) - (5.66)$.

5.6 $(n+3)$-dimensional Static Spacetime

In this section, we apply the boundary stress tensor method to $(n+3)$-dimensional static spacetime. We show that Δ^{ab} makes no contribution with respect to the conserved quantities and obtain the conserved charges by using (5.5).

We examine the boundary stress tensor method associated with the MM-counterterm in $(n+3)$-dimensional static spacetime. In this spacetime, we check that $\Delta^{ab} = 0$, and prove that the boundary stress tensor yields conserved charges agreed with the usual definition [5] [71].

From the Schwarzschild-Tangherlini solution (also in [71]), the metric is

$$ds^2 = -\left(1 - \frac{\mu}{r^n}\right)dt^2 + \left(1 - \frac{\mu}{r^n}\right)^{-1}dr^2 + r^2 d\Omega_{n+1}^2, \tag{5.147}$$

where μ is related to the mass M

$$M = \frac{(n+1)A_{n+1}}{16\pi G}\mu, \qquad A_{n+1} = \frac{2\pi^{(n+2)/2}}{\Gamma((n+2)/2)}, \tag{5.148}$$

and comparing (5.147) with our metric (5.30), they are related by

$$\gamma^{(1)} = -\frac{1}{2}\mu, \qquad \alpha = \frac{1}{2}\mu, \qquad \gamma^{(2)} = 0, \qquad \mu_{AB}^{(1)} = \mu_{AB}^{(2)} = 0. \tag{5.149}$$

Substituting these values to the results $(5.129) - (5.130)$ for $n > 1$ and (5.136) for $n = 1$, it is straightforwardly proved that $[\Delta^{ab}]^{(i)} = 0$ for $i = 1, 2$ for a general n. Since Δ^{ab} vanishes for $n > 1$, the boundary stress tensor becomes

$$T_{ab} = -\frac{1}{8\pi G}\frac{1}{r^{n-1}}\left(\frac{n}{2r^2}h_{ab}^{(1)} + \frac{1}{r^2}\gamma^{(1)}h_{ab}^{(0)} + \frac{n}{(n-1)}\alpha\mu_{ab}^{(0)} + \frac{1}{(n-1)}\gamma^{(1)}\mu_{ab}^{(0)} + \frac{1}{(n-1)}D_aD_b\alpha\right), \tag{5.150}$$

and the conserved charge is directly obtained

$$
\begin{aligned}
Q[\xi^t] &= \frac{1}{8\pi G}\int d^{n+1}x\sqrt{\gamma^{(0)}}u^{(0)t}T_{tt}^{(1)}\xi^{(0)t}, \\
&= \frac{1}{8\pi G}r^{n+1}A_{n+1}(-1)\left(-\frac{(n+1)}{2r^{n+1}}\mu\right), \\
&= \frac{(n+1)}{(n+2)}M.
\end{aligned}
\tag{5.151}
$$

For $n = 1$ the boundary stress tensor has the form

$$T_{ab} = -\frac{1}{8\pi G}\left(\frac{1}{2r^2}h_{ab}^{(1)} - \frac{1}{2}\mu_{ab}^{(1)}\right), \tag{5.152}$$

and the conserved charge is

$$Q[\xi^t] = \frac{1}{8\pi G}\int_0^{2\pi} d\varphi \int_0^{\pi} d\theta\ r^2 \sin\theta(-1)\left(-\frac{1}{r^2}\mu\right) = M, \tag{5.153}$$

which corresponds to [71].

5.7 Summary and Discussion

In this chapter, the MM-counterterm was studied in asymptotically flat static spacetime, and for the boundary condition the cylindrical coordinate has been chosen. We began with defining the most general form of the asymptotically static metric in $(n+3)$ dimensions, and then solved the decomposed Einstein equations and the MM-relation at the asymptotic boundary of the spacetime. We found the MM-counterterm solution $\hat{K}_{ab}$ to be uniquely determined for $n \geq 2$, but had ambiguities for $n = 1$.

For $n = 1$, at sub-leading order these ambiguities can be nullified by choosing $\mu_{ab}^{(1)} = -2\alpha\mu_{ab}^{(0)}$ and $D_a D_b \alpha = -\alpha\mu_{ab}^{(0)} - \gamma^{(1)}\mu_{ab}^{(0)}$. The quantity Δ_{ab} consequently vanishes. At sub-sub-leading order we found that while these ambiguities in $\hat{K}_{ab}$ cannot ensure that the resultant contribution to Δ_{ab} vanishes, as displayed in $(5.135) - (5.136)$, they can be chosen to ensure that Δ_{ab} does not contribute to the conserved charge. These results are similar to those obtained for the hyperbolic case [64], which has manifestly vanishing $[\Delta^{ab}]^{(0)}$ and $[\Delta^{ab}]^{(1)}$, but non-vanishing $[\Delta^{ab}]^{(2)}$. The stress-energy tensor is conserved provided (5.146) holds, which can be obtained by applying $(5.64) - (5.66)$.

For $n \geq 2$ we find at both sub-leading and sub-sub-leading orders that $\hat{K}_{ab}$ is determined. The quantity Δ^{ab} turns out to be non-zero, as shown in $(5.128) - (5.130)$. This result indicates that the boundary stress tensor should be T_{ab} in (5.18) not T_{ab}^{π} in (5.4). However we find that Δ^{ab} does not contribute to the conserved charge (see $(5.138, 5.139)$); only T_{ab}^{π} produces conserved charges and so the form of the conserved quantity formula (5.5) is still valid. We also investigated the divergence of the boundary stress tensor, and found that $\mathcal{D}^a T_{ab} = 0$.

We applied the boundary stress tensor method with the solution of the MM-counterterm to the specific case, which is a static black hole in $(n+3)$-dimensional static spacetime,

61

and found that Δ^{ab} manifestly is zero. We also obtained the conserved charge from the boundary stress tensor. This agrees with the ADM mass, demonstrating that the boundary stress tensor with MM-counterterm is also applicable using cylindrical boundary conditions.

As mentioned in Section 5.2.2, the asymptotic behaviours of the hyperbolic boundary case and cylindrical boundary case are distinguished. In the hyperbolic case, all components of the induced metric h_{ab} can be expanded to the same order in r, and so are covariant under the variation. However in the cylindrical case the induced metric h_{ab} is again decomposed into tt- and angular components; these components have expansions to different orders in r. They do not covariantly transform, thereby not permitting inference of results from the hyperbolic case to the cylindrical case. Furthermore, these two boundary conditions yield different solutions from the decomposed Einstein equations. In the hyperbolic case, the sub-sub-leading order of the Ricci tensor and the trace of the sub-sub-leading order of h_{ab} become zero, so they in turn affect the sub-sub-leading order of $\hat{K}_{ab}$ and subsequently imply that the sub-sub-leading order of Δ^{ab} is zero. By contrast, in the cylindrical case the sub-sub-leading order of the Ricci tensor and the trace of the sub-sub-leading order of h_{ab} are not zero; they partly contribute to the sub-sub-leading order of Δ^{ab}, rendering it nonzero. Despite these differing properties between two boundary conditions, we found that the MM-counterterm is still valid yielding different descriptions of the boundary stress tensor in more than 4 dimensions for the respective cases.

These results for the MM-counterterm applied to asymptotically flat spacetimes are an optimistic sign for holographic renormalization, and we anticipate that the MM-counterterm is a good candidate to be employed, if one finds a holographic correspondence for the Minkowski spacetime in the future.

Chapter 6

Deformations of Lifshitz Holography

6.1 Introduction

In this chapter, we deal with the Lifshitz spacetime/quantum critical theory correspondence, which is one of applications of gravity/condensed matter theory correspondences. The quantum criticality was found by investigating phase transitions of modern materials several decades ago. It was observed that a precarious point exists between two stable phases of matter such as superconductors and ferroelectrics (or ferromagnets) in circumstances in which the temperature of a system has been driven to absolute zero and some external parameter such as pressure or a magnetic field is applied. Since the critical fluctuations are quantum mechanical in nature, this point is called the quantum critical point and exhibits universally distinct characteristics upon fanning out to finite temperatures. Over this region, which shares the same properties with the critical point, the quantum phase transition emerges, and its properties are intensively discussed in chapter 3.

In quantum critical theory, time scales differently from space

$$t \to \lambda^z t, \quad \vec{x} \to \lambda \vec{x} \tag{6.1}$$

where z is the dynamical critical exponent; $z = 1$ corresponds to conformal invariance, whereas $z \neq 1$ implies an anisotropic scaling invariance. Its geometrical dual description is conjectured to be

$$ds^2 = l^2 \left(-\frac{dt^2}{r^{2z}} + \frac{dr^2}{r^2} + \frac{dx^2 + dy^2}{r^2} \right) \tag{6.2}$$

which is called Lifshitz spacetime and obviously satisfies

$$t \to \lambda^z t, \quad r \to \lambda r, \quad \vec{x} \to \lambda \vec{x}. \tag{6.3}$$

When $z = 1$, the metric (6.2) is that of (asymptotic) AdS spacetime, and (6.1) recovers the conformal symmetry of the CFT. When $z \neq 1$, (6.1) restores the scaling symmetry of quantum critical theories. Thus, in Lifshitz spacetime/Quantum Critical Theory (Lifshitz/QCT), the anisotropic scaling symmetry, when $z \neq 1$, is same for both gravity and field theory, and it becomes the foundation for gravity/gauge correspondence.

In gravity theory, non-trivial spacetimes that asymptote to the anisotropic metric (6.2) can be generated by having an anisotropic energy-momentum tensor with a contribution of matter fields such as a massive vector field. An alternate approach also can be made by including higher curvature terms into the Einstein action [34]; by appropriately tuning the different gravitational constants, metrics asymptotic to (6.2) can be obtained. In this chapter, we follow the first approach, investigating the Einstein action coupled to a massive vector field in $(n + 1)$ dimensions.

In Lifshitz field theory, an interesting feature associated with renormalization group flow is shown as follows. When $z = 2$, the action of the Lifshitz field is

$$S_{\text{Lif}} = \frac{1}{2} \int d\tau d^2 x \left((\partial_\tau \phi)^2 - \kappa (\nabla^2 \phi)^2 \right) \tag{6.4}$$

which has an anisotropic scaling invariance. This action describes strongly correlated electron systems and its fixed points of the system seem to flow to a non-Abelian gauge theory by perturbing the action with a term $-(\nabla \phi)^2$. Applying this feature to the holographic duality picture, holographic renormalization flow is expected, for example, from a UV-Lifshitz fixed point to an AdS fixed point under the relevant perturbation, and its existence is numerically found in [56], where a Proca field is added and its essential physics for $z = 2$ in (3+1) dimensions is that of a marginally relevant operator in the quantum critical theory, which induces a flow from the $z = 2$ theory to a relativistic $z = 1$ infrared fixed point.

In this chapter, we consider $(n + 1)$-dimensional Lifshitz spacetime and $((n - 1) + 1)$-dimensional Quantum Critical Theory(QCT), and study their holographic duality. While QCT is well described in a $2 + 1$ dimensional context, more general theories of physics including the standard model and gravity are implemented in a higher-dimensional context. The success of the AdS/CFT correspondence therefore provides motivation to understand the extent to which the broader notions of Lifshitz/QCT duality are applicable in higher dimensions, and what different behaviour emerges. Motivated by these interests, we especially focus on the marginally relevant operators in the QCT extended to higher dimensions, with the goal of understanding their behaviour from the perspective of holographic duality.

As previous work in this subject has concentrated on the (2+1)-dimensional case [25], we generalize the idea to $(n + 1)$ dimensions with the same purposes; one of them is to

show an implication of renormalization group flow from Lifshitz spacetime in the Ultraviolet (UV) regime to AdS spacetime in the Infrared (IR) regime in any dimensionality at zero temperature, which is found in [18],[56]. The other purpose is to form a description of physical quantities near the critical point at finite temperature. To do so, we first consider that the Lifshitz spacetime is in the UV regime and the AdS spacetime is in the IR regime. At the boundary of the spacetime i.e. $r \to 0$, we obtain the asymptotic solutions of Lifshitz spacetime and expand the solutions to sub-leading orders by introducing a momentum scaling Λ. Here in order to yield non-trivial solutions at sub-leading order, the equations of motion restrict us to have $z = n - 1$. Due to $\Lambda \sim 0$, the Lifshitz spacetime is slightly deformed by it, and from the perspective of the holographic correspondence, the deformed solutions of the spacetime correspond to the marginally relevant operators of the field theory. By constructing proper counterterms with these asymptotic solutions, we obtain the well-defined action, and derive the free energy density and energy density. We also find the expanded black hole solutions at near horizon $r = r_+$ to configure finite temperature theory. Then we fix the undetermined parameters in the both metrics by using numerical integration, and based on these values of the metrics investigate the behaviour of physical quantities such as the free energy density $\mathcal{F}$ and the energy density $\mathcal{E}$. Thus we observe what properties are shown from those quantities depending on Λ^z/T.

In section 6.2, the action, equations of motion, and basic setup are introduced, along with an ansatz for which all constants are fine-tuned and normalized for both Lifshitz and AdS spacetime. In section 6.3, asymptotic solutions consistent with marginally relevant operators are derived by bringing in a dynamically generated momentum scale Λ (assumed very small), which deforms Lifshitz spacetime in the high energy regime. In section 6.4, we carry out holographic renormalization by building relevant counterterms. In section 6.5, we match our asymptotic near-Lifshitz solutions with the results of numerical integration of the expanded black hole solutions, and then in section 6.6 compute physical quantities such as the free energy density $\mathcal{F}$, and the energy density $\mathcal{E}$ for $n = 3, 4, 5, 6, 7$, and 8. In section 6.7, we summarize and include a discussion of results.

6.2   Einstein Gravity with a Massive Vector fields

The action for gravity in $(n + 1)$-dimensional spacetime coupled to a massive vector field is described by

$$S = \int d^{n+1}x\sqrt{-g}\left(\frac{1}{2\kappa_{n+1}{}^2}[R + 2\tilde{\Lambda}] - \frac{1}{g_v{}^2}\left[\frac{1}{4}H^2 + \frac{\gamma}{2}B^2\right]\right) \tag{6.5}$$

where $\kappa_{n+1} = \sqrt{8\pi G_{n+1}}$ in which G_{n+1} is the $(n+1)$ dimensional gravitational constant, and $H = dB$ and g_v is the $(n+1)$ dimensional coupling constant of the vector field. The equations of motion are

$$\frac{1}{\kappa_{n+1}{}^2}\left(R_{\mu\nu} - \frac{1}{2}g_{\mu\nu}R - \tilde{\Lambda}g_{\mu\nu}\right) = \frac{1}{g_v{}^2}\left(H_{\mu\rho}H_\nu{}^\rho - \frac{1}{4}g_{\mu\nu}H^2\right) + \frac{\gamma}{g_v{}^2}\left(B_\mu B_\nu - \frac{1}{2}g_{\mu\nu}B^2\right), \quad (6.6)$$

and

$$\nabla_\mu H^{\mu\nu} - \gamma B^\nu = 0 \qquad (6.7)$$

where γ is the squared mass of the vector field. For the action to yield solutions asymptotic to those having the scaling symmetry (6.3), we require the spacetime metric

$$ds^2 = l^2\left(-\frac{dt^2}{r^{2z}} + \frac{dr^2}{r^2} + \frac{dx^2 + dy^2 + \cdots}{r^2}\right) \qquad (6.8)$$

to be a solution to the field equations, where z is arbitrary. Note that in these coordinates $r \to 0$ corresponds to the boundary of the spacetime.

The vector potential yielding a stress-energy supporting this metric is given by

$$B = \frac{g_v l}{\kappa_{n+1}} \frac{q}{r^z} dt. \qquad (6.9)$$

These ansatz and boundary conditions fine-tune the cosmological constant to be

$$\tilde{\Lambda} = \frac{(z-1)^2 + n(z-2) + n^2}{2l^2}, \qquad (6.10)$$

and the squared mass and the charge of the vector field to be

$$\gamma = \frac{(n-1)z}{l^2}, \qquad\qquad q^2 = \frac{z-1}{z}. \qquad (6.11)$$

Regardless of the dimensionality of the spacetime, setting $z = 1$ in (6.8) yields AdS_{n+1} solution

$$ds^2_{AdS} = a\, l^2\left(-\frac{dt^2}{r^2} + \frac{dr^2}{r^2} + \frac{dx^2 + dy^2 + \cdots}{r^2}\right) \qquad (6.12)$$

where the vector potential vanishes. As the cosmological constant has been already fixed due to the Lifshitz boundary condition we introduce a scaling constant, a, into the AdS metric and adjust its value to be

$$a = \frac{n(n-1)}{(z-1)^2 + n(z-2) + n^2}. \qquad (6.13)$$

Once we fix the cosmological constant (6.10) with space dimension n and dynamical critical exponent z, then those values determine the scaling constant for the AdS spacetime metric.

In order to describe the renormalization group flow which involves breaking the anisotropy of the spacetime by running from the UV Lifshitz to the IR AdS, we employ the ansatz

$$ds^2 = l^2\left(-f(r)dt^2 + \frac{dr^2}{r^2} + p(r)(dx^2 + dy^2 + \cdots)\right), \tag{6.14}$$

$$B = \frac{g_v l}{\kappa_{n+1}} h(r) dt \tag{6.15}$$

so for the Lifshitz spacetime

$$\text{Lifshitz}: f = \frac{1}{r^{2z}} \quad p = \frac{1}{r^2}, \quad h = \frac{\sqrt{z-1}}{\sqrt{z}}\frac{1}{r^z}, \tag{6.16}$$

whereas for the AdS_{n+1} spacetime

$$\text{AdS}: f = p = \frac{n}{(3n-4)}r^{-2\sqrt{\frac{3n-4}{n}}}, \quad h = 0. \tag{6.17}$$

With (6.14) and (6.15), the equations of motion yield three independent non-linear ODEs for $\{f(r), p(r), h(r)\}$

$$2\chi + \frac{z(4n-6)h(r)^2}{f(r)} - \frac{rf'(r)}{f(r)} + \frac{r^2 f'(r)^2}{2f(r)^2} - \frac{(3n-5)r^2 f'(r)p'(r)}{2f(r)p(r)}$$
$$- \frac{(n-2)^2 r^2 p'(r)^2}{2p(r)^2} - \frac{r^2 f''(r)}{f(r)} = 0,$$

$$-\frac{2zh(r)^2}{f(r)} - \frac{rp'(r)}{p(r)} + \frac{r^2 f'(r)p'(r)}{2f(r)p(r)} + \frac{r^2 p'(r)^2}{2p(r)^2} - \frac{r^2 p''(r)}{p(r)} = 0,$$

$$\chi + \frac{(n-1)zh(r)^2}{f(r)} - \frac{r^2 h'(r)^2}{f(r)} - \frac{(n-1)r^2 f'(r)p'(r)}{2f(r)p(r)} - \frac{(n-2)(n-1)r^2 p'(r)^2}{4p(r)^2} = 0, \tag{6.18}$$

where $\chi = (n-1)^2 + (n-2)z + z^2$. We shall rewrite the equations of the motion with the new variables

$$p(r) = e^{\int^r \frac{q(s)}{s} ds}, \quad f(r) = e^{\int^r \frac{m(s)}{s} ds}, \quad h(r) = k(r)\sqrt{f(r)}. \tag{6.19}$$

These variables have the added benefit of turning the second order differential equations into first order and postponing the determination of rescaling ambiguities on f, p, and h.

For further simplification, we introduce a new variable

$$x(r) = \left(4\chi + 4(n-1)zk(r)^2 - 2(n-1)m(r)q(r) - (n-2)(n-1)q(r)^2\right)^{\frac{1}{2}}. \quad (6.20)$$

Putting (6.19) and (6.20) into (6.18) gives

$$rx'(r) = -2(n-1)zk(r) - \frac{(n-1)}{2}q(r)x(r),$$

$$rq'(r) = \frac{\chi}{(n-1)} - zk(r)^2 - \frac{n}{4}q(r)^2 - \frac{1}{4(n-1)}x(r)^2,$$

$$rk'(r) = -\frac{\chi}{(n-1)}\frac{k(r)}{q(r)} - \frac{zk(r)^3}{q(r)} + \frac{(n-2)}{4}k(r)q(r) - \frac{x(r)}{2} + \frac{1}{4(n-1)}\frac{k(r)x(r)^2}{q(r)}. \quad (6.21)$$

So far we have worked with a general value of z in $(n+1)$ dimensions. We are interested in studying the effects of marginal operators, which have scaling dimension $z+n-1$ in Lifshitz spacetime, because of the different scaling of the time coordinate. While it has been shown that the linearized equation of motion for the scalar part of constant perturbations in a Lifshitz background in $(3+1)$ dimensions [79] (and the gravitational field has solutions that are marginal for general z), the vector field only admits a single degenerate solution at the special value of $z = 2$, where the vector operator also becomes marginal. Applying this analysis to $(n+1)$ dimensions [18], the condition for having a single degenerate solution for the vector field becomes $z = n - 1$, and this condition also is required from the equations of motion to ensure non-trivial sub-leading orders of the asymptotic solutions. Henceforth we deal with the case satisfying $z = n - 1$.

Then, in terms of the new variables $k(r)$, $q(r)$, and $x(r)$, Lifshitz spacetime is described by

$$\text{Lifshitz}: \quad q = -2 \quad x = 2\sqrt{z-1}\sqrt{z}, \quad k = \frac{\sqrt{z-1}}{\sqrt{z}}, \quad (6.22)$$

whereas for AdS spacetime

$$\text{AdS}: \quad q = -2\sqrt{\frac{3n-4}{n}}, \quad x = 0, \quad k = 0. \quad (6.23)$$

6.3 Asymptotic Behaviour

We consider the spacetime slightly thermally heated and so slightly deformed from the pure Lifshitz case, restricting our considerations to $z = n - 1$. Under these assumptions,

the general asymptotic solutions near the boundary i.e. $r \to 0$ become

$$k(r) = \frac{\sqrt{z-1}}{\sqrt{z}}$$

$$\times \left(1 + \frac{1}{(z-1)^2 \log(r\Lambda)} + \frac{(z-1)(-3z+2(z-1)^3\lambda) + 2(1-3z)\log(-\log(r\Lambda))}{2z(z-1)^4 \log^2(r\Lambda)} + \cdots\right)$$

$$+ (r\Lambda)^{2z} \log^2(r\Lambda)\left(\beta\left(1 + \frac{2(3z-1)\log(-\log(r\Lambda))}{z(z-1)^2\log(r\Lambda)} + \cdots\right) + \alpha\left(\frac{1}{\log(r\Lambda)} + \right.\right.$$

$$\left.\left.\frac{(2z^2-4z+1) - 2(z-1)^4(2z-1)\lambda + 2(6z^2-5z+1)\log(-\log(r\Lambda))}{2z(z-1)^2(2z-1)\log^(r\Lambda)} + \cdots\right)\right),$$

$$(6.24)$$

$$q(r) = -2\left(1 - \frac{1}{(z-1)\log(r\Lambda)} - \frac{z + 2(z-1)^4\lambda - 2(3z-1)\log(-\log(r\Lambda))}{2z(z-1)^3\log^2(r\Lambda)} + \cdots\right)$$

$$- \frac{2\sqrt{z-1}\sqrt{z}}{2z-1}(r\Lambda)^{2z}$$

$$\times \log^2(r\Lambda)\left(\beta\left(1 + \frac{-z(4z^2-7z+2) + 2(2z-1)(3z-1)\log(-\log(r\Lambda))}{z(z-1)^2(2z-1)\log(r\Lambda)} + \cdots\right)\right.$$

$$\left.+ \alpha\left(\frac{1}{\log(r\Lambda)} - \frac{(2z^2-4z+1) + 2(z-1)^4\lambda - 2(3z-1)\log(-\log(r\Lambda))}{2z(z-1)^2\log^2(r\Lambda)} + \cdots\right)\right),$$

$$(6.25)$$

$$x(r) = 2\sqrt{z-1}\sqrt{z}\left(1 + \frac{z}{(z-1)^2\log(r\Lambda)} + \frac{(z-1)^4\lambda + (1-3z)\log(-\log(r\Lambda))}{(z-1)^4\log^2(r\Lambda)} + \cdots\right)$$

$$- \frac{2z^2}{2z-1}(r\Lambda)^{2z}$$

$$\times \log^2(r\Lambda)\left(\beta\left(1 + \frac{-z(4z^2-5z+1) + 2(6z^2-5z+1)\log(-\log(r\Lambda))}{z(z-1)^2(2z-1)\log(r\Lambda)} + \cdots\right)\right.$$

$$\left.+ \alpha\left(\frac{1}{\log(r\Lambda)} - \frac{(2z-1)^2 + 2(z-1)^4\lambda - 2(3z-1)\log(-\log(r\Lambda))}{2z(z-1)^2\log^2(r\Lambda)} + \cdots\right)\right), \quad (6.26)$$

where Λ is a momentum scale, which generates a marginally relevant modes, and Λ^z becomes an energy scale. As $\Lambda \to 0$, the solution recovers the pure Lifshitz spacetime. The parameters α and β describe other modes of the solution, and λ is nothing but a 'gauge choice' [25]. In other words λ is related to defining the scale Λ, and the solution $\{k, q, x\}$ transforms as

$$F(\Lambda r; \alpha, \beta; \lambda) = F(e^{\lambda'/z}\Lambda r; e^{-2\lambda'}(\alpha - \lambda'\beta), e^{-2\lambda'}\beta; \lambda + \lambda') \quad (6.27)$$

where F stands for the k, q and x functions. This is easily verified by noting that the solutions k, q and x with $\lambda = 0$ can be obtained by setting $\lambda' = -\lambda$, and replacing Λr, α, and β with $e^{-\lambda/z}\Lambda r$, $e^{2\lambda}(\alpha + \lambda\beta)$, and $e^{2\lambda}\beta$ respectively, and then re-expanding the solutions under the assumption $|\log(\Lambda r)| \gg |\lambda|$. Here we fix this ambiguity by setting $\lambda = 0$.

Since the Lifshitz spacetime lies in the high energy regime, we expand the solutions by introducing an arbitrary scale μ so that we can control the energy scale, and write

$$\log(r\Lambda) = \log(r\mu) - \log\frac{\mu}{\Lambda}. \tag{6.28}$$

In the high energy regime where $\mu \gg \Lambda$, we can have an approximation such as

$$\left|\frac{1}{\log\frac{\mu}{\Lambda}}\right|, \quad \left|\frac{\log(r\mu)}{\log\frac{\mu}{\Lambda}}\right| \leqslant 1. \tag{6.29}$$

Upon expansion, equations (6.24) $\sim$ (6.26) become

$$k(r) = \frac{\sqrt{z-1}}{\sqrt{z}}$$
$$\times \left(1 + \frac{1}{(z-1)^2\log(\frac{\mu}{\Lambda})} - \frac{3z(z-1) + 2z(z-1)^2\log(r\mu) + 2(3z-1)\log(-\log(\frac{\mu}{\Lambda}))}{2z(z-1)^4\log^2(\frac{\mu}{\Lambda})} + \cdots\right),$$
$$\tag{6.30}$$

$$q(r) = -2\left(1 - \frac{1}{(z-1)\log(\frac{\mu}{\Lambda})} + \frac{-z + 2z(z-1)^2\log(r\mu) + 2(3z-1)\log(-\log(\frac{\mu}{\Lambda}))}{2z(z-1)^3\log^2(\frac{\mu}{\Lambda})} + \cdots\right),$$
$$\tag{6.31}$$

$$x(r) = 2\sqrt{z-1}\sqrt{z}\left(1 + \frac{z}{(z-1)^2\log(\frac{\mu}{\Lambda})} - \frac{z(z-1)^2\log(r\mu) + (3z-1)log(-\log(\frac{\mu}{\Lambda}))}{(z-1)^4\log^2(\frac{\mu}{\Lambda})} + \cdots\right).$$
$$\tag{6.32}$$

Using these solutions for $k(r), q(r)$ and $x(r)$, we employ the change of variables (6.19) and

(6.20) in reverse to obtain the original form of the solutions

$$f(\rho) = \frac{F_0^2}{(r\Lambda)^{2z}(-\log(r\Lambda))^{\frac{2z}{z-1}}}\left(1 - \frac{(7z-4) + 2(3z-1)\log(-\log(r\Lambda))}{(z-1)^3\log(r\Lambda)}\right.$$
$$-\frac{(23z^4 - 142z^3 + 152z^2 - 57z + 6)}{4z(z-1)^6\log^2(r\Lambda)}$$
$$\left.+ \frac{(3z-1)^2(5z-2)\log(-\log(r\Lambda)) + (3z-1)^3\log^2(-\log(r\Lambda))}{z(z-1)^6\log^2(r\Lambda)} + \cdots\right) \qquad (6.33)$$

$$p(\rho) = \frac{P_0^2(-\log(r\Lambda))^{\frac{2}{z-1}}}{(r\Lambda)^2}\left(1 + \frac{(5z-2) + 2(3z-1)\log(-\log(r\Lambda))}{z(z-1)^3\log(r\Lambda)}\right.$$
$$+ \frac{(31z^4 - 64z^3 + 106z^2 - 69z + 14)}{4z^2(z-1)^6\log^2(r\Lambda)}$$
$$\left.+ \frac{(3z^3 + 26z^2 - 21z + 4)\log(-\log(r\Lambda)) + (3z-1)^2(z-3)\log^2(-\log(r\Lambda))}{z^2(z-1)^6\log^2(r\Lambda)} + \cdots\right)$$
$$(6.34)$$

where F_0 and P_0 are constants. These expressions (6.33)-(6.34) also should be computed in the high energy regime by applying (6.29)

$$f(\rho) = \frac{1}{r^{2z}}\left(1 + \frac{7z - 4 + 2z(z-1)^2\log(r\mu) + 2(3z-1)\log(\log(\frac{\mu}{\Lambda}))}{(z-1)^3\log(\frac{\mu}{\Lambda})} + \cdots\right), \qquad (6.35)$$

$$p(\rho) = \frac{1}{r^2}\left(1 - \frac{5z - 2 + 2z(z-1)^2\log(r\mu) + 2(3z-1)\log(\log(\frac{\mu}{\Lambda}))}{z(z-1)^3\log(\frac{\mu}{\Lambda})} + \cdots\right) \qquad (6.36)$$

upon rescaling the t and x coordinates to

$$t \to \left(\Lambda\,\log^{\frac{1}{z-1}}(\frac{\mu}{\Lambda})\right)^z\frac{1}{F_0}t, \quad x \to \frac{\Lambda}{\log^{z-1}(\frac{\mu}{\Lambda})}\frac{1}{P_0}x. \qquad (6.37)$$

6.4   Holographic Renormalization

In this section we derive physical quantities such as free energy density or energy density at an asymptotic boundary of the deformed Lifshitz spacetime. We begin with the definition of the free energy density

$$F = -T\log\mathcal{Z} = TS_\epsilon(g_*) \qquad (6.38)$$

71

where S_ϵ and g_* are respectively the Euclidean action and the metric, and $\mathcal{Z}$ is the partition function. Upon carrying out a variation of the on-shell action, boundary terms arise, and to cancel these out a Gibbons-Hawking boundary term is added into the action. After Euclideanization, the action and the metric can be explicitly written as

$$S_\epsilon = \int d^{n+1}x \sqrt{g} \left(\frac{1}{2\kappa_{n+1}^2}[R + 2\tilde{\Lambda}] - \frac{1}{g_v^2}[\frac{1}{4}H^2 + \frac{\gamma}{2}B^2] \right) + \frac{1}{\kappa_{n+1}^2} \int d^n x \sqrt{\gamma} K, \quad (6.39)$$

$$ds_\epsilon^2 = l^2 \left(f(r)d\tau^2 + \frac{dr^2}{r^2} + p(r)(dx^2 + dy^2 + \cdots) \right), \quad (6.40)$$

where ϵ indicates the Euclidean version of the quantities.

Calculating the free energy density (the free energy per unit $(n-1)$-dimensional spatial volume), the Einstein-Hilbert action and Gibbons-Hawking term yield

$$\mathcal{F}_{\text{EH}} = -\frac{l^{n-1}}{2\kappa_{n+1}^2} \lim_{r\to 0} r \sqrt{f(r)} p'(r) p(r)^{\frac{n-3}{2}}, \quad (6.41)$$

$$\mathcal{F}_{\text{GH}} = \frac{1}{\kappa_{n+1}^2} \lim_{r\to 0} \sqrt{\gamma} K = \frac{l^{n-1}}{\kappa_{n+1}^2} \lim_{r\to 0} r \left(\sqrt{f(r)} p(r)^{\frac{n-1}{2}} \right)' \quad (6.42)$$

where γ_{ab} is the induced metric on the boundary and $K_{\mu\nu}$ is the extrinsic curvature defined as $K_{\mu\nu} = \nabla_\mu n_\nu$ in which n_ν is the normal vector on the boundary surface. The free energy is $F = \int d^{n-1}x \mathcal{F}$. However for the marginally relevant modes both (6.41) and (6.42) are divergent as the boundary ($r \to 0$) is approached. We incorporate boundary counterterms [79, 10, 65, 78] into the action as a remedy for this problem. We construct these counterterms as a power series in $B^2 = B^\mu B_\mu$ [25], so as to satisfy covariance at the boundary, obtaining

$$\mathcal{F}_{\text{C.T.}} = \frac{1}{2l\kappa_{n+1}^2} \lim_{r\to 0} \sqrt{\gamma} \sum_{j=0}^{2} C_j \left(-\frac{\kappa_{n+1}^2}{g_v^2} B^2 - \frac{(z-1)}{z} \right)^j \quad (6.43)$$

$$= \frac{l^{n-1}}{2\kappa_{n+1}^2} \lim_{r\to 0} \sqrt{f(r)} p(r)^{\frac{n-1}{2}} \sum_{j=0}^{2} C_j \left(k(r)^2 - \frac{(z-1)}{z} \right)^j \quad (6.44)$$

where we have used $(B^2 - (z-1)/z)$ instead of B^2, since these must vanish for the pure Lifshitz case. The coefficients C_j are not constants but rather a series of logarithmic functions, with at least three needed to eliminate divergences.

The final expression for the free energy density is

$$\mathcal{F} = \mathcal{F}_{\text{EH}} + \mathcal{F}_{\text{GH}} + \mathcal{F}_{\text{C.T.}}$$

$$= \frac{l^{n-1}}{2\kappa_{n+1}{}^2} \lim_{r\to 0} \sqrt{f(r)}p(r)^{\frac{n-1}{2}} \left(\frac{(n-2)rp'(r)}{p(r)} + \frac{rf'(r)}{f(r)} + \sum_{j=0}^{2} C_j \left(k(r)^2 - \frac{(z-1)}{z} \right)^j \right).$$
(6.45)

To obtain the energy density, we use the definition of the boundary stress tensor to the case in which additional non-vanishing boundary fields are present [50]. From the variation of the action, we obtain

$$\delta S = \frac{\sqrt{\gamma}}{2}\tau^{ab}\delta\gamma_{ab} + \mathcal{J}^a \delta B_a.$$
(6.46)

where τ^{ab} is the boundary stress tensor. However we are here dealing not with scalar matter fields but with massive vector fields, and so the usual charge defined by

$$Q = -\int d^{n-2}x \sqrt{\sigma}\xi_a k_b \tau^{ab}$$
(6.47)

where $\sqrt{\sigma} = \sqrt{\gamma_{xx} \cdots \gamma_{zz}}$ is the spatial volume element, ξ_a is a boundary Killing fields, and k_b is the unit normal vector to the boundary Cauchy surface, is not conserved. The boundary stress tensor τ^{ab} must therefore be redefined so as to fix the matter fields in the boundary. Employing the vielbein frame defined by

$$\gamma_{ab} = \eta_{\hat{a}\hat{b}}e_a^{\hat{a}}e_b^{\hat{b}}, \quad \eta = \text{diag}(\pm 1, 1, 1, \cdots)$$
(6.48)

where

$$e^{\hat{t}} = e_a^{\hat{t}}dx^a = \sqrt{f}d\tau, \quad e^{\hat{x}_i} = \sqrt{p}\,dx_i.$$
(6.49)

We find that the variation of the free energy density retains its original form, but that τ^{ab} is replaced with $\mathcal{T}^{ab}$, where

$$\delta S = \sqrt{\gamma}\mathcal{T}_{\hat{a}}^a \delta e_a^{\hat{a}} + \mathcal{J}^{\hat{a}}\delta B_{\hat{a}},$$
(6.50)

with

$$\mathcal{T}^{ab} = \mathcal{T}_{\hat{a}}^a e^{b\hat{a}}, \quad \mathcal{T}^{ab} = \tau^{ab} + \frac{1}{\sqrt{\gamma}}\mathcal{J}^{(a}B^{b)}.$$
(6.51)

The energy density is then given by

$$\mathcal{E} = \sqrt{\gamma}\tau^t{}_t + \mathcal{J}^t B_t$$
(6.52)

and the pressure is

$$\mathcal{P} = -\sqrt{\gamma}\tau^x{}_x. \tag{6.53}$$

Computing the distinct components of $\mathcal{E}$, we find

$$\tau^{ab} = \frac{2}{\sqrt{\gamma}}\frac{\delta S}{\delta\gamma_{ab}} = \frac{1}{\kappa_{n+1}{}^2}(K\gamma^{ab} - K^{ab}) + \frac{1}{2l\kappa_{n+1}{}^2}\sum_{j=0}^{2}C_j\left(\gamma^{ab}\left(-\frac{\kappa_{n+1}{}^2}{g_v^2}B^2 - \frac{(z-1)}{z}\right)^j\right.$$
$$\left. + \frac{2j\kappa_{n+1}{}^2}{g_v^2}B^aB^b\left(-\frac{\kappa_{n+1}{}^2}{g_v^2}B^2 - \frac{(z-1)}{z}\right)^{j-1}\right), \tag{6.54}$$

and

$$\mathcal{J}^{\hat{t}} = \sqrt{f(r)}\frac{\delta S}{\delta B_t},$$
$$= \frac{l^{n-2}}{g_v\kappa_{n+1}}\lim_{r\to0}\sqrt{f(r)}p(r)^{\frac{n-1}{2}}\left(\frac{r(k(r)\sqrt{f(r)})'}{\sqrt{f(r)}} + k(r)\sum_{j=0}^{2}jC_j\left(k(r)^2 - \frac{(z-1)}{z}\right)^{j-1}\right),$$
$$= \frac{l^{n-2}}{g_v\kappa_{n+1}}\lim_{r\to0}\sqrt{f(r)}p(r)^{\frac{n-1}{2}}\left(-\frac{1}{2}x(r) + k(r)\sum_{j=0}^{2}jC_j\left(k(r)^2 - \frac{(z-1)}{z}\right)^{j-1}\right), \tag{6.55}$$

and other component of $\mathcal{J}^a$ become zero. Putting these together into (6.52) yields

$$\mathcal{E} = \frac{l^{n-1}}{2\kappa_{n+1}{}^2}\lim_{r\to0}\sqrt{f(r)}p(r)^{\frac{n-1}{2}}\left(\frac{(n-1)rp'(r)}{p(r)} - x(r)k(r) + \sum_{j=0}^{2}C_j\left(k(r)^2 - \frac{(z-1)}{z}\right)^j\right) \tag{6.56}$$

and

$$\mathcal{P} = -\mathcal{F}. \tag{6.57}$$

To obtain a well-defined action principle, physical quantities of $\mathcal{F}$ (6.45), $\mathcal{E}$ (6.55), and $\mathcal{J}^{\hat{t}}$ (6.56) should be finite with the asymptotic solutions (6.24)-(6.26), and the counterterms

to render them finite are found to be

$$C_0 = 2(2z - 1) - \frac{2z^2}{(2z-1)(z-1)^3 \log^2(r\Lambda)} + \frac{(4z^4 + 2z^3 - 3z^2 - 2z + 1)}{(z-1)^5(2z-1)^2 \log^3(r\Lambda)}$$
$$+ \frac{4z(3z-1)\log(-\log(r\Lambda))}{(z-1)^5(2z-1)\log^3(r\Lambda)} + \cdots , \tag{6.58}$$

$$C_1 = z + \frac{2z^3}{(2z-1)(z-1)^2 \log(r\Lambda)}$$
$$- \frac{z(14z^3 - z^2 - 10z + 3) + 4z^2(2z-1)(3z-1)\log(-\log(r\Lambda))}{2(2z-1)^2(z-1)^4 \log^2(r\Lambda)}$$
$$- \frac{1}{\log^3(r\Lambda)} \left(\frac{z^2(34z^4 - 54z^3 + 72z^2 - 46z + 9) + 8a(2z-1)^2(z-1)^5}{2z(2z-1)^2(z-1)^6} \right.$$
$$\left. - \frac{(6z^4 + 25z^3 - 45z^2 + 21z - 3)\log(-\log(r\Lambda))}{(2z-1)^2(z-1)^6} - \frac{2z(3z-1)^2 \log^2(-\log(r\Lambda))}{(z-1)^6(2z-1)} \right) + \cdots , \tag{6.59}$$

$$C_2 = \frac{z^2(1 - 3z)}{4(2z-1)(z-1)} + \frac{z^2(15z^2 - 14z + 3)}{4(2z-1)^2(z-1)^3 \log(r\Lambda)} + \frac{a}{\log^2(r\Lambda)}$$
$$- \frac{z(3z-1)^2(5z-3)\log(-\log(r\Lambda))}{4(2z-1)^2(z-1)^5 \log^2(r\Lambda)} \tag{6.60}$$

where the first two are infinite series in $1/\log(r\Lambda)$ that include powers of $\log(-\log(r\Lambda))$ such that the order of the $\log(-\log(r\Lambda))$ terms do not exceed the order of the $1/\log(r\Lambda)$ terms. It is sufficient for C_2 to retain terms up to second order in $1/\log(r\Lambda)$. Note that there exists an ambiguity a in these expressions. This ambiguity does not affect numerical evaluation of the free energy density and the energy density that we shall later compute, though it does affect $\mathcal{J}^{\hat{t}}$, reflecting the reaction of the system to changes in the boundary Proca field. Our counterterm construction (6.58) – (6.60) is minimal; additional terms such as $C_3(B^2 - (z-1)/z)^3$ or $C_4(B^2 - (z-1)/z)^4$ would also yield solutions.

Applying (6.58)-(6.60) into (6.45), (6.55) and (6.56), the physical quantities become

$$\mathcal{F} = \frac{l^{n-1}}{\kappa_{n+1}^2} \frac{\sqrt{z}}{\sqrt{z-1}(2z-1)} \left(z\alpha - \frac{(2z^3 - 2z^2 - 2z + 1)}{(2z-1)(z-1)^4} \beta \right), \tag{6.61}$$

$$\mathcal{E} = -\frac{l^{n-1}}{\kappa_{n+1}^2} \frac{\sqrt{z}}{\sqrt{z-1}(2z-1)} \left(z\alpha + \frac{(2z^3 - 4z^2 + 4z - 1)}{(2z-1)(z-1)^4} \beta \right), \tag{6.62}$$

$$\mathcal{J}^{\hat{t}} = \frac{1}{g_v} \frac{l^{n-2}}{\kappa_{n+1}} \left(\frac{z(20z^5 + 18z^4 - 22z^3 - 23z^2 + 24z - 5)}{2(z-1)^4(2z-1)^3} + \frac{4(z-1)a}{z} \right) \beta. \tag{6.63}$$

75

Since the pure Lifshitz solution does not depend on α and β, we expect in this case that

$$\mathcal{F} = \mathcal{E} = \mathcal{J}^{\hat{t}} = 0 \tag{6.64}$$

regardless of the dimension of spacetime.

6.5   Finite Temperature

In this section, we consider the finite temperature theory by obtaining the expanded black hole solution near horizon. Our goal is to describe the renormalization group (RG) flow of the marginally relevant modes, and to predict behaviour of physical quantities such as the free energy density $\mathcal{F}$ and the energy density $\mathcal{E}$ near critical regimes in order to provide a way of understanding the quantum phase transition from one phase to the critical point via the holographic dictionary. For these purposes, we find that the RG flow is ensured in the zero temperature limit $\Lambda^z/T \to \infty$ with $\Lambda \sim 0$ fixed, as found in [56]. We also investigate the behaviours of $\mathcal{F}/Ts$ and $\mathcal{E}/Ts$ as functions of $\log(\Lambda^z/T)$ at high temperature regime $\Lambda^z/T \to 0$.

6.5.1   Expansion and Physical quantities near horizon

We assume a black hole solution which is defined by $f(r_+) = 0$ in the metric form of (6.14). With an ansatz for the expanded form of the black hole solution, which are constructed in a way that regularity requires g_{tt} to have a double zero at the horizon and g_{xx} remains nonzero, the equations of the motion (6.18) yield

$$f(r) = f_0\left(\left(1 - \frac{r}{r_+}\right)^2 + \left(1 - \frac{r}{r_+}\right)^3 + \frac{(-6z^2 + 14z + 7)z + 8(3z - 2)h_0^2}{12z}\left(1 - \frac{r}{r_+}\right)^4 + \cdots\right), \tag{6.65}$$

$$p(r) = p_0\left(1 + \frac{(3z - 1)z - 4h_0^2}{2z}\left(1 - \frac{r}{r_+}\right)^2 + \frac{(3z - 1)z - 4h_0^2}{2z}\left(1 - \frac{r}{r_+}\right)^3 + \cdots\right), \tag{6.66}$$

$$h(r) = \sqrt{f_0}\left(h_0\left(1 - \frac{r}{r_+}\right)^2\right.$$
$$\left. + h_0\left(1 - \frac{r}{r_+}\right)^3 + h_0\left(\frac{z(-9z^2 + 10z + 20) + 8h_0^2(3z - 1)}{24z}\right)\left(1 - \frac{r}{r_+}\right)^4 + \cdots\right) \tag{6.67}$$

76

where the constants f_0 and p_0 are associated with scaling ambiguities of the coordinates $\{t, x, y, \cdots\}$, which function as the clock and rulers of the system. Upon fixing these, the only variable left in the metric is h_0. Different values of h_0 correspond to different black holes and so we have a 1-parameter family of black hole solutions.

With (6.65)-(6.67), thermodynamic quantities can be calculated near the horizon of the black hole. The temperature T is a quantity coming from demanding regularity of the spacetime at the horizon, which is satisfied by identifying the imaginary time coordinate τ with the spherical coordinate ϕ such as $\phi = \beta\tau$ with $\rho^2 = \alpha(r - r_+)^2$. That is, the Euclideanized metric components (τ, r) correspond to (ρ, ϕ) components of the spherical coordinate

$$f(r)d\tau^2 + \frac{dr^2}{r^2} \sim d\rho^2 + \rho^2 d\phi^2, \tag{6.68}$$

and substituting τ with ϕ and r with ρ, it yields that $\alpha = \frac{1}{r_+}$ and $\beta = r_+\sqrt{\frac{1}{2}\frac{d^2 f}{dr^2}}$ where $T = \frac{\beta}{2\pi}$. The entropy density, s, obtained from the definition of the entropy, $S = \frac{A}{4G_{n+1}}$. Then we find

$$T = \frac{r_+}{2\pi}\sqrt{\frac{1}{2}\frac{d^2 f(r)}{dr^2}}\bigg|_{r=r_+}, \tag{6.69}$$

$$s = 2\pi\frac{l^{n-1}}{\kappa_{n+1}^2}p(r_+)^{\frac{n-1}{2}}, \tag{6.70}$$

where $S = \int s\, d^{n-1}x$.

The horizon flux, Φ, of the massive vector field is

$$\Phi = \oint \sqrt{h}\vec{H} \cdot d\vec{A} = \oint \phi\, d^{n-1}x \tag{6.71}$$

where

$$\phi = \frac{l^{n-2}g_v r_+}{\kappa_{n+1}}\left(\frac{p(r)^{\frac{n-1}{2}}}{\sqrt{f(r)}}\frac{dh(r)}{dr}\right)\bigg|_{r=r_+} \tag{6.72}$$

is the horizon flux density. Using (6.65)-(6.67) we obtain

$$T = \frac{\sqrt{f_0}}{2\pi}, \quad s = 2\pi p_0^{\frac{n-1}{2}}\frac{l^{n-1}}{\kappa_{n+1}^2}, \quad \phi = 2h_0 p_0^{\frac{n-1}{2}}\left(\frac{l^{n-2}g_v}{\kappa_{n+1}}\right). \tag{6.73}$$

for the temperature, entropy density, and horizon flux density, and as shown above, those are determined by parameters (f_0, p_0, and h_0) of the metric.

77

6.5.2 Integrated First law of thermodynamics

Before embarking on our numerical calculations, in this section we obtain relationships between the free energy density and the energy density derived in section 6.4 via the thermodynamic variables s and T.

First, by using the asymptotic solutions (6.24) – (6.26) we construct an r-independent RG-invariant quantity

$$
\begin{aligned}
\bar{K} &= -\frac{1}{2}\sqrt{f(r)}p(r)^{\frac{n-1}{2}}\left(-q(r) + m(r) + k(r)x(r)\right), \\
&= -\frac{\sqrt{f(r)}p(r)^{\frac{n-1}{2}}}{4(n-1)q(r)}\left(4\chi + 4(n-1)zk(r)^2 - n(n-1)q(r)^2 - x(r)^2 + 2(n-1)q(r)k(r)x(r)\right),
\end{aligned}
\tag{6.74}
$$

where plugging (6.30)-(6.32) into the above gives

$$
\bar{K} = \frac{2\sqrt{z}}{\sqrt{z-1}(1-2z)}\left(z\alpha - \frac{(z^2 - 3z + 1)}{(1-2z)(z-1)^2}\beta\right).
\tag{6.75}
$$

Near the horizon, this RG-invariant quantity is calculated by using (6.65)-(6.67) and expressed in terms of T and s by applying (6.73), which is

$$
\bar{K} = \sqrt{f_0}p_0^{\frac{n-1}{2}} = Ts\frac{\kappa_{n+1}^2}{l^{n-1}}.
\tag{6.76}
$$

Next, from the free energy density (6.45) and the energy density (6.56) we obtain the following relation

$$
\begin{aligned}
&\frac{1}{2}\sqrt{f(r)}p(r)^{\frac{n-1}{2}}\left(\frac{(n-1)rp'(r)}{p(r)} - x(r)k(r) + \sum_{j=0}^{2}C_j\left(k(r)^2 - \frac{(z-1)}{z}\right)^j\right) \\
&= \frac{1}{2}\sqrt{f(r)}p(r)^{\frac{n-1}{2}}\left(\frac{(n-2)rp'(r)}{p(r)} + \frac{rf'(r)}{f(r)} + \sum_{j=0}^{2}C_j\left(k(r)^2 - \frac{(z-1)}{z}\right)^j\right) + \bar{K},
\end{aligned}
\tag{6.77}
$$

which is more simply expressed as

$$
\mathcal{E} = \mathcal{F} + \frac{l^{n-1}}{\kappa_{n+1}^2}\bar{K}.
\tag{6.78}
$$

This relation is easily checked using (6.61), (6.62) and (6.76).

Finally, combining (6.76) with (6.78) gives

$$\mathcal{F} = \mathcal{E} - Ts. \tag{6.79}$$

which is the integrated form of the first law for these black holes. We will use this to check the accuracy of our numerical results in section 6.6.

Considering the limit $\Lambda = 0$, since anisotropic scale invariance still holds, from the Ward identity we expect that the pressure is equal to the energy [86]. From (6.57), we have

$$\mathcal{F}_0 = -\mathcal{E}_0 \qquad (\Lambda = 0), \tag{6.80}$$

and in conjunction with (6.79), we obtain an analytic prediction for when the marginally relevant modes are not excited

$$\mathcal{F}_0 = -\mathcal{E}_0 = -\frac{1}{2}Ts_0 \quad (\Lambda = 0), \tag{6.81}$$

which will be used for a consistency check on our numerical results in section 6.6. Note that the relation $\mathcal{F} = -\mathcal{E}$ also holds for $\Lambda \sim 0$ case when $\beta = 0$, as is easily seen from equations (6.61) and (6.62).

6.6 Exploring Near the Quantum Critical Point

6.6.1 Integrating towards the Lifshitz Boundary

To investigate Lifshitz spacetime in the UV-region, $T \gg \Lambda^z$, we re-expand the asymptotic solutions into the high energy regime by using (6.29), and set the arbitrary scale $\mu \sim r_+^{-1}$, thereby making the spacetime near-Lifshitz. This spacetime approaches an asymptotically pure-Lifshitz having the black hole by supplying heat at much greater temperatures or higher energy scales.

In this section, we numerically connect the expanded near-horizon black hole solution with the near-Lifshitz asymptotic solution. By matching two solutions, we determine values of $\log(\Lambda r_+)$ for given h_0, and then use these values to fix values of f_0 and p_0. With these values fixed we compute the free energy density $\mathcal{F}$ and energy density $\mathcal{E}$ versus $\log(r/r_+)$ varying the value of h_0. By collecting these data, we plot the free energy density and energy density as functions of $\log(\Lambda^z/T)$ and find their fitting functions, which gives the sub-leading dependence of the free energy and energy density as a function of $\log(\Lambda^z/T)$ for $\Lambda \neq 0$. We also discuss how renormalization group flow is described in our context. In our numerical work, we use r/r_+ as our radial variable, and unitless quantities such as $\mathcal{F}/Ts$, $\mathcal{E}/Ts$, and Λ^z/T are considered.

Matching Λ

For extracting Λ, we start with the asymptotic solutions $k(r)$, $q(r)$, and $x(r)$ in (6.30)-(6.32), which are expanded ones to high energy regime by introducing the arbitrary scale $\mu \gg \Lambda$ eventually setting $\mu \to r_+^{-1}$. In the asymptotic solutions, we have only the variable $\log(\Lambda r_+)$ to be fixed. While near the horizon, the expanded black hole solutions (6.65)–(6.67) are changed to functions of $k(r)$, $q(r)$, and $x(r)$ by (6.19) and (6.20), and in this process f_0 and p_0 drop out and h_0 only remains. Now, given values of h_0, we numerically integrate the near horizon solution toward the boundary satisfying the equations of motion (6.21), and match the numerical solutions with the asymptotic expectation by adjusting the value of $\log(\Lambda r_+)$ in the middle region. In our numerical work, the integration starts at $\log(r/r_+) \sim -0.015$ and ends at $\log(r/r_+) \sim -10^4$. Our numerical results for the k function are shown in Figure 6.1, where the red dashed line is a fit for the asymptotic expectation, the blue solid line corresponds to the numerical results, and the dots signify the values used for finding the matching condition. We note that the agreement between our numerical results and the asymptotic expectations is very strong.

The important outcome of this procedure is that a maximum value of h_0 is obtained. In other words, if we keep increasing the value of h_0 then beyond a certain point we are not able to find a matching condition connecting our numerical result to the asymptotic expectation. Physically this means that at a large value of flux, the metric functions grow exponentially as the boundary is approached, so they do not ever reach the boundary. This means that under the condition of large flux and high temperature $\Lambda^z/T \to 0$, the spacetime having the black hole (6.65)–(6.67) is no longer deformed, but rather is asymptotic to pure Lifshitz spacetime. We also find that the maximum values of h_0 linearly increased according to the critical exponent, z (or the spatial dimension) of the spacetime, n. We present this behaviour in Figure B.1, and explicitly denote the maximum values of h_0 in Table 6.1.

On the other hand, a minimum value of the flux also exists and its value becomes zero at the horizon. In this case, the massive vector field disappears and the spacetime is described by an asymptotically AdS black hole.

Examining the situation for h_0 between 0 and h_{min} is non-trivial. However for a very small amount of flux, we expect that the renormalization group flow is recovered in the zero temperature limit $\Lambda^z/T \to \infty$, which is found in [56]. That is, this result implies that tuning the horizon flux via h_0 interpolates between the zero temperature RG flow [56] and asymptotic Lifshitz black holes [79, 86, 14, 62, 29, 15].
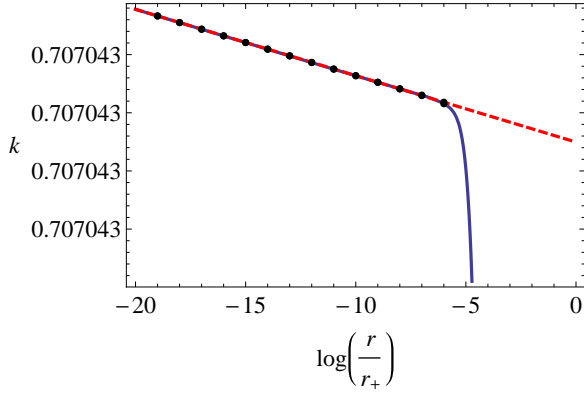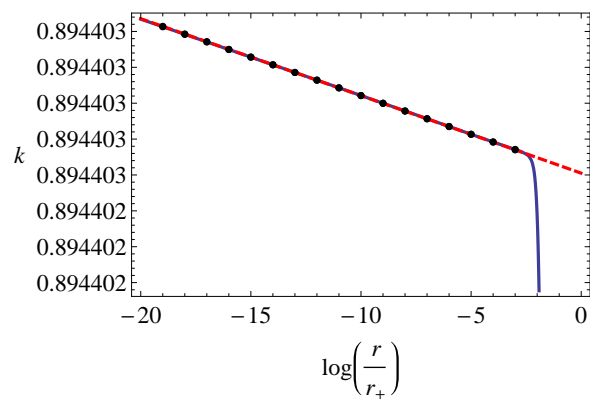
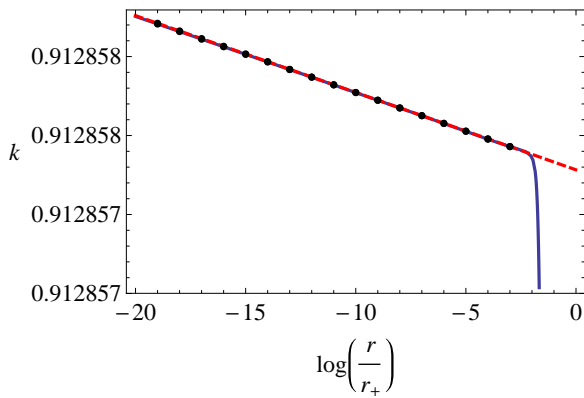(a) $z = 2$ and $h_0 = 0.97128$, $\log(\Lambda r_+) = -11141.7$
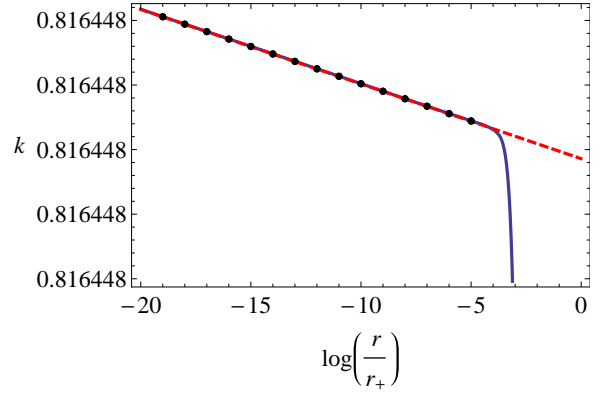
(b) $z = 3$ and $h_0 = 1.63428$, $\log(\Lambda r_+) = -4188.2$
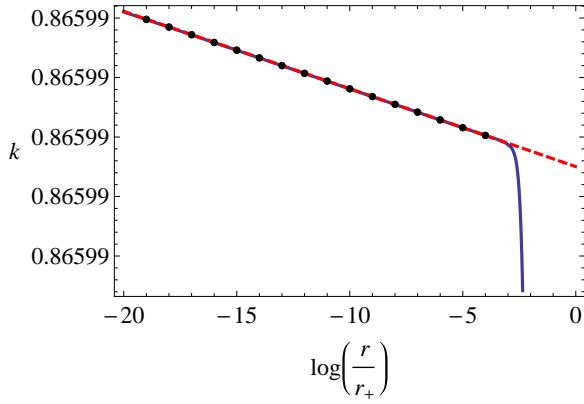
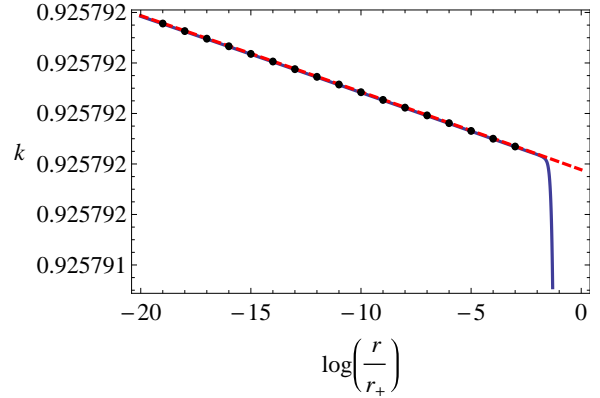(c) $z = 4$ and $h_0 = 2.28218$, $\log(\Lambda r_+) = -2709.4$

(d) $z = 5$ and $h_0 = 2.92548$, $\log(\Lambda r_+) = -2270.6$

(e) $z = 6$ and $h_0 = 3.56678$, $\log(\Lambda r_+) = -2726$

(f) $z = 7$ and $h_0 = 4.20680$, $\log(\Lambda r_+) = -908.7$
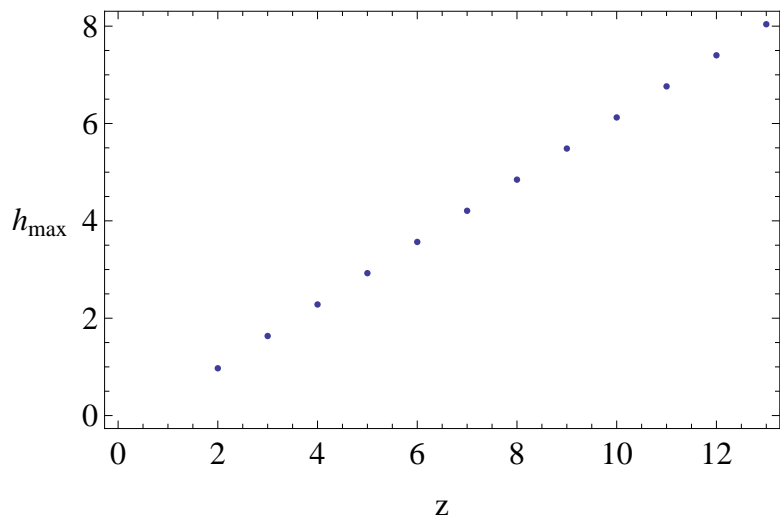
Figure 6.1: Extracting $\log(\Lambda r_+)$

Figure 6.2: h_{max} versus z

	h_{max}
$z = 2$	0.9713
$z = 3$	1.6343
$z = 4$	2.2822
$z = 5$	2.9255
$z = 6$	3.5668
$z = 7$	4.2070
$z = 8$	4.8465
$z = 9$	5.4856
$z = 10$	6.1244
$z = 11$	6.7629
$z = 12$	7.4012
$z = 13$	8.0394
$\vdots$	$\vdots$

Table 6.1: maximum value of h_0

Matching f_0, and p_0

Since, given h_0, $\log(\Lambda r_+)$ is fixed, f_0 and p_0 arising in (6.65) – (6.67) can be determined by repeating the previous process with the functions of f, p, and h. Here we start with (6.35)–(6.36), where we can neglect the α and β involved in the exponent terms because these contribute much less than the logarithmic terms as the boundary is approached (technically these unknowns are hard to fix). Applying the same numerical technique, we start to integrate the near horizon solution towards the boundary governed by the equation of motion (6.18). Over a finite range, provided values of h_0 and $\log(\Lambda r_+)$, the numerical solutions and asymptotic expectations (6.35)–(6.36) are matched by finding values of $f_0 r_+{}^{2z}$ and $p_0 r_+{}^2$. Our numerical calculations are carried out over a range of 4 to 9 dimensional spacetime. The results are shown in Figures 6.3 and 6.4 where the red dashed line is a plot of the asymptotic expectation and the blue solid line is the numerical result.

Using the fixed constants Λ, f_0, and p_0 we can find matching values for temperature (in unitless) via

$$\log\left(\frac{\Lambda^z}{T}\right) = z\,\log(\Lambda r_+) + \log(2\pi) - \frac{1}{2}\log(f_0 r_+^{2z}). \tag{6.82}$$

We also compute the entropy density, derived in (6.73) and determined by $f_0 r_+^{2z}$ and $p_0 r_+^2$, and plot s/T as a function of $\log(\Lambda^z/T)$ in Figure E.1.

Energy Density, and Free Energy Density

Now we move to the free energy density (6.45) and energy density (6.56). Putting the numerical results of k, q, and x functions into (6.45) by using (6.19) and (6.20), and applying the counterterm (6.58) – (6.60), the free energy density and the energy density are respectively depicted in Figures 6.5 and 6.6. We find that the free energy density and the energy density have a flat region over some finite range of $\log(r/r_+)$, yielding a stable constant value for these quantities. In these figures we also illustrate oscillating and divergent behaviours as the boundary is approached. Recall that initially the physical quantities having marginally relevant modes diverge at the boundary, necessitating the addition of counterterms to render them finite. The counterterms should be expanded in an infinite series in $\log(\Lambda r)$. However in practice the counterterms (6.58) – (6.60) are truncated at a finite order, while our numerical results include higher orders than ones we considered in the analytic calculation. This limitation is responsible for the unstable behavior near the boundary that appears in Figure 6.5 and 6.6. In other words, the terms
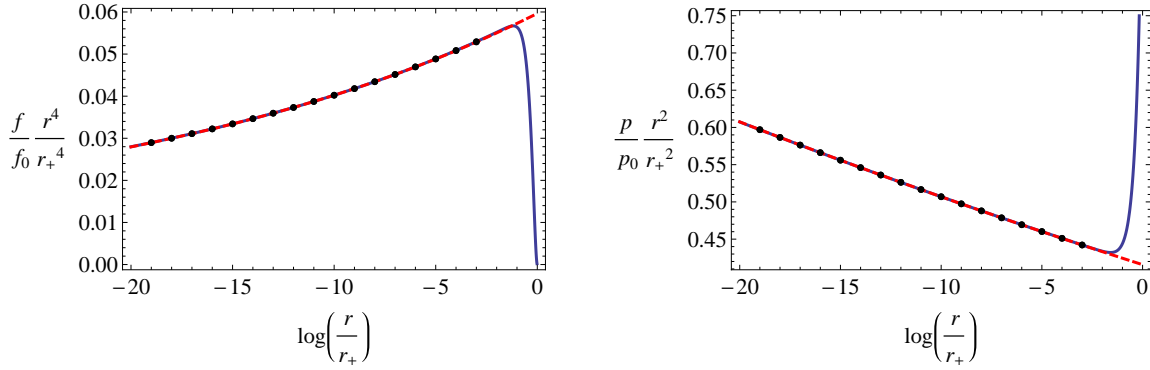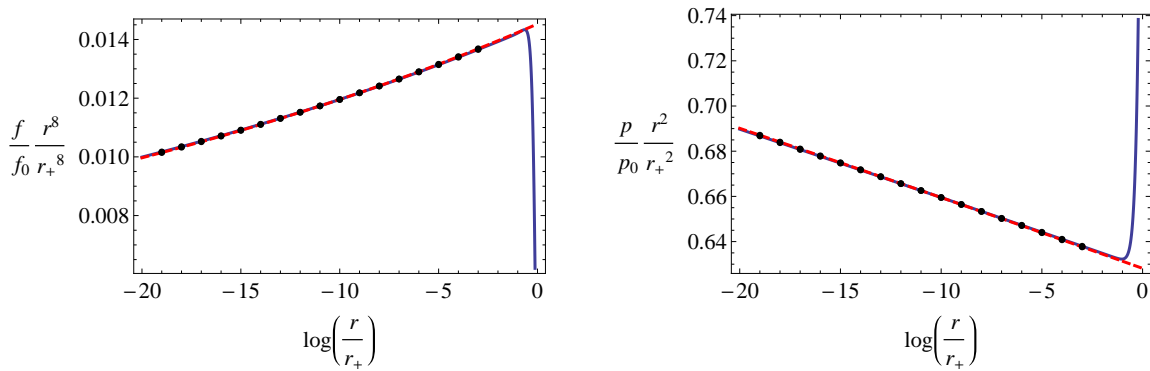
(a) For $z = 2$ and $h_0 = 0.962$, which corresponds to $\log(\Lambda r_+) = -106.8$, the red dashed line is matched to the blue solid line at $f_0 r_+^4 = 29.04$ (left) and at $p_0 r_+^2 = 1.8428$ (right). The dots correspond to the values used for finding the matching condition.
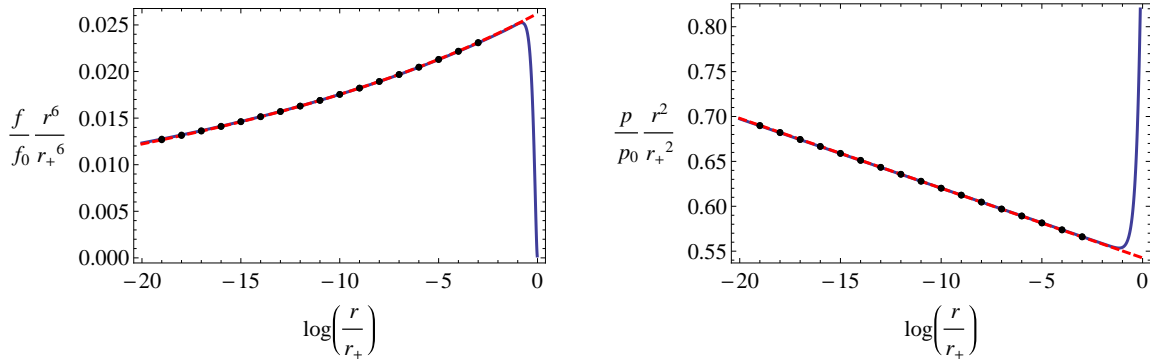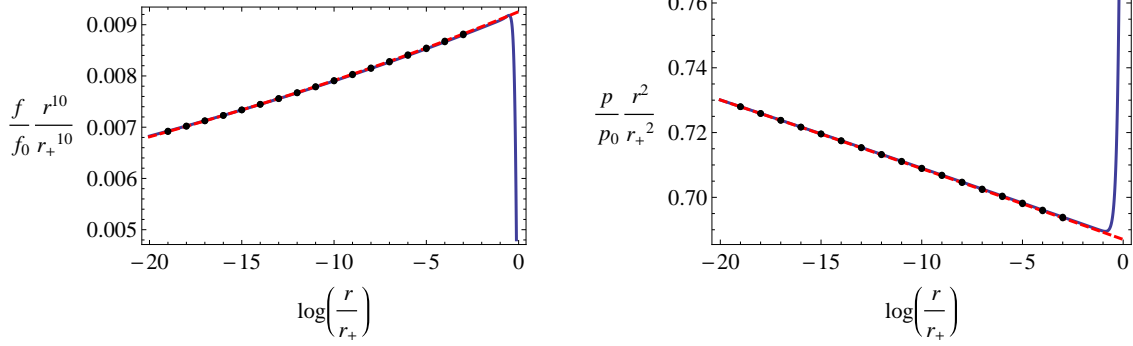

(b) For $z = 3$ and $h_0 = 1.628$, which corresponds to $\log(\Lambda r_+) = -72.6$, the red dashed line is matched to the blue solid line at $f_0 r_+^6 = 44.266$ (left) and at $p_0 r_+^2 = 1.7579$ (right). The dots correspond to the values used for finding the matching condition.
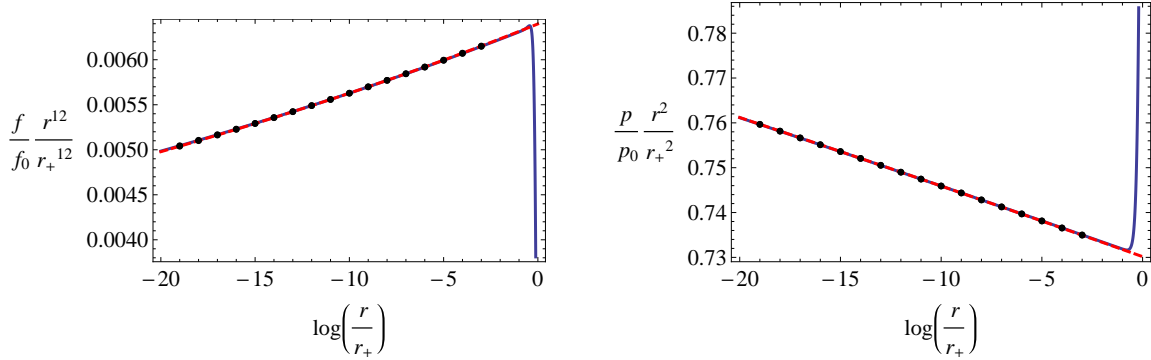

(c) For $z = 4$ and $h_0 = 2.2798$, which corresponds to $\log(\Lambda r_+) = -133.4$, the red dashed line is matched to the blue solid line at $f_0 r_+^8 = 71.40$ (left) and at $p_0 r_+^2 = 1.5781$ (right). The dots correspond to the values used for finding the matching condition.
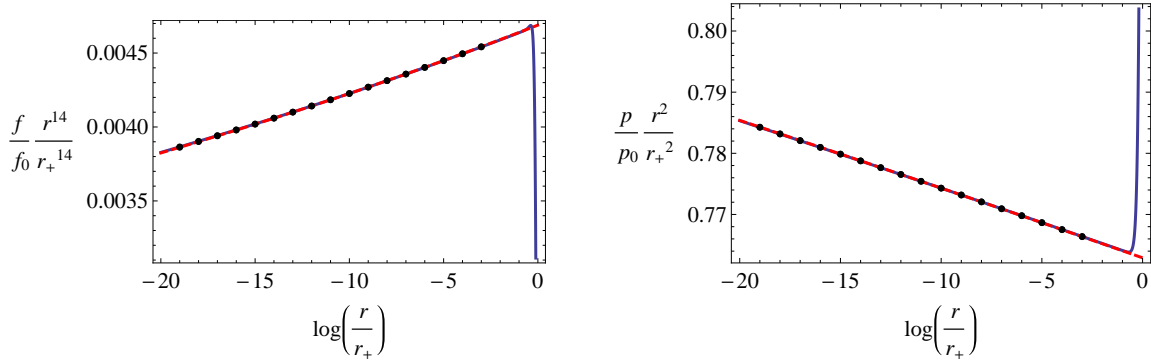
Figure 6.3: Extracting f_0 and p_0 for $z = 2, 3$, and 4

(a) For $z = 5$ and $h_0 = 2.9238$, which corresponds to $\log(\Lambda r_+) = -155.6$, the red dashed line is matched to the blue solid line at $f_0 r_+^{10} = 109.953$ (left) and at $p_0 r_+^2 = 1.45079$ (right). The dots correspond to the values used for finding the matching condition.

(b) For $z = 6$ and $h_0 = 3.5655$, which corresponds to $\log(\Lambda r_+) = -183$, the red dashed line is matched to the blue solid line at $f_0 r_+^{12} = 157.777$ (left) and at $p_0 r_+^2 = 1.36751$ (right). The dots correspond to the values used for finding the matching condition.

(c) For $z = 7$ and $h_0 = 4.206$, which corresponds to $\log(\Lambda r_+) = -220.2$, the red dashed line is matched to the blue solid line at $f_0 r_+^{14} = 214.442$ (left) and at $p_0 r_+^2 = 1.3098$ (right). The dots correspond to the values used for finding the matching condition.

Figure 6.4: Extracting f_0 and p_0 for $z = 5, 6$, and 7

85

in the parenthesis in (6.45) and (6.56) no longer exhibit smooth behavior as the boundary is approached but slowly start to oscillate due to the (imperfect) matching between the numerical results and the truncated counterterm power series. These oscillations increase as r decreases, and furthermore are amplified by the factor of $\sqrt{f}p^{z/2}$, which is rapidly growing when $r \to 0$. Note that the figures 3 and 4 depict $fr^{2z}/f_0 r_+^{2z}$ and $pr^2/p_0 r_+^2$ and are monotonically decreasing and increasing respectively at small r, whereas the functions f and p rapidly grow in that region.

As the spacetime dimension increases we find that the flat region gets narrower and the divergence behaviour starts more quickly from the horizon. The main reason for this is due to the $\sqrt{f}p^{z/2}$ factor commonly appearing in the free energy density (6.45) and the energy density (6.56); both $\sqrt{f}$ and $p^{z/2}$ vary as $1/r^z$ (as shown in (6.36)) as the boundary $r \to 0$ is approached, whereas the quantities in the parentheses of (6.45) and (6.56) contain no divergent terms.

6.6.2 Behaviours of $\mathcal{F}$ and $\mathcal{E}$ near Quantum Critical Regimes

In this section, we plot data of the free energy density per Ts ($\mathcal{F}/Ts$) and the energy density per Ts ($\mathcal{E}/Ts$), which are collected for various values h_0 in previous sections, as functions of $\log(\Lambda^z/T)$. Figure 6.7 and 6.8 present our results for the quantities $\mathcal{F}/Ts$, $\mathcal{E}/Ts$, and $\mathcal{F}/\mathcal{E}$. We also include the fitting function depicted as a solid line. As expected from analytic considerations for the leading order terms of $\mathcal{F}/Ts$ and $\mathcal{E}/Ts$ for $\Lambda = 0$, which is (6.81), we recover from our numerical results the same value for the leading order terms. In addition, the sub-leading contribution depending on $\log(\Lambda^z/T)$ due to marginally relevant modes with fixed $\Lambda \sim 0$ are numerically found in Figure 6.7 and 6.8. For each z, the fitting functions of $\mathcal{F}/Ts$, $\mathcal{E}/Ts$, and $\mathcal{F}/\mathcal{E}$ are presented in Table 6.2.

In addition, the marginally relevant mode should be consistent with the first law of black hole thermodynamics, which is $-\mathcal{F}/Ts + \mathcal{E}/Ts - 1 = 0$. We plot this in Figure 6.9 as a check on the accuracy on our numerical results. We find that our numerical errors are found between the order of 10^{-3} and 10^{-4}.
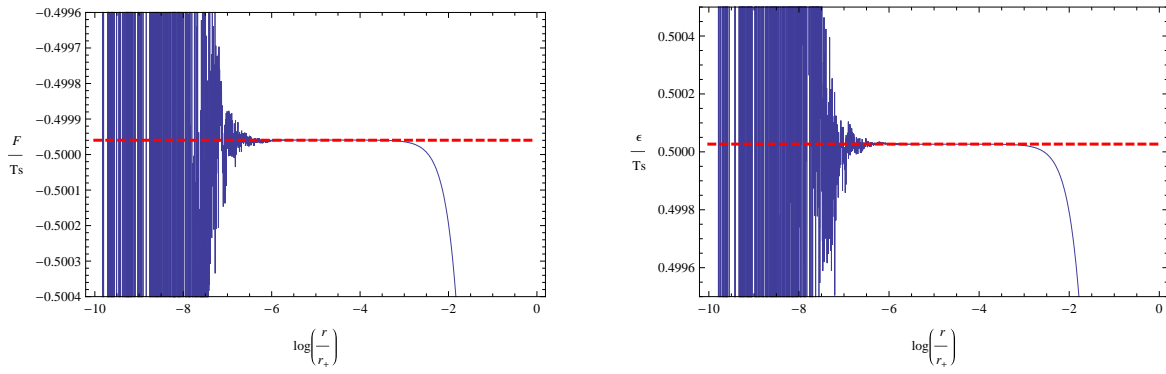
(a) When $z = 2$ and $h_0 = 0.97102$, corresponding to $\log(\Lambda^2/T) \sim -5270$, the left is the numerical result of free energy density $\mathcal{F}$ over Ts and the right is the numerical result of energy density $\mathcal{E}$ over Ts, as a function of $\log(r/r_+)$. The quantity is well defined in the intermediate region. Red dashed line is reading-off the constant value of $\mathcal{F}/Ts$ in the intermediate regime.
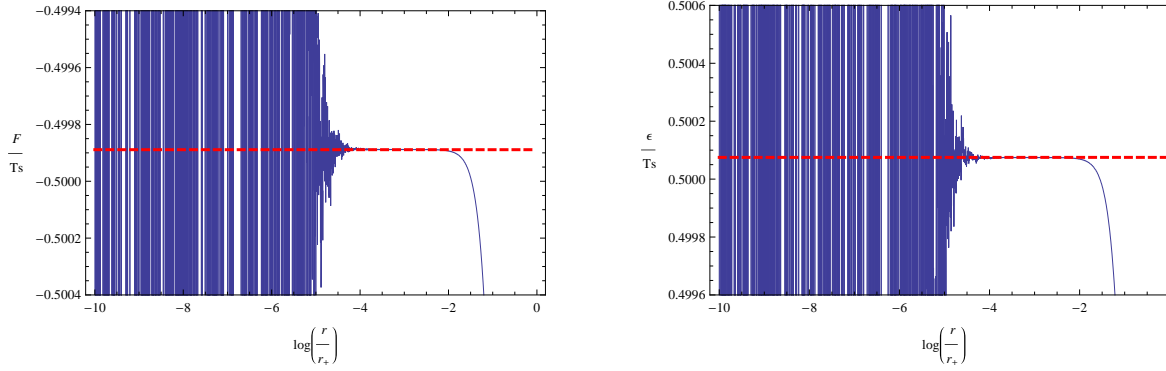
(b) When $z = 3$ and $h_0 = 1.63422$, corresponding to $\log(\Lambda^2/T) \sim -8000$, the left is the numerical result of free energy density $\mathcal{F}$ over Ts and the right is the numerical result of energy density $\mathcal{E}$ over Ts, as a function of $\log(r/r_+)$. The quantity is well defined in the intermediate region. Red dashed line is reading-off the constant value of $\mathcal{F}/Ts$ in the intermediate regime.
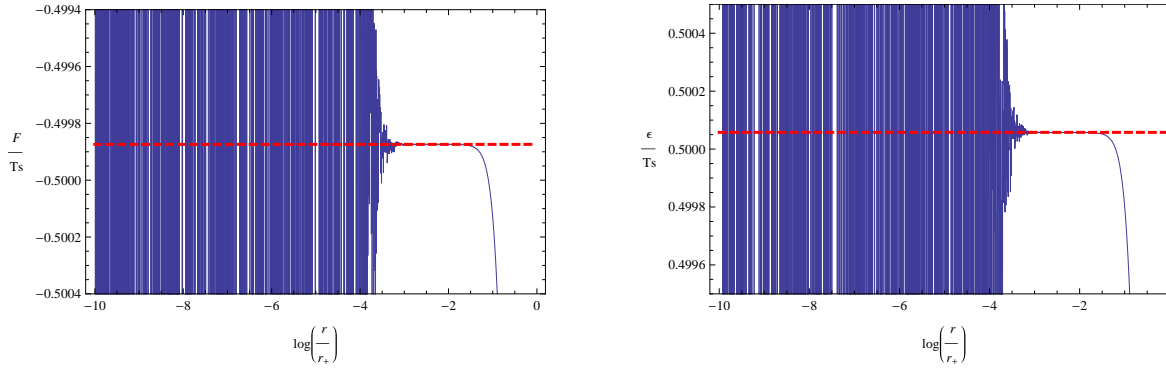
(c) When $z = 4$ and $h_0 = 2.28212$, corresponding to $\log(\Lambda^2/T) \sim -7000$, the left is the numerical result of free energy density $\mathcal{F}$ over Ts and the right is the numerical result of energy density $\mathcal{E}$ over Ts, as a function of $\log(r/r_+)$. The quantity is well defined in the intermediate region. Red dashed line is reading-off the constant value of $\mathcal{F}/Ts$ in the intermediate regime.
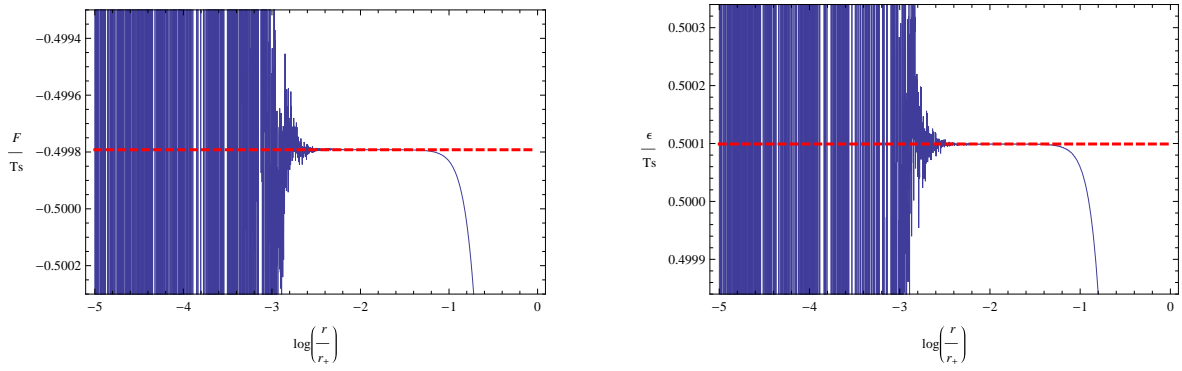
Figure 6.5: $\mathcal{F}/Ts$ and $\mathcal{E}/Ts$ versus $\log(\frac{r}{r_+})$ for $z = 2$, 3, and 4

(a) When $z = 5$ and $h_0 = 2.92526$, corresponding to $\log(\Lambda^2/T) \sim -4100$, the left is the numerical result of free energy density $\mathcal{F}$ over Ts and the right is the numerical result of energy density $\mathcal{E}$ over Ts, as a function of $\log(r/r_+)$. The quantity is well defined in the intermediate region. Red dashed line is reading-off the constant value of $\mathcal{F}/Ts$ in the intermediate regime.
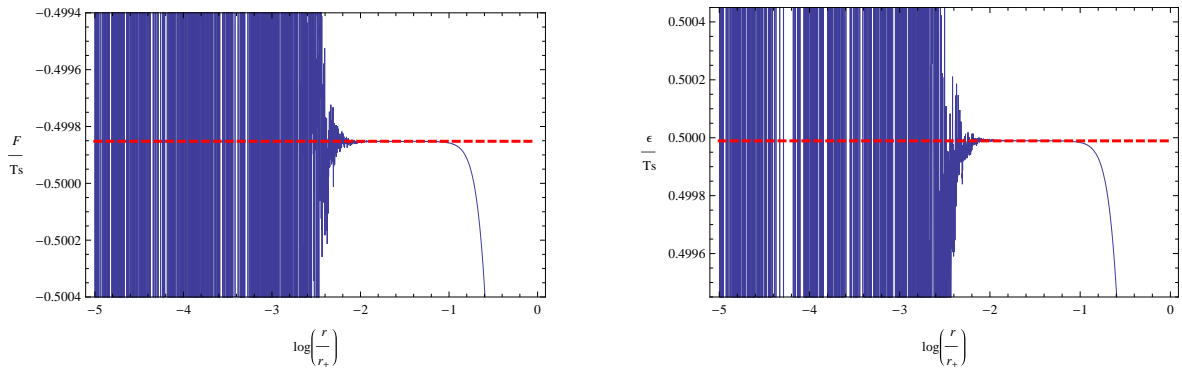

(b) When $z = 6$ and $h_0 = 3.56670$, corresponding to $\log(\Lambda^2/T) \sim -8700$, the left is the numerical result of free energy density $\mathcal{F}$ over Ts and the right is the numerical result of energy density $\mathcal{E}$ over Ts, as a function of $\log(r/r_+)$. The quantity is well defined in the intermediate region. Red dashed line is reading-off the constant value of $\mathcal{F}/Ts$ in the intermediate regime.
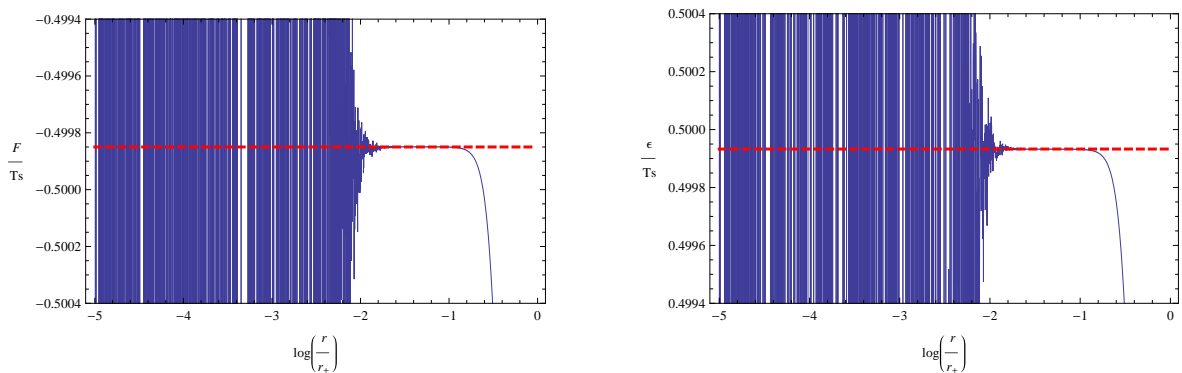

(c) When $z = 7$ and $h_0 = 4.20694$, corresponding to $\log(\Lambda^2/T) \sim -14000$, the left is the numerical result of free energy density $\mathcal{F}$ over Ts and the right is the numerical result of energy density $\mathcal{E}$ over Ts, as a function of $\log(r/r_+)$. The quantity is well defined in the intermediate region. Red dashed line is reading-off the constant value of $\mathcal{F}/Ts$ in the intermediate regime.
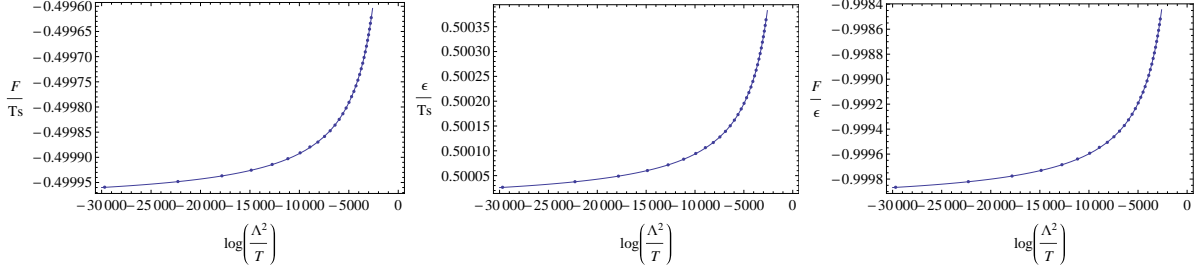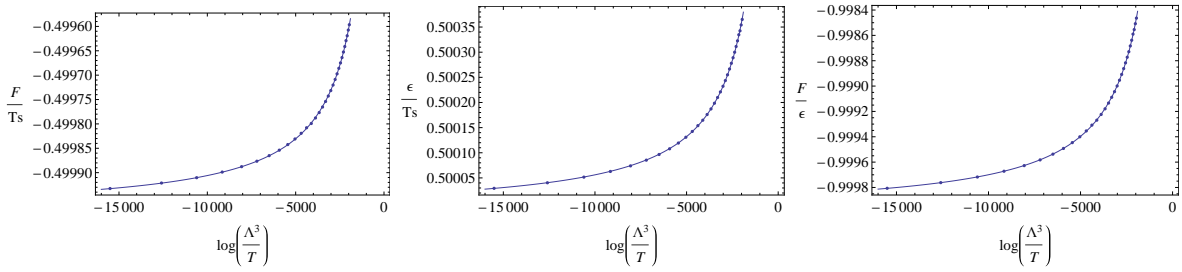
Figure 6.6: $\mathcal{F}/Ts$ and $\mathcal{E}/Ts$ versus $\log(\frac{r}{r_+})$ for $z = 5$, 6, and 7

(a) For $z = 2$. Dots are numerical results running h_0 from 0.9713 to 0.9707, which corresponds to $\log(\Lambda^2/T)$ from about -30000 to -2700. Solid line is the fitting function in table 1.

(b) For $z = 3$. Dots are numerical results running h_0 from 1.6343 to 1.6337, which corresponds to $\log(\Lambda^3/T)$ from about -15500 to -2000. Solid line is the fitting function in table 1.
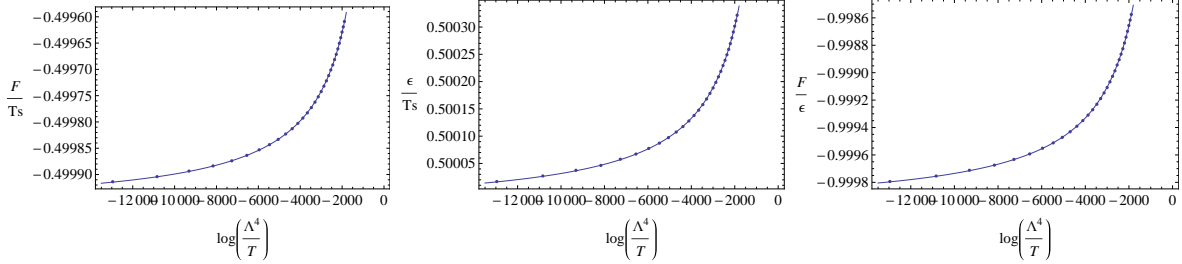
(c) For $z = 4$. Dots are numerical results running h_0 from 2.2822 to 2.2816, which corresponds to $\log(\Lambda^4/T)$ from about -13000 to -1900. Solid line is the fitting function in table 1.

Figure 6.7: Plots of $\mathcal{F}/Ts$, $\mathcal{E}/Ts$, and $\mathcal{F}/\mathcal{E}$ versus $\log(\Lambda^z/T)$ for $z = 2$, 3, and 4.

89
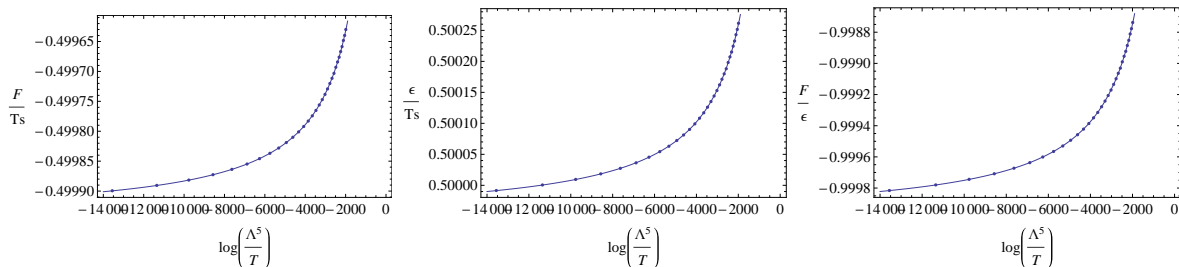
(a) For $z = 5$. Dots are numerical results running h_0 from 2.9255 to 2.9249, which corresponds to $\log(\Lambda^5/T)$ from about -14000 to -2000. Solid line is the fitting function in table 6.2.

(b) For $z = 6$. Dots are numerical results running h_0 from 3.5668 to 3.5662, which corresponds to $\log(\Lambda^6/T)$ from about -21000 to -2200. Solid line is the fitting function in table 6.2.
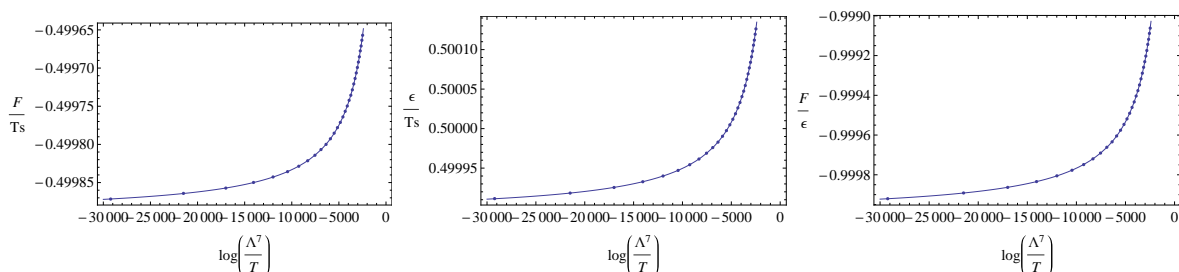
(c) For $z = 7$. Dots are numerical results running h_0 from 4.2070 to 4.2064, which corresponds to $\log(\Lambda^7/T)$ from about -30000 to -2200. Solid line is the fitting function in table 6.2.
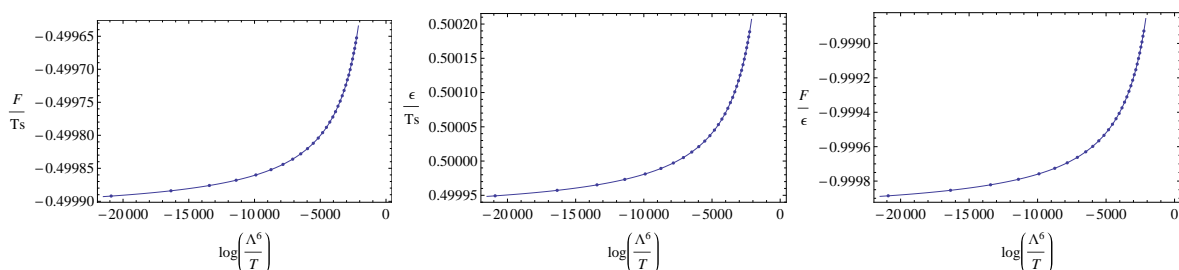
Figure 6.8: Plots of $\mathcal{F}/Ts$, $\mathcal{E}/Ts$, and $\mathcal{F}/\mathcal{E}$ versus $\log(\Lambda^z/T)$ for $z = 5$, 6, and 7.
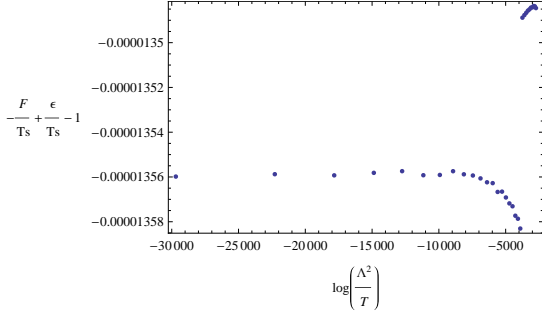
(a) Plots of $-\mathcal{F}/Ts + \mathcal{E}/Ts - 1$ for $z = 2$ and h_0 from 0.9713 to 0.9707.
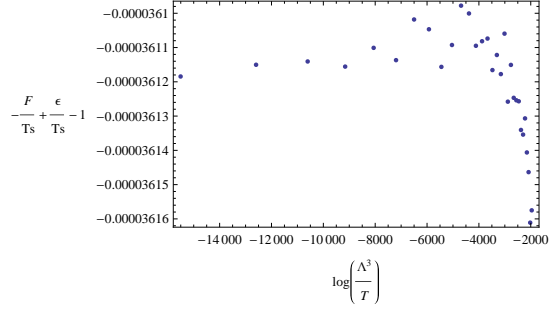
(b) Plots of $-\mathcal{F}/Ts + \mathcal{E}/Ts - 1$ for $z = 3$ and h_0 from 1.6343 to 1.6337.
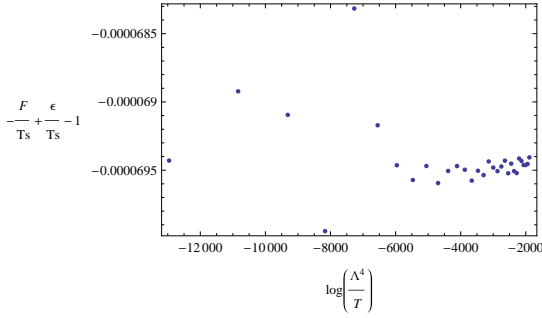
(c) Plots of $-\mathcal{F}/Ts + \mathcal{E}/Ts - 1$ for $z = 4$ and h_0 from 2.2822 to 2.2816.
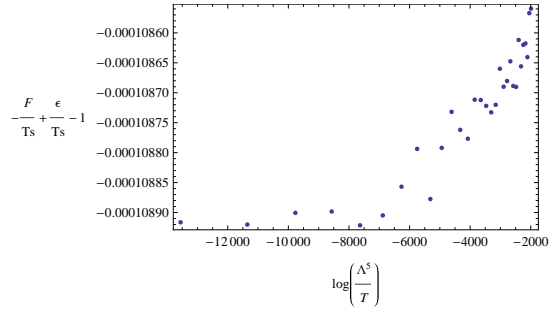
(d) Plots of $-\mathcal{F}/Ts + \mathcal{E}/Ts - 1$ for $z = 5$ and h_0 from 2.9255 to 2.9249.
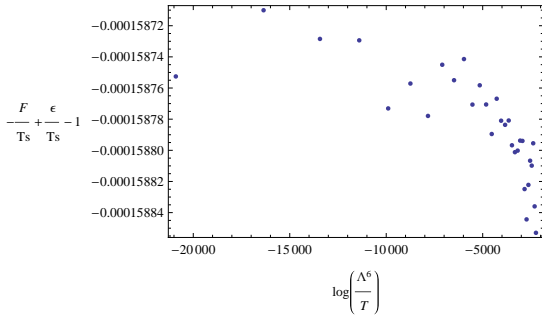
(e) Plots of $-\mathcal{F}/Ts + \mathcal{E}/Ts - 1$ for $z = 6$ and h_0 from 3.5668 to 3.5662.

(f) Plots of $-\mathcal{F}/Ts + \mathcal{E}/Ts - 1$ for $z = 7$ and h_0 from 4.2070 to 4.2064.

Figure 6.9: Plots of errors from $-\mathcal{F}/Ts + \mathcal{E}/Ts - 1$

	free energy density over Ts ($\frac{\mathcal{F}}{Ts} =$)	energy density over Ts ($\frac{\mathcal{E}}{Ts} =$)	free energy density over energy density ($\frac{\mathcal{F}}{\mathcal{E}} =$)
$z = 2$	$-\frac{1}{2} - \frac{1}{\log \Lambda^2/T} + \cdots$	$\frac{1}{2} - \frac{1}{\log \Lambda^2/T} + \cdots$	$-1 - \frac{4}{\log \Lambda^2/T} + \cdots$
$z = 3$	$-\frac{1}{2} - \frac{0.76}{\log \Lambda^3/T} + \cdots$	$\frac{1}{2} - \frac{0.76}{\log \Lambda^3/T} + \cdots$	$-1 - \frac{3}{\log \Lambda^3/T} + \cdots$
$z = 4$	$-\frac{1}{2} - \frac{0.67}{\log \Lambda^4/T} + \cdots$	$\frac{1}{2} - \frac{0.67}{\log \Lambda^4/T} + \cdots$	$-1 - \frac{2.7}{\log \Lambda^4/T} + \cdots$
$z = 5$	$-\frac{1}{2} - \frac{0.63}{\log \Lambda^5/T} + \cdots$	$\frac{1}{2} - \frac{0.63}{\log \Lambda^5/T} + \cdots$	$-1 - \frac{2.50}{\log \Lambda^5/T} + \cdots$
$z = 6$	$-\frac{1}{2} - \frac{0.60}{\log \Lambda^6/T} + \cdots$	$\frac{1}{2} - \frac{0.60}{\log \Lambda^6/T} + \cdots$	$-1 - \frac{2.40}{\log \Lambda^6/T} + \cdots$
$z = 7$	$-\frac{1}{2} - \frac{0.58}{\log \Lambda^7/T} + \cdots$	$\frac{1}{2} - \frac{0.58}{\log \Lambda^7/T} + \cdots$	$-1 - \frac{2.33}{\log \Lambda^7/T} + \cdots$
$\vdots$	$\vdots$	$\vdots$	$\vdots$

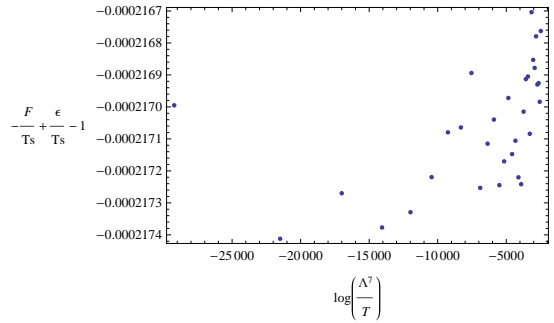Table 6.2: fitting functions for $\frac{\mathcal{F}}{Ts}$, $\frac{\mathcal{E}}{Ts}$, and $\frac{\mathcal{F}}{\mathcal{E}}$

6.7 Summary and Discussion

We investigated the Lifshitz/quantum critical theory correspondence. In gravity theory, we obtained the asymptotic solutions, which are expanded to sub-leading orders where the equations of motion restrict the value of z to be $z = n - 1$ so as to have non-trivial solutions of the marginally relevant mode, and found the expanded black hole solutions, which are characterized by the horizon flux (or h_0), at near horizon. From the perspective of the holographic correspondence, the asymptotic gravitational solutions correspond to the marginally relevant operators of the field theory residing on the boundary of the spacetime, and the quantum critical property at finite temperature is described. In this configuration, one of our aims was to describe the renormalization group flow of the marginally relevant operators between UV-Lifshtiz and IR-AdS at zero temperature limit $\Lambda^z/T \rightarrow \infty$ based on the studies [56],[18]. The other aim was to investigate the thermodynamic behaviours of physical quantities depending on Λ^z/T at finite temperatures in terms of the dimensionality of the spacetime

With these purposes, we derived the equations of motion for Einstein gravity and obtained asymptotic solutions in terms of functions k, q, and x and also in functions of f, p, and h (used separately for later numerical work). Then we derived the free energy density $\mathcal{F}$ and the energy density $\mathcal{E}$, and performed the holographic renormalization with

the gravitational action at the asymptotic boundary of the spacetime, where the relevant counterterms are constructed to prevent the divergent terms. Moving to the horizon, we obtained near-horizon expansions of (planar) black hole solutions, and calculated physical variables such as the entropy density s, the temperature T, and horizon flux ϕ defined at the horizon $r = r_+$, which are expressed by the metric parameters f_0, p_0, and Λ for given h_0. Before carrying out the numerical work, we proved that our analytical results are consistent with the integrated first law of thermodynamics, and also made the prediction that $\mathcal{F}_0/Ts = -\mathcal{E}_0/Ts = 1/2$ at $\Lambda = 0$, which means the marginally relevant modes are turned off. Then we numerically computed the free energy density $\mathcal{F}/Ts$, and the energy density $\mathcal{E}/Ts$ in spacetime dimensions 4 to 9 for given h_0, which are chosen near below values from the maximum of h_0, and then plotted their data as functions of $\log(\Lambda^z/T)$ for each dimension.

Our results indicate that the basic physics of Lifshitz/QCT duality [25] is valid in higher dimensions. Regardless of dimensionality, with a small value of h_0, renormalization group flow under the marginally relevant operators for UV-Lifshitz to IR-AdS can be obtained in the zero temperature limit $\Lambda^z/T \to \infty$, commensurate with the 4-dimensional case [18, 56]. Namely, in the zero temperature limit $\Lambda^z/T \to \infty$, which implies the zero limit of h_0, the AdS spacetime emerges, and so it implies that the renormalization group flow is recovered by controlling h_0 to be very small. In high temperature regime $\Lambda^z/T \to 0$, we calculated the free energy density over Ts and the energy density over Ts for given various h_0, and plotted data as functions of $\log(\Lambda^z/T)$. As analytically expected, the leading-order values of $\mathcal{F}/Ts$ and $\mathcal{E}/Ts$ for $\Lambda = 0$ are numerically recovered as shown in table 6.2. Moreover, the sub-leading dependence of these quantities are found in terms of $\log(\Lambda^z/T)$, with fixed $\Lambda \sim 0$. This illustrates how physical quantities such as $\mathcal{F}/Ts$ and $\mathcal{E}/Ts$ change as functions of $\log(\Lambda^z/T)$ upon approaching the critical point from a given phase. We consequently found that higher dimensional Lifshitz black holes can hold more horizon flux of the massive vector field, since the maximum value of h_0 increased with increasing n. The sub-leading values generated by the marginally relevant modes on the $\mathcal{F}/Ts$ and $\mathcal{E}/Ts$ have a weaker dependence on temperature T as dimensionality increases, as shown in table 6.2.

Chapter 7

Deformation of Lifshitz Holography with Gauss-Bonnet term

7.1 Introduction

Continuing from Chapter 6 [25],[75], we investigate deformations of Lifshitz holography with a Gauss-Bonnet term in $(n + 1)$ dimensions. Gauss-Bonnet gravity generalizes Einstein gravity to include quadratic curvature terms. The equations of motion consist of the Einstein equations modified by additional quadratic curvature terms (with coupling constant α) in such a way that the higher derivative terms cancel out. Unfortunately, as the additional terms in the equations of motion identically vanish in four dimensional spacetime, effects from such terms manifest only in 5 dimensions or more. There are various motivations for considering such higher dimensional gravitational theories.

First, in gravity theory, considering higher curvature terms expands the array of black hole solutions of Einstein gravity to Gauss-Bonnet-Einstein black hole solutions. Examples include the Boulware-Deser solution for spherically symmetric spacetime [17],[89] and the Gauss-Bonnet black hole solution in AdS spacetime [22],[26],[28],[72], and the properties of these black hole solutions have been studied [54],[87]. In supersting/M-theory the Gauss-Bonnet term naturally arises in the effective low energy limit and leads to ghost-free nontrivial gravitational self interactions [91]. Also in cosmology, it provides one approach to understand the current acceleration of the universe in the context of the dark energy problem [59],[73]. In brane-world scenarios it yields additional interesting features [24],[31]. From the holographic correspondence point of view, involving condensed matter systems,

one expects that the higher curvature correction will induce interesting new effects [41],[57] or provide a better explanation for physical phenomena shown in abnormal materials.

The main purpose of this chapter is to find what role the Gauss-Bonnet coupling plays in deformed Gauss-Bonnet-Lifshitz (GB-Lifshitz) holography. In 5 dimensions this is the simplest extension that can yield interesting effects in a four-dimensional theory; we shall here examine any dimensionality. To do so, we assume GB-Lifshitz spacetime in the ultraviolet (UV) energy regime and Gauss-Bonnet-AdS (GB-AdS) spacetime in the infrared (IR) energy regime, and consider the special condition $z = (n-1) - 2(n-2)\tilde{\alpha}$, where z is the dynamic critical exponent and $\tilde{\alpha}$ is the rescaled Gauss-Bonnet coupling constant (defined below). This condition allows the massive vector field to describe the marginally relevant operator, when the operator is expanded to sub-leading orders. To generate the sub-leading orders of the gravitational solutions at the boundary, we introduce a momentum scale Λ, which is very small ($\Lambda \sim 0$) and expand the solutions as a power series in this quantity. Then these sub-leading terms slightly deform the GB-Lifshitz spacetime, which lies in high energy scale $\Lambda^z/T \to 0$, at the asymptotic region. We also consider the finite temperature theory by finding (planar) black hole solutions, which are expanded near the horizon. From the duality perspective, this configuration leads us to expect that the gravitational solution at the boundary of the deformed spacetime gives information about how marginally relevant operators behave near critical points at finite temperature in quantum critical theory. Thus we observe the behaviours of the physical quantities such as the free energy density or the energy density, which show the properties of the marginally relevant operators, according to different values of $\tilde{\alpha}$. While at zero temperature limit $\Lambda^z/T \to \infty$ at fixed $\Lambda \sim 0$, the GB-AdS spacetime can appear and then it might be possible to find the renormalization group flow between the deformed GB-Lifshitz and GB-AdS spacetime for future such as [18],[56].

In section 7.2, the Gauss-Bonnet-Einstein action with negative cosmological constant coupled to a massive vector field is introduced, and its equations of motion are derived. In section 7.3, we consider asymptotically Lifshitz spacetime in the high energy regime, slightly deformed by a small value Λ, and calculate its asymptotic solutions. In section 7.4, with these asymptotic solutions we perform holographic renormalization by constructing the relevant counterterms so as to achieve a well-defined action principle. By doing so, we obtain a well-defined free energy density $\mathcal{F}$ and energy density $\mathcal{E}$. Moving near the black hole horizon, in section 7.5, we derive the expanded black hole solutions in this region, and obtain the thermodynamic variables defined at the horizon. Also we check that our analytic calculations agree with the integrated form of the first thermodynamic law. In section 7.6, we carry out numerical work with the asymptotic solutions and the expanded black hole solutions. Choosing various values of $\tilde{\alpha} = \frac{1}{4}, \frac{1}{10}, 0, -\frac{1}{20}, -\frac{1}{2(n-2)}, -\frac{3}{10}$, we then fix

the undetermined parameters (Λ, f_0, and p_0) appearing in the metric for given $\tilde{\alpha}$ and h_0, which are variables characterizing black hole solutions, using numerical integration. Based on these fixed values, we explore the physical quantities, and finally plot the free energy density and the energy density depending $\log(\Lambda^z/T)$ and find their fitting functions. From this data, we analyze the physical behaviour of the free energy density and the energy density according to $\tilde{\alpha}$ (or z) in section 7.7.

7.2 Higher curvature gravity with a massive vector field

We start with $(n+1)$ dimensional gravitational action modified by higher curvature terms and coupled to a massive vector field

$$S = \int d^{n+1}x\sqrt{-g}\left(\frac{1}{2\kappa_{n+1}^2}[R + 2\tilde{\Lambda} + \alpha\mathcal{L}_{GB}] - \frac{1}{g_v^2}\left[\frac{1}{4}H^2 + \frac{\gamma}{2}B^2\right]\right) \tag{7.1}$$

where $\kappa_{n+1} = \sqrt{8\pi G_{n+1}}$, $\tilde{\Lambda}$ is cosmological constant, α is the Gauss-Bonnet coupling constant and $\mathcal{L}_{GB} = R^2 - 4R_{\mu\nu}R^{\mu\nu} + R_{\mu\nu\alpha\beta}R^{\mu\nu\alpha\beta}$. $H = dB$, and g_v and γ are the coupling constant and the squared mass of the vector field respectively. This action yields equations of motion for the gravitational field

$$G_{\mu\nu} + \alpha L_{\mu\nu} - \tilde{\Lambda}g_{\mu\nu} = \kappa_{n+1}^2 T_{\mu\nu} \tag{7.2}$$

where

$$G_{\mu\nu} = R_{\mu\nu} - \frac{1}{2}g_{\mu\nu}R, \tag{7.3}$$

$$L_{\mu\nu} = 2\left(RR_{\mu\nu} - 2R_{\mu\alpha}R^\alpha_{\ \nu} - 2R^{\alpha\beta}R_{\mu\alpha\nu\beta} + R_\mu^{\ \alpha\beta\gamma}R_{\nu\alpha\beta\gamma}\right) - \frac{1}{2}g_{\mu\nu}\mathcal{L}_{GB}, \tag{7.4}$$

$$T_{\mu\nu} = \frac{1}{g_v^2}\left(H_{\mu\rho}H_\nu^{\ \rho} - \frac{1}{4}g_{\mu\nu}H^2\right) + \frac{\gamma}{g_v^2}\left(B_\mu B_\nu - \frac{1}{2}g_{\mu\nu}B^2\right), \tag{7.5}$$

and for the massive vector field

$$\nabla_\mu H^{\mu\nu} - \gamma B^\nu = 0. \tag{7.6}$$

At the asymptotic region (i.e. $r \to 0$), for $z \neq 1$ we require the equations of motion to admit the metric

$$ds^2 = l^2\left(-\frac{dt^2}{r^{2z}} + \frac{dr^2}{r^2} + \frac{dx^2 + dy^2 + \cdots}{r^2}\right) \tag{7.7}$$

96

which is supported by the vector potential described by

$$B = \frac{g_v l}{\kappa_{n+1}} \frac{q}{r^z} dt. \tag{7.8}$$

These ansatz and boundary conditions fine-tune the cosmological constant to be

$$\tilde{\Lambda} = \frac{\chi_1}{2l^2} - \tilde{\alpha} \frac{\chi_2}{l^2} \tag{7.9}$$

where we replaced the coupling constant of the Gauss-Bonnet α with $\tilde{\alpha}$, which is

$$\tilde{\alpha} = \frac{\alpha(n-2)(n-3)}{l^2}, \tag{7.10}$$

and the squared mass and the squared charge to be

$$\gamma = \frac{(n-1)z}{l^2}, \qquad q^2 = \frac{z-1}{z}(1 - 2\tilde{\alpha}) \tag{7.11}$$

where the χ_1 and χ_2 are defined by

$$\chi_1 = z^2 + (n-2)z + (n-1)^2, \qquad \chi_2 = z^2 + (n-2)z + \frac{(n-1)(n-2)}{2}. \tag{7.12}$$

For given (n, z, α) we require that AdS_{n+1} spacetime is also a solution to the equations with cosmological constant (7.9). In this case the metric is

$$ds^2_{AdS} = a\, l^2 \left(-\frac{dt^2}{r^2} + \frac{dr^2}{r^2} + \frac{dx^2 + dy^2 + \cdots}{r^2} \right) \tag{7.13}$$

where the a is the scaling constant defined by

$$a = \frac{n(n-1) + \sqrt{n(n-1)(1 - 2\tilde{\alpha})(n(n-1) - 4\chi_2\tilde{\alpha})}}{2(\chi_1 - 2\chi_2\tilde{\alpha})} \tag{7.14}$$

appears because the cosmological constant (7.9) has been already fixed due to the Lifshitz boundary condition.

In order to configure the spacetime to induce renormalization flow from UV Lifshitz spacetime to IR AdS spacetime at finite temperature (thereby recovering isotropic scaling symmetry at low energy), we employ the ansatz

$$ds^2 = l^2 \left(-f(r)dt^2 + \frac{dr^2}{r^2} + p(r)(dx^2 + dy^2 + \cdots) \right), \tag{7.15}$$

$$B = \frac{g_v l}{\kappa_{n+1}} h(r)dt, \tag{7.16}$$

97

and these yield the solution for the Lifshitz spacetime

$$\text{Lifshitz}: \quad f = \frac{1}{r^{2z}}, \quad p = \frac{1}{r^2}, \quad h = \frac{\sqrt{(z-1)(1-2\tilde{\alpha})}}{\sqrt{z}} \frac{1}{r^z} \tag{7.17}$$

and for AdS_{n+1} spacetime

$$\text{AdS}: \quad f = p = ar^{-2/\sqrt{a}}, \quad h = 0. \tag{7.18}$$

Plugging the ansatz (7.15) and (7.16) into (7.2) and (7.6) yields

$$-\frac{2zh(r)^2}{f(r)} - \frac{rp'(r)}{p(r)} + \frac{r^2 f'(r)p'(r)}{2f(r)p(r)} + \frac{r^2 p'(r)^2}{2p(r)^2} - \frac{r^2 p''(r)}{p(r)} + \frac{\tilde{\alpha}}{2} \left(\frac{r^3 p'(r)^3}{p(r)} - \frac{r^4 f'(r)p'(r)^3}{2f(r)p(r)^3} \right.$$
$$\left. - \frac{r^4 p'(r)^4}{2p(r)^4} + \frac{r^4 p'(r)^2 p''(r)}{p(r)^3} \right) = 0, \tag{7.19}$$

$$2\chi_1 + \frac{2(2n-3)zh(r)^2}{f(r)} - \frac{rf'(r)}{f(r)} + \frac{r^2 f'(r)^2}{2f(r)^2} - \frac{(3n-5)r^2 f'(r)p'(r)}{2f(r)p(r)} - \frac{(n-2)^2 r^2 p'(r)^2}{2p(r)^2}$$
$$- \frac{r^2 f''(r)}{f(r)} + \tilde{\alpha} \left(-4\chi_2 + \frac{3r^3 f'(r)p'(r)^2}{2f(r)p(r)^2} - \frac{r^4 f'(r)^2 p'(r)^2}{4f(r)^2 p(r)^2} - \frac{r^3 p'(r)^3}{p(r)^3} + \frac{3(n-3)r^4 f'(r)p'(r)^3}{4f(r)p(r)^3} \right.$$
$$\left. + \frac{(n^2 - 7n + 16)r^4 p'(r)^4}{8p(r)^4} + \frac{r^4 p'(r)^2 f''(r)}{2f(r)p(r)^2} + \frac{r^4 f'(r)p'(r)p''(r)}{f(r)p(r)^2} - \frac{r^4 p'(r)^2 p''(r)}{p(r)^3} \right) = 0, \tag{7.20}$$

$$\chi_1 + \frac{(n-1)zh(r)^2}{f(r)} - \frac{r^2 h'(r)^2}{f(r)} - \frac{(n-1)r^2 f'(r)p'(r)}{2f(r)p(r)} - \frac{(n-1)(n-2)r^2 p'(r)^2}{4p(r)^2}$$
$$+ \tilde{\alpha} \left(-2\chi_2 + \frac{(n-1)r^4 f'(r)p'(r)^3}{4f(r)p(r)^3} + \frac{(n-1)(n-4)r^4 p'(r)^4}{16p(r)^4} \right) = 0. \tag{7.21}$$

For simplification we change variables via

$$p(r) = e^{\int^r \frac{q(s)}{s} ds}, \quad f(r) = e^{\int^r \frac{m(s)}{s} ds}, \quad h(r) = k(r)\sqrt{f(r)} \tag{7.22}$$

where $m(r)$ is defined by using a new variable

$$y(r) = \left(4\chi_1 + 4(n-1)zk(r)^2 - 2(n-1)m(r)q(r) - (n-1)(n-2)q(r)^2 \right.$$
$$\left. + \tilde{\alpha}(-8\chi_2 + (n-1)m(r)q(r)^3 + \frac{1}{4}(n-1)(n-4)q(r)^4) \right)^{1/2}, \tag{7.23}$$

98

upon which (7.19)-(7.21) are rewritten as

$$ry'(r) = -2(n-1)zk(r) - \frac{(n-1)}{2}q(r)y(r), \tag{7.24}$$

$$rq'(r) = \frac{\chi_1}{(n-1)} - zk(r)^2 - \frac{n}{4}q(r)^2 - \frac{y(r)^2}{4(n-1)} + \frac{\tilde{\alpha}}{(2-\tilde{\alpha}q(r)^2)}$$
$$\times \left(-\frac{4\chi_2}{(n-1)} + \frac{\chi_1 q(r)^2}{(n-1)} - zk(r)^2 q(r)^2 - \frac{n}{8}q(r)^4 - \frac{q(r)^2 y(r)^2}{4(n-1)} \right), \tag{7.25}$$

$$rk'(r) = -\frac{y(r)}{2} + \frac{k(r)y(r)^2}{4(n-1)q(r)} - \frac{zk(r)^3}{q(r)} + \frac{(n-2)}{4}k(r)q(r) - \frac{\chi_1 k(r)}{(n-1)q(r)} + \frac{\tilde{\alpha}}{(2-\tilde{\alpha}q(r)^2)}$$
$$\times \left(\frac{4\chi_2 k(r)}{(n-1)q(r)} - \frac{\chi_1 k(r)q(r)}{(n-1)} - zk(r)^3 q(r) + \frac{nk(r)q(r)^3}{8} + \frac{k(r)q(r)y(r)^2}{4(n-1)} \right). \tag{7.26}$$

In terms of the new variables $k(r), q(r)$, and $y(r)$, the Lifshitz spacetime is described by

$$\text{Lifshitz}: q = -2, \quad y = 2\sqrt{z}\sqrt{(z-1)(1-2\tilde{\alpha})}, \quad k = \frac{\sqrt{(z-1)(1-2\tilde{\alpha})}}{\sqrt{z}}, \tag{7.27}$$

whereas for GB-AdS spacetime,

$$\text{GB-AdS}: q = -\frac{2}{\sqrt{a}}, \quad y = 0, \quad k = 0. \tag{7.28}$$

7.3 Asymptotic behaviour

Here we expand the asymptotic solutions (7.27) to sub-leading orders, which are generated by a momentum scale $\Lambda \sim 0$, so that the Lifshitz spacetime becomes slightly deformed. Here the non-trivial solution for the sub-leading orders, which become marginally relevant modes for the massive vector field, are only allowed under the condition

$$z = (n-1) - 2(n-2)\tilde{\alpha}. \tag{7.29}$$

by equations of motion (7.24)-(7.26). Henceforth we deal with the case satisfying the above condition. Then the sub-leading orders admit the following form of the (Lifshitz spacetime)

solution

$$k(r) = \frac{\sqrt{(z-1)(1-2\tilde{\alpha})}}{\sqrt{z}}\left[1 + \frac{z + (2z^2 - 5z - 1)\tilde{\alpha} - 2(z+1)(z-2)\tilde{\alpha}^2}{(z-1)^2(z + (2-4z)\tilde{\alpha})\log(r\Lambda)}\right.$$

$$+ \frac{1}{2(z-1)^4(z+(2-4z)\tilde{\alpha})^2\log^2(r\Lambda)}\left((z-1)\left(-3z^2 - 4z^2(z-7)\tilde{\alpha} + (10z^3 - 65z^2\right.\right.$$

$$\left.\left. - 20z + 3)\tilde{\alpha}^2 - 2(z+1)(z^2 - 26z + 1)\tilde{\alpha}^3 - 4(z+1)^2(z+2)\tilde{\alpha}^4\right)\right.$$

$$+ \frac{2}{(z+(2-4z)\tilde{\alpha})}\left(z^2(1-3z) - 2z(4z^3 - 25z^2 + 13z - 2)\tilde{\alpha} - (4z^5 - 87z^4 + 315z^3\right.$$

$$\left.\left. - 189z^2 + 41z - 4)\tilde{\alpha}^2 + \cdots\right)\log(-\log(r\Lambda))\right) + \cdots\right]$$

$$+ (r\Lambda)^{2z+m_1}\log^{2-m_2}(r\Lambda)\left[\xi\left(1 + \frac{\log(-\log(r\Lambda))}{(z-1)^2(z - (z+1)\tilde{\alpha})(z - (2-4z)\tilde{\alpha})^3\log(r\Lambda)}\right.\right.$$

$$\left.\left. \times\left(2z^3(3z-1) + 2z^2(2z^3 - 51z^2 + 33z - 6)\tilde{\alpha} + \cdots\right) + \cdots\right) + \zeta\left(\frac{1}{\log(r\Lambda)} + \cdots\right)\right],$$

$$\text{(7.30)}$$

$$q(r) = -2\left[1 - \frac{z - (3z+1)\tilde{\alpha} + 2(z+1)\tilde{\alpha}^2}{(z-1)(z+(2-4z)\tilde{\alpha})\log(r\Lambda)} - \frac{1}{(z-1)^3(z+(2-4z)\tilde{\alpha})^2\log^2(r\Lambda)}\right.$$

$$\times\left(\frac{1}{2(z+2\tilde{\alpha})}\left(z^3 - 2z^2(z^2 + 2z + 2)\tilde{\alpha} + z(8z^3 + 13z^2 + 14z + 5)\tilde{\alpha}^2 - 2(5z^4 + 15z^3\right.\right.$$

$$\left.\left. + 12z^2 + 7z + 1)\tilde{\alpha}^3 + 4(z+1)(z^3 + 6z^2 + 2z + 1)\tilde{\alpha}^4\right) + \frac{1}{(z+(2-4z)\tilde{\alpha})}\right.$$

$$\left.\left. \times\left(-z^2(3z-1) - 2z(z^3 - 21z^2 + 12z - 2)\tilde{\alpha} + \cdots\right)\log(-\log(r\Lambda))\right) + \cdots\right]$$

$$- \frac{2\sqrt{z-1}\sqrt{z}}{(2z-1)\sqrt{1-2\tilde{\alpha}}}(r\Lambda)^{2z+m_1}\log^{2-m_2}(r\Lambda)$$

$$\times\left[\xi\left(1 + \frac{1}{(z-1)^2(2z-1)(z+(2-4z)\tilde{\alpha})\log(r\Lambda)}\left(\frac{-1}{(2z-1)}\left(z(4z^2 - 7z + 2)\right.\right.\right.\right.$$

$$\left.\left.\left.\left. + (10z^3 - 21z^2 + 11z - 4)\tilde{\alpha} - 2(z+1)\tilde{\alpha}^2\right) + \cdots\right) + \cdots\right) + \zeta\left(\frac{1}{\log(r\Lambda)} + \cdots\right)\right],$$

$$\text{(7.31)}$$

$$y(r) = 2\sqrt{z}\sqrt{(z-1)(1-2\tilde{\alpha})}\left[1 + \frac{z^2 - z(z+3)\tilde{\alpha} + 2(z+1)\tilde{\alpha}^2}{(z-1)^2(z+(2-4z)\tilde{\alpha})\log(r\Lambda)}\right.$$

$$+ \frac{\log(-\log(r\Lambda))}{(z-1)^4(z+(2-4z)\tilde{\alpha})^3\log^2(r\Lambda)}\left(z^3(1-3z) - 2z^2(z^3 - 18z^2 + 8z - 1)\tilde{\alpha}\right.$$

$$\left.+ z(7z^4 - 123z^3 + 21z^2 + 8z - 1)\tilde{\alpha}^2 + \cdots\right) + \cdots\Bigg]$$

$$- \frac{2z(z-2\tilde{\alpha})}{(2z-1)(1-2\tilde{\alpha})}(r\Lambda)^{2z+m_1}\log^{2-m_2}(r\Lambda)\left[\xi\left(1 + \frac{1}{(z-1)^2(z+(2-4z)\tilde{\alpha})\log(r\Lambda)}\right.\right.$$

$$\times\left(\frac{-z(4z-1)(z-1) + (14z^2 - 7z + 5)(z-1)\tilde{\alpha} - 2(2z+1)(z+1)(z-1)\tilde{\alpha}^2}{(2z-1)}\right.$$

$$\left.\left.+ \frac{(2z^3(3z-1) + 2z^2(2z^3 - 51z^2 + 33z - 6)\tilde{\alpha})\log(-\log(r\Lambda))}{(z-(z+1)\tilde{\alpha})(z+(z-4z)\tilde{\alpha})^2}\right) + \cdots\right)$$

$$+ \zeta\left(\frac{1}{\log(r\Lambda)} + \cdots\right)\bigg]. \tag{7.32}$$

where m_1 and m_2 become respectively

$$m_1(z,\tilde{\alpha}) = \frac{2(z-1)\tilde{\alpha}}{1-2\tilde{\alpha}}, \qquad m_2(z,\tilde{\alpha}) = -\frac{2\tilde{\alpha}(z-(z+1)\tilde{\alpha})}{z+(2-4z)\tilde{\alpha}}. \tag{7.33}$$

Here $2z + m_1$ is equivalent to $z + n - 1$ by using (7.29). Note that the denominator of m_2 must not be zero so as to ensure that the logarithmic term $\log^{2-m_2}$ remains finite; recall that we want slightly perturbed metric from the origin. Since (7.33) becomes singular when $\tilde{\alpha} = \frac{z}{2(-1+2z)}$, where $\tilde{\alpha}$ decreases with increasing z, approaching $\frac{1}{4}$ as $z \to \infty$, we require $\tilde{\alpha} \leq \frac{1}{4}$, where the equality is removed when $z = \infty$. This ensures m_2 is finite for any $z \geq 2$. In Fig.7.1, we depict m_2 versus z by varying $\tilde{\alpha}$; we find that the value of m_2 does not exceed $-\frac{5}{4}$ for $|\tilde{\alpha}| < 1$ and any positive z.

In (7.30)-(7.32), a momentum scale Λ is taken to be very small compared to the energy scale, where the Lifshitz spacetime lies. Thus Λ slightly deforms the Lifshitz spacetime and by doing so generates the marginally relevant mode; the pure Lifshitz spacetime solutions (7.27) are recovered when $\Lambda \to 0$. Futhermore we see from (7.30)-(7.32) that these solutions contain different modes due to the arbitrary parameters ξ and ζ. This introduces an ambiguity related to defining the scale of Λ since the solution is invariant under the transformation

$$F(\Lambda r; \zeta, \xi; \lambda) = F(e^{\lambda'/z}\Lambda r; e^{-2\lambda'}(\zeta - \lambda'\xi), e^{-2\lambda'}\xi; \lambda + \lambda') \tag{7.34}$$

101

where F stands for k, q, and y functions. We fix $\lambda = 0$ in (7.30)-(7.32) as in previous work where $\tilde{\alpha} = 0$ [25] and [75].

By substituting (7.30)-(7.32) into the relation (7.22) and (7.23), the original functions f and p are obtained as

$$
\frac{f}{l^2} = F_0^2 \frac{\log^{-2\frac{m_2}{m_1}z}(r\Lambda)}{(r\Lambda)^{2z}} \left[1 - \frac{1}{(z-1)^3(z+(2-4z)\tilde{\alpha})^3 \log(r\Lambda)} \left(z^3(7z-4) + 2z^2(4z^3 - 49z^2 \right. \right.
$$

$$
+ 37z - 7)\tilde{\alpha} - z(64z^4 - 487z^3 + 406z^2 - 111z + 8)\tilde{\alpha}^2 + \cdots + \left(2z^3(3z-1) + 4z^2(z^3 \right.
$$

$$
\left. \left. - 21z^2 + 12z - 2)\tilde{\alpha} + \cdots \right) \log(-\log(r\Lambda)) \right) + \cdots \right], \tag{7.35}
$$

$$
\frac{p}{l^2} = P_0^2 \frac{\log^{2\frac{m_2}{m_1}}(r\Lambda)}{(r\Lambda)^2} \left[1 + \frac{1}{(z-1)^3(z+(2-4z)\tilde{\alpha})^3 \log(r\Lambda)} \left(z^2(5z-2) + 2z(3z^3 - 38z^2 \right. \right.
$$

$$
+ 24z - 4)\tilde{\alpha} - (38z^4 - 377z^3 + 280z^2 - 69z + 8)\tilde{\alpha}^2 + \cdots + \left(2z^2(3z-1) + 4z(z^3 - 21z^2 \right.
$$

$$
\left. \left. + 12z - 2)\tilde{\alpha} - (22z^4 - 398z^3 + 274z^2 - 66z + 8)\tilde{\alpha}^2 + \cdots \right) \log(-\log(r\Lambda)) \right) + \cdots \right] \tag{7.36}
$$

where F_0 and P_0 are integration constants. As we are assuming the Lifshitz spacetime in

(a) $\tilde{\alpha} \in \{-1, -1/2, -3/10, -1/4\}$ (b) $\tilde{\alpha} \in \{1/7, 1/6, 1/5, 1/4\}$
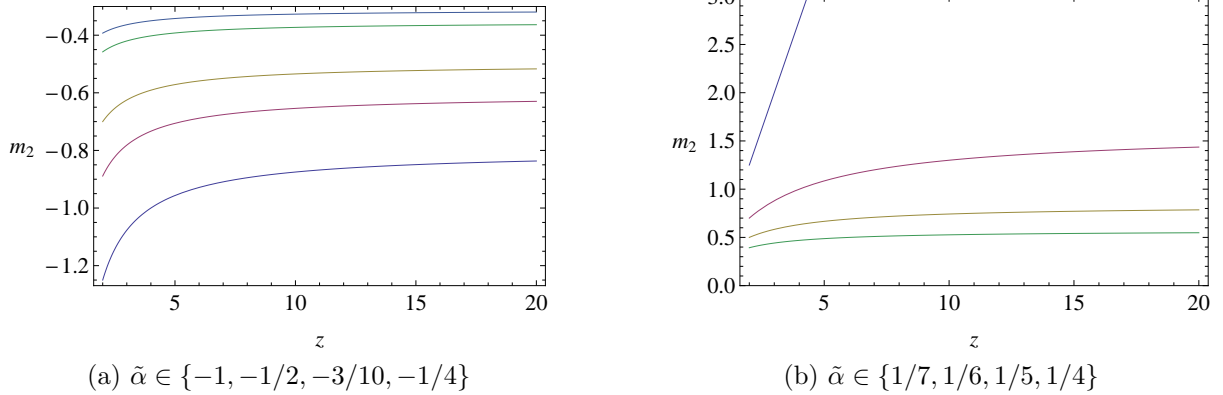
Figure 7.1: m_2 versus z for increasing values of $\tilde{\alpha}$ from bottom to top.

high energy regime, we introduce an arbitrary scale μ

$$\log(r\Lambda) = \log(r\mu) - \log\frac{\mu}{\Lambda}, \tag{7.37}$$

and expand the asymptotic solutions into UV regions where $\mu \gg \Lambda$

$$\left|\frac{1}{\log\frac{\mu}{\Lambda}}\right|, \qquad \left|\frac{\log(r\mu)}{\log\frac{\mu}{\Lambda}}\right| \ll 1, \tag{7.38}$$

and then (7.35) and (7.36) become

$$
\begin{aligned}
f = \frac{1}{r^{2z}} &\left[1 + \frac{1}{(z-1)^3(z-(2-4z)\tilde{\alpha})^3 \log(\frac{\mu}{\Lambda})} \left(z^3\left(7z - 4 + 2z(z-1)^2 \log(r\mu)\right.\right.\right. \\
&\left. + 2(3z-1)\log(\log(\frac{\mu}{\Lambda}))\right) + 2z^2\left(4z^3 - 49z^2 + 37z - 7 - (11z-3)z(z-1)^2 \log(r\mu)\right. \\
&\left.\left.\left. + 2(z^3 - 21z^2 + 12z - z)\log(\log(\frac{\mu}{\Lambda}))\right)\tilde{\alpha} + \cdots \right) + \cdots \right],
\end{aligned} \tag{7.39}
$$

$$
\begin{aligned}
p = \frac{1}{r^2} &\left[1 - \frac{(1 - 2\tilde{\alpha})}{(z-1)^3(z-(2-4z)\tilde{\alpha})^3 \log(\frac{\mu}{\Lambda})} \left(z^2\left(5z - 2 + 2z(z-1)^2 \log(r\mu)\right.\right.\right. \\
&\left. + 2(3z-1)\log(\log(\frac{\mu}{\Lambda}))\right) + 2z\left(3z^3 - 33z^2 + 22z - 4 - 3z(z-1)^2(3z-1)\log(r\mu)\right. \\
&\left.\left.\left. + 2(z^3 - 18z^2 + 11z - 2)\log(\log(\frac{\mu}{\Lambda}))\right)\tilde{\alpha} + \cdots \right) + \cdots \right]
\end{aligned} \tag{7.40}
$$

where t and x coordinates are rescaled by

$$t \to \left(\Lambda \log^{\frac{m_2}{m_1}}\left(\frac{\mu}{\Lambda}\right) \right)^z \frac{1}{F_0} t, \qquad x \to \frac{\Lambda}{\log^{\frac{m_2}{m_1}}\left(\frac{\mu}{\Lambda}\right)} \frac{1}{P_0} x. \tag{7.41}$$

7.4 Holographic Renormalization

As we are considering the spacetime at finite temperature, the action is related to the free energy by the definition

$$F = -T \log \mathcal{Z} = T S_\epsilon(g_*) \tag{7.42}$$

where S_ϵ and g_* indicate the Euclidean action and metric respectively. At the asymptotic boundary near $r \to 0$, the action includes the boundary term to yield the bulk equations of motions such as

$$S_\epsilon = S_{\text{bulk},\epsilon} + S_{\text{boundary},\epsilon} \tag{7.43}$$

103

where each term is written as

$$S_{\text{bulk},\epsilon} = \int d^{n+1}x \sqrt{g} \left(\frac{1}{2\kappa_{n+1}^2} [R + 2\tilde{\Lambda} + \alpha \mathcal{L}_{GB}] - \frac{1}{g_v{}^2} \left[\frac{1}{4} H^2 + \frac{\gamma}{2} B^2 \right] \right),$$

$$S_{\text{boundary}} = \frac{1}{\kappa_{n+1}^2} \int_\Sigma d^n x \sqrt{\gamma} \left(K + 2\alpha (J - 2\hat{G}^{ab} K_{ab}) \right) \tag{7.44}$$

and where $\hat{G}^{ab}$ is the n-dimensional Einstein tensor on Σ corresponding to γ_{ab} and $J = J_{ab}\gamma^{ab}$ in which

$$J_{ab} = \frac{1}{3}(2KK_{ac}K^c{}_b + K_{cd}K^{cd}K_{ab} - 2K_{ac}K^{cd}K_{db} - K^2 K_{ab}). \tag{7.45}$$

Defining $F = \int d^{n-1}x \, \mathcal{F}$, the free energy density $\mathcal{F}$, which is the free energy density per unit $(n-1)$-dimensional spatial volume, is

$$\mathcal{F}_{\text{bulk}} = -\frac{l^{n-1}}{2\kappa_{n+1}^2} \lim_{r \to 0} r \sqrt{f(r)} p'(r) p(r)^{\frac{n-3}{2}} \left(1 - \alpha \frac{(n-2)r^2}{l^2} \frac{p'(r)}{p(r)} \left(\frac{(n-3)}{2} \frac{p'(r)}{p(r)} + \frac{f'(r)}{f(r)} \right) \right),$$

$$\mathcal{F}_{\text{boundary}} = \frac{l^{n-1}}{\kappa_{n+1}^2} \lim_{r \to 0} \left(r \left(\sqrt{f(r)} p(r)^{\frac{n-1}{2}} \right)' - \alpha \frac{(n-1)(n-2)r^3}{6l^2} \frac{p'(r)^2}{f(r)p(r)} \left(\sqrt[3]{f(r)} p(r)^{\frac{n-3}{2}} \right)' \right). \tag{7.46}$$

Considering the boundary of the spacetime near $r \to 0$, these quantities are divergent upon insertion of (7.39) - (7.40), and so counterterms are required to render them finite. These counterterms also should be constructed so as to preserve the covariance of the action at the boundary and to yield a well-defined variational principle. To meet the first condition, one convenient option would be to employ $B^2 = B^\mu B_\mu$ and to consider its combination, which could be any form if cancelling divergences were the only criterion. We take the counterterms in the combination of $C_0 + C_1 B^2 + C_2 B^4 + \cdots$ and then replace B^2 with $-\frac{\kappa_{n+1}^2}{g_v^2} B^2 - \frac{(z-1)(1-2\tilde{\alpha})}{z}$, because the counterterm should vanish for the pure Lifshitz spacetime.

The counterterms are precisely expressed by

$$\mathcal{F}_{\text{c.t}} = \frac{l^{n-1}}{2\kappa_{n+1}^2} \lim_{r \to 0} \sqrt{f(r)} p(r)^{\frac{n-1}{2}} \left(\sum_{j=0}^{2} C_j \left(-\frac{\kappa_{n+1}^2}{g_v^2} B^2 - \frac{(z-1)(1-2\tilde{\alpha})}{z} \right)^j \right)$$

$$= \frac{l^{n-1}}{2\kappa_{n+1}^2} \lim_{r \to 0} \sqrt{f(r)} p(r)^{\frac{n-1}{2}} \left(\sum_{j=0}^{2} C_j \left(k(r)^2 - \frac{(z-1)(1-2\tilde{\alpha})}{z} \right)^j \right) \tag{7.47}$$

104

where C_j are not constants but rather series in $1/\log(r\Lambda)$, which expand similarly to (7.30) - (7.32). Thus the free energy density is finally written as

$$
\begin{aligned}
\mathcal{F} =& \mathcal{F}_{\text{bulk}} + \mathcal{F}_{\text{boundary}} + \mathcal{F}_{\text{c.t}} \\
=& \frac{l^{n-1}}{2\kappa_{n+1}^2} \lim_{r \to 0} \sqrt{f(r)} p(r)^{\frac{n-1}{2}} \left(\frac{(n-2)rp'(r)}{p(r)} + \frac{rf'(r)}{f(r)} + \tilde{\alpha}\left(-\frac{r^3}{2}\frac{f'(r)}{f(r)}\frac{p'(r)^2}{p(r)^2} - \frac{(n-4)}{6}\frac{r^3 p'(r)^3}{p(r)^3} \right) \right. \\
& \left. + \sum_{j=0}^{2} C_j\left(k(r)^2 - \frac{(z-1)(1-2\tilde{\alpha})}{z} \right)^j \right).
\end{aligned}
\tag{7.48}
$$

The counterterms are also compatible with the well-defined variational principle of the on-shell action, and this process defines the boundary stress tensor, which yields the conserved quantities. Here we obtain some physical quantities such as energy density $\mathcal{E}$, pressure $\mathcal{P}$, and flow $\mathcal{J}^i$ by finding the boundary stress tensor. To do this we start with the variation of the action known as

$$
\delta\mathcal{F} = \frac{\sqrt{\gamma}}{2}\tau^{ab}\delta\gamma_{ab} + \mathcal{J}^a\delta B_a
\tag{7.49}
$$

where τ^{ab} contributes to yield conserved quantities via

$$
Q = -\int d^{n-1}x\sqrt{\sigma}\xi_a k_b \tau^{ab}
\tag{7.50}
$$

where $\sqrt{\sigma} = \sqrt{\sigma_{x_1 x_1}\cdots\sigma_{x_{n-1}x_{n-1}}}$ is the spatial volume element, ξ_a are boundary Killing fields, and k_a is the unit vector normal to the boundary surface. In the presence of the non-scalar fields, the boundary stress tensor τ^{ab} should be modified to include the contribution of the massive vector fields, and to do so, we employ the vielbein frame at the boundary of the metric

$$
\gamma_{ab} = \eta_{\hat{a}\hat{b}}e_a^{\hat{a}}e_b^{\hat{b}}, \quad \eta = \text{diag}(\pm 1, 1, 1, \cdots)
\tag{7.51}
$$

where

$$
e^{\hat{t}} = e_a^{\hat{t}}dx^a = \sqrt{f}d\tau, \quad e^{\hat{x_i}} = \sqrt{p}\,dx_i.
\tag{7.52}
$$

Then (7.49) is rewritten with the new boundary stress tensor $\mathcal{T}^{ab}$

$$
\delta\mathcal{F} = \sqrt{\gamma}\,\mathcal{T}^a_{\hat{a}}\delta e_a^{\hat{a}} + \mathcal{J}^{\hat{a}}\delta B_{\hat{a}}
\tag{7.53}
$$

where

$$
\mathcal{T}^{ab} = T^a_{\hat{a}}e^{b\hat{a}}, \qquad \mathcal{T}^{ab} = \tau^{ab} + \frac{1}{\sqrt{\gamma}}\mathcal{J}^{(a}B^{b)}.
\tag{7.54}
$$

105

The energy density is expressed as

$$\mathcal{E} = \sqrt{\sigma} k_a \xi_b T^{ab} = \sqrt{\gamma} \tau^t{}_t + \mathcal{J}^t B_t \tag{7.55}$$

and the pressure is given by

$$\mathcal{P} = -\sqrt{\gamma} \tau^x{}_x. \tag{7.56}$$

From the variation of the action (7.43)-(7.45) with respect to the γ_{ab}, we obtain for τ^{ab} the expression

$$
\begin{aligned}
\tau^{ab} = \frac{2}{\sqrt{\gamma}} \frac{\delta \mathcal{F}}{\delta \gamma_{ab}} = \frac{1}{\kappa_{n+1}^2} \Bigg[& (K\gamma^{ab} - K^{ab}) + 2\alpha (J\gamma^{ab} - 3J^{ab} - 2\hat{P}^{acdb} K_{cd}) \\
& + \frac{1}{2l} \sum_{j=0}^{2} C_j \left(\gamma^{ab} \left(-\frac{\kappa_{n+1}^2}{g_v{}^2} B^2 - \frac{(z-1)(1-2\tilde{\alpha})}{z} \right)^j \right. \\
& \left. + \frac{2j\kappa_{n+1}{}^2}{g_v{}^2} B^a B^b \left(-\frac{\kappa_{n+1}^2}{g_v{}^2} B^2 - \frac{(z-1)(1-2\tilde{\alpha})}{z} \right)^{j-1} \right) \Bigg]
\end{aligned}
\tag{7.57}
$$

where

$$\hat{P}_{abcd} = \hat{R}_{abcd} + 2\hat{R}_{b[c}g_{d]a} - 2\hat{R}_{a[c}g_{d]b} + \hat{R}g_{a[c}g_{d]b}, \tag{7.58}$$

in which the $\hat{R}$'s are various contractions of Riemann tensors defined on the n-dimensional hypersurface associated with γ_{ab}. From the variation of the action with respect to the vector field strength B_t, $\mathcal{J}^{\hat{t}}$ we obtain

$$
\begin{aligned}
\mathcal{J}^{\hat{t}} &= \sqrt{f(r)} \frac{\delta S}{\delta B_t}, \\
&= \frac{l^{n-2}}{g_v \kappa_{n+1}} \lim_{r \to 0} \sqrt{f(r)} p(r)^{\frac{n-1}{2}} \left(\frac{r(k(r)\sqrt{f(r)})'}{\sqrt{f(r)}} + k(r) \sum_{j=0}^{2} jC_j \left(k(r)^2 - \frac{(z-1)(1-2\tilde{\alpha})}{z} \right)^{j-1} \right) \\
&= \frac{l^{n-2}}{g_v \kappa_{n+1}} \lim_{r \to 0} \sqrt{f(r)} p(r)^{\frac{n-1}{2}} \left(-\frac{1}{2} y(r) + k(r) \sum_{j=0}^{2} jC_j \left(k(r)^2 - \frac{(z-1)(1-2\tilde{\alpha})}{z} \right)^{j-1} \right)
\end{aligned}
\tag{7.59}
$$

where other components of $\mathcal{J}^{\hat{a}}$ vanish. Then the energy density becomes

$$
\begin{aligned}
\mathcal{E} = \frac{l^{n-1}}{2\kappa_{n+1}^2} \lim_{r \to 0} \sqrt{f(r)} p(r)^{\frac{n-1}{2}} \Bigg[& (n-1) \frac{rp'(r)}{p(r)} - k(r)y(r) + \tilde{\alpha} \left(-\frac{(n-1)}{6} \frac{r^3 p'(r)^3}{p(r)^3} \right) \\
& + \sum_{j=0}^{2} C_j \left(k(r)^2 - \frac{(z-1)(1-2\tilde{\alpha})}{z} \right)^j \Bigg],
\end{aligned}
\tag{7.60}
$$

106

and the pressure takes the same form of the free energy density with inverse sign

$$\mathcal{P} = -\mathcal{F}. \tag{7.61}$$

To ensure a finite value of the action and a well-defined variational principle $\delta S = 0$, we expect our counterterms (7.47) to render the free energy density (7.48), the flow (7.59), and the energy density (7.60) finite when $r \to 0$. Expanding these functions with the asymptotic solution (7.30)-(7.32), they take the form

$$F \sim \frac{1}{r^{z+n-1}} \left(F_1 [\frac{1}{\log(r\Lambda)}] + \cdots (r\Lambda)^{z+n-1} \log^{2-m_2}(r\Lambda) \left(F_2 [\frac{1}{\log(r\Lambda)}] + \cdots \right) \right) + \text{counterterms} \tag{7.62}$$

where F stands for $\mathcal{F}$, $\mathcal{E}$, and $\mathcal{J}^{\hat{t}}$, and F_1 and F_2 indicate the parts involving series of $\log(r\Lambda)$ in the expression of $\mathcal{F}$, $\mathcal{E}$, and $\mathcal{J}^{\hat{t}}$. As shown in (7.62), divergences occur as $r \to 0$. The divergences due to $\frac{1}{r^{z+n-1}}$ are eliminated by the two coefficients C_0 and C_1, expanded as a series in $1/\log(r\Lambda)$. To prevent the divergences due to $\log^{2-m_2}(r\Lambda)$, another coefficient

C_2 of the counterterm is required. Then C_0, C_1, and C_2 become

$$C_0 = -\frac{2(-3 + 6z + (6 - 14z)\tilde{\alpha} + 4(-2 + 3z)\tilde{\alpha}^2)}{-3 + 6\tilde{\alpha}}$$
$$+ \frac{2(z - 2\tilde{\alpha})(1 + 2(-2 + z)\tilde{\alpha})(-z + (1 + z)\tilde{\alpha})^3}{(z - 1)^3(2z - 1)(z + (2 - 4z)\tilde{\alpha})^2 \log^2(r\Lambda)}$$
$$+ \frac{(z - (1 + z)\tilde{\alpha})^2}{3(2z - 1)^2(z - 1)^5(z + (2 - 4z)\tilde{\alpha}^3)\log^3(r\Lambda)}\Bigg(3z(1 - 2z - 3z^2 + 2z^3 + 4z^4)$$
$$+ (-3 - 21z + 109z^2 + 33z^3 - 146z^4 - 48z^5 + 16z^6)\tilde{\alpha} + \cdots\Bigg) + \cdots, \tag{7.63}$$

$$C_1 = z - \frac{2z(z - 2\tilde{\alpha})(z - (1 + z)\tilde{\alpha})^2}{(z - 1)^2(2z - 1)(2\tilde{\alpha} - 1)(z + (2 - 4z)\tilde{\alpha})\log(r\Lambda)}$$
$$- \frac{z(-z + (1 + z)\tilde{\alpha})}{2(2z - 1)^2(z - 1)^4(2\tilde{\alpha} - 1)(z + (2 - 4z)\tilde{\alpha})^2 \log^2(r\Lambda)}\Bigg(z(3 - 10z - z^2 + 14z^3)$$
$$+ (-3 - 9z + 113z^2 - 103z^3 - 70z^4 + 24z^5)\tilde{\alpha} + \cdots\Bigg) + \cdots, \tag{7.64}$$

$$C_2 = \frac{z^2(1 - 3z + 4z\tilde{\alpha})}{4(z - 1)(2z - 1)(2\tilde{\alpha} - 1)^2} + \frac{z^2}{4(2z - 1)^2(z - 1)^3(2\tilde{\alpha} - 1)^2(z + (2 - 4z)\tilde{\alpha})\log(r\Lambda)}$$
$$\times \Bigg(z(3 - 14z + 15z^2) + (-3 + 3z + 65z^2 - 119z^3 + 30z^4)\tilde{\alpha} + \cdots\Bigg) + \frac{\Delta}{\log^2(r\Lambda)}$$
$$+ \frac{z^2 \log(-\log(r\Lambda))}{4(1 - 2z)^2(-1 + z)^5(1 - 2\tilde{\alpha}^2(-z + (1 + z)\tilde{\alpha})(-z + (-2 + 4z)\tilde{\alpha})^3 \log^2(r\Lambda)}$$
$$\times \Bigg((1 - 3z)^2z^3(-3 + 5z) + z^2(-9 + 110z - 532z^2 + 1154z^3 - 955z^4 + 120z^5)\tilde{\alpha} + \cdots\Bigg). \tag{7.65}$$

where C_0 and C_1 keep expanding in an infinite series in $1/\log(r\Lambda)$ as the asymptotic solutions expand. However C_2 just consists of a finite number of terms, because the $\log^{2-m_2}(r\Lambda)$ quantity in (7.62) is divided by $1/\log^i(r\Lambda)$ (where $i = 1, 2, \cdots$) from F_2 and so when i becomes $2 - m_2$ divergences due to $\log^{2-m_2}(r\Lambda)$ vanish. These solutions, however, have an ambiguity Δ as shown in (7.65). It turns out that Δ does not affect numerical work for the free energy density and the energy density, as we shall show in the next section.

Inserting the solution (7.63)-(7.65) into (7.48), (7.59), and (7.60), we find

$$\mathcal{F} = \frac{l^{n-1}}{\kappa_{n+1}^2} \frac{\sqrt{z}}{\sqrt{(z-1)(1-2\tilde{\alpha})}} \left((z-(z+1)\tilde{\alpha})\zeta + \frac{X}{(2z-1)(z-1)^2(z-(-2+4z)\tilde{\alpha})^3}\xi \right),$$
(7.66)

$$\mathcal{E} = -\frac{l^{n-1}}{\kappa_{n+1}^2} \frac{(z-2\tilde{\alpha})}{\sqrt{(z-1)z}(2z-1)(1-2\tilde{\alpha})^{3/2}}$$
$$\times \left((z-(z+1)\tilde{\alpha})\zeta - \frac{Y}{(2z-1)(z-1)^2(z-(-2+4z)\tilde{\alpha})^3}\xi \right),$$
(7.67)

$$\mathcal{J}^{\hat{t}} = \frac{1}{g_v} \frac{l^{n-2}}{\kappa_{n+1}} \frac{1}{(1-2z)^2(1-2\tilde{\alpha})^2} \left(-(z-1)(z-2\tilde{\alpha})\tilde{\alpha}\,\zeta + \frac{4(z-1)(1-2\alpha)^3\Delta}{z}\xi \right.$$
$$\left. + \frac{Z}{2(z-1)^4(1-2z)(z-(1+z)\tilde{\alpha})(z-(-2+4z)\tilde{\alpha})^3}\xi \right),$$
(7.68)

where X, Y, and Z are functions of z and $\tilde{\alpha}$, and are displayed in (F.1). This result implies for the pure Lifshitz spacetime to be

$$\mathcal{F} = \mathcal{E} = \mathcal{J}^{\hat{t}} = 0,$$
(7.69)

since $\zeta = \xi = 0$ for the pure Lifshitz solution.

7.5 Finite Temperature

We have so far worked near boundary of the spacetime. We now move to the near-horizon region of a black hole. In this section, we first obtain (planar) black hole solutions expanded near the horizon, and find some thermodynamic quantities such as temperature T, entropy density s, horizon flux density of the massive vector field ϕ at near horizon $r = r_+$. Then we prove the integrated first law by constructing an RG-invariant quantity $\bar{K}$, and find the relation $\mathcal{F}_0 = -\eta(n, \tilde{\alpha})\mathcal{E}_0$ from the integrated law of thermodynamics and the trace Ward identity.

7.5.1 Expansion and Physical quantities near the horizon

Let us consider a black hole solution defined by $f(r_+) = 0$, and expand the solution near horizon $r = r_+$. The expansions in powers of $(1 - \frac{r}{r_+})$ are determined by equation of motion

109

We find

$$f(r) = f_0\left(\left(1 - \frac{r}{r_+}\right)^2 + \left(1 - \frac{r}{r_+}\right)^3 + \frac{1}{12(1 - 2\tilde{\alpha})^2(z - 2\tilde{\alpha})^2}\right.$$

$$\times \left(z(8h_0^2(-2 + 3z) + z(7 + 14z - 6z^2)) + 2(32h_0^4 + 16h_0^2(1 + z - 6z^2)\right.$$

$$\left.\left. + z(-18 - 30z - 35z^2 + 29z^3))\tilde{\alpha} + \cdots\right)\left(1 - \frac{r}{r_+}\right)^4 + \cdots\right), \tag{7.70}$$

$$p(r) = p_0\left(1\right.$$

$$+ \frac{(4h_0^2 + z - 3z^2 - (16h_0^2 + z - 11z^2)\tilde{\alpha} + 2(-1 + 8h_0^2 + z - 8z^2)\tilde{\alpha}^2 + 8z^2\tilde{\alpha}^3)}{2(z - 2\tilde{\alpha})(-1 + 2\tilde{\alpha})}\left(1 - \frac{r}{r_+}\right)^2$$

$$+ \frac{(4h_0^2 + z - 3z^2 - (16h_0^2 + z - 11z^2)\tilde{\alpha} + 2(-1 + 8h_0^2 + z - 8z^2)\tilde{\alpha}^2 + 8z^2\tilde{\alpha}^3)}{2(z - 2\tilde{\alpha})(-1 + 2\tilde{\alpha})}\left(1 - \frac{r}{r_+}\right)^3$$

$$\left. + \cdots\right), \tag{7.71}$$

$$h(r) = \sqrt{f_0}h_0\left(\left(1 - \frac{r}{r_+}\right)^2 + \left(1 - \frac{r}{r_+}\right)^3 + \frac{1}{24(1 - 2\tilde{\alpha})^2(z - 2\tilde{\alpha})^2}\right.$$

$$\left(z(z(20 + 10z - 9z^2) + 8h_0^2(-1 + 3z)) + 4(8h_0^4 - 4h_0^2(-1 + 2z + 9z^2)\right.$$

$$\left.\left. + z(-21 - 27z - 5z^2 + 14z^3))\tilde{\alpha} + \cdots\right)\left(1 - \frac{r}{r_+}\right)^4 + \cdots\right) \tag{7.72}$$

where f_0 and p_0 are constants, which are not determined by equations of motion, and control the scaling of the metric by redefining the coordinates so that $dt'^2 = f_0^2 dt^2$ and $dx_i'^2 = p_0^2 dx_i^2$. In the next section, we tune f_0 and p_0 with $\log(\frac{\Lambda}{\mu})$ shown in (7.39) and (7.40) at the energy scale $\mu = \frac{1}{r_+}$ by matching near horizon solutions (numerically integrated towards asymptotics) and the asymptotic solutions. If f_0 and p_0 are fixed by doing so, the expanded black hole solutions (7.70)-(7.72) are characterized by two parameters h_0 and $\tilde{\alpha}$. Namely, (7.70)-(7.72) describe a two-parameter family $\{h_0, \tilde{\alpha}\}$ of black hole solutions.

Thermodynamic properties of (7.70)-(7.72) are found by calculating temperature T and entropy density s near horizon. The temperature is determined by demanding the periodicity of the imaginary time coordinate τ so that spacetime becomes regular at $r = r_+$, and the entropy is defined by $S = \frac{A}{4G_{n+1}}$ which is proportional to the area of the black

hole. Using our metric (7.15), the T and s can be written as

$$T = \frac{r_+}{2\pi}\sqrt{\left.\frac{1}{2}\frac{d^2 f(r)}{dr^2}\right|_{r=r_+}}, \tag{7.73}$$

$$s = 2\pi\frac{l^{n-1}}{\kappa_{n+1}^2}p(r_+)^{\frac{n-1}{2}} \tag{7.74}$$

where $S = \int s\, d^{n-1}x$. We also can calculate the horizon flux Φ of the massive vector field defined by

$$\Phi = \oint \sqrt{\gamma}\vec{H}\cdot d\vec{A} = \oint \phi\, d^{n-1}x \tag{7.75}$$

where

$$\phi = \frac{l^{n-2}g_v r_+}{\kappa_{n+1}}\left(\frac{p(r)^{\frac{n-1}{2}}}{\sqrt{f(r)}}\frac{dh(r)}{dr}\right)\Bigg|_{r=r_+} \tag{7.76}$$

is the horizon flux density. Plugging near horizon solutions (7.70)-(7.71) into (7.59)–(7.73), each quantity becomes

$$T = \frac{\sqrt{f_0}}{2\pi}, \qquad s = 2\pi p_0^{\frac{n-1}{2}}\frac{l^{n-1}}{\kappa_{n+1}^2}, \qquad \phi = 2h_0 p_0^{\frac{n-1}{2}}\frac{l^{n-2}g_v}{\kappa_{n+1}}. \tag{7.77}$$

7.5.2 Integrated First Law of Thermodynamics

So far we obtained the asymptotic solutions (7.30)-(7.32), and calculated the free energy density (7.48) and the energy density (7.60). Then we derived the near horizon solutions (7.70)-(7.71), and computed thermodynamic quantities such as temperature T and the entropy density s near horizon in (7.77). Now we check the consistency of our calculations by proving the integrated first law of thermodynamics.

To connect the physical variables of the asymptotic region and near horizon region, we construct an RG-invariant quantity $\bar{K}$ to be a constant at both regions. First, by using the asymptotic solution, we combine the functions q, k, y and m in an invariant combination. Then $\bar{K}$ takes the form

$$\bar{K} = \frac{\sqrt{f(r)}p(r)^{\frac{n-1}{2}}}{2}\left[q(r) - m(r) - k(r)y(r) - \tilde{\alpha}\left(\frac{1}{2}q(r)^3 - \frac{1}{2}m(r)q(r)^2\right)\right] \tag{7.78}$$

$$= \frac{\sqrt{f(r)}p(r)^{\frac{n-1}{2}}}{4q(r)}\left[\frac{1}{(n-1)}y(r)^2 + nq(r)^2 - 4zk(r)^2 - 2k(r)q(x)y(x) - \frac{4\chi_1}{(n-1)}\right.$$

$$\left. + \tilde{\alpha}\left(-\frac{n}{4}q(r)^4 + \frac{8\chi_2}{(n-1)}\right)\right] \tag{7.79}$$

111

which produces with (7.30)-(7.32)

$$\bar{K} = \frac{2(z - (1+z)\tilde{\alpha})}{\sqrt{z-1}\sqrt{z}(1-2z)(1-2\tilde{\alpha})^{\frac{3}{2}}} \left((z - (1+z)\tilde{\alpha})\zeta - \frac{\xi}{(1-2z)(z-1)^2(z+(2-4z)\tilde{\alpha})^3} \right.$$

$$\times \left(-z^3(1-3z+z^2) + z^2(-6+28z-48z^2+21z^3-4z^4)\tilde{\alpha} + z(-12+95z-287z^2 \right.$$

$$+ 424z^3 - 262z^4 + 72z^5)\tilde{\alpha}^2 + (-8+116z-514z^2+1193z^3-1630z^4+1125z^5$$

$$- 322z^6)\tilde{\alpha}^3 + (28-231z+685z^2-1283z^3+1887z^4-1558z^5+472z^6)\tilde{\alpha}^4 - 2(7-27z$$

$$\left. \left. - 62z^2 + 246z^3 - 47z^4 - 231z^5 + 90z^6)\tilde{\alpha}^5 + 4(1+z)^2(2-17z+41z^2-32z^3+4z^4)\tilde{\alpha}^6 \right) \right).$$

$$(7.80)$$

Employing the expression for the free energy density (7.48) and the energy density(7.60), we obtain the algebraic relation

$$\frac{1}{2}\sqrt{f(r)}p(r)^{\frac{n-1}{2}} \left[\frac{(n-1)rp'(r)}{p(r)} - k(r)y(r) + \tilde{\alpha} \left(-\frac{(n-1)}{6}\frac{r^3p'(r)^3}{p(r)^3} \right) \right.$$

$$\left. + \sum_{j=0}^{2} C_j \left(k(r)^2 - \frac{(z-1)(1-2\tilde{\alpha})}{z} \right)^j \right]$$

$$= \frac{1}{2}\sqrt{f(r)}p(r)^{\frac{n-1}{2}} \left[\frac{(n-2)rp'(r)}{p(r)} + \frac{rf'(r)}{f(r)} + \tilde{\alpha} \left(-\frac{r^3}{2}\frac{f'(r)}{f(r)}\frac{p'(r)^2}{p(r)^2} - \frac{(n-4)}{6}\frac{rp'(r)^3}{p(r)^3} \right) \right.$$

$$\left. + \sum_{j=0}^{2} C_j \left(k(r)^2 - \frac{(z-1)(1-2\tilde{\alpha})}{z} \right)^j \right] + \bar{K} \qquad (7.81)$$

or simply

$$\mathcal{E} = \mathcal{F} + \frac{l^{n-1}}{\kappa_{n+1}^2}\bar{K}. \qquad (7.82)$$

Next, let us calculate $\bar{K}$ with (7.70)-(7.71) at $r = r_+$. This yields for $\bar{K}$

$$\bar{K} = \sqrt{f_0}P_0^{\frac{n-1}{2}} = Ts\frac{\kappa_{n+1}^2}{l^{n-1}} \qquad (7.83)$$

and by plugging the above into (7.82), we find

$$\mathcal{F} = \mathcal{E} - Ts \qquad (7.84)$$

112

which is the integrated form of the first law of thermodynamics. We have therefore proved that our analytic calculation agrees with the first law of thermodynamics. We shall make use of (7.84) for checking our numerical calculations, which are performed with the aim of observing the behaviour of the marginally relevant modes where $\Lambda \sim 0$, in section 6.

For $\Lambda = 0$, in [75] it was expected regardless of dimensionality that

$$\mathcal{F}_0 = -\mathcal{E}_0 = -\frac{1}{2}Ts_0 \tag{7.85}$$

which is derived by using $\mathcal{F}_0 = -\mathcal{E}_0$ from the trace Ward identity in [86], and (7.61). This fact was also proved by the numerical calculation in [75]. More generally, using (7.61) we expect $\mathcal{P}_0 = \frac{z}{n-1}\mathcal{E}_0$ implying

$$\mathcal{F}_0 = -\frac{z}{n-1}\mathcal{E}_0 \tag{7.86}$$

in any dimensionality. In the Gauss-Bonnet case we are considering, $z = n - 1 - 2(n-2)\tilde{\alpha}$ leads us to expect

$$\mathcal{F}_0 = -\eta(n, \tilde{\alpha})\mathcal{E}_0 \quad \text{where} \quad \eta(n, \tilde{\alpha}) = 1 - \frac{2(n-2)}{(n-1)}\tilde{\alpha}, \tag{7.87}$$

and

$$\frac{\mathcal{F}_0}{Ts} = -\frac{n-1-2\tilde{\alpha}(n-2)}{2(n-1)-2\tilde{\alpha}(n-2)}, \qquad \frac{\mathcal{E}_0}{Ts} = \frac{n-1}{2(n-1)-2\tilde{\alpha}(n-2)}. \tag{7.88}$$

In the next section we shall numerically compute $\eta(n, \tilde{\alpha})$ function for $n = 4, 5, \ldots, 9$ for all values of $\tilde{\alpha}$ we consider. We will see that our results are consistent with eqs. (7.87) and (7.88) in all dimensions.

7.6 Exploring Near the Quantum Critical Point

In holographic duality picture at zero temperature, we can imagine that the matter fields residing on the boundary of the spacetime become those of the conformal field theory, which is dual to the AdS spacetime in IR regimes, or the Lifshitz-like field theory (or quantum critical theory), which is dual to the Lifshitz spacetime in UV regimes. Our interests are to consider this configuration at finite temperature in the presence of the massive vector field and the Gauss-Bonnet terms in the gravity action, and to investigate the thermodynamic behaviour of the deformed GB-Lifshitz spacetime with a black hole,

which from the duality perspective corresponds to the marginally relevant operators near the quantum critical point. To generate the marginally relevant modes, the momentum scale Λ is introduced into the asymptotic Lifshitz metric, and it is assumed that $\Lambda \sim 0$, which is much smaller than the background temperature T ($\Lambda^z \ll T$). Hence it slightly deforms the Lifshitz spacetime, recovering the pure Lifshitz spacetime for $\Lambda = 0$.

In this section, our aims are to show the implications of the Gauss-Bonnet terms for holographic renormalization flow and to observe the behaviour of physical quantities such as the free energy density $\mathcal{F}/Ts$ and the energy density $\mathcal{E}/Ts$ as functions of $\log(\Lambda^z/T)$.

To do these, we first fix the undetermined parameters Λ, f_0, and p_0 (in the numerical calculation we consider the quantities Λr_+, $\frac{f}{f_0}\frac{r^z}{r_+^z}$, and $\frac{p}{p_0}\frac{r^2}{r_+^2}$). This is performed by numerically integrating the near horizon solution towards the boundary and reading off the matching values of Λ, f_0, and p_0. Based on these values the thermodynamic functions $\mathcal{F}$ and $\mathcal{E}$ are numerically integrated from near horizon to the boundary, and their numerical values are found for each h_0 in section 7.6.1. In section 7.6.2 we plot the data for $\mathcal{F}$ and $\mathcal{E}$ in a function of $\log(\frac{\Lambda^z}{T})$, and find the numerical data corresponding to $\eta(n, \tilde{\alpha})$ in (7.87).

7.6.1   Integrating towards the Lifshitz Boundary

As mentioned in section 5.1, we have scaling ambiguities in the metric due to the undetermined constants f_0 and p_0. We here find values of Λ for each h_0 by matching the numerical integration of near horizon solutions with the asymptotic solutions at the middle regions, and tune f_0 and p_0 with the matching value of Λ for the same h_0 by using the same method. For the numerical calculation, we set up the arbitrary scale $\mu = r_+^{-1}$ and use dimensionless quantities: r/r_+, Λr_+, $\mathcal{F}/Ts$, $\mathcal{E}/Ts$ and Λ^z/T.

Before performing the numerical work, we need to find the range of $\tilde{\alpha}$ and to decide the specific values of $\tilde{\alpha}$, as (7.70)-(7.72) describe two-parameter family $\{h_0, \tilde{\alpha}\}$ of black hole solutions, where the values of h_0 are variously taken for each $\tilde{\alpha}$ and will be discussed further in the following subsection.

Analyzing the asymptotic solutions (7.30)-(7.32) in section 2, recall that m_2 yields the restriction $\tilde{\alpha} \leq \frac{1}{4}$, where equality is attained when $z = \infty$. We expect that $|\tilde{\alpha}| < 1$ since the Gauss-Bonnet term associated with the coupling constant $\tilde{\alpha}$ via (7.10) is considered as a small correction to Einstein gravity. Then the range of $\tilde{\alpha}$ becomes

$$-1 < \tilde{\alpha} \leq \frac{1}{4}, \tag{7.89}$$

and this corresponds to the range

$$\frac{n}{2} \leq z < 3n - 5 \tag{7.90}$$

upon using $z = n - 1 - 2(n - 2)\tilde{\alpha}$ from (7.29). To observe the $\tilde{\alpha}$-dependence for a broad range of values, we sparsely choose the values of $\tilde{\alpha}$, which are the two positive values $\frac{1}{4}$, $\frac{1}{10}$, and three negative values $-\frac{1}{20}$ (bigger than $-\frac{1}{2(n-2)}$), $-\frac{1}{2(n-2)}$, $-\frac{3}{10}$ (smaller than $-\frac{1}{2(n-2)}$), and we also consider $\tilde{\alpha} = 0$ [75] for comparison. Table 7.1 lists the cases that we consider.

		z				
	$\tilde{\alpha} = \frac{1}{4}$	$\tilde{\alpha} = \frac{1}{10}$	$\tilde{\alpha} = 0$	$\tilde{\alpha} = -\frac{1}{20}$	$\tilde{\alpha} = -\frac{1}{2(n-2)}$	$\tilde{\alpha} = -\frac{3}{10}$
$n = 4$	2	2.6	3	3.2	4	4.2
$n = 5$	2.5	3.4	4	4.3	5	5.8
$n = 6$	3	4.2	5	5.4	6	7.4
$n = 7$	3.5	5	6	6.5	7	9
$n = 8$	4	5.8	7	7.6	8	10.6
$n = 9$	4.5	6.6	8	8.7	9	12.2

Table 7.1: values of z according to n and $\tilde{\alpha}$

Matching Λ

In the asymptotic solutions (7.30)-(7.32), Λ is the only unfixed quantity. To fix Λ, we expand these solutions into the high energy regimes by introducing the arbitrary scale μ and using the condition (7.38), which assumed that $\mu \gg \Lambda$. Then we set $\mu = r_+$, which means that our asymptotic solutions are described at the energy scale r_+, and fit the asymptotic solutions towards the horizon.

Near the horizon the expanded black hole solutions (7.70)-(7.72) should be changed to in functions of k, q, and y by using the relations (7.38) so as to avoid the scale ambiguities

of f_0 and p_0 for now. Then we numerically integrate the solutions towards the boundary by obeying the equations of the motion (7.24)-(7.26).

At the middle region, we match the fitting of the asymptotic solutions with the numerical integration for given h_0 by controlling the value of $\log \Lambda r_+$ as shown in Fig.7.2, which displays the function k for $n = 4$ and for each value of $\tilde{\alpha}$ in Table7.1. The red dashed line is the fitted asymptotic solution, that is the one including $\log \Lambda r_+$, and the blue solid line is the result of numerical integration of the horizon solution. In our numerical work, the integration is performed from $\log(r/r_+) \sim -0.15$ to $\log(r/r_+) \sim -10^4$.

Note that in Fig.7.2, the graph (f) shows the different behaviour from (a)-(e) by having a positive slope, which means that the k function decreases as the boundary is approached. This positive-slope pattern is observed only for the k function in the range $\tilde{\alpha} < -1/(2(n-2))$, which is equivalent to $z > n$; for $\tilde{\alpha} \geq -1/(2(n-2))$ or $z \leq n$, the slope of k is negative, meaning it increases as the boundary is approached. The signs of the slopes of q and y versus $\log(r/r_+)$ are negative for all values of $\tilde{\alpha}$. Note that k is defined via $h = k\sqrt{f}$ from (7.22), where f is the $-g_{tt}$-component of the metric and h is the vector field potential. Hence k only has information about the charge of the vector field and the Gauss-Bonnet coupling constant $\tilde{\alpha}$. Fig.7.2-(f) illustrates that when $z > n$ the weight for the charge of the vector field and $\tilde{\alpha}$ near the horizon become larger than at the boundary.

This process is performed by varying h_0. Beyond the maximum value of $\log \Lambda r_+$, the numerical integration of the near horizon solution exponentially grows as the boundary is approached, and so does not match the asymptotic solution. This means that if the horizon flux ϕ in (7.77) is too large, which corresponds to high temperature, the deformation of the spacetime is not allowed any more and becomes the asymptotically pure Gauss-Bonnet-Lifshitz spacetime (having a black hole). Hence there exists a maximum value of h_0.

The maximum values of h_0 are recorded in Table 7.2, and show linearly increasing dependence on the dimensionality of spacetime for the same $\tilde{\alpha}$. For decreasing $\tilde{\alpha}$ the slope gets larger as shown in Fig.7.3, where dots are the numerical data of the maximum value of h_0 and the data obtained with the same value of $\tilde{\alpha}$ are connected with the line. For $n = 4$, the dependence of $\tilde{\alpha}$ (or z) on the maximum values of h_0 are also found in Fig.7.4, where the dots the maximum values of h_0, and the lines are the fitting functions obtained from the data. These are not linear; rather $h_{max} \sim -0.633878 + 0.553198z + 0.0680033z^2$ for Fig.7.4(a) and $h_{max} \sim 1.63775 - 3.84487\tilde{\alpha} + 1.08805\tilde{\alpha}^2$ for Fig.7.4(b). These results indicate that h_0 obviously depends on $\tilde{\alpha}$.
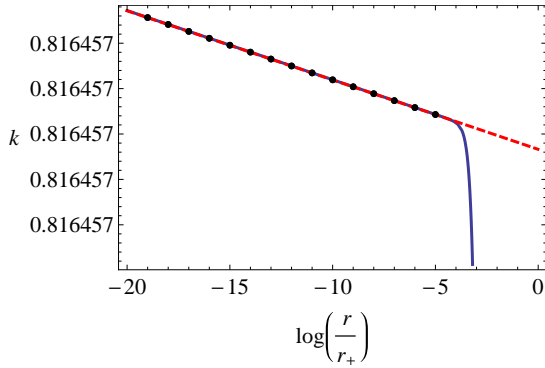
A minimum value of the flux also exists; its value becomes zero at the horizon. In this case, the influence of the massive vector field vanishes, and so the spacetime is described completely by an asymptotically Gauss-Bonnet AdS black hole.
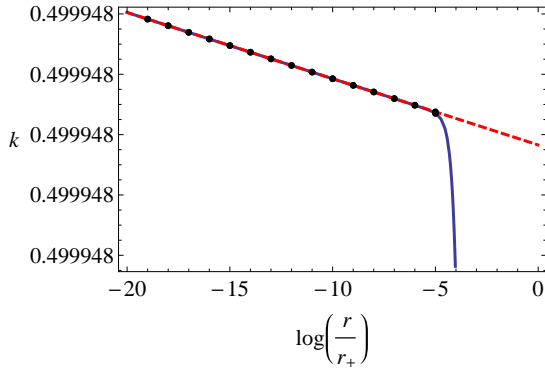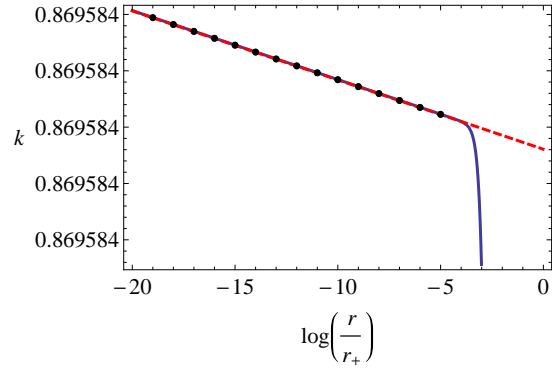
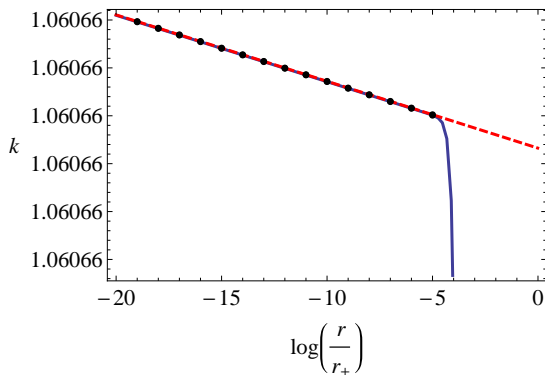(a) For $\tilde{\alpha} = 1/4$ and $n = 4$, $h_0 = 0.75120$ corresponds to $\log(\Lambda r_+) = -23874.4$
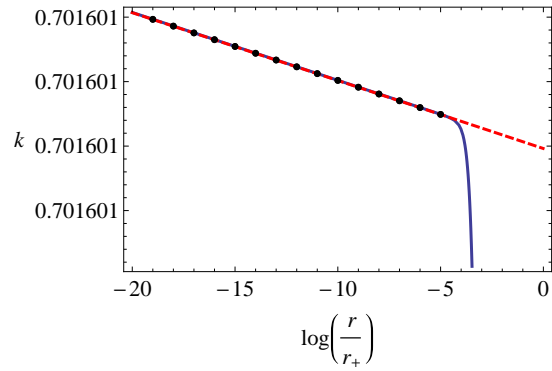
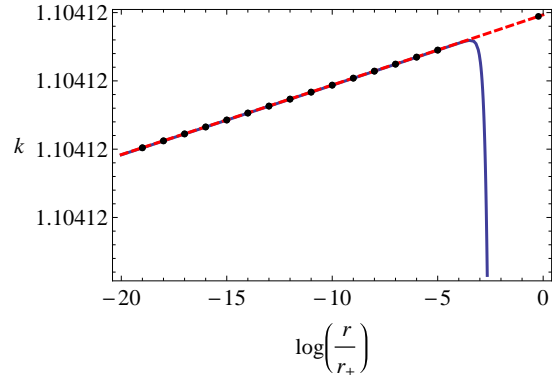(b) For $\tilde{\alpha} = 1/10$ and $n = 4$, $h_0 = 1.26160$ corresponds to $\log(\Lambda r_+) = -8611.8$

(c) For $\tilde{\alpha} = 0$ and $n = 4$, $h_0 = 1.63430$ corresponds to $\log(\Lambda r_+) = -5167.9$

(d) For $\tilde{\alpha} = -1/20$ and $n = 4$, $h_0 = 1.82980$ corresponds to $\log(\Lambda r_+) = -3422$

(e) For $\tilde{\alpha} = -1/4$ and $n = 4$, $h_0 = 2.66868$ corresponds to $\log(\Lambda r_+) = -4137.2$

(f) For $\tilde{\alpha} = -3/10$ and $n = 4$, $h_0 = 2.89170$ corresponds to $\log(\Lambda r_+) = -2110.4$

Figure 7.2: Extracting $\log(\Lambda r_+)$

117

Very small values of h_0 correspond to the zero temperature limit $\Lambda^z/T \to \infty$; in this limit the AdS spacetime emerges in the IR regime. Hence for fixed $\Lambda \sim 0$, the slightly deformed UV Lifshitz spacetime and IR AdS spacetime with Gauss-Bonnet corrections emerge instead. Thus we might expect holographic renormalization group flow at zero temperature similar to the $\tilde{\alpha} = 0$ case [56], [18] . The presence and nature of the renormalization flow interpolating both spacetimes for $\tilde{\alpha} \neq 0$ has not yet been studied yet; it remains for future work.
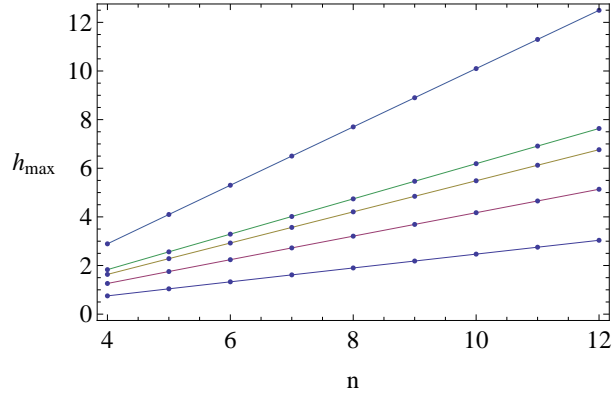
Figure 7.3: Dots are the maximum value of h_0 for given n and $\tilde{\alpha}$, and dots sharing the same $\tilde{\alpha}$ are connected with the same color of line to distinguish them. From the bottom, each different color of line respectively indicates $\tilde{\alpha} = \frac{1}{4}, \frac{1}{10}, 0, -\frac{1}{20}$, and $-\frac{3}{10}$.

	h_{max}					
	$\tilde{\alpha} = \frac{1}{4}$	$\tilde{\alpha} = \frac{1}{10}$	$\tilde{\alpha} = 0$	$\tilde{\alpha} = -\frac{1}{20}$	$\tilde{\alpha} = -\frac{1}{2(n-2)}$	$\tilde{\alpha} = -\frac{3}{10}$
$n = 4$	0.7512	1.2616	1.6343	1.8298	2.6687	2.8917
$n = 5$	1.0416	1.7528	2.2822	2.5622	3.2519	4.0981
$n = 6$	1.3288	2.2394	2.9255	3.2900	3.8614	5.3005
$n = 7$	1.6147	2.7239	3.5668	4.0158	4.4818	6.5012
$n = 8$	1.8998	3.2073	4.2070	4.7406	5.1079	7.7011
$n = 9$	2.1844	3.6900	4.8465	5.4647	5.7372	8.9004
$n = 10$	2.4688	4.1723	5.4856	6.1884	6.3686	10.0992
$n = 11$	2.7530	4.6543	6.1244	6.9118	7.0013	11.2977
$n = 12$	3.0371	5.1361	6.7629	7.6346	7.6349	12.4958

Table 7.2: the maximum values of h_0 for each values of n and $\tilde{\alpha}$

(a) the maximum value of h_0 on z
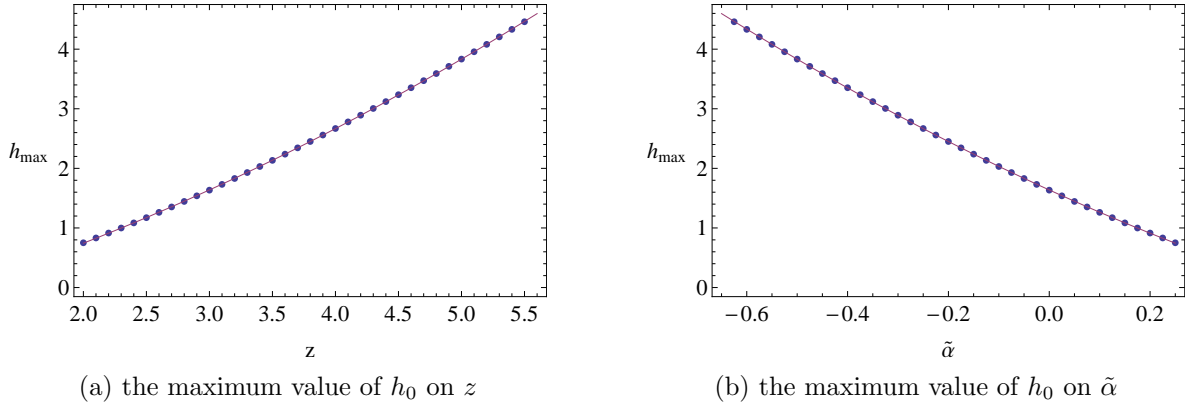
(b) the maximum value of h_0 on $\tilde{\alpha}$

Figure 7.4: dependence of z or $\tilde{\alpha}$ on h_{max} when $n = 4$.

Matching f_0 and p_0

We have other variables left to be determined, which are f_0 and p_0 in (7.70)-(7.72). Since Λ is fixed, we tune f_0 and p_0 based on the value of Λ for each set $\{h_0, \tilde{\alpha}\}$ by using the same method applied for Λ.

We bring the asymptotic solutions (7.39)-(7.40) expanded in the high energy regime in terms of μ, where $\mu = r_+^{-1}$, and fit the solutions with the determined value of Λ (given $\{h_0, \tilde{\alpha}\}$) to the horizon. Near the horizon, we numerically integrate the equations of motion (7.19)-(7.21) towards the boundary using (7.70)-(7.72) as initial conditions. At the middle region, we adjust $f_0 r_+^{2z}$ or $p_0 r_+^2$ and read off the values for which both solutions agree. This process for f and p functions is depicted in Figures 7.5 and 7.6 for $\tilde{\alpha} = 1/4, 1/10, 0, -1/20, -1/4, -3/10$ in $n = 4$. The red dashed line is the fit of the boundary solution and the blue solid line is the numerical result of the near horizon solution. For $n = 5, 6, 7, 8, 9$ higher-dimensional cases we find similar patterns for the same values of $\tilde{\alpha}$.

Since we have now fixed Λ, f_0, and p_0, the thermodynamic quantities calculated in (7.77) can be determined. The temperature is given by

$$\log\left(\frac{\Lambda^z}{T}\right) = z \log(\Lambda r_+) + \log(2\pi) - \frac{1}{2}\log(f_0 r_+^{2z}) \tag{7.91}$$

which is computed from the known values of Λ and f_0. In next sections, we collect all data on the free energy density $\mathcal{F}/Ts$ and the energy density $\mathcal{E}/Ts$ for given $\{h_0, \tilde{\alpha}\}$, where the specific value of h_0 corresponds to each set of values $\{\Lambda, f_0, p_0\}$, and fit their results
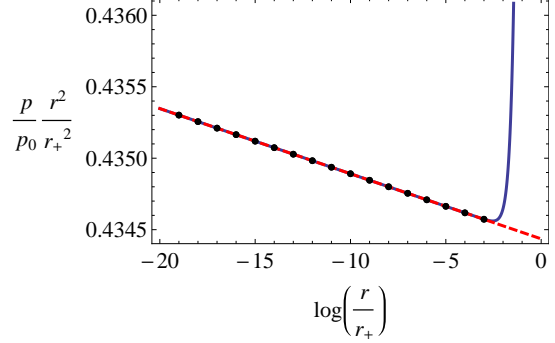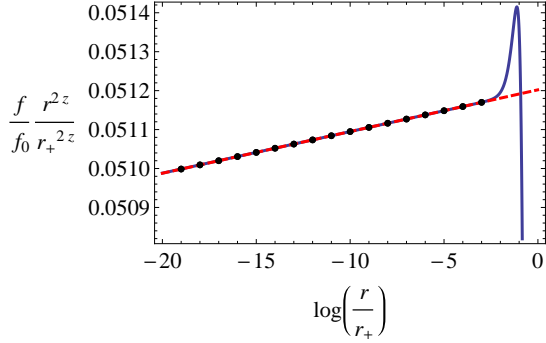
(a) For $\tilde{\alpha} = 1/4$ ($z = 2$) and $h_0 = 0.75120$, which corresponds to $\log(\Lambda r_+) = -23874.4$, the red dashed line is matched to the blue solid line at $f_0 r_+^{2z} = 19.66$ (left) and $p_0 r_+^2 = 2.2942$ (right)
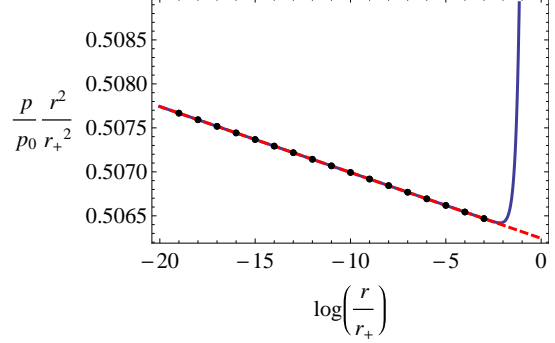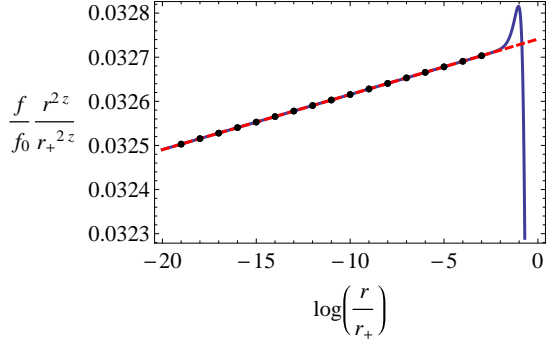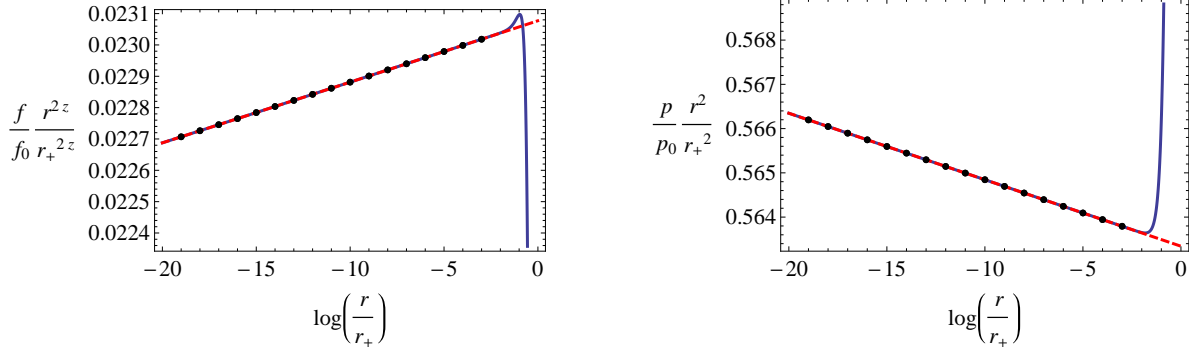

(b) For $\tilde{\alpha} = 1/10$ (z=2.6) and $h_0 = 1.26160$, which corresponds to $\log(\Lambda r_+) = -8611.8$, the red dashed line is matched to the blue solid line at $f_0 r_+^{2z} = 30.66$ (left) and $p_0 r_+^2 = 1.9725$ (right)
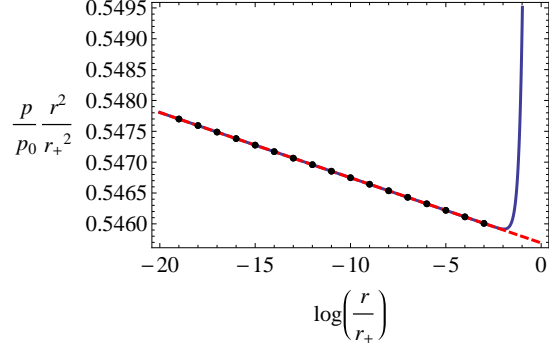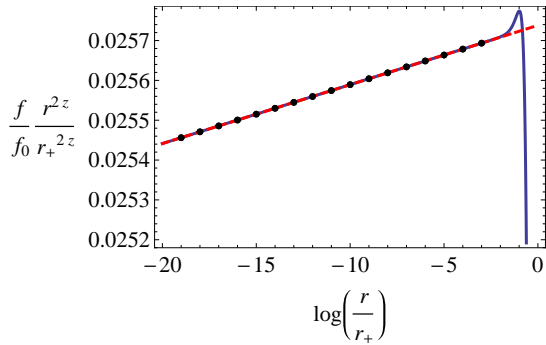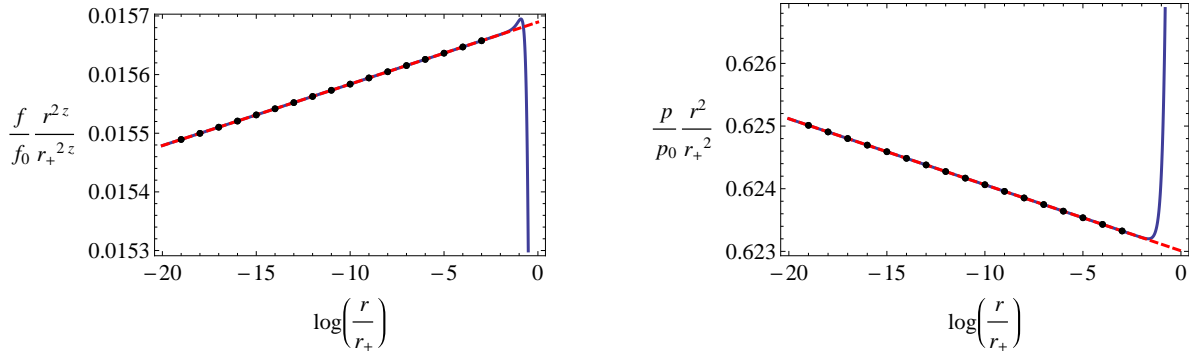

(c) For $\tilde{\alpha} = 0$ (z=3) and $h_0 = 1.63430$, which corresponds to $\log(\Lambda r_+) = 5167.9$, the red dashed line is matched to the blue solid line at $f_0 r_+^{2z} = 39.00$ (left) and $p_0 r_+^2 = 1.8303$ (right)
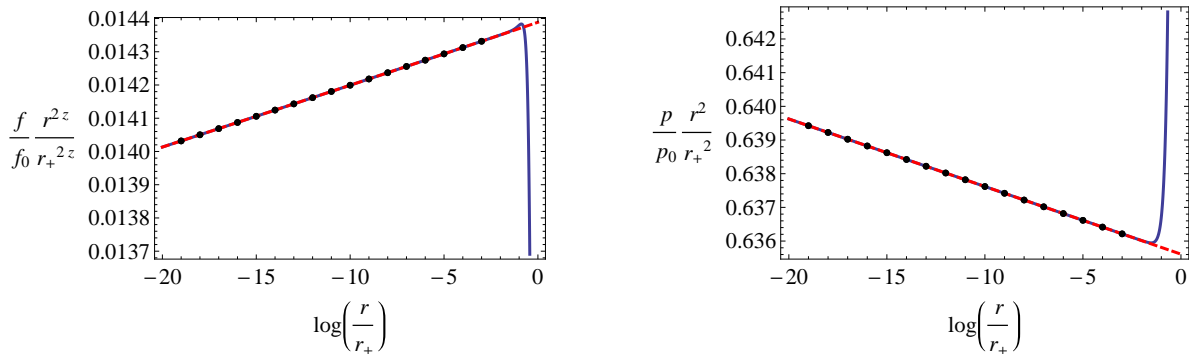
Figure 7.5: Extracting f_0 and p_0 for positive and zero $\tilde{\alpha}$ in $n = 4$

(a) For $\tilde{\alpha} = -1/20$ ($z = 3.2$) and $h_0 = 1.82980$, which corresponds to $\log(\Lambda r_+) = -3422$, the red dashed line is matched to the blue solid line at $f_0 r_+^{2z} = 43.53$ (left) and $p_0 r_+^2 = 1.7727$ (right)

(b) For $\tilde{\alpha} = -1/4$ ($z = 4$) and $h_0 = 2.66868$, which corresponds to $\log(\Lambda r_+) = -4137.2$, the red dashed line is matched to the blue solid line at $f_0 r_+^{2z} = 63.88$ (left) and $p_0 r_+^2 = 1.6042$ (right)

(c) For $\tilde{\alpha} = -3/10$ ($z = 4.2$) and $h_0 = 2.89170$, which corresponds to $\log(\Lambda r_+) = -2110.4$, the red dashed line is matched to the blue solid line at $f_0 r_+^{2z} = 69.76$ (left) and $p_0 r_+^2 = 1.5719$ (right)

Figure 7.6: Extracting f_0 and p_0 for negative $\tilde{\alpha}$ in $n = 4$

to a function of $\log \Lambda^z/T$. We consider the dimensionless quantities $\mathcal{F}/Ts$ and $\mathcal{E}/Ts$. For the entropy density s from (7.77), we consider the dimensionless quantity $s/T^{(n-1)/z}$ as a function of $\log(\Lambda/T)$, plotted in Fig.F.1.
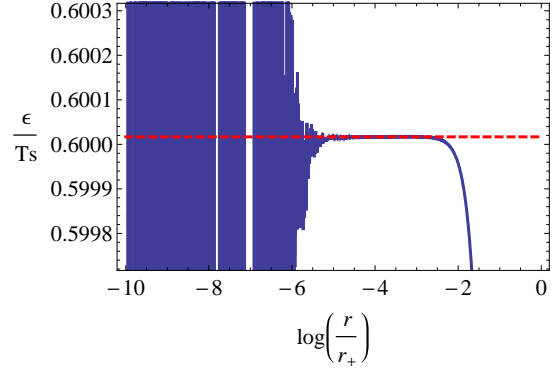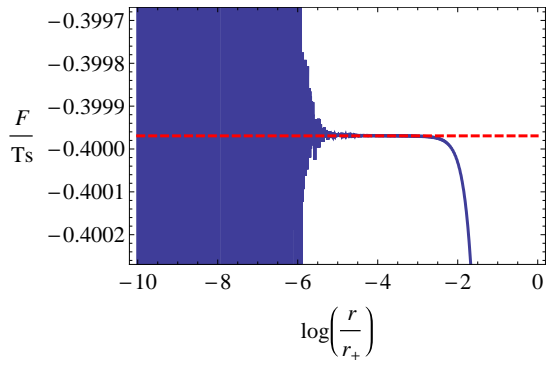
Free Energy Density and Energy Density

The dimensionless quantities $\mathcal{F}/Ts$ and $\mathcal{E}/Ts$, respectively the free energy density (7.48) and the energy density (7.60), are numerically integrated from the horizon towards the boundary for given $\{h_0, \tilde{\alpha}\}$. The results are depicted in Figures 7.7 and 7.8, where the blue line is the numerical result and the red dashed line is read off from the stable value in the flat region. As shown in Figures 7.7 and 7.8, $\mathcal{F}/Ts$ and $\mathcal{E}/Ts$ yield constant values over some finite range of $\log(r/r_+)$, but oscillate infinitely upon approaching the boundary. The reason for these diverging and oscillating behaviours can be found in the holographic renormalization process in section 3. Recall that the free energy density and the energy density diverge as $r \to 0$, and so the counterterms (7.63)-(7.65) were constructed to render them finite. As mentioned, C_0 and C_1 expand to infinite series in $\log(\Lambda r_+)$; however only terms up to $1/\log^4(\Lambda r)$ (15 terms for each of C_0 and C_1) are computed due to limitations of the analytic calculation. This finite number of terms is employed in the numerical calculation of $\mathcal{F}/Ts$ and $\mathcal{E}/Ts$. On the other hand, the numerical work includes higher orders (i.e. higher than $1/\log^4 \Lambda r$), and so the diverging properties are not totally eliminated by our analytic solutions using counterterms.

In Figures 7.8 (b) and (c), which corresponds to cases of $z = 4$ and $z = 4.2$ respectively, unstable behaviours are observed near the horizon. To see the whole pattern the scales are zoomed out in Figure 7.9. This pattern of having a sharp peak near the horizon commonly appears for the range $z \gtrsim n$ for any n and h_0. This unstable behaviour of $\mathcal{F}/Ts$ and $\mathcal{E}/Ts$ for $z \gtrsim n$ can be understood via the same rationale for the different pattern of the k-function for $z > n$. That is, as z gets bigger and approaches $z \sim n$ due to the decreasing value of $\tilde{\alpha}$, the effect of both the charge of the vector field and $\tilde{\alpha}$ gets bigger near the horizon than at the boundary, causing unstable behaviour in both $\mathcal{F}/Ts$ and $\mathcal{E}/Ts$.

7.6.2   Behaviours of $\mathcal{E}$ and $\mathcal{F}$ near Quantum Critical Regimes

Collecting data for each of the values of $\{h_0, \tilde{\alpha}\}$, we plot $\mathcal{F}/Ts$ and $\mathcal{E}/Ts$ as functions of $\log \Lambda^z/T$ and find their fitting functions. These results are displayed in Figures 7.11 and 7.12, for which $n = 4$; the dots are the numerical results and the solid line is the fitting function found. The fitting functions for each n are recorded in Tables 7.3, F.1, F.2, F.3,

(a) For $\tilde{\alpha} = 1/4$ ($z = 2$) and $h_0 = 0.75120$, which corresponds to $\log(\Lambda r_+) = -23874.4$. Blue line is the numerical results of the free energy density over Ts (left) and the energy density over Ts (right), and red dashed line is reading-off the constant value in the intermediate regime.
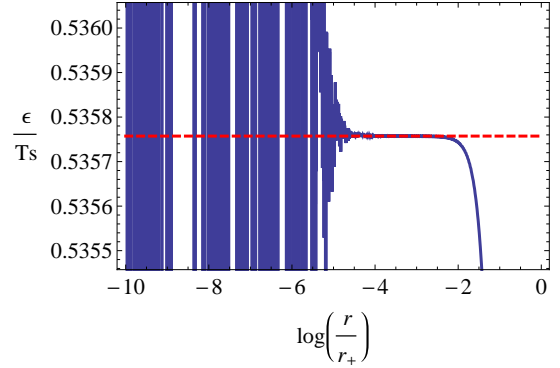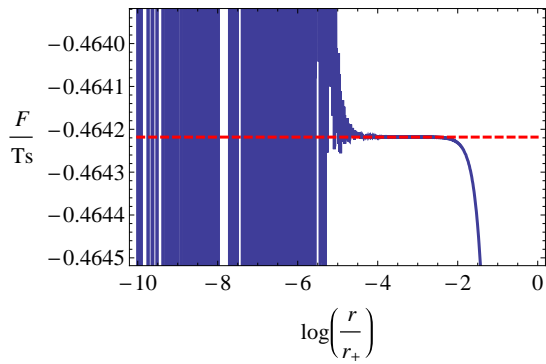
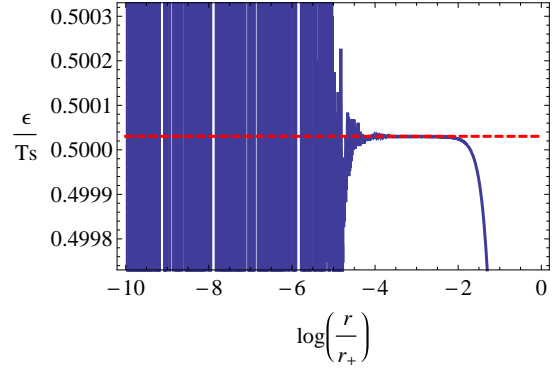(b) For $\tilde{\alpha} = 1/10$ ($z = 2.6$) and $h_0 = 1.26156$, which corresponds to $\log(\Lambda r_+) = -5648.3$. Blue line is the numerical results of the free energy density over Ts (left) and the energy density over Ts (right), and red dashed line is reading-off the constant value in the intermediate regime.

(c) For $\tilde{\alpha} = 0$ (z=3) and $h_0 = 1.63430$, which corresponds to $\log(\Lambda r_+) = 5167.9$. Blue line is the numerical results of the free energy density over Ts (left) and the energy density over Ts (right), and red dashed line is reading-off the constant value in the intermediate regime.

Figure 7.7: $\mathcal{F}/Ts$ and $\mathcal{E}/Ts$ versus $\log(\frac{r}{r_+})$ for positive and zero $\tilde{\alpha}$ in $n = 4$
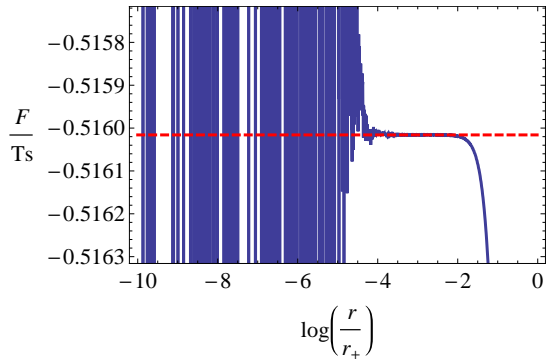
(a) For $\tilde{\alpha} = -1/10$ ($z = 3.2$) and $h_0 = 1.82976$, which corresponds to $\log(\Lambda r_+) = -2523.1$. Blue line is the numerical results of the free energy density over Ts (left) and the energy density over Ts (right), and red dashed line is reading-off the constant value in the intermediate regime.
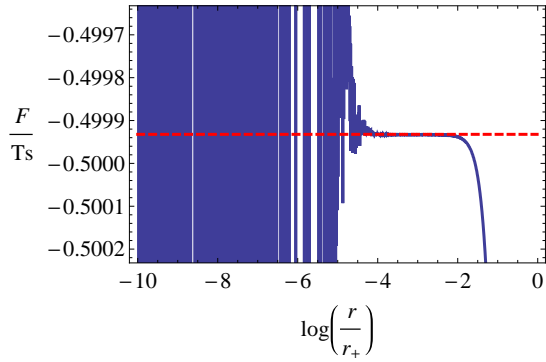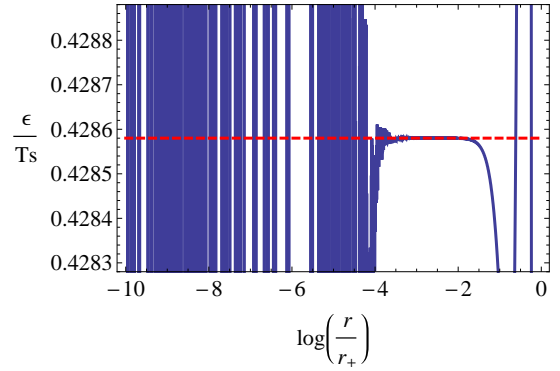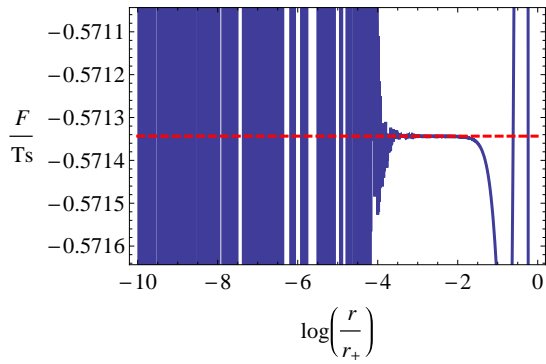

(b) For $\tilde{\alpha} = -1/4$ ($z = 4$) and $h_0 = 2.66868$, which corresponds to $\log(\Lambda r_+) = -4137.2$. Blue line is the numerical results of the free energy density over Ts (left) and the energy density over Ts (right), and red dashed line is reading-off the constant value in the intermediate regime.
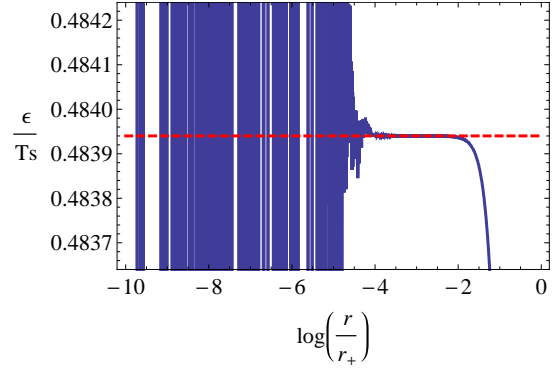

(c) For $\tilde{\alpha} = -3/10$ ($z = 4.2$) and $h_0 = 2.89170$, which corresponds to $\log(\Lambda r_+) = -2110.4$. Blue line is the numerical results of the free energy density over Ts (left) and the energy density over Ts (right), and red dashed line is reading-off the constant value in the intermediate regime.
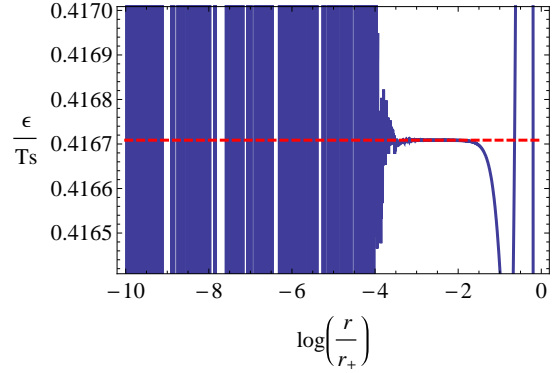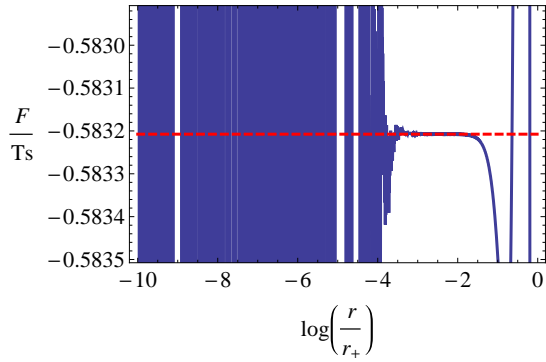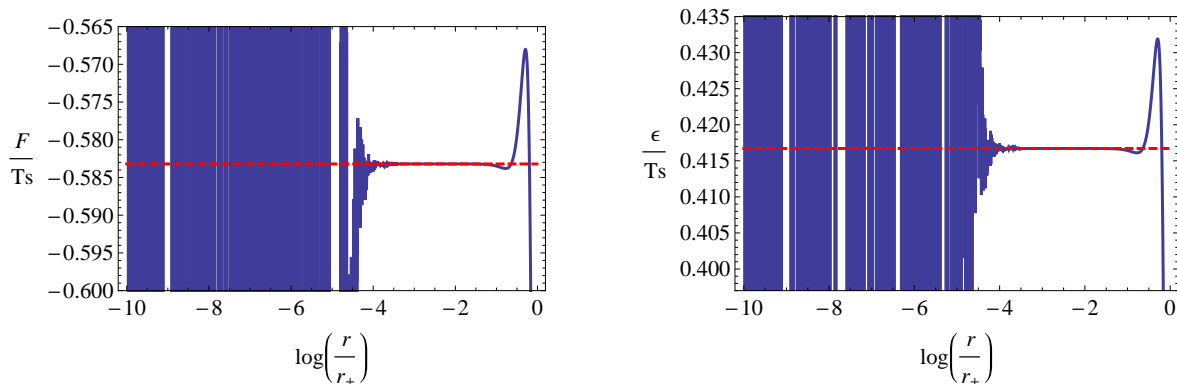
Figure 7.8: $\mathcal{F}/Ts$ and $\mathcal{E}/Ts$ versus $\log(\frac{r}{r_+})$ for negative $\tilde{\alpha}$ in $n = 4$

125

(a) enlarged graphs of the Fig.7.8-(c)

Figure 7.9: $\mathcal{F}/Ts$ and $\mathcal{E}/Ts$ versus $\log(\frac{r}{r_+})$ for negative $\tilde{\alpha}$ in $n = 4$

F.4, and F.5. We subsequently check that our numerical results for $\mathcal{F}/Ts$ and $\mathcal{E}/Ts$ with the marginally relevant modes agree with the integrated first law of thermodynamics in (7.84) with an error of less than 10^{-4} as shown in Fig. 7.13.

It is straightforward to show using the data in the rightmost columns of tables 7.3, F.1, F.2, F.3, F.4, and F.5, that the values of $\mathcal{F}_0/\mathcal{E}_0 = -\eta(n, \tilde{\alpha})$ are consistent with the expression (7.87). We illustrate the $n = 4$ case in Fig. 7.10, where the red dots are the numerical data and the solid line is the expression for $\eta(4, \tilde{\alpha})$ given in eq. (7.87). We recover the values of $\mathcal{F}_0/Ts$ and $\mathcal{E}_0/Ts$ in (7.88) in the absence of the marginally relevant mode ($\Lambda = 0$) at finite temperature.

We also observed how $\mathcal{F}/Ts$ and $\mathcal{E}/Ts$ behave with the marginally relevant modes according to different values of n and $\tilde{\alpha}$ when $\Lambda^z/T \to 0$. When $\Lambda \neq 0$ the marginally relevant modes (generated by small values of Λ) contribute at sub-leading order to $\mathcal{F}/Ts$ and $\mathcal{E}/Ts$ as functions of $\log \Lambda^z/T$, where $\Lambda^z/T \to 0$. From Figures 7.11, 7.12 and Tables 7.3, F.1, F.2, F.3, F.4, and F.5, we see that for the same dimension n, as z increases (or $\tilde{\alpha}$ decreases), this sub-leading contribution decreases. Furthermore, for the same value of $\tilde{\alpha}$, as z increases (or n increases), this sub-leading contribution also decreases. That is, when z increases due to either decreasing $\tilde{\alpha}$ or increasing n by $z = n - 1 - 2(n-2)\tilde{\alpha}$, this sub-leading contribution decreases.

126
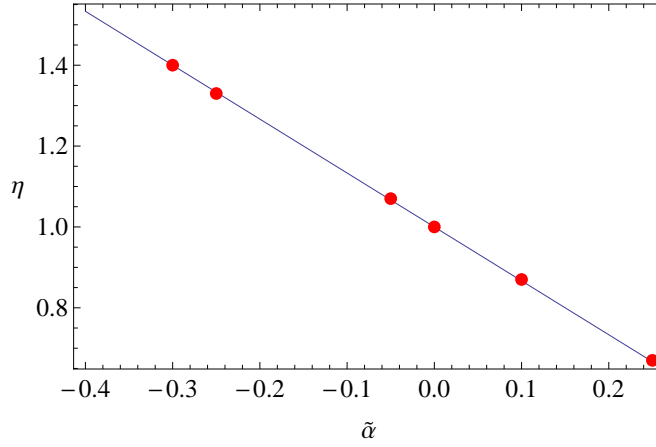
Figure 7.10: For $n = 4$, red dots are the numerical data and blue solid line is the fitting of the η function

7.7 Summary and Discussion

Our main purpose has been to understand how the Gauss-Bonnet coupling constant $\tilde{\alpha}$, defined in (7.10), plays a role in the deformation of Lifshitz holography in $(n+1)$ dimensions.

$(n = 4)$	$\frac{\mathcal{F}}{Ts}$	$\frac{\mathcal{E}}{Ts}$	$\frac{\mathcal{F}}{\mathcal{E}}$
$\tilde{\alpha} = 1/4$ or $z = 2$	$-0.40 - \frac{1.21}{\log \Lambda^z/T} + \cdots$	$0.60 - \frac{1.21}{\log \Lambda^z/T} + \cdots$	$-0.67 - \frac{3.37}{\log \Lambda^z/T} + \cdots$
$\tilde{\alpha} = 1/10$ or $z = 2.6$	$-0.46 - \frac{0.83}{\log \Lambda^z/T} + \cdots$	$0.54 - \frac{0.83}{\log \Lambda^z/T} + \cdots$	$-0.87 - \frac{2.89}{\log \Lambda^z/T} + \cdots$
$\tilde{\alpha} = 0$ or $z = 3$	$-0.50 - \frac{0.76}{\log \Lambda^z/T} + \cdots$	$0.50 - \frac{0.76}{\log \Lambda^z/T} + \cdots$	$-1.0 - \frac{3.00}{\log \Lambda^z/T} + \cdots$
$\tilde{\alpha} = -1/20$ or $z = 3.2$	$-0.52 - \frac{0.73}{\log \Lambda^z/T} + \cdots$	$0.48 - \frac{0.74}{\log \Lambda^z/T} + \cdots$	$-1.1 - \frac{3.13}{\log \Lambda^z/T} + \cdots$
$\tilde{\alpha} = -1/4$ or $z = 4$	$-0.57 - \frac{0.69}{\log \Lambda^z/T} + \cdots$	$0.43 - \frac{0.69}{\log \Lambda^z/T} + \cdots$	$-1.3 - \frac{3.76}{\log \Lambda^z/T} + \cdots$
$\tilde{\alpha} = -3/10$ or $z = 4.2$	$-0.58 - \frac{0.69}{\log \Lambda^z/T} + \cdots$	$0.42 - \frac{0.69}{\log \Lambda^z/T} + \cdots$	$-1.4 - \frac{3.95}{\log \Lambda^z/T} + \cdots$
$\vdots$	$\vdots$	$\vdots$	$\vdots$

Table 7.3: fitting functions for $\frac{\mathcal{F}}{Ts}$, $\frac{\mathcal{E}}{Ts}$, and $\frac{\mathcal{F}}{\mathcal{E}}$

127
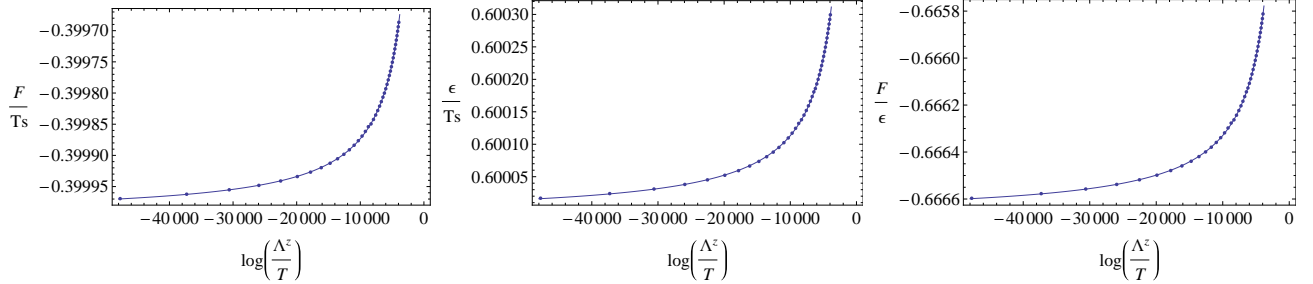
(a) For $\alpha = \frac{1}{4}$ (or $z = 2$). Dots are numerical results running h_0 from 0.75120 to 0.75038, which corresponds to $\log \Lambda^z/T$ from -47748.5 to -3945.48. Solid line is the fitting function denoted in Table 7.3.
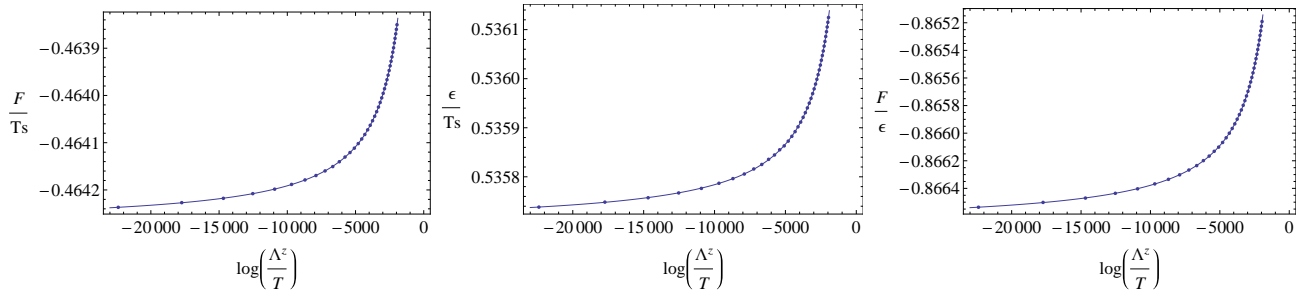
(b) For $\alpha = \frac{1}{10}$ (or $z = 2.6$). Dots are numerical results running h_0 from 1.26160 to 1.26078, which corresponds to $\log \Lambda^z/T$ from -22390.6 to -1960.29. Solid line is the fitting function denoted in Table 7.3.
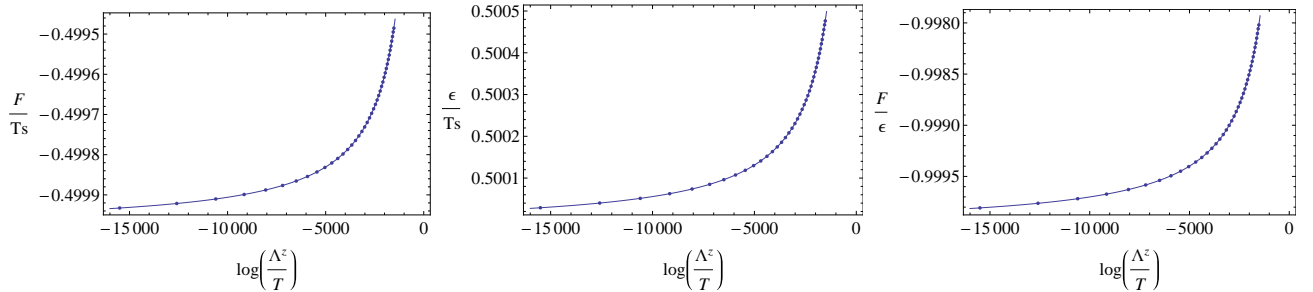
(c) For $\alpha = 0$ (or $z = 3$). Dots are numerical results running h_0 from 1.63430 to 1.63348, which corresponds to $\log \Lambda^z/T$ from -15503.7 to -15522.51. Solid line is the fitting function denoted in Table 7.3.

Figure 7.11: Plots of $\mathcal{F}/Ts$, $\mathcal{E}/Ts$ and $\mathcal{F}/\mathcal{E}$ versus $\log(\Lambda^z/T)$ for positive and zero $\tilde{\alpha}$ in $n = 4$
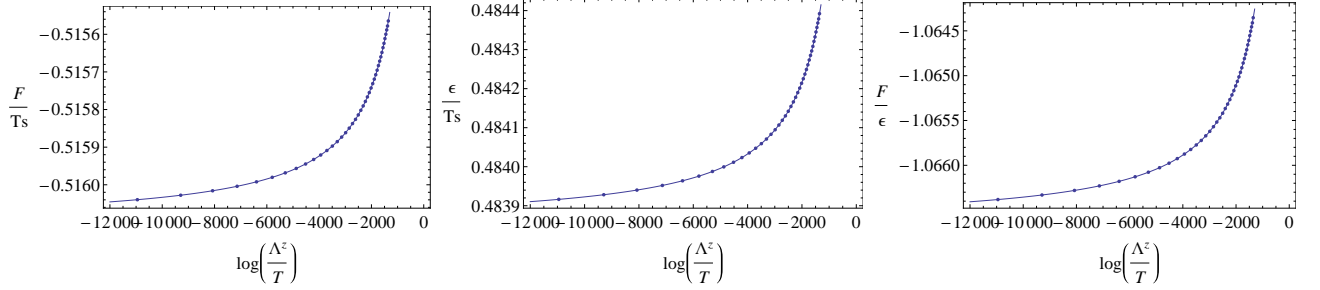
(a) For $\alpha = -\frac{1}{20}$ (or $z = 3.2$). Dots are numerical results running h_0 from 1.82980 to 1.82898, which corresponds to $\log \Lambda^z/T$ from -10950.4 to -1354.62. Solid line is the fitting function denoted in Table 7.3.
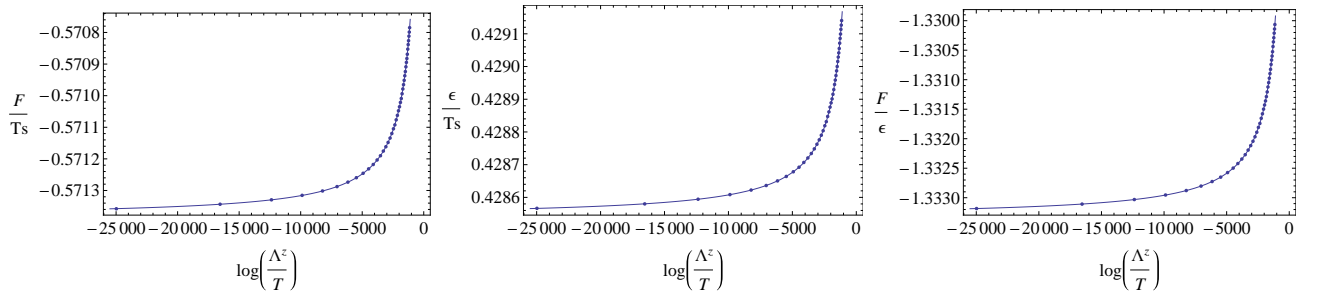
(b) For $\tilde{\alpha} = -\frac{1}{4}$ (or $z = 4$). Dots are numerical results running h_0 from 2.66870 to 2.66788, which corresponds to $\log \Lambda^z/T$ from -24978.2 to -1147.85. Solid line is the fitting function denoted in Table 7.3.
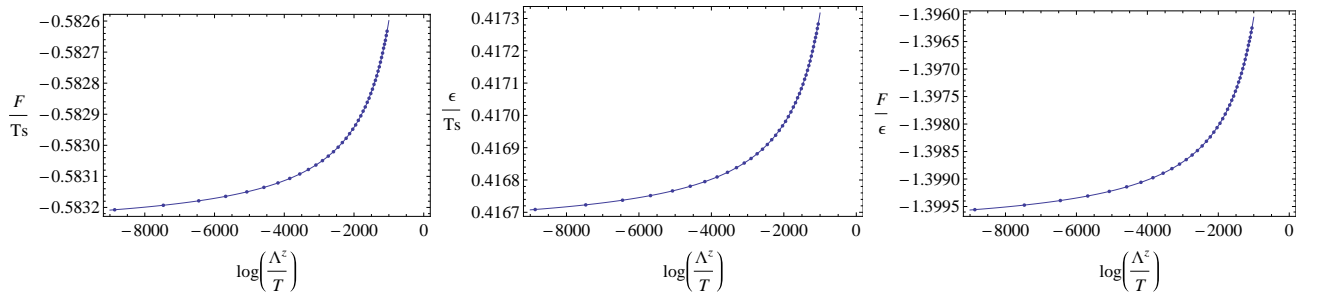
(c) For $\tilde{\alpha} = -\frac{3}{10}$ (or $z = 4.2$). Dots are numerical results running h_0 from 2.89170 to 2.89088, which corresponds to $\log \Lambda^z/T$ from -8863.96 to -1051.13. Solid line is the fitting function denoted in Table 7.3.

Figure 7.12: Plots of $\mathcal{F}/Ts$, $\mathcal{E}/Ts$ and $\mathcal{F}/\mathcal{E}$ versus $\log(\Lambda^z/T)$ for negative $\tilde{\alpha}$ in $n = 4$.
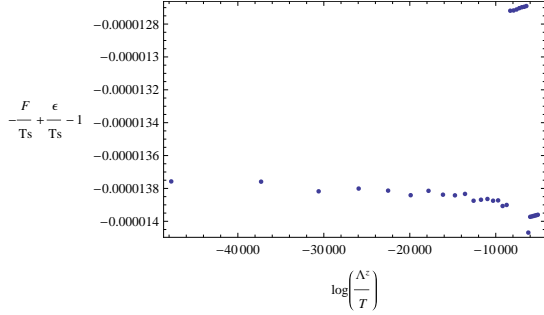
(a) For $\tilde{\alpha} = \frac{1}{4}$ ($or\,z = 2$) and h_0 runs from 0.75120 to 0.75038.
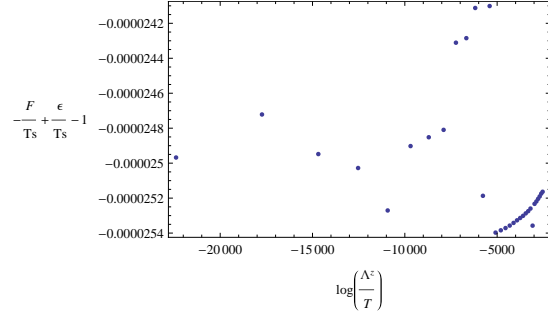
(b) For $\tilde{\alpha} = \frac{1}{10}$ (or $z = 2.6$) and h_0 from 1.26160 to 1.26078.
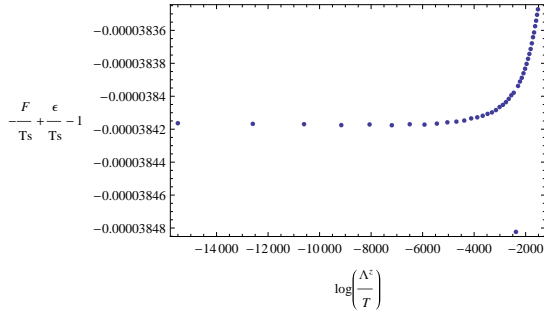
(c) For $\tilde{\alpha} = 0$ (or $z = 3$) and h_0 runs from 1.63430 to 1.63348
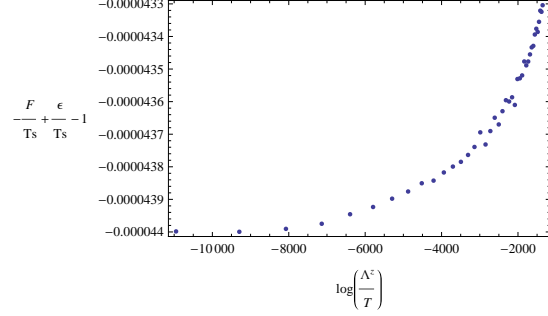
(d) For $\tilde{\alpha} = -\frac{1}{20}$ (or $z = 3.2$) and h_0 runs from 1.82980 to 1.82898
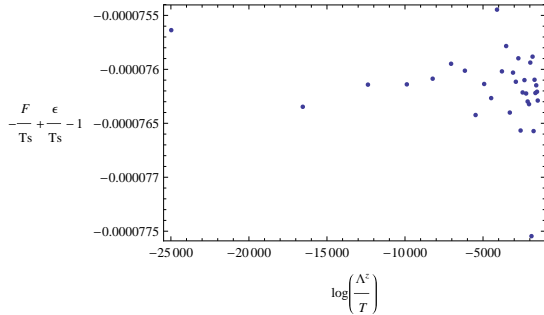
(e) For $\tilde{\alpha} = -\frac{1}{4}$ (or $z = 4$) and h_0 runs from 2.66870 to 2.66788
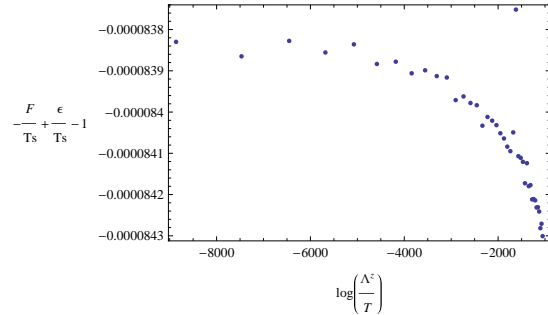
(f) For $\tilde{\alpha} = -\frac{3}{10}$ (or $z = 4.2$). h_0 runs from 2.89170 to 2.89088

Figure 7.13: Plots of errors from $-\mathcal{F}/Ts + \mathcal{E}/Ts - 1$

130

First recall where $\tilde{\alpha}$ makes a contribution. In the Lifshitz spacetime without the Gauss-Bonnet term ($\tilde{\alpha} = 0$), the anisotropy of the spacetime is governed by the massive vector field. This vector field allows a marginal mode only at $z = (n-1)$ [75]. When the Gauss-Bonnet term is included in the Lifshitz gravity action, the marginal mode is now restricted by $z = n - 1 - 2(n-2)\tilde{\alpha}$. In other words z is determined not only by the massive vector field but also by the value of $\tilde{\alpha}$. Considering the marginal mode in the pure Lifshitz case (i.e.$\Lambda = 0$) for the metric (7.15), $\tilde{\alpha}$ contributes to the function $f = \frac{1}{r^{2z}}$ in the metric via z and also modifies the charge of the massive vector field by $q^2 = \frac{z-1}{z}(1 - 2\tilde{\alpha})$. However, in the deformed Lifshitz spacetime (i.e. considering marginally relevant modes generated by $\Lambda \sim 0$), $\tilde{\alpha}$ modifies both f and p in the metric with Λ and involves the massive vector field, as shown in (7.30)-(7.32) or (7.35)-(7.36).

We found the asymptotic solutions in (7.30)-(7.32), and obtained the free energy density in (7.48) and the energy density in (7.60) by holographic renormalization. We next derived the near-horizon expansion of the black hole solution in (7.70)-(7.72), characterized by two parameters h_0 and $\tilde{\alpha}$, and calculated thermodynamic quantities such as temperature T and entropy density s in (7.77). As our metric solutions contain undetermined parameters Λ in the asymptotic solution and f_0 and p_0 in the near horizon solution, we numerically integrate the horizon solution towards the boundary and match it with the asymptotic solution plotted towards the horizon by controlling Λ, f_0, and p_0 for given $\{h_0, \tilde{\alpha}\}$. After fixing those parameters, we numerically explored physical quantities such as the free energy density and the energy density.

Numerically we found that there exists a maximum value of h_0, which corresponds to high temperature $\Lambda^z/T \to 0$. The smaller the value of $\tilde{\alpha}$ (or larger z) , the larger the maximum value of h_0. This explicitly demonstrates that $\tilde{\alpha}$ modifies h_0 or the horizon flux of the vector field via h_0. The dependence of the maximum value of h_0 both on $\tilde{\alpha}$ and n is shown in Fig.(7.3), and for $n = 4$ the maximum value of h_0 according to z or α are depicted in Figures (7.4) (a) and (b) respectively.

Smaller values of h_0 correspond to decreased temperature. For a very small value of h_0, the zero temperature limit $\Lambda^z/T \to \infty$ is approached. Due to fixed $\Lambda \sim 0$, our spacetime can be configured as a slightly deformed Lifshitz spacetime in the UV regime and as an AdS spacetime in the IR regime. Hence we expect holographic renormalization group flow at zero temperature from UV Gauss-Bonnet-Lifshitz to IR Gauss-Bonnet-AdS. Such renormalization flow was discovered in the AdS case [18], [56], but when $\tilde{\alpha} \neq 0$ the situation remains unknown, and an interesting problem for further research.

To investigate the behaviour of physical quantities with the metric solution of the deformed Lifshitz spaetime at high energy scale, which is expected to give information

about the marginally relevant operators near the critical regime at finite temperature via holographic duality, we confined ourselves to values of h_0 that are a little less than its maximum value (which corresponds to the high temperature regime $\Lambda^z/T \to 0$), and obtained the numerical results as shown in Table 7.4. For $\tilde{\alpha} \geq 0$, the value of z becomes less than $n-1$ – this case appears to have stable properties as no unstable behaviour is observed for the k-function and the fitting for $\mathcal{F}/Ts$ and $\mathcal{E}/Ts$. However for $0 > \tilde{\alpha} > -\frac{1}{2(n-2)}$, the value of z is in the range $n-1 < z < n$, and instability is expected due to the free energy density being larger than the energy density. Even worse properties emerge for $-\frac{1}{2(n-2)} \lesssim \tilde{\alpha}$, where $\mathcal{F}/Ts$ and $\mathcal{E}/Ts$ both have an oscillatory sharp peak near the horizon and the free energy density is bigger than the energy density. Here "$\sim$" indicates near the value of $-\frac{1}{2(n-2)} \pm \epsilon$ or $n \pm \epsilon$, where ϵ is small.

When $\Lambda = 0$, we analytically predicted the 0th order expressions for the free energy density and the energy density from the integrated first law of thermodynamics and the trace Ward identity. Our numerical results are consistent with these expressions, indicating that the trace Ward identity is valid in the GB case (at least for $z = n - 1 - 2(n-2)\tilde{\alpha}$).

Finally we found the sub-leading behaviour of $\mathcal{F}/Ts$ and $\mathcal{E}/Ts$ as a function of $\log \Lambda^z/T$, which is expected to be the contribution from the marginally relevant mode at finite temperature. As the value of z gets bigger due to either decreasing $\tilde{\alpha}$ or increasing n, the factor associated with the sub-leading order (i.e. the magnitude of coefficient of $\log \Lambda^z/T$) becomes smaller as shown in Tables 7.3, F.1, F.2,F.3, F.4, F.5.

	$\tilde{\alpha} \geq 0$	$0 > \tilde{\alpha} > -\frac{1}{2(n-2)}$	$-\frac{1}{2(n-2)} \lesssim \tilde{\alpha}$
value of z	$z \leq n-1$	$n-1 < z < n$	$n \lesssim z$
k **function**	Increases as the boundary is approached, as shown in Fig.7.2-(a),(b),(c)	Increases as the boundary is approached, as shown in Fig.7.2-(d),(e)	Decreases as the boundary is approached, as shown in Fig.7.2-(f)
$\mathcal{F}/Ts$ **and** $\mathcal{E}/Ts$ **depending on** $\log(r/r_+)$	No unstable behaviour seen near the horizon in Fig.7.7-(a),(b),(c)	No unstable behaviour seen near the horizon in Fig.7.8-(a)	Large oscillating peak; unstable behaviour observed near the horizon as shown in Fig.7.8-(b),(c), and Fig.7.9
Comparing magnitude of $\|\mathcal{F}_0/Ts\|$ **and** $\|\mathcal{E}_0/Ts\|$	$\left\|\frac{\mathcal{F}_0}{Ts}\right\| \leq \left\|\frac{\mathcal{E}_0}{Ts}\right\|$ as shown in Table 7.3,F.1,F.2,F.3,F.4 F.5	$\left\|\frac{\mathcal{F}_0}{Ts}\right\| > \left\|\frac{\mathcal{E}_0}{Ts}\right\|$ as shown in Table 7.3,F.1,F.2,F.3,F.4 F.5	$\left\|\frac{\mathcal{F}_0}{Ts}\right\| > \left\|\frac{\mathcal{E}_0}{Ts}\right\|$ as shown in Table 7.3,F.1,F.2,F.3,F.4, F.5

Table 7.4: These results are obtained at high temperature (i.e. h_0 is near maximum or $\Lambda^z/T \to 0$).

133

Chapter 8

Conclusion

This thesis is an effort to obtain a comprehensive understanding of the holographic correspondence, and to demonstrate its applications to new regimes of the AdS/CFT correspondence.

To achieve the former purpose, we found three important factors to establish the holographic correspondence from the original conjecture of the AdS/CFT correspondence [60] and subsequent primary studies [85, 90], which are summarized as follows. The first is that having the same isometry group for gravity theory and field theory is a crucial condition to accomplish duality. The second is that gauge/gravity correspondence can be interpreted as a UV/IR connection. The third is that the gravitational partition function is equivalent to the generating functional of field theory, which provides more a precise picture of holographic correspondence and gives a way for direct applications. Chapters 2,3, and 4 are devoted to this purpose to understand the above factors in detail.

For the latter purpose, regarding holographic renormalization, the Mann-Marolf (MM) counterterm method for the asymptotically Minkowski spacetime is studied in chapter 5, and as applications for the holographic correspondence, the Lifshitz spacetime/quantum critical theory correspondence is investigated in chapter 6, and 7.

The properties of AdS_{n+1} spacetime in chapter 2 can be summarized as follows. The symmetry of the spacetime is represented by the isometry group $SO(2, n)$, which is the same as that of conformal field theory. The AdS spacetime has a uniquely determined conformal boundary at spacelike infinity, and by applying the boundary analysis, the general solution of the metric near the conformal boundary of the spacetime can be generated. From this solution, the divergent terms in the action are easily isolated, and so it automatically constructs the counterterm and leads the holographic renormalization as shown in chapter

4. We also pointed out the importance of the well-defined asymptotic boundary, which is a place in which matter fields from the conformal theory reside, and where the gravitational information is transferred to matter fields.

In chapter 3, we studied the quantum phase transition involving quantum criticality and renormalization group flow associated with this scale invariant property of a lattice system to accommodate the profound understanding for chapter 6 and 7.

As an application of the holographic renormalization, the Minkowski spacetime is intensively studied. Different from the AdS spacetime, the conformal boundary of the Minkowski spacetime can be either null infinity or spacelike infinity. Both have difficulties to be considered as a place where field theory resides, as discussed in chapter 2. If one disposes the conformal boundaries, various asymptotic boundaries can be considered. The standard boundaries that we usually use are hyperbolic coordinates, which is $\rho = $ constant, and cylindrical coordinates, which is $r = $ constant where $r^2 = \rho^2 - t^2$. As different boundary conditions show different asymptotic behaviours at the boundary of a spacetime, it seems hard to expect to build a universal set of local counterterms satisfying all different boundary conditions, but it looks more optimal to have the counterterm as solutions derived from a given differential equation or an algebraic equation for each boundary condition. The MM-counterterm method validates this perspective in the sense that the solutions of the MM-counterterm are derived from the given algebraic equation, which is called the MM-relation, and yields local counterterms for each boundary conditions. It is verified that the MM-counterterms yield conserved quantities, which agree with the well-defined ones, for the hyperbolic coordinates [64] and also for the cylindrical coordinates in $(n + 3)$ dimensions in chapter 5 [75].

In the results, it is noted that the the 4 dimensional case is dealt with separately from the other higher dimensions as it has ambiguities in the counterterm solutions, which are not shown in other dimensions. For the sub-leading order, the ambiguity is removed by the condition of fixing the supertranslation symmetry, but for the sub-sub-leading order, the ambiguities can be fixed in a way not to disturb conserved charges. Also the form of the boundary stress tensor is the same as the hyperbolic boundary case in 4 dimensions, but has additional terms in higher than 4 dimensions. We find that these additional terms are impotent and do not contribute to conserved charges.

In this study, the cylindrical coordinates provide great benefits by giving direct applications for many gravitational systems, since that is the most popular coordinate. However, despite this benefit, the difficulty of the cylindrical coordinate associated with the MM-counterterm method arises in its calculation, which is more complicated than the hyperbolic case due to different asymptotic behaviours. That is, hyperbolic coordinates are

manifestly covariant under variation of the metric with respect to a normal coordinate to a boundary surface, but the cylindrical coordinate is not. More improvement regarding the MM-counterterm in the cylindrical coordinate can be made by investigating it in stationary coordinates, which are applicable to rotating gravitational systems.

From the perspective of the holographic correspondence, a holographic dual field theory for the Minkowski case has not been found yet, but a conformal field theory can be a candidate if a connection between the isometry groups of the Minkowski spacetime and conformal field theory is found. Also if a field theory dual is found, it is expected that the MM-counterterm will be employed to construct the holographic renormalization.

New regimes for the holographic correspondence were applied to the Lifshitz spacetime/quantum critical theory in condensed matter physics in chapters 6 and 7. The Lifshitz/qct correspondence is based on the same anisotropic symmetry of gravity and gauge theory. On the gravity side, the anisotropic spacetime is generated by adding massive vector fields into the gravity action or is adjusted by adding higher curvature terms such as the Gauss-Bonnet term, which work in a way to cooperate with the massive vector fields. The properties of the Lifshitz spacetime have been recently studied and were found to possess a naked singularity [27, 52]. On this topic, more research needs to be done. On the field theory side, the anisotropic scaling occurs due to the property of critical slowing down, which is that the temporal correlation function of the order parameter decays slower and slower in the vicinity of a quantum critical point. Above this, unusual phenomena had been discovered near the quantum critical point, but a theory explaining the phenomena has not been found. Some properties of quantum criticality associated with the second order phase transition are studied in chapter 3. Inspired by the AdS/CFT correspondence, it is expected that the holographic correspondence provides a new framework to understand quantum critical phenomena.

In the study of the deformation of the Lifshitz spacetime (chapter 6 and 7), we considered the Lifshitz spacetime in the UV regime and the AdS spacetime in the IR regime in $(n+1)$ dimensions. At the asymptotic boundary i.e. $r \to 0$, the solution of the pure Lifshitz spacetime is expanded to the sub-leading orders, which are generated by $\Lambda \sim 0$, and so the Lifshitz spacetime is slightly deformed at the asymptotic region. Here the non-trivial sub-leading orders, which are the marginally relevant modes for the massive vector field, of the asymptotic solution are only allowed for $z = (n-1) - 2(n-2)\tilde{\alpha}$, where z is the dynamical critical exponent. Also we find the expanded black hole solution, which is characterized by the Gauss-Bonnet coupling constant $\tilde{\alpha}$ and the horizon flux of the massive vector field, near the horizon $r = r_+$. By numerical integration of the expanded black hole solution toward the asymptotic region, we match both solutions at the middle regions, and based on these values evaluate physical quantities such as the free energy density over Ts
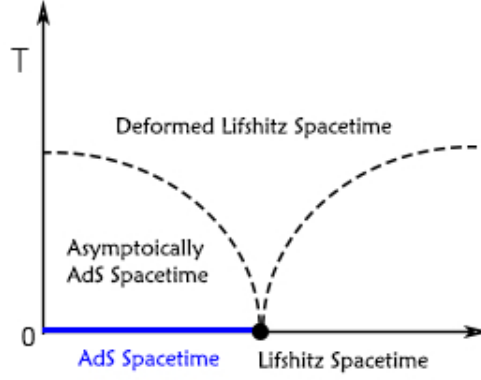
Figure 8.1: holographic phase transition

(temperature times entropy density) and the energy density over Ts.

The main results are as follows. We found the contributions of the marginally relevant operators by observing the physical quantities depending on temperature according to n and $\tilde{\alpha}$, which show a weaker dependence on temperature as z increases or $\tilde{\alpha}$ decreases. Moreover, we found the linear function $\eta(\tilde{\alpha}) \sim 1.00 - \frac{2n-2}{n-1}\tilde{\alpha}$, which relates $\mathcal{F}_0 = -\eta(\tilde{\alpha})\mathcal{E}_0$ when the marginally relevant operators are turned off. The numerical data calculated for $\eta(\tilde{\alpha})$ function were computed to two decimal places. When $\tilde{\alpha} < 0$, the free energy density over Ts becomes bigger than the energy density over Ts, so it is expected that the system becomes unstable and this instability gets worse when $\tilde{\alpha} < -\frac{1}{2(n-2)}$.

From the perspective of the holographic correspondence, at the high temperature limit (i.e. $\Lambda^z/T \to 0$) of the gravity theory with fixed $\Lambda \sim 0$, this configuration describes the strongly coupled physics approaching the quantum critical phase at finite temperature from the critical point due to marginally relevant operators. While at the zero temperature limit (i.e. $\Lambda^z/T \to \infty$) of the gravity theory with fixed $\Lambda \sim 0$, this configuration yields the renormalization group flow from the Lifshitz-like field theory to the conformal field theory. Then compared to the quantum phase diagram, which is studied in chapter 3, we might draw the (hypothetic) holographic phase diagram as shown in 8.1, where only two fixed points (the trivial fixed point is for AdS and the critical fixed point is for Lifshitz spacetime) exist, two phases are drawn and the one on the right is not defined in this configuration.

As examples for other applications of the holographic correspondence, the study of heavy ion physics (e.g. strongly coupled quark-gluon plasma) has been successful [38, 43, 53]. Condensed matter theory has also been actively studied. Especially, as most metallic

137

systems are strongly coupled and can be engineered in laboratories, it has benefits to have the possibility of direct experimental tests. There are some applicable candidates to be studied with respect to this subject such as the dual description of the Hall effect [39, 74] or Nernst effect. Recently, the most studied subject is high-temperature (high-T_c) superconductors [47, 49, 51], which were experimentally discovered in many materials, but unlike conventional superconductors, a high-T_c superconductor cannot be explained by BCS theory. In the context of the holographic correspondence, the key problem for resolving this mechanism is to build a proper gravitational model.

APPENDICES

Appendix A

Useful Coordinates of AdS Spacetime

The AdS_{n+1} spacetime can be represented as the hyperboloid

$$-U^2 - V^2 + X_1^2 + \cdots + X_n^3 = -l^2 \tag{A.1}$$

where l is the radius of curvature. This can be embedded in flat spacetime with

$$ds^2 = -dU^2 - dV^2 + dX_1^2 + \cdots + dX_n^2 \tag{A.2}$$

which has two-timelike directions and n-spacelike directions. This spacetime has closed timelike curves (CTC) as shown in Fig.A.1. However if one does not identify the time-like direction with the circle S^1 we can obtain the universal covering spacetime of AdS spacetime.

There are several known coordinates of AdS_{n+1} spacetime for convenience of use and these coordinates are obtained by proper coordinate transformation from (A.2). Here we demonstrate four cases, where three of them will be used in chapter 5, as follows.

A.1 Global Coordinates

If we parameterize the hyperboloid in (A.2) in the following way:

$$U = l \cosh r \sin t, \; V = l \cosh r \cos t, \; X_1 = l \sinh r \cos \theta_1, \; X_2 = l \sinh r \sin \theta_1 \cos \theta_2, \; \cdots,$$

$$X_{n-1} = l \sinh r \cos \theta_{n-1} \prod_{i=1}^{n-2} \sin \theta_i, \qquad X_n = l \sinh r \prod_{i=1}^{n} \sin \theta_i \tag{A.3}$$
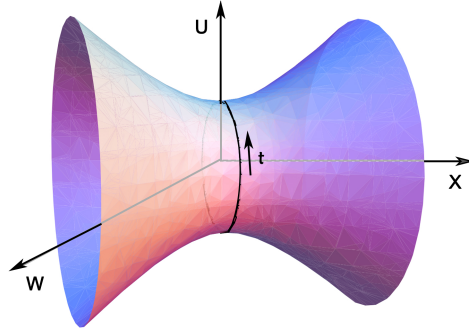
Figure A.1: Closed Timelike Curves

where t, θ, ϕ are periodic and have ranges of $-\pi \leq t \leq \pi$, $0 \leq \theta_n \leq \pi$, $0 \leq \theta_i \leq 2\pi$ where $i = 1, \cdots, n-1$, and $r \geq 0$, the static form of the metric is obtained

$$ds^2 = l^2 \left(-\cosh^2 r \, dt^2 + dr^2 + \sinh^2 r \, d\Omega_{n-1}^2 \right). \tag{A.4}$$

At $t = const.$ and $r = R$, this spacetime with the radius R has the surface area $\frac{2\pi^{n/2}}{\Gamma(\frac{n}{2})} \sinh^2 R$, and proper time $d\tau = dt \cosh R$ elapses much faster at large distance.

Now let us redefine the parameter r in (A.4) with θ by

$$\tan\left(\frac{\theta}{2} + \frac{\pi}{4}\right) = e^r \tag{A.5}$$

where θ is defined in a range of $0 \leq \theta < \frac{\pi}{2}$ and this reparameterization brings the infinity of r to be the finite value. One finds the metric of

$$ds^2 = \frac{l^2}{\cos^2\theta}\left(-dt^2 + d\theta^2 + \sin^2\theta d\Omega_{n-1}^2 \right), \tag{A.6}$$

which becomes singular at $\theta = \frac{\pi}{2}$, and so the spacetime does not expand at and beyond these points. Thus these points are defined as the boundary of AdS and yield the conformal structure, which will be discussed in the next subsection. This coordinate also shows that the AdS covers the region $0 \leq \theta < \frac{\pi}{2}$ of Einstein static universe, which are illustrated in Fig.A.2a where the Einstein static universe is depicted by a cylinder and the AdS takes half of the cylinder.

(a) Global Coordinate　　　　　　　(b) Diamond Shape
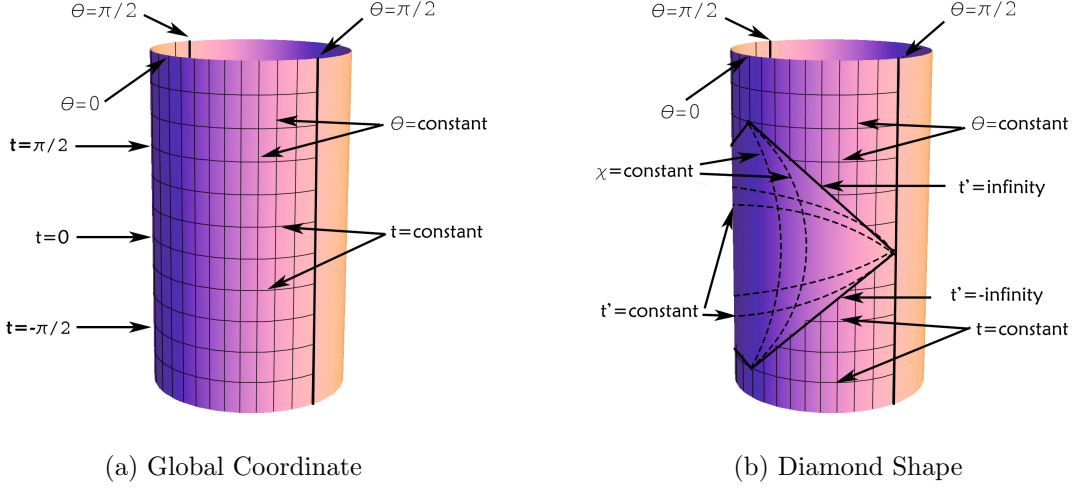
Figure A.2: Diagrams

A.2　Diamond Patch of AdS Spacetime

Let us redefine the parameters in (A.2) by

$$U = l\cos\frac{t'}{l}, \qquad V = l\sin\frac{t'}{l}, \tag{A.7}$$

$$X_1 = l\cos\frac{t'}{l}\sinh\chi\cos\theta_1, \qquad X_2 = l\cos\frac{t'}{l}\sinh\chi\sin\theta_1\cos\theta_2, \qquad \cdots,$$

$$X_{n-1} = l\cos\frac{t'}{l}\sinh\chi\cos\theta_{n-1}\prod_{i=1}^{n-2}\sin\theta_i, \qquad X_n = l\cos\frac{t'}{l}\sinh\chi\prod_{i=1}^{n}\sin\theta_i$$

and it yields

$$ds^2 = -dt'^2 + l^2\sin^2\frac{t'}{l}\left(d\chi^2 + \sinh^2\chi\, d\Omega_{n-1}^2\right). \tag{A.8}$$

This coordinate system covers only part of the AdS spacetime, which is the diamond shape region in Fig.A.2b and has apparent singularities at $t' = 0$ and π. This metric becomes identical with $k = -1$ Robertson-Walker spacetime which is

$$ds^2 = -dt^2 + R^2(t)\left(\frac{1}{1+r^2}dr^2 + r^2 d\Omega_{n-1}^2\right) \tag{A.9}$$

by using $r = \sinh\chi$.

142

A.3 Static Coordinates

If we introduce a coordinate transformation following

$$U = (l^2 + r^2)^{1/2} \cos \frac{t}{l}, \qquad V = (l^2 + r^2)^{1/2} \sin \frac{t}{l}, \tag{A.10}$$

$$X_1 = r \cos \theta_1, \;\; X_2 = r \cos \theta_2, \;\; \cdots, \;\; X_{n-1} = r \cos \theta_{n-1} \prod_{i=1}^{n-2} \sin \theta_i, \;\; X_n = r \prod_{i=1}^{n} \sin \theta_i,$$

we obtain the familiar form of the metric

$$ds^2 = -\left(1 + \frac{r^2}{l^2}\right) dt^2 + \left(1 + \frac{r^2}{l^2}\right)^{-1} dr^2 + r^2 d\Omega_{n-1}^2. \tag{A.11}$$

A.4 Poincarè Coordinates

Another interesting coordinate transformation is

$$X_n - U = \frac{l}{x_0}, \qquad X_n + U = l\left(x_0 + \frac{1}{x_0}\left(\eta^2 - \sum_{i=1}^{n-1} x_i^2\right)\right), \qquad V = \frac{l}{x_0}\eta,$$

$$X_i = \frac{l}{x_0} x_i, \qquad \text{where} \qquad i = 1, \ldots, n - 1 \tag{A.12}$$

where η, x, and y only take real values and $z \geq 0$, and then one finds

$$ds^2 = \frac{l^2}{x_0^2}\left(-dt^2 + \sum_{i=0}^{n} dx_i^2\right). \tag{A.13}$$

This coordinate only cover half of the AdS spacetime and the other half will be covered by expanding it to $z \leq 0$.

Appendix B

Field Theoretical Renormalization

This appendix deals with the renormalization process so as to have a more profound understanding of holographic renormalization, (the subject of chapter 4) and to naturally develop the arguments of the renormalization group, which plays an important role in the context of the holographic correspondence associated with condensed matter physics. Here we demonstrate the regularization procedure and calculate the leading order of self-energy in ϕ^4 theory by using dimensional regularization, and then discuss about the concepts of renormalization and renormalizability. We also derive the renormalization equation under the minimal subtraction scheme and apply this to obtain the running coupling constant for the one-loop case for ϕ^4 theory. Finally, we discuss properties of the renormalization group.

B.1 Regularization Method: Dimensional Regularization

As introduced in chapter 1, perturbation theory is accompanied with loop contributions, which are divergent in the integration of correlation function. The process of rendering a divergent integral to be calculable is called regularization, and the most common regularizations are

- Cutoff Regularization or Pauli-Villars Regularization

- Dimensional Regularization.

The cutoff regularization is quite a traditional method: the main idea is to bring a cut off momentum Λ instead of sending $k \to \infty$ in the integration of the propagator, but the problem is that the cut off momentum dependence usually causes unphysical features such as violating a symmetry of the theory. While in Pauli-Villars (PV) heavy-mass particles are introduced with that have the opposite statistics to the physical particles, so that the loops from these heavy particles come in with a minus sign. The infinite-mass limit is taken at the end.

Dimensional regularization might be the most convenient and practical method. It basically takes the dimension of the spacetime to be D, which is regarded as a continuous variable, and integrates products of Green's functions that are Euclideanized. Then in the resultant calculation, the divergence always shows up a form of the pole of the gamma function, and the divergent part and the finite part are separated.

Here we calculate the amputated one-loop correction or the self-energy for the leading order of the ϕ^4 theory by using dimensional regularization method:

$$
-i\Sigma_1(p): \qquad \text{[diagram]} \qquad
\begin{aligned}
&= -\frac{i\lambda}{2} \int \frac{d^4k}{(2\pi)^4} \frac{1}{k^2 - m^2 + i\epsilon} \\
&= -\frac{i\lambda}{2} \int \frac{d^4k_E}{(2\pi)^4} \frac{-i}{k_E^2 + m^2 + i\epsilon}.
\end{aligned}
\tag{B.1}
$$

where Wick rotation is used in the second line:

$$
\begin{aligned}
t &= -i\tau, \\
k^0 &= ik_E^0
\end{aligned}
\qquad \Rightarrow \qquad
d^4k = i\, d^4k_E, \quad k^2 = -k_E^2.
\tag{B.2}
$$

If the dimension of the spacetime is changed to D, the integral variables turn to

$$
\frac{d^4k}{(2\pi)^4} \to \mu^{4-D} \frac{d^Dk}{(2\pi)^D},
\tag{B.3}
$$

and then the self-energy is written as

$$
-i\Sigma_1(p) \equiv -\frac{i\lambda}{2} \int \frac{d^4k_E}{(2\pi)^4} \frac{-i}{k_E^2 + m^2 + i\epsilon} \to -\frac{i\lambda}{2}\mu^{4-D} \int \frac{d^Dk_E}{(2\pi)^D} \frac{1}{k_E^2 + m^2}.
\tag{B.4}
$$

Applying the following identity

$$
\frac{1}{A} = \int_0^\infty ds\, e^{-As},
\tag{B.5}
$$

145

it yields

$$-i\Sigma_1(p) = -\frac{i\lambda}{2}\mu^{4-D}\int\frac{d^D k_E}{(2\pi)^D}\int_0^\infty ds\; e^{-(k_E^2+m^2)s} = -\frac{i\lambda}{2}\mu^{4-D}\int_0^\infty ds\; e^{-m^2 s}\int\frac{d^D k_E}{(2\pi)^D}e^{-k_E^2 s}$$

$$\text{(B.6)}$$

$$= -\frac{i\lambda}{2}\mu^{4-D}\int_0^\infty ds\; e^{-m^2 s}\frac{1}{(2\pi)^D}\left(\frac{\pi}{s}\right)^{\frac{D}{2}} = -\frac{i\lambda}{2}\mu^{4-D}\frac{1}{(4\pi)^{\frac{D}{2}}}\int_0^\infty ds\; s^{-\frac{D}{2}}e^{-m^2 s}$$

$$\text{(B.7)}$$

$$= -\frac{i\lambda}{2}\mu^{4-D}\frac{(m^2)^{\frac{D}{2}-1}}{(4\pi)^{\frac{D}{2}}}\,\Gamma(1-D/2)$$

$$\text{(B.8)}$$

where the Gaussian integral and the definition of Gamma function are used

$$\int d^D x\; e^{-Ax^2} = \left(\frac{\pi}{A}\right)^{\frac{D}{2}}, \qquad \Gamma(z) = \int_0^\infty t^{z-1}e^{-t}dt.$$

$$\text{(B.9)}$$

If $D = 4$, (B.8) is divergent as $\Gamma(-1) = \infty$. To separate the pole giving the infinity of the Gamma function, we use

$$\Gamma(n+1) = n\Gamma(n) = n!,$$

$$\text{(B.10)}$$

and define $\epsilon = 4 - D$, then the Gamma function in (B.8) is manipulated

$$\Gamma(1-D/2) = \Gamma(-1+\epsilon/2) = \frac{1}{-1+\frac{\epsilon}{2}}\Gamma(\epsilon/2) = \frac{1}{-1+\frac{\epsilon}{2}}\frac{1}{\left(\frac{\epsilon}{2}\right)}\Gamma(1+\epsilon/2)$$

$$= -\frac{2}{\epsilon} - 1 + \gamma + \mathcal{O}(\epsilon)$$

$$\text{(B.11)}$$

where $\gamma = 0.57721\cdots$ and is called Euler-Mascheroni constant. From dimensional analysis (in units of mass) we find

$$d^D x(\partial\phi)^2 \;\rightarrow\; -D + 2 + 2[\phi] = 0 \;\Rightarrow\; [\phi] = \frac{D-2}{2},$$

$$d^D x\lambda\,\phi^4 \;\rightarrow\; -D + [\lambda] + 4\frac{D-2}{2} = 0 \;\Rightarrow\; [\lambda] = 4 - D,$$

$$\text{(B.12)}$$

so when $D = 4$ the coupling constant is dimensionless, but when $D \neq 4$ it has dimensionality $mass^{4-D}$. However, as the coupling constant λ in (B.4) is combined with the factor μ, which does not exist in the original Lagrangian but was newly introduced by the dimensional regularization process in (B.3), it becomes dimensionless again. Expanding μ in terms of small ϵ yields

$$\lambda = \lambda\mu^{4-D} = \lambda e^{(4-D)\ln\mu} = \lambda(1 + \epsilon\ln\mu + \cdots).$$

$$\text{(B.13)}$$

146

With (B.11) and (B.13) the leading-order of the self-energy (B.8) is expanded as

$$-i\Sigma_1(p) = -\frac{i\lambda}{2}\frac{(m^2)^{\frac{D}{2}-1}}{(4\pi)^{\frac{D}{2}}}\left(-\frac{2}{\epsilon}-1+\gamma+\cdots\right)(1+\epsilon\ln\mu+\cdots)$$

$$= i\lambda\frac{(m^2)^{\frac{D}{2}-1}}{(4\pi)^{\frac{D}{2}}}\frac{1}{\epsilon}+i\lambda\frac{(m^2)^{\frac{D}{2}-1}}{(4\pi)^{\frac{D}{2}}}(\ln\mu+\cdots)$$

$$= i\lambda\frac{(m^2)^{\frac{D}{2}-1}}{(4\pi)^{\frac{D}{2}}}\frac{1}{\epsilon}+\text{finite} \tag{B.14}$$

where the finite part depends on μ. Restoring the original dimensionality by substituting $D = 4$, we obtain

$$-i\Sigma_1(p) = i\lambda\frac{m^2}{(4\pi)^2}\frac{1}{\epsilon}+\text{finite} \equiv -i\Sigma_{1,inf}-i\Sigma_{1,fin} \tag{B.15}$$

where as $\epsilon \to 0$, the first term diverges, and so the infinity part and the finite part are separated from the $\Sigma_1(p)$. Considering higher orders, we can write

$$\Sigma \equiv \Sigma_{inf}+\Sigma_{fin}. \tag{B.16}$$

B.2 Renormalization

By the regularization, the infinite part of a divergent integral becomes isolated, and so the next step is to find a way to deal with it. This infinity can be absorbed into parameter redefinitions (i.e. $m \to m_R$) or be removed by adding counterterms $1/2\Sigma_{inf}\phi^2$ to the Lagrangian. This process of eliminating the divergences is called renormalization. Alternatively, we can define the renormalization as a procedure of working with measured quantities instead of bare quantities.

Let us start with the original (or bare) Lagrangian

$$\mathcal{L} = \frac{1}{2}(\partial\phi)^2-\frac{1}{2}m^2\phi^2-\frac{g}{4!}\phi^4 \tag{B.17}$$

and redefine the parameters as follows

$$\phi_R = Z_\phi^{-\frac{1}{2}}\phi, \tag{B.18}$$

$$m_R^2 = m^2+\delta m^2, \tag{B.19}$$

$$g_R = Z_g^{-1}Z_\phi^2 g \tag{B.20}$$

where Z_ϕ is called the *field-strength renormalization* factor, ϕ, m^2, and g are bare quantities containing the infinity, and ϕ_R, m_R^2, and g_R are the renormalized quantities. In order to cancel the infinity of the bare quantities, the counterterms are added

$$\mathcal{L} = \mathcal{L}_R + \mathcal{L}_{C.T} \tag{B.21}$$

where

$$\mathcal{L}_R = \frac{1}{2}(\partial\phi_R)^2 - \frac{1}{2}m_R^2\phi_R^2 - \frac{g_R}{4!}\phi_R^4 \tag{B.22}$$

$$\mathcal{L}_{C.T} = \frac{1}{2}(Z_\phi - 1)(\partial\phi_R)^2 - \frac{1}{2}\Big[(Z_\phi - 1)m_R^2 - \delta m^2 Z_\phi\Big]\phi_R^2 - \frac{1}{4!}g_R(Z_g - 1)\phi_R^4$$

$$= \frac{1}{2}\delta_z(\partial\phi_R)^2 - \frac{1}{2}\delta_m\phi_R^2 - \frac{1}{4!}\delta_\lambda\phi_R^4 \tag{B.23}$$

where

$$\delta_z = Z_\phi - 1, \qquad \delta_m = (Z_\phi - 1)m_R^2 - \delta m^2 Z_\phi, \qquad \delta_\lambda = g_R(Z_g - 1). \tag{B.24}$$

In fact, we need to impose the renormalization conditions on (B.24) to fix the renormalized parameters with the observed ones as follows

$$= \frac{i}{p^2 - m^2} + \text{(terms regular at } p^2 = m^2) \tag{B.25}$$

$$= -i\lambda \qquad \text{at } s = 4m^2, \ t = u = 0 \tag{B.26}$$

where $s = (p_1 + p_2)^2$, $t = (p_1 - p_3)^2$, and $u = (p_1 - p_4)^2$ are Mandelstam variables.

This renormalization procedure can also be interpreted from an alternative point of view. From the beginning, we can start with the renormalized Lagrangian (B.22) and consider it as a tree-level Lagrangian and then do perturbation on g_R, which induces divergent diagrams. This divergence is resolved by adding the counterterms, and so the divergence at 1-loop order will be removed by the first order of the counterterm $\mathcal{L}_{C.T}^{(1)}$

$$\mathcal{L} = \mathcal{L}_R + \mathcal{L}_{C.T}^{(1)} \tag{B.27}$$

and one on the 2-loop order will also canceled by adding $\mathcal{L}_{C.T}^{(2)}$

$$\mathcal{L} = \mathcal{L}_R + \mathcal{L}_{C.T}^{(1)} + \mathcal{L}_{C.T}^{(2)}. \tag{B.28}$$

Then, as a result the full Lagrangian is obtained

$$
\begin{aligned}
\mathcal{L} &= \mathcal{L}_R + \mathcal{L}_{C.T}^{(1)} + \mathcal{L}_{C.T}^{(2)} + \cdots \\
&= \mathcal{L}_R + \mathcal{L}_{C.T}
\end{aligned}
\tag{B.29}
$$

where note that if all orders of the $\mathcal{L}_{C.T}^{(i)}$ have the same structure as the $\mathcal{L}_R$; for example if the $\mathcal{L}_{C.T}^{(i)}$ has the form given in (B.22):

$$
\mathcal{L}_{C.T}^{(i)} = \frac{1}{2}\delta Z_\phi^{(i)}(\partial\phi_R)^2 - \frac{1}{2}\delta m^{2(i)}\phi_R^2 - \frac{1}{4!}\delta g^{(i)}\phi_R^4,
\tag{B.30}
$$

and these counterterms are enough to get rid of the divergence in the above $(B.27) - (B.29)$, then it is said that the theory is renormalizable. However, if different forms of the counterterms from the $\mathcal{L}_R$ are need to deter the infinity then the theory is non-renormalizable.

Then let us calculate the renormalized two-point correlation function,

$$
G_2(p) = \frac{1}{p^2 - m^2 - \Sigma(p) + i\epsilon}.
$$

As the physical mass is defined by the pole of the propagator, $[G_2(p)]^{-1} = 0$ at $p^2 = m_{phy}^2$ and yields

$$
m_{phy}^2 - m^2 - \Sigma(m_{phy}^2, m^2) = 0 \qquad \Rightarrow \qquad m_{phy}^2 = m^2 + \delta m^2
\tag{B.31}
$$

where $\delta m^2 = \Sigma(m_{phy}^2, m^2)$. If expanding $\Sigma(p)$ near at a, which is substituted by m_{phy}, it is calculated

$$
\begin{aligned}
\Sigma(p) &= \Sigma(p^2, m^2)\Big|_{p^2=a} + (p^2 - a)\Sigma'(p^2, m^2)\Big|_{p^2=a} + \tilde{\Sigma}(p) + \cdots \\
&= \Sigma(m_{phy}^2, m^2) + (p^2 - m_{phy}^2)\,\Sigma'(m_{phy}^2, m^2) + \tilde{\Sigma}(p) + \cdots \\
&= \delta m^2 + (p^2 - m_{phy}^2)\,\Sigma'(m_{phy}^2, m^2) + \tilde{\Sigma}(p) + \cdots
\end{aligned}
\tag{B.32}
$$

where $\tilde{\Sigma}(p)$ indicates the higher orders of the series. Plugging (B.32) to (B.2), the two-point correlation function has the form

$$
\begin{aligned}
G_2(p) &= \frac{i}{p^2 - m_{phy}^2 - (p^2 - m_{phy}^2)\,\Sigma'(m_{phy}^2) - \tilde{\Sigma}(p) + i\epsilon} \\
&= \frac{i}{(p^2 - m_{phy}^2)(1 - \Sigma') - \tilde{\Sigma}(p) + i\epsilon} \simeq \frac{1}{(1 - \Sigma')}\frac{i}{p^2 - m_{phy}^2 - \tilde{\Sigma}(p) + i\epsilon} \\
&\simeq \frac{iZ_\phi}{p^2 - m_{phy}^2 - \tilde{\Sigma}(p) + i\epsilon}
\end{aligned}
\tag{B.33}
$$

149

where $Z_\phi = \frac{1}{1-\Sigma'}$. Upon redefining the field $\phi_R = Z_\phi^{-\frac{1}{2}}\phi$, the renormalized two-point correlation function is obtained

$$G_2(x,y) = \langle\Omega|T\{\phi(x)\phi(y)\}|\Omega\rangle = Z_\phi\langle\Omega|T\{\phi_R(x)\phi_R(y)\}|\Omega\rangle \quad . \tag{B.34}$$

This result also can be generalized to n-point Green's functions (or n-point correlation function)

$$G_N(x_1,\cdots,x_N;m,g) = Z_\phi^{\frac{N}{2}}G_{NR}(x_1,\cdots,x_N;m_R,g_R) \tag{B.35}$$

where the G_{NR} is finite. In terms of the amputated Green functions, it yields

$$\begin{aligned}
G_N^{amp}(p_1,\cdots,p_N;m,g) &= \frac{1}{G_2(p_1)}\cdots\frac{1}{G_2(p_N)}G_N(p_1,\cdots,p_N) \\
&= \frac{1}{Z_\phi^N}Z_\phi^{\frac{N}{2}}G_N^{amp}(p_1,\cdots,p_N) \\
&= Z_\phi^{-\frac{N}{2}}G_{NR}^{amp}(p_1,\cdots,p_N:m_R,g_R) \tag{B.36}
\end{aligned}$$

where G_{NR}^{amp} is a quantity appearing in scattering matrix.

B.3   Renormalization Scheme: Minimal Subtraction

In the renormalization procedure, the bare Lagrangian parameters are separated into the renormalized quantity and the diverging quantity, for example

$$m^2 = m_R^2 - \delta m^2$$

where m_R^2 is finite and δm^2 includes infinity. In the traditional view, we set up $m_R^2 = m_{phy}^2$, where m_{phy}^2 is the pole of the propagator, but there is no special reason to take the renormalized mass m_R as the physical mass value. As long as m_R is finite, we can obtain a well-defined Green function and derive the unique final result unrelated to the choice of the m_R. This idea, that a renormalization quantity is arbitrary, can also be applied to $\phi_R = Z_\phi^{-1/2}\phi$ and $g_R = Z_g^{-1}Z_\phi^2\,g$ in which

$$\phi_R' = {Z'}_\phi^{-\frac{1}{2}}\phi = \left(\frac{Z_\phi}{Z'_\phi}\right)\phi_R \;, \qquad g_R' = \left(\frac{Z_g}{Z'_g}\frac{{Z'}_\phi^2}{Z_\phi^2}\right)g_R \tag{B.37}$$

where the quantities in the parenthesis should be finite. There exist a lot of ways to separate the Lagrangian or Lagrangian parameters into an infinite part and a finite part; the different ways of doing it are provided by *renormalization schemes* (or renormalization prescriptions). Note that

1. There are many kinds of renormalization schemes.
   e.g. mass-shell scheme, minimal subtraction scheme, BPHZ scheme, $\cdots$

2. The choice of renormalization scheme depends on the physical situation.
   The most commonly used one is the minimal subtraction method under dimensional regularization

3. Regularization and scheme are different.
   e.g. the mass-shell scheme can be applied with the dimensional regularization or the cutoff regularization

4. In some cases, a regularization automatically requires a special scheme.
   e.g. $\sum_{n=1}^{\infty} n = \zeta(-1) = -\frac{1}{12}$

5. A physical result is unchanged by a scheme.
   e.g. as the full Lagrangian is the same, the pole of the propagator also remains the same regardless of the renormalization mass

In the dimensional regularization, every divergence shows up as the pole of a Γ-function. For example the one-loop calculation of ϕ^4 theory yields

$$V(p^2) = -\frac{1}{2}\frac{1}{(4\pi)^{\frac{D}{2}}}\Gamma(2 - D/2)\int_0^1 dx\frac{1}{[m^2 - x(1-x)p^2]^{2-D/2}}$$

where the Γ-function is expanded to $\Gamma(2 - D/2) \simeq \frac{2}{\epsilon} + \cdots$ on a small value of $\epsilon = 4 - D$. The minimal subtraction scheme considers the $(1/\epsilon)$ pole of the Γ-function as the infinity part and removes it by setting the Lagrangian parameters to have a form of

$$m^2 = m_R^2 - \delta m^2 = m_R^2 - \sum_{r=1}^{\infty}\frac{b_r(g_R)}{\epsilon^r}, \tag{B.38}$$

$$g = \mu^\epsilon\left[g_R + \sum_{r=1}^{\infty}\frac{a_r(g_R)}{\epsilon^r}\right], \tag{B.39}$$

$$\phi = \phi_R\left[1 + \sum_{r=1}^{\infty}\frac{c_r(g_R)}{\epsilon^r}\right] \tag{B.40}$$

where the coefficients a_r, b_r, and c_r are functions of only g, and completely determined by the UV divergence of the r-loops diagrams. The quantity μ is the parameter introduced in (B.3) and identified with the energy scale E of the renormalization group. That is, changing the arbitrary scale μ corresponds to changing the energy; in other words, it means changing of the renormalization scheme by redefining the renormalized part and the infinite part.

B.4 Renormalization Group

As stated above, there is an arbitrariness to separate the divergent part and the finite part in the renormalization process, and this arbitrariness basically becomes the basis of the renormalization group. The general concept of the renormalization group is to see how a physical system (e.g. m, g, Green's functions etc.) is changed when the scheme is changed. Here we consider the renormalization group under the minimal subtraction scheme, in which physical quantities depend on the renormalization scale μ.

Let us consider a bare Green function $G_N(p_i; g, m)$, which is independent of μ by construction; it then satisfies

$$\frac{d}{d\mu} G_N = 0, \tag{B.41}$$

whereas the renormalized Green function satisfies

$$G_N(p_i; g, m) = Z_\phi^{\frac{N}{2}} G_{NR}(p_i; g_R(\mu), m_R(\mu), \mu) \tag{B.42}$$

yielding

$$0 = \frac{d}{d\mu} G_N = \frac{N}{2} Z_\phi^{\frac{N}{2}-1} \frac{dZ_\phi}{d\mu} G_{NR} + Z_\phi^{\frac{N}{2}} \frac{d}{d\mu} G_{NR}. \tag{B.43}$$

Rearranging the above on G_{NR}

$$\frac{d}{d\mu} G_{NR} = -\frac{N}{2} \frac{d\ln Z_\phi}{d\mu} G_{NR},$$

$$\left(\frac{\partial}{\partial\mu} + \frac{dg_R}{d\mu} \frac{\partial}{\partial g_R} + \frac{dm_R^2}{d\mu} \frac{\partial}{\partial m_R^2} \right) G_{NR} = -\frac{N}{2} \frac{d\ln Z_\phi}{d\mu} G_{NR} \tag{B.44}$$

and multiplying μ, we finally obtain RG equation :

$$\left[\mu\frac{\partial}{\partial\mu} + \beta\frac{\partial}{\partial g_R} + \gamma_m m_R^2 \frac{\partial}{\partial m_R^2} + N\gamma \right] G_{NR} = 0 \tag{B.45}$$

where the coefficients are defined as

$$\beta = \mu\frac{dg_R}{d\mu}, \tag{B.46}$$

$$\gamma_m = \mu\frac{d\ln m_R^2}{d\mu}, \tag{B.47}$$

$$\gamma = \frac{1}{2}\mu\frac{d}{d\mu}\ln Z_\phi. \tag{B.48}$$

To calculate these under minimal subtraction scheme, we use the fact that bare parameters are RG invariant. The coupling constant in (B.39) expands as

$$g = \mu^\epsilon \left[g_R + \frac{1}{\epsilon} a_1(g_R) + \frac{1}{\epsilon^2} a_2(g_R) + \cdots \right] \tag{B.49}$$

and as g is independent on μ, we find

$$0 = \mu \frac{dg}{d\mu} = \epsilon \mu^\epsilon \left[g_R + \frac{1}{\epsilon} a_1(g_R) + \frac{1}{\epsilon^2} a_2(g_R) + \cdots \right] + \mu^\epsilon \left[\mu \frac{dg_R}{d\mu} + \frac{1}{\epsilon} a_1' \mu \frac{dg_R}{d\mu} + \cdots \right],$$

$$0 = \epsilon g_R + a_1(g_R) + \frac{1}{\epsilon} a_2(g_R) + \cdots + \left[1 + \frac{1}{\epsilon} a_1' + \frac{1}{\epsilon^2} a_2' + \cdots \right] \mu \frac{dg_R}{d\mu}. \tag{B.50}$$

Then the derivative of the coupling constant with respect to μ takes the form of

$$\mu \frac{dg_R}{d\mu} = - \left(1 + \frac{1}{\epsilon} a_1' + \frac{1}{\epsilon^2} a_2' + \cdots \right)^{-1} \left(\epsilon g_R + a_1(g_R) + \frac{1}{\epsilon} a_2(g_R) + \cdots \right)$$

$$= \beta(g_R(\mu), \epsilon) \tag{B.51}$$

and this can be written as

$$\left(1 + \frac{1}{\epsilon} a_1' + \frac{1}{\epsilon^2} a_2' + \cdots \right) \left(\beta_0(g_R) + \epsilon \beta_1(g_R) + \epsilon^2 \beta_2(g_R) + \cdots \right)$$

$$= - \left(\epsilon g_R + a_1(g_R) + \frac{1}{\epsilon} a_2(g_R) + \cdots \right). \tag{B.52}$$

Expanding both sides of the equation and comparing powers of ϵ, each order of ϵ yields

$$\beta_k = 0 \qquad \text{for} \qquad k \geq 2, \tag{B.53}$$

$$\beta_1 = -g_R, \tag{B.54}$$

$$\beta_0 + \beta_1 \frac{da_1}{dg_R} = \beta_0 - g_R \frac{da_1}{dg_R} = -a_1, \tag{B.55}$$

and when $\epsilon \to 0$ the $\beta(g_R, \epsilon) = \beta_0(g_R) + \epsilon \beta_1(g_R)$ becomes $\beta_0(g_R)$. Thus the beta function is determined by calculating (B.55), which is solved by finding the coefficients of $1/\epsilon$ from the Feynman diagram.

For the γ_m and the γ in (B.47) and (B.48), the same procedure is applied.

B.5 Physical Interpretation of RG

In context of the Renormalization Group (henceforth RG), the new parameter μ, called the renormalization scale or sliding scale, is introduced and it is important to understand the role of the parameter. The μ defines a characteristic momentum scale we would like to investigate, and in the end our main objective through RG is to study the dependence of physical quantities on the scale μ.

One notable feature of RG theory is to produce more accurate results than ones from perturbation theory by solving the differential equations $(B.46) - (B.48)$, which is from the fact that physical quantities are unrelated to the renormalization scheme. For the coupling constant in ϕ^4 theory, while the RG equation results in

$$g_R(\mu') = \frac{g_R(\mu)}{1 - \frac{3}{16\pi^2} g_R(\mu) \ln \frac{\mu'}{\mu}}, \tag{B.56}$$

the perturbation theory for small $g(\mu)$ yields

$$g(\mu') \simeq g(\mu) + \frac{3}{16\pi^2} g^2(\mu) \ln \frac{\mu'}{\mu} + \mathcal{O}\left(g^3 \left(\ln \frac{\mu'}{\mu}\right)^2\right). \tag{B.57}$$

Comparing the two results $(B.56)$ and $(B.57)$, the RG equation includes higher-powers of logarithms occurring at higher-order in perturbation theory.

In general, the graph of the β-function can be sorted into four cases and for each case the behaviour of the coupling constant depending on μ can be predicted as follows

- **case (a)** : on given $g(\mu)$ and μ, if $\mu' \to \infty$ (or big enough) then $g(\mu') \to \infty$ Thus perturbation theory breaks down and the theory itself becomes ill-defined in that regime. This case applies to ϕ^4 theory and to most theories except Yang-Mills theory.

- **case (b)** : it describes $g(\mu) \to \infty$ as $\mu \to \infty$, but different from the case (a), g is finite in a certain range (or finite scale). e.g. $\beta(g) \sim bg^k$ where $k < 1$.

- **case (c)** : it contains a point where $\beta(g) = 0$ at $g = g_*$. That is, if $g < g_*$ it satisfies $\beta = \mu \frac{dg}{d\mu} > 0$, so g increases as μ increases, but if $g > g_*$ it satisfies $\beta = \mu \frac{dg}{d\mu} < 0$, so g decreases as μ increases. Thus near $g \simeq g_*$ the beta function is approximately described by $\beta(g) \simeq a(g_* - g)$ where $a > 0$, and then the RG equation yields

$$\int \frac{1}{\beta} dg = \int \frac{dg}{a(g_* - g)} = \int \frac{1}{\mu} d\mu \;\; \Rightarrow \;\; g = g_* - \mu^{-a}. \tag{B.58}$$

154
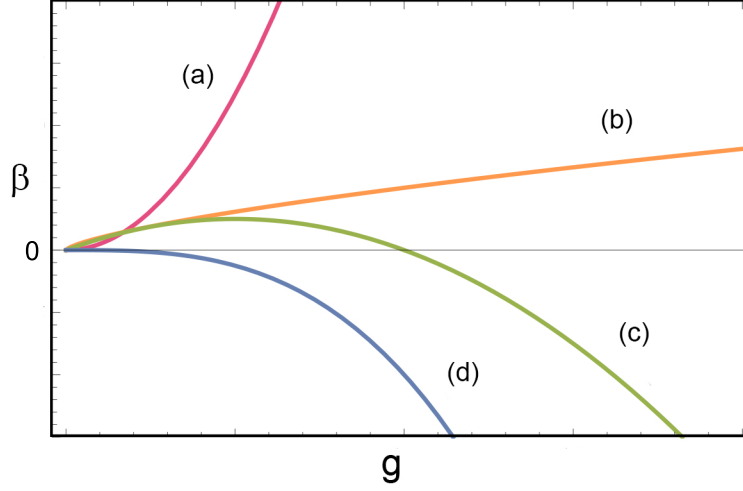
Figure B.1: beta function versus coupling constant, (a),(b),(c), and (d) are labeled from the top graph.

Therefore when $\mu \to \infty$, the coupling constant g approaches to g_*, where the g_* is called "UV fixed point".

- **case (d)** : as $\beta = \mu \frac{dg}{d\mu} < 0$, g decreases as μ increases. Thus the bigger the scale μ is, the better the perturbation becomes. Especially when $\mu \to \infty$ the g goes to 0, and so in this case $g = 0$ becomes "UV fixed point". This theory is said to be "asymptotically free" and is applied to Yang-Mills theory.

Now let us consider γ in (B.48), which is one of coefficients of the RG equation,

$$\gamma = \frac{1}{2}\mu \frac{d}{d\mu} \ln Z_\phi.$$

Making a change of the renormalization scale $\mu \to \mu'$, the relation between the renormalized fields is

$$\phi_R = Z_\phi^{-\frac{1}{2}}\phi \qquad \to \qquad \phi_R' = Z_\phi'^{-\frac{1}{2}}\phi = \left(\frac{Z_\phi'}{Z_\phi}\right)^{-\frac{1}{2}} \phi_R = \zeta^{-1}(\mu', \mu)\phi_R \tag{B.59}$$

where $\zeta^{-1} = \frac{Z_\phi'}{Z_\phi}$. Applying this relation to γ by replacing $Z_\phi^{1/2}$ with ζ, the coefficient γ is rewritten as

$$\gamma(g(\mu')) = \mu' \frac{d}{d\mu'} \ln \zeta(\mu', \mu). \tag{B.60}$$

155

Then ζ finally takes a form of

$$\zeta(\mu', \mu) = \exp\left[\int_\mu^{\mu'} \frac{d\mu}{\mu} \gamma(g(\mu))\right] = \exp\left[\int_{g(\mu)}^{g(\mu')} dg \frac{\gamma(g)}{\beta(g)}\right]. \tag{B.61}$$

For the specific case of having the UV fixed point at $g = g_*$ (like case (c)), if μ' approaches to ∞, γ can be expanded near g_* as

$$\gamma(g) \simeq \gamma(g_*) + \gamma_1(g - g_*) + \cdots, \tag{B.62}$$

and then plugging this to (B.61), ζ is obtained.

$$\zeta(\mu', \mu) \simeq \exp\left[\gamma(g_*) \int_\mu^{\mu'} \frac{d\mu}{\mu} + \cdots\right] = e^{\gamma(g_*) \ln \frac{\mu'}{\mu}} = \left(\frac{\mu'}{\mu}\right)^{\gamma(g_*)}. \tag{B.63}$$

Thus the renormalized field at the new renormalization scale μ' becomes

$$\phi'_R \simeq \left(\frac{\mu'}{\mu}\right)^{-\gamma(g_*)} \phi_R \tag{B.64}$$

where $\gamma(g_*)$ is called "anomalous dimension".

B.6   Renormalizability

In order to check if a theory is renormalizable, it helps to classify diagrams by the appearance of ultraviolet divergences. As this divergence is roughly predicted to occur when the power of momentum in numerator is bigger than the one in the denominator, we define the *superficial degree of divergence*, D, as

$$D \equiv \text{power of momentum in numerator} - \text{power of momentum in denorminator} \tag{B.65}$$

and then can roughly expect

$$\begin{array}{llll} D > 0 & : & \text{divergence} \propto \Lambda^D & \text{(B.66)} \\ D = 0 & : & \text{divergence} \propto \log \Lambda & \text{(B.67)} \\ D < 0 & : & \text{no divergence} & \text{(B.68)} \end{array}$$

156

where Λ is a momentum cutoff. Considering the N-point Green's function in momentum space

$$(2\pi)^d \delta^{(d)}(p_1 + \cdots + p_N) G_N(p_1, \cdots, p_N)$$
$$= \int d^d x_1 \cdots d^d x_N e^{i(p_1 \cdot x_1 + \cdots + p_N \cdot x_N)} G_N(x_1, \cdots, x_N), \tag{B.69}$$

the dimensional analysis of this in mass dimension gives

$$[G_N(p)] + [\delta^d(p)] = N[d^d x] + [G_N(x)]$$
$$\Rightarrow \quad [G_N(p)] + (-d) = N(-d) + N\left(\frac{d-2}{2}\right)$$
$$\Rightarrow \quad [G_N(p)] = -N\left(\frac{d+2}{2}\right) + d \tag{B.70}$$
$$\Rightarrow \quad [G_2(p)] = -2 \tag{B.71}$$

and then the mass dimension of the amputated Green function is calculated

$$[G_N^{amp}(p)] = -N[G_2(p)] + [G_N(p)]$$
$$= d - N\left(\frac{d-2}{2}\right). \tag{B.72}$$

In view of Feynman diagram, as all external momentum and masses in the propagator can be neglected in UV-region, the structure of the n-th order Feynman diagram is simply described by

$$g^n \int d^d k_1 d^d k_2 \cdots \frac{1}{k_1^2 \, k_2^2 \cdots} \tag{B.73}$$

and this mass dimension becomes

$$D + n[g]. \tag{B.74}$$

Then from (B.72) and (B.74) we find that the superficial degree of divergence takes

$$D = d - N\left(\frac{d-2}{2}\right) - n[g]. \tag{B.75}$$

Thus the divergence crucially depends on whether the mass dimension of the coupling is negative or positive. If $[g] < 0$ it is non-renormalizable; if $[g] > 0$ it is super-renormalizable; if $[g] = 0$ it is renormalizable. However this analysis is quite naive, and exceptional cases often happen. The trivial case is that a diagram with no propagator and no loops has

157

$D = 0$, but does not diverge. Also it is possible that a diagram would include a divergent subdiagram, which makes worse the divergence, or a symmetry such as the Ward identity could cancel or reduce the divergence.

A more qualitative classification on renormalizability is as follows

- Super-Renormailzable Theory:

    - Only a finite number of Feynman diagrams superficially diverge.
    - OR, Coupling constant has positive mass dimension
    - e.g. ϕ^3 theory in 4 dimensions

- Renormalizable Theory:

    - Only a finite number of amplitudes superficially diverge; however, divergences occur at all orders in perturbation theory.
    - OR, Coupling constant is dimensionless.
    - e.g. ϕ^4 theory in 4 dimensions, QED, Electro-Weak, QCD

- Non-Renormalizable Theory:

    - All amplitudes are divergent at a sufficiently high order in perturbation theory.
    - OR, Coupling constant has negative mass dimension.
    - e.g. ϕ^6 theory in 4 dimensions, Fermi theory of weak interaction

Appendix C

Wilsonian RG Equation

Here we understand the renormalization group in another context in order to make a bridge between the field theoretical renormalization group and the the statistical renormalization group, which is discussed in chapter 3. To begin with, we suppose a theory with the initial UV cutoff Λ_0 (e.g. Planck scale, ElectroWeak scale, etc.) and consider its generating functional to be

$$Z[J] = \int [\mathcal{D}\phi] e^{iS^{\Lambda_0}[\phi] + iJ\phi} \tag{C.1}$$

where S^{Λ_0} denotes integration for all modes below Λ_0. Now let us separate the integration section into two parts as

$$\phi_H \equiv \text{high momentum mode}, p > \Lambda$$
$$\phi_L \equiv \text{low momentum mode}, p < \Lambda \tag{C.2}$$

where $\Lambda < \Lambda_0$, and then write

$$\phi = \phi_H + \phi_L, \qquad J = J_H + J_L, \tag{C.3}$$
$$[\mathcal{D}\phi] = [\mathcal{D}\phi_L][\mathcal{D}\phi_H], \tag{C.4}$$

so that (C.1) turns to

$$Z[J] = \int [\mathcal{D}\phi_L] \int [\mathcal{D}\phi_H] e^{iS[\phi_L + \phi_H] + i(J_L + J_H)(\phi_L + \phi_H)}$$
$$= \int [\mathcal{D}\phi_L] \int [\mathcal{D}\phi_H] e^{iS[\phi_L + \phi_H] + i(J_L \phi_L + J_H \phi_H)}. \tag{C.5}$$

Let us suppose that we are interested only in low energy process ($p < \Lambda$). This allows us to set $J_H = 0$ and to integrate it on ϕ_H

$$Z[J] = \int [\mathcal{D}\phi_L] e^{iS_{\mathrm{eff}}^{\Lambda}[\phi_L] + iJ_L\phi_L} \tag{C.6}$$

where

$$e^{iS_{\mathrm{eff}}^{\Lambda}[\phi_L]} \equiv \int [\mathcal{D}\phi_H] e^{iS[\phi_L + \phi_H]} \tag{C.7}$$

which is called "Wilsonian low-energy effective action". The $S_{\mathrm{eff}}^{\Lambda}[\phi_L]$ can be considered as the action of a theory with the UV cutoff Λ and would yield the same result as the initial action $S^{\Lambda_0}[\phi]$ for the low energy scale, since this takes the same form of the generating functional $Z[J]$ as seen in (C.1) and (C.6). Around the cutoff Λ, let us assume the infinitesimal change from Λ to $\Lambda - d\Lambda$. Then the effective action would change

$$S_{\mathrm{eff}}^{\Lambda} \to S_{\mathrm{eff}}^{\prime \Lambda - d\Lambda} \equiv S^{\Lambda} - dS_{\mathrm{eff}}^{\Lambda} \tag{C.8}$$

and then the variation of S with respect to Λ would take the form

$$\Lambda \frac{dS_{\mathrm{eff}}^{\Lambda}}{d\Lambda} = F[S_{\mathrm{eff}}^{\Lambda}] \tag{C.9}$$

where $F[S_{\mathrm{eff}}^{\Lambda}]$ is provisional and should be found.

Returning to (C.1), let us separate the action into the interaction part and the free part

$$S^{\Lambda_0}[\phi] = \frac{1}{2} \int \phi D^{\Lambda_0^{-1}} \phi + S_{\mathrm{int}}^{\Lambda_0}[\phi] \tag{C.10}$$

where D^{Λ_0} is the free propagator with the UV cutoff Λ_0. Dividing the propagator into two parts

$$D^{\Lambda_0} = D^{\Lambda} + D_{\Lambda}^{\Lambda_0} \tag{C.11}$$

where D^{Λ} and $D_{\Lambda}^{\Lambda_0}$ indicate the low energy and the high energy part of propagators respectively, the generating functional (C.1) becomes

$$\begin{aligned} Z[J] &= \int [\mathcal{D}\phi_L][\mathcal{D}\phi_H] e^{-\frac{1}{2}\phi_L D^{\Lambda^{-1}}\phi_L - \frac{1}{2}\phi_H D_{\Lambda}^{\Lambda_0^{-1}}\phi_H - S_{\mathrm{int}}^{\Lambda_0}[\phi_L + \phi_H] + J(\phi_L + \phi_H)} \\ &= \int [\mathcal{D}\phi_L] e^{-\frac{1}{2}\phi_L D^{\Lambda^{-1}}\phi_L - W^{\Lambda}[\phi_L, J]} \end{aligned} \tag{C.12}$$

where

$$e^{-W^\Lambda[\phi_L, J]} = \int [\mathcal{D}\phi_H] e^{-\frac{1}{2}\phi_H D_\Lambda^{\Lambda_0^{-1}} \phi_H - S_{\text{int}}^{\Lambda_0}[\phi_L + \phi_H] + J(\phi_L + \phi_H)}. \tag{C.13}$$

It is noted that if $\phi_L = 0$, $e^{-W^\Lambda[0, J]}$ becomes a generating functional of a theory both of UV cutoff Λ_0 and IR cutoff Λ with the propagator $D_\Lambda^{\Lambda_0}$. Changing variables by using $\phi_H = \phi - \phi_L$

$$-\frac{1}{2}\phi_H D_\Lambda^{\Lambda_0^{-1}} \phi_H = -\frac{1}{2}\phi D_\Lambda^{\Lambda_0^{-1}} \phi - \frac{1}{2}\phi_L D_\Lambda^{\Lambda_0^{-1}} \phi_L + \phi D_\Lambda^{\Lambda_0^{-1}} \phi_L, \tag{C.14}$$

(C.13) yields

$$e^{-W^\Lambda[\phi_L, J]} = e^{-\frac{1}{2}\phi_L D_\Lambda^{\Lambda_0^{-1}} \phi_L} \int [\mathcal{D}\phi] e^{-\frac{1}{2}\phi D_\Lambda^{\Lambda_0^{-1}} \phi - S_{\text{int}}^\Lambda[\phi] + (J + D_\Lambda^{\Lambda_0^{-1}} \phi_L)\phi}. \tag{C.15}$$

and redefining variables with $\tilde{J} = J + D_\Lambda^{\Lambda_0^{-1}} \phi_L$, the first term out of the functional integration on the right side expands as

$$\begin{aligned}
-\frac{1}{2}\phi_L D_\Lambda^{\Lambda_0^{-1}} \phi_L &= -\frac{1}{2}(\tilde{J} - J) D_\Lambda^{\Lambda_0}(\tilde{J} - J) \\
&= -\frac{1}{2}\tilde{J} D_\Lambda^{\Lambda_0} \tilde{J} + J D_\Lambda^{\Lambda_0} \tilde{J} - \frac{1}{2} J D_\Lambda^{\Lambda_0} J \\
&= -\frac{1}{2}\tilde{J} D_\Lambda^{\Lambda_0} \tilde{J} + \frac{1}{2} J D_\Lambda^{\Lambda_0} J + J\phi_L,
\end{aligned} \tag{C.16}$$

and the first term inside of the functional integration changes to

$$-\frac{1}{2}\phi D^{\Lambda_0^{-1}} \phi = -\frac{1}{2}(\phi - \tilde{J} D_\Lambda^{\Lambda_0}) D_\Lambda^{\Lambda_0^{-1}} (\phi - D_\Lambda^{\Lambda_0} \tilde{J}) + \frac{1}{2}\tilde{J} D_\Lambda^{\Lambda_0} \tilde{J}. \tag{C.17}$$

Thus the (C.15) becomes

$$\begin{aligned}
e^{-W^\Lambda[\phi_L, J]} &= e^{\frac{1}{2} J D_\Lambda^{\Lambda_0} J + J\phi_L} e^{-\frac{1}{2} J D_\Lambda^{\tilde{\Lambda}_0} \tilde{J}} e^{-S_{\text{int}}^{\Lambda_0}[\frac{\delta}{\delta J}]} e^{\frac{1}{2}\tilde{J} D_\Lambda^{\Lambda_0} \tilde{J}} \\
&= e^{\frac{1}{2} J D_\Lambda^{\Lambda_0} J + J\phi_L} e^{-S_{\text{int}}^\Lambda[\phi_L + D_\Lambda^{\Lambda_0} J]}
\end{aligned} \tag{C.18}$$

and by replacing (C.13) with (C.18) its generating functional (C.12) takes a form of

$$Z[J] = \int [\mathcal{D}\phi_L] e^{-\frac{1}{2}\phi_L D^{\Lambda^{-1}} \phi_L - S_{\text{int}}^\Lambda[\phi_L + D_\Lambda^{\Lambda_0} J] + J\phi_L + \frac{1}{2} J D_\Lambda^{\Lambda_0} J}. \tag{C.19}$$

Again considering the low energy scale regime, we set $J_H = 0$; consequently $J = J_L$ and $D_\Lambda^{\Lambda_0} J = 0$ are obtained. The interacting part of the action is yielded

$$S_{\text{int}}^\Lambda[\phi_L + D_\Lambda^{\Lambda_0} J] = S_{\text{int}}^\Lambda[\phi_L] \tag{C.20}$$

where $S_{\text{int}}^\Lambda[\phi_L]$ becomes the interaction part of Wilsonian effective action.

To derive the RG equation, let us apply $\phi_L = 0$ into

$$W^\Lambda[\phi_L, J] = \frac{1}{2} J D_\Lambda^{\Lambda_0} J + J\phi_L + S_{\text{int}}^\Lambda[\phi_L + D_\Lambda^{\Lambda_0} J], \tag{C.21}$$

which yields

$$W^\Lambda[0, J] = \frac{1}{2} J D_\Lambda^{\Lambda_0} J + S_{\text{int}}^\Lambda[D_\Lambda^{\Lambda^0} J]. \tag{C.22}$$

In the low energy scale, the derivation of (C.13) with respect to Λ becomes

$$\frac{d}{d\Lambda} e^{W^\Lambda[0, J]} = -\frac{1}{2} \frac{\delta}{\delta J} \left(\frac{d}{d\Lambda} D_\Lambda^{\Lambda_0^{-1}} \right) \frac{\delta}{\delta J} e^{-W^\Lambda[0, J]} \tag{C.23}$$

and this is expressed again in terms of S_{int}^Λ as follows

$$\frac{dS_{\text{int}}^\Lambda[\phi]}{d\Lambda} = -\frac{1}{2} \int \frac{d^4 p}{(2\pi)^4} \frac{dD^{\Lambda(p)}}{d\Lambda} \left[\frac{\delta^2 S_{\text{int}}^\Lambda}{\delta\phi(p)\delta\phi(-p)} - \frac{\delta S_{\text{int}}^\Lambda}{\delta\phi(p)} \frac{\delta S_{\text{int}}^\Lambda}{\delta\phi(-p)} \right] \tag{C.24}$$

which is called the Wilsonian exact RG equation.

Let us find a simple connection of the Wilsonian effective action with conventional QFT quantities. Repeating (C.22), $W^\Lambda[0, J]$ indicates generating functional of connected Green functions with IR cutoff Λ, and $S_{\text{int}}^\Lambda[D_\Lambda^{\Lambda_0} J]$ is the Wilsonian effective action with UV cutoff Λ. Also (C.24) can be written in a familiar form, which is compared with LSZ formula, as

$$\frac{\delta^n S_{\text{int}}^\Lambda[\phi]}{\delta\phi(p_1) \cdots \delta\phi(p_n)} \bigg|_{\phi=0} = \prod_{i=1}^{n} \underbrace{D_\Lambda^{\Lambda_0^{-1}}(p_i)}_{\text{amputated}} \underbrace{\frac{\delta^n W^\Lambda[J]}{\delta J(p_1) \cdots \delta J(p_n)} \bigg|_{J=0}}_{\text{connected Green function}}. \tag{C.25}$$

Thus the Wilsonian effective action means not only the low energy effective action with UV cutoff Λ but also the generating functional of amputated and connected Green functions with IR cutoff Λ.

Then it is important to understand how a theory is influenced according to the cut-off scale Λ. Let us expand S_{int}^{Λ} in terms of (infinitely many) local operators $\mathcal{O}_i$ such as $(\partial\phi)^2, \phi^4, \phi^6, (\partial^2\phi)^2$, and etc

$$S_{\text{int}}^{\Lambda} = \sum_i \int d^4x g_i \mathcal{O}_i \tag{C.26}$$

where g_i are coupling constants. Among the infinitely many terms in S^{Λ}, significant contributions of operators can be obtained by counting their mass dimensions. Provided that the mass dimension of an operator $\mathcal{O}_i$ is $[\mathcal{O}_i] = \delta_i$, the coupling constant has the mass dimension $[g_i] = 4 - \delta_i$ and can be redefined with the dimensionless coupling constant λ_i as

$$g_i = \lambda_i \Lambda^{4-\delta_i}. \tag{C.27}$$

Then the initial action (C.26) is re-written as

$$S_{\text{int}}^{\Lambda} = \sum_i \lambda_i \Lambda^{4-\delta_i} \int d^4x \mathcal{O}_i \tag{C.28}$$

where Λ is a characteristic scale of S^{Λ} and so $\lambda_i \sim 1$ is expected. Assuming a theory in the energy scale E, the operators $\mathcal{O}_i$ has the scale of E^{δ_i}, and so we can predict the effect of the operator in the UV cutoff Λ to be

$$g_i \int d^4x \mathcal{O}_i \sim \lambda_i \left(\frac{E}{\Lambda}\right)^{\delta_i - 4}. \tag{C.29}$$

If $\delta_i > 4$, the operator becomes "irrelevant" in low energy regimes (for small values of E) and this case is comparable to non-renormalizability in the ordinary RG theory. In a case of $\delta_i = 0$, it is said that the operator is "marginal" and comparable to renormalizable. If $\delta_i < 4$ the operator becomes "relevant" and corresponds to super-renormalizability. Thus in the Wilsonian picture, the non-renormalizable terms are physically unimportant in the low energy regime, and the non-renormalizable terms in the action S do not influence processes at low energy scales; (super-)renormalizable terms are enough for describing the low energy process.

Appendix D

Useful Commutation Relation

D.1 Useful Commutation Relation

$$
\begin{aligned}
D_k D_l \Big(D^k D^l \alpha \Big) =& D_k D^2 (D^k \alpha) = D_k [D^2, D^k] \alpha + D^2 D^2 \alpha \\
=& -D_k \Big(\mathcal{R}^{(0)km}{}_m{}^l D_l \alpha \Big) + D^2 D^2 \alpha \\
=& \frac{n}{r^2} D^2 \alpha + D^2 D^2 \alpha
\end{aligned}
\tag{D.1}
$$

$$
\begin{aligned}
D^2 \Big(D^a D^b \alpha \Big) =& [D^2, D^a] D^b \alpha + D^a [D^2, D^b] \alpha + D^a D^b (D^2 \alpha) \\
=& -\mathcal{R}^{(0)e}{}_c{}^{ca} D_e D^b \alpha - \mathcal{R}^{(0)eb}{}_c{}^a D^c D_e \alpha - D^c \Big(\mathcal{R}^{(0)eb}{}_c{}^a D_e \alpha \Big) \\
& - D^a \Big(\mathcal{R}^{(0)e}{}_c{}^{cb} D_e \alpha \Big) + D^a D^b (D^2 \alpha) \\
=& 2 \mathcal{R}^{(0)caeb} D_c D_e + \frac{2n}{r^2} D^a D^b \alpha + D^a D^b D^2 \alpha
\end{aligned}
\tag{D.2}
$$

$$
\begin{aligned}
D_k D^a (D^k D^b \alpha) =& [D_k, D^a](D^k D^b \alpha) + D^a [D^2, D^b] \alpha + D^a D^b (D^2 \alpha) \\
=& -\mathcal{R}^{(0)e}{}_c{}^{ca} D_e D^b \alpha - \mathcal{R}^{(0)ebca} D_c D_e \alpha - D^a \Big(\mathcal{R}^{(0)e}{}_c{}^{ca} D_e \alpha \Big) + D^a D^b (D^2 \alpha) \\
=& \mathcal{R}^{(0)caeb} D_c D_e \alpha + \frac{2n}{r^2} D^a D^b \alpha + D^a D^b D^2 \alpha
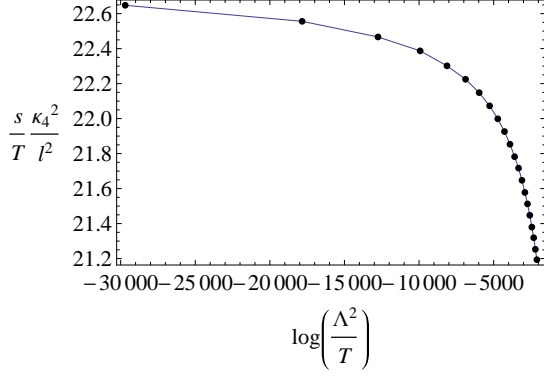\end{aligned}
\tag{D.3}
$$

where the commutation of two covariant derivatives acting on w_c and t_{ab} is
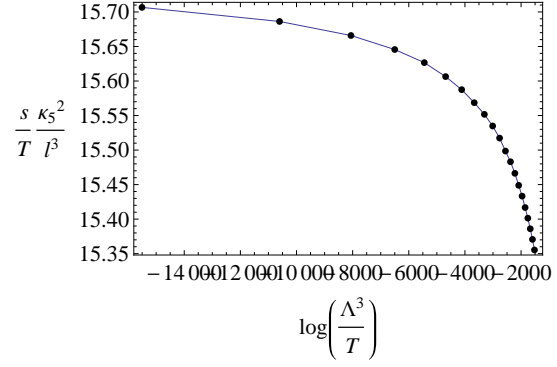
$$[D_a, D_b] w_c = \mathcal{R}^{(0)}_{abc}{}^d w_d$$
$$[D_a, D_b] t_c{}^d = \mathcal{R}^{(0)}_{abc}{}^e t_e{}^d + \mathcal{R}^{(0)}_{ab}{}^d{}_e t_c{}^e. \tag{D.4}$$
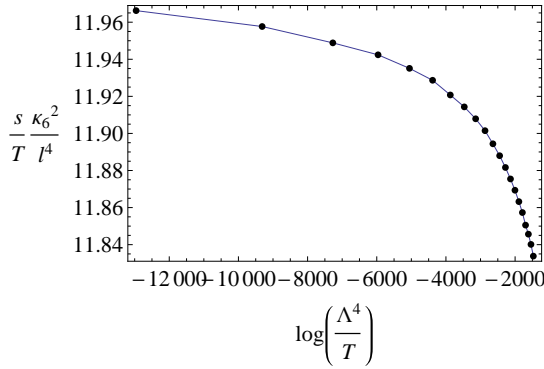
Appendix E

Graphs of Entropy Density for Chapter 6

(a) Dots are calculated under that $z = 2$ and h_0 runs from 0.9713 to 0.9705 in increments of 0.00004 and are joined by straight lines.

(b) Dots are calculated under that $z = 3$ and h_0 runs from 1.6343 to 1.6335 in increments of 0.00004 and are joined by straight lines.

(c) Dots are calculated under that $z = 4$ and h_0 runs from 2.2822 to 2.2814 in increments of 0.00004 and are joined by straight lines.

(d) Dots are calculated under that $z = 5$ and h_0 runs from 2.9255 to 2.9247 in increments of 0.00004 and are joined by straight lines.
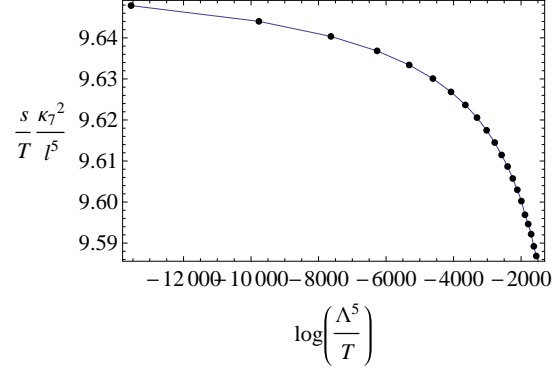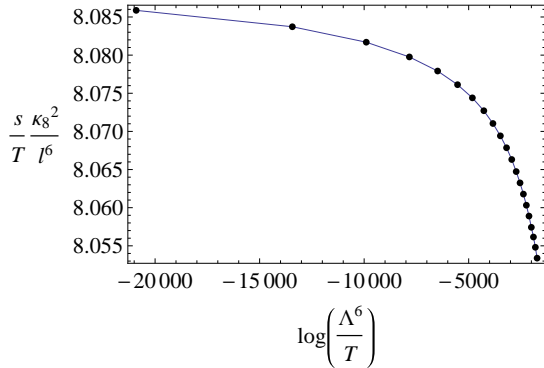
(e) Dots are calculated under that $z = 6$ and h_0 runs from 3.5668 to 3.566 in increments of 0.00004 and are joined by straight lines.
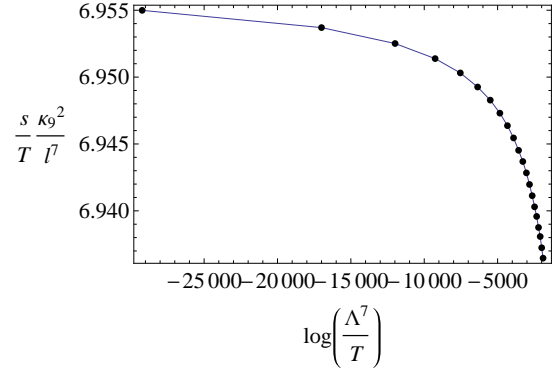
(f) Dots are calculated under that $z = 7$ and h_0 runs from 4.2070 to 4.2062 in increments of 0.00004 and are joined by straight lines.

Figure E.1: Entropy density per unit temperature versus $\log(\Lambda^z/T)$

Appendix F

Supplements for Chapter 7

F.1   X,Y, and Z in $\mathcal{F}$, $\mathcal{E}$, and $\mathcal{J}^{\hat{t}}$ in (7.66)-(7.68)

$$
\begin{aligned}
X =\,& z^3(-1 + 2z + 2z^2 - 2z^3) + z^2(-6 + 27z - 34z^2 - 14z^3 + 18z^4)\tilde{\alpha} - z(12 - 101z \\
& + 309z^2 - 406z^3 + 144z^4 + 12z^5)\tilde{\alpha}^2 + (-8 + 120z - 574z^2 + 1405z^3 - 1842z^4 \\
& + 1053z^5 - 194z^6)\tilde{\alpha}^3 + (20 - 191z + 693z^2 - 1595z^3 + 2383z^4 - 1718z^5 + 408z^6)\tilde{\alpha}^4 \\
& - 2(-1 + 21z - 150z^2 + 262z^3 + 49z^4 - 295z^5 + 90z^6)\tilde{\alpha}^5 + 4(1 + z)^2(2 - 17z \\
& + 41z^2 - 32z^3 + 4z^4)\tilde{\alpha}^6
\end{aligned}
\tag{F.1}
$$

$$
\begin{aligned}
Y =\,& z^3(-1 + 4z - 4z^2 + 2z^3) + z^2(-6 + 31z - 70z^2 + 66z^3 - 30z^4)\tilde{\alpha} + z(-12 + 95z \\
& - 311z^2 + 560z^3 - 502z^4 + 200z^5)\tilde{\alpha}^2 + (-8 + 112z - 490z^2 + 1209z^3 - 1934z^4 \\
& + 1689z^5 - 618z^6)\tilde{\alpha}^3 + (28 - 215z + 589z^2 - 1155z^3 + 2095z^4 - 2134z^5 + 792z^6)\tilde{\alpha}^4 \\
& + (-14 + 38z + 220z^2 - 668z^3 + 126z^4 + 654z^5 - 308z^6)\tilde{\alpha}^5 + 4(1 + z)^2(2 - 17z \\
& + 41z^2 - 32z^3 + 4z^4)\tilde{\alpha}^6)
\end{aligned}
\tag{F.2}
$$

$$
\begin{aligned}
Z =\,& z^5(-5 + 24z - 23z^2 - 22z^3 + 18z^4 + 20z^5) + z^4(11 + 23z - 395z^2 + 703z^3 - 40z^4 \\
& - 318z^5 - 176z^6)\tilde{\alpha} + z^3(1 - 140z + 402z^2 + 2050z^3 - 6461z^4 + 3610z^5 + 1106z^6 \\
& + 776z^7)\tilde{\alpha}^2 + z^2(-37 + 105z + 1198z^2 - 7062z^3 + 2299z^4 + 25593z^5 - 29948z^6 \\
& + 6308z^7 - 3832z^8)\tilde{\alpha}^3 + 2z(53 - 351z + 1059z^2 - 4788z^3 + 22016z^4 - 31125z^5 \\
& - 13341z^6 + 49514z^7 - 24299z^8 + 7982z^9)\tilde{\alpha}^4 - 2(-16 + 328z - 2401z^2 + 7052z^3 \\
& - 16915z^4 + 62838z^5 - 119335z^6 + 51832z^7 + 66435z^8 - 58018z^9 + 18952z^{1}0)\tilde{\alpha}^5 \\
& + 4(-28 + 218z - 1604z^2 + 3369z^3 - 1768z^4 + 22651z^5 - 76922z^6 + 67311z^7 \\
& + 11872z^8 - 31725z^9 + 12002z^{1}0)\tilde{\alpha}^6 - 8(-7 - 46z - 23z^2 - 1092z^3 + 8439z^4 \\
& - 11616z^5 - 8665z^6 + 21748z^7 - 2820z^8 - 8226z^9 + 3844z^{1}0)\tilde{\alpha}^7 + 16(1 + z)^2(-2 \\
& + 23z - 322z^2 + 1396z^3 - 2240z^4 + 665z^5 + 1724z^6 - 1676z^7 + 480z^8)\tilde{\alpha}^8 \qquad \text{(F.3)}
\end{aligned}
$$

F.2 Graph of Entropy Density depending on $\log(\Lambda^z/T)$
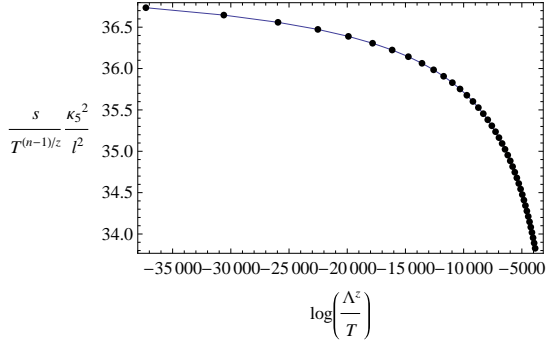
(a) For $\tilde{\alpha} = \frac{1}{4}$ ($or z = 2$) and h_0 runs from 0.75120 to 0.75038 in increments of 0.00002. Dots are the numerical results and joined by straight line.
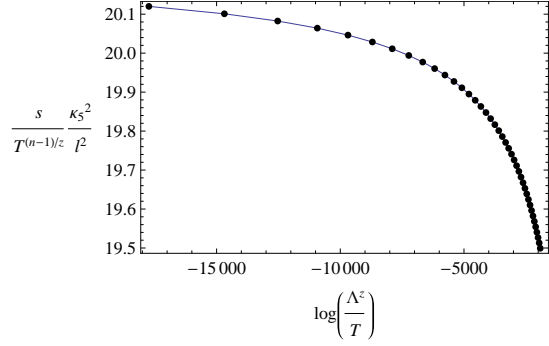
(b) For $\tilde{\alpha} = \frac{1}{10}$ (or $z = 2.6$) and h_0 from 1.26160 to 1.26078 in increments of 0.00002. Dots are the numerical results and joined by straight line.
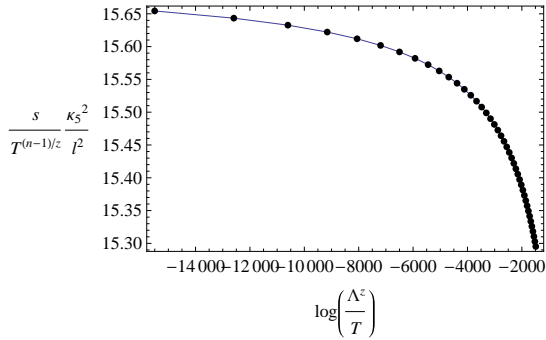
(c) For $\tilde{\alpha} = 0$ (or $z = 3$) and h_0 runs from 1.63430 to 1.63348 in increments of 0.00002. Dots are the numerical results and joined by straight line.
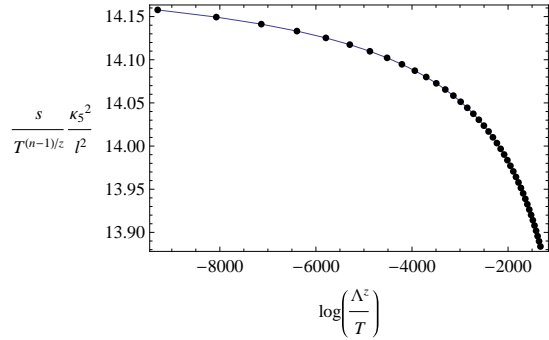
(d) For $\tilde{\alpha} = -\frac{1}{20}$ (or $z = 3.2$) and h_0 runs from 1.82980 to 1.82898 in increments of 0.00002. Dots are the numerical results and joined by straight line.
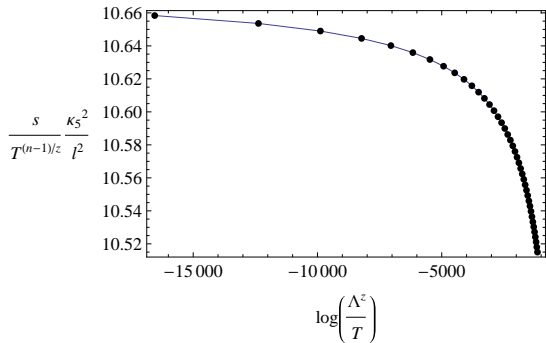
(e) For $\tilde{\alpha} = -\frac{1}{4}$ (or $z = 4$) and h_0 runs from 2.66870 to 2.66788 in increments of 0.00002. Dots are the numerical results and joined by straight line.

(f) For $\tilde{\alpha} = -\frac{3}{10}$ (or $z = 4.2$). h_0 runs from 2.89170 to 2.89088 in increments of 0.00002. Dots are the numerical results and joined by straight line.

Figure F.1: Dimensionless entropy density per unit temperature versus $\log \Lambda^z/T$ for each $\tilde{\alpha}$ in $n = 4$

170

F.3 Table $\mathcal{F}/Ts$ and $\mathcal{E}/Ts$ for $n = 5, 6, 7, 8$ and 9

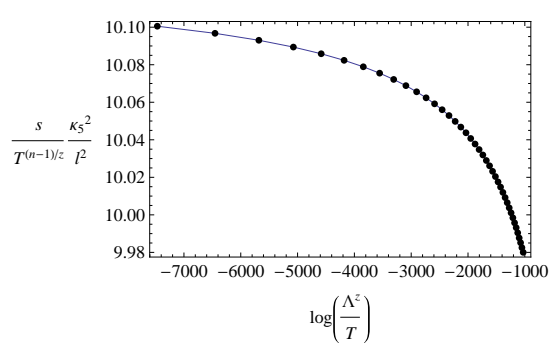| $(n = 5)$	$\frac{\mathcal{F}}{Ts}$	$\frac{\mathcal{E}}{Ts}$	$\frac{\mathcal{F}}{\mathcal{E}}$
$\tilde{\alpha} = 1/4$ or $z = 2.5$	$-0.38 - \frac{1.29}{\log \Lambda^z/T} + \cdots$	$0.62 - \frac{1.29}{\log \Lambda^z/T} + \cdots$	$-0.63 - \frac{3.42}{\log \Lambda^z/T} + \cdots$
$\tilde{\alpha} = 1/10$ or $z = 3.4$	$-0.46 - \frac{0.75}{\log \Lambda^z/T} + \cdots$	$0.54 - \frac{0.75}{\log \Lambda^z/T} + \cdots$	$-0.85 - \frac{2.56}{\log \Lambda^z/T} + \cdots$
$\tilde{\alpha} = 0$ or $z = 4$	$-0.50 - \frac{0.67}{\log \Lambda^z/T} + \cdots$	$0.50 - \frac{0.67}{\log \Lambda^z/T} + \cdots$	$-1.00 - \frac{2.67}{\log \Lambda^z/T} + \cdots$
$\tilde{\alpha} = -1/20$ or $z = 4.3$	$-0.52 - \frac{0.65}{\log \Lambda^z/T} + \cdots$	$0.48 - \frac{0.65}{\log \Lambda^z/T} + \cdots$	$-1.08 - \frac{2.78}{\log \Lambda^z/T} + \cdots$
$\tilde{\alpha} = -1/6$ or $z = 5$	$-0.56 - \frac{0.63}{\log \Lambda^z/T} + \cdots$	$0.44 - \frac{0.62}{\log \Lambda^z/T} + \cdots$	$-1.25 - \frac{3.17}{\log \Lambda^z/T} + \cdots$
$\tilde{\alpha} = -3/10$ or $z = 5.8$	$-0.59 - \frac{0.60}{\log \Lambda^z/T} + \cdots$	$0.41 - \frac{0.61}{\log \Lambda^z/T} + \cdots$	$-1.45 - \frac{3.63}{\log \Lambda^z/T} + \cdots$
$\vdots$	$\vdots$	$\vdots$	$\vdots$

Table F.1: fitting functions for $\frac{\mathcal{F}}{Ts}$, $\frac{\mathcal{E}}{Ts}$, and $\frac{\mathcal{F}}{\mathcal{E}}$ in $n = 5$

$(n=6)$	$\frac{\mathcal{F}}{Ts}$	$\frac{\mathcal{E}}{Ts}$	$\frac{\mathcal{F}}{\mathcal{E}}$
$\tilde{\alpha}=1/4$ or $z=3$	$-0.37-\frac{1.43}{\log\Lambda^z/T}+\cdots$	$0.62-\frac{1.41}{\log\Lambda^z/T}+\cdots$	$-0.60-\frac{3.65}{\log\Lambda^z/T}+\cdots$
$\tilde{\alpha}=1/10$ or $z=4.2$	$-0.46-\frac{0.71}{\log\Lambda^z/T}+\cdots$	$0.54-\frac{0.71}{\log\Lambda^z/T}+\cdots$	$-0.84-\frac{2.40}{\log\Lambda^z/T}+\cdots$
$\tilde{\alpha}=0$ or $z=5$	$-0.50-\frac{0.63}{\log\Lambda^z/T}+\cdots$	$0.50-\frac{0.63}{\log\Lambda^z/T}+\cdots$	$-1.00-\frac{2.51}{\log\Lambda^z/T}+\cdots$
$\tilde{\alpha}=-1/20$ or $z=5.4$	$-0.52-\frac{0.60}{\log\Lambda^z/T}+\cdots$	$0.48-\frac{0.60}{\log\Lambda^z/T}+\cdots$	$-1.08-\frac{2.61}{\log\Lambda^z/T}+\cdots$
$\tilde{\alpha}=-1/8$ or $z=6$	$-0.55-\frac{0.58}{\log\Lambda^z/T}+\cdots$	$0.45-\frac{0.58}{\log\Lambda^z/T}+\cdots$	$-1.20-\frac{2.81}{\log\Lambda^z/T}+\cdots$
$\tilde{\alpha}=-3/10$ or $z=7.4$	$-0.60-\frac{0.57}{\log\Lambda^z/T}+\cdots$	$0.40-\frac{0.57}{\log\Lambda^z/T}+\cdots$	$-1.48-\frac{3.48}{\log\Lambda^z/T}+\cdots$
$\vdots$	$\vdots$	$\vdots$	$\vdots$

Table F.2: fitting functions for $\frac{\mathcal{F}}{Ts}$, $\frac{\mathcal{E}}{Ts}$, and $\frac{\mathcal{F}}{\mathcal{E}}$ in $n=6$

$(n=7)$	$\frac{\mathcal{F}}{Ts}$	$\frac{\mathcal{E}}{Ts}$	$\frac{\mathcal{F}}{\mathcal{E}}$
$\tilde{\alpha}=1/4$ or $z=3.5$	$-0.37-\frac{1.58}{\log\Lambda^z/T}+\cdots$	$0.63-\frac{1.59}{\log\Lambda^z/T}+\cdots$	$-0.58-\frac{3.97}{\log\Lambda^z/T}+\cdots$
$\tilde{\alpha}=1/10$ or $z=5$	$-0.45-\frac{0.68}{\log\Lambda^z/T}+\cdots$	$0.55-\frac{0.68}{\log\Lambda^z/T}+\cdots$	$-0.83-\frac{2.30}{\log\Lambda^z/T}+\cdots$
$\tilde{\alpha}=0$ or $z=6$	$-0.50-\frac{0.60}{\log\Lambda^z/T}+\cdots$	$0.50-\frac{0.60}{\log\Lambda^z/T}+\cdots$	$-1.00-\frac{2.40}{\log\Lambda^z/T}+\cdots$
$\tilde{\alpha}=-1/20$ or $z=6.5$	$-0.52-\frac{0.58}{\log\Lambda^z/T}+\cdots$	$0.48-\frac{0.58}{\log\Lambda^z/T}+\cdots$	$-1.08-\frac{2.50}{\log\Lambda^z/T}+\cdots$
$\tilde{\alpha}=-1/10$ or $z=7$	$-0.54-\frac{0.56}{\log\Lambda^z/T}+\cdots$	$0.46-\frac{0.56}{\log\Lambda^z/T}+\cdots$	$-1.17-\frac{2.63}{\log\Lambda^z/T}+\cdots$
$\tilde{\alpha}=-3/10$ or $z=9$	$-0.60-\frac{0.54}{\log\Lambda^z/T}+\cdots$	$0.40-\frac{0.54}{\log\Lambda^z/T}+\cdots$	$-1.5-\frac{3.37}{\log\Lambda^z/T}+\cdots$
$\vdots$	$\vdots$	$\vdots$	$\vdots$

Table F.3: fitting functions for $\frac{\mathcal{F}}{Ts}$, $\frac{\mathcal{E}}{Ts}$, and $\frac{\mathcal{F}}{\mathcal{E}}$ in $n=7$

$(n = 8)$	$\frac{\mathcal{F}}{Ts}$	$\frac{\mathcal{E}}{Ts}$	$\frac{\mathcal{F}}{\mathcal{E}}$
$\tilde{\alpha} = 1/4$ or $z = 4$	$-0.36 - \frac{1.76}{\log \Lambda^z/T} + \cdots$	$0.64 - \frac{1.73}{\log \Lambda^z/T} + \cdots$	$-0.57 - \frac{4.32}{\log \Lambda^z/T} + \cdots$
$\tilde{\alpha} = 1/10$ or $z = 5.8$	$-0.45 - \frac{0.66}{\log \Lambda^z/T} + \cdots$	$0.55 - \frac{0.67}{\log \Lambda^z/T} + \cdots$	$-0.83 - \frac{2.23}{\log \Lambda^z/T} + \cdots$
$\tilde{\alpha} = 0$ or $z = 7$	$-0.50 - \frac{0.58}{\log \Lambda^z/T} + \cdots$	$0.50 - \frac{0.58}{\log \Lambda^z/T} + \cdots$	$-1.00 - \frac{2.33}{\log \Lambda^z/T} + \cdots$
$\tilde{\alpha} = -1/20$ or $z = 7.6$	$-0.52 - \frac{0.56}{\log \Lambda^z/T} + \cdots$	$0.48 - \frac{0.56}{\log \Lambda^z/T} + \cdots$	$-1.09 - \frac{2.45}{\log \Lambda^z/T} + \cdots$
$\tilde{\alpha} = -1/12$ or $z = 8$	$-0.53 - \frac{0.56}{\log \Lambda^z/T} + \cdots$	$0.47 - \frac{0.55}{\log \Lambda^z/T} + \cdots$	$-1.14 - \frac{2.53}{\log \Lambda^z/T} + \cdots$
$\tilde{\alpha} = -3/10$ or $z = 10.6$	$-0.60 - \frac{0.53}{\log \Lambda^z/T} + \cdots$	$0.40 - \frac{0.53}{\log \Lambda^z/T} + \cdots$	$-1.51 - \frac{3.35}{\log \Lambda^z/T} + \cdots$
$\vdots$	$\vdots$	$\vdots$	$\vdots$

Table F.4: fitting functions for $\frac{\mathcal{F}}{Ts}$, $\frac{\mathcal{E}}{Ts}$, and $\frac{\mathcal{F}}{\mathcal{E}}$ in $n = 8$

$(n = 9)$	$\frac{\mathcal{F}}{Ts}$	$\frac{\mathcal{E}}{Ts}$	$\frac{\mathcal{F}}{\mathcal{E}}$
$\tilde{\alpha} = 1/4$ or $z = 4.5$	$-0.36 - \frac{1.89}{\log \Lambda^?/T} + \cdots$	$0.64 - \frac{1.89}{\log \Lambda^z/T} + \cdots$	$-0.56 - \frac{4.59}{\log \Lambda^z/T} + \cdots$
$\tilde{\alpha} = 1/10$ or $z = 6.6$	$-0.45 - \frac{0.66}{\log \Lambda^z/T} + \cdots$	$0.55 - \frac{0.66}{\log \Lambda^z/T} + \cdots$	$-0.83 - \frac{2.19}{\log \Lambda^z/T} + \cdots$
$\tilde{\alpha} = 0$ or $z = 8$	$-0.50 - \frac{0.57}{\log \Lambda^z/T} + \cdots$	$0.50 - \frac{0.57}{\log \Lambda^z/T} + \cdots$	$-1.0 - \frac{2.29}{\log \Lambda^z/T} + \cdots$
$\tilde{\alpha} = -1/20$ or $z = 8.7$	$-0.52 - \frac{0.55}{\log \Lambda^z/T} + \cdots$	$0.48 - \frac{0.55}{\log \Lambda^z/T} + \cdots$	$-1.09 - \frac{2.40}{\log \Lambda^z/T} + \cdots$
$\tilde{\alpha} = -1/14$ or $z = 9$	$-0.53 - \frac{0.54}{\log \Lambda^z/T} + \cdots$	$0.47 - \frac{0.54}{\log \Lambda^z/T} + \cdots$	$-1.13 - \frac{2.46}{\log \Lambda^z/T} + \cdots$
$\tilde{\alpha} = -3/10$ or $z = 12.2$	$-0.60 - \frac{0.51}{\log \Lambda^z/T} + \cdots$	$0.40 - \frac{0.51}{\log \Lambda^z/T} + \cdots$	$-1.53 - \frac{3.28}{\log \Lambda^z/T} + \cdots$
$\vdots$	$\vdots$	$\vdots$	$\vdots$

Table F.5: fitting functions for $\frac{\mathcal{F}}{Ts}$, $\frac{\mathcal{E}}{Ts}$, and $\frac{\mathcal{F}}{\mathcal{E}}$ in $n = 9$

References

[1] Enrique Alvarez, Jorge Conde, and Lorenzo Hernandez. Goursat's problem and the holographic principle. *Nucl.Phys.*, B689:257–291, 2004.

[2] Giovanni Arcioni and Claudio Dappiaggi. Exploring the holographic principle in asymptotically flat space-times via the BMS group. *Nucl.Phys.*, B674:553–592, 2003.

[3] Giovanni Arcioni and Claudio Dappiaggi. Holography in asymptotically flat space-times and the BMS group. *Class.Quant.Grav.*, 21:5655, 2004.

[4] Giovanni Arcioni and Claudio Dappiaggi. Holography and BMS field theory. *AIP Conf.Proc.*, 751:176–178, 2005.

[5] Richard L. Arnowitt, Stanley Deser, and Charles W. Misner. The Dynamics of general relativity. *Gen.Rel.Grav.*, 40:1997–2027, 2008.

[6] A. Ashtekar and R.O. Hansen. A unified treatment of null and spatial infinity in general relativity. I - Universal structure, asymptotic symmetries, and conserved quantities at spatial infinity. *J.Math.Phys.*, 19:1542–1566, 1978.

[7] A. Ashtekar and A. Magnon-Ashtekar. Energy-Momentum in General Relativity. *Phys. Rev. L.*

[8] A. Ashtekar and Joseph D. Romano. Spatial infinity as a boundary of space-time. *Class.Quant.Grav.*, 9:1069–1100, 1992.

[9] Dumitru Astefanesei, Robert B. Mann, and Cristian Stelea. Note on counterterms in asymptotically flat spacetimes. *Phys.Rev.*, D75:024007, 2007.

[10] Koushik Balasubramanian and John McGreevy. An Analytic Lifshitz black hole. *Phys.Rev.*, D80:104039, 2009.

[11] Vijay Balasubramanian and Per Kraus. A Stress tensor for Anti-de Sitter gravity. *Commun.Math.Phys.*, 208:413–428, 1999.

[12] R. Beig. INTEGRATION OF EINSTEIN'S EQUATIONS NEAR SPATIAL INFIN-ITY. 1983.

[13] R. Beig and B. G. Schmidt. Einstein's equations near spatial infinity. 1982.

[14] Gaetano Bertoldi, Benjamin A. Burrington, and Amanda Peet. Black Holes in asymp-totically Lifshitz spacetimes with arbitrary critical exponent. *Phys.Rev.*, D80:126003, 2009.

[15] Gaetano Bertoldi, Benjamin A. Burrington, and Amanda W. Peet. Thermodynamics of black branes in asymptotically Lifshitz spacetimes. *Phys.Rev.*, D80:126004, 2009.

[16] H. Bondi, M.G.J. van der Burg, and A.W.K. Metzner. Gravitational waves in gen-eral relativity. 7. Waves from axisymmetric isolated systems. *Proc.Roy.Soc.Lond.*, A269:21–52, 1962.

[17] David G. Boulware and Stanley Deser. String Generated Gravity Models. *Phys.Rev.Lett.*, 55:2656, 1985.

[18] Harry Braviner, Ruth Gregory, and Simon F. Ross. Flows involving Lifshitz solutions. *Class.Quant.Grav.*, 28:225028, 2011.

[19] Irene Bredberg, Cynthia Keeler, Vyacheslav Lysov, and Andrew Strominger. Wilso-nian Approach to Fluid/Gravity Duality. *JHEP*, 1103:141, 2011.

[20] J. David Brown, J. Creighton, and Robert B. Mann. Temperature, energy and heat capacity of asymptotically anti-de Sitter black holes. *Phys.Rev.*, D50:6394–6403, 1994.

[21] J. David Brown and Jr. York, James W. Quasilocal energy and conserved charges derived from the gravitational action. *Phys.Rev.*, D47:1407–1419, 1993.

[22] Rong-Gen Cai. Gauss-Bonnet black holes in AdS spaces. *Phys.Rev.*, D65:084014, 2002.

[23] Rong-Gen Cai and Qi Guo. Gauss-Bonnet black holes in dS spaces. *Phys.Rev.*, D69:104025, 2004.

[24] Christos Charmousis and Jean-Francois Dufaux. General Gauss-Bonnet brane cos-mology. *Class.Quant.Grav.*, 19:4671–4682, 2002.

[25] Miranda C.N. Cheng, Sean A. Hartnoll, and Cynthia A. Keeler. Deformations of Lifshitz holography. *JHEP*, 1003:062, 2010.

[26] Y.M. Cho and Ishwaree P. Neupane. Anti-de Sitter black holes, thermal phase transition and holography in higher curvature gravity. *Phys.Rev.*, D66:024044, 2002.

[27] Keith Copsey and Robert Mann. Pathologies in Asymptotically Lifshitz Spacetimes. *JHEP*, 1103:039, 2011.

[28] Mirjam Cvetic, Shin'ichi Nojiri, and Sergei D. Odintsov. Black hole thermodynamics and negative entropy in de Sitter and anti-de Sitter Einstein-Gauss-Bonnet gravity. *Nucl.Phys.*, B628:295–330, 2002.

[29] Ulf H. Danielsson and Larus Thorlacius. Black holes in asymptotically Lifshitz spacetime. *JHEP*, 0903:070, 2009.

[30] Claudio Dappiaggi, Valter Moretti, and Nicola Pinamonti. Rigorous steps towards holography in asymptotically flat spacetimes. *Rev.Math.Phys.*, 18:349–416, 2006.

[31] Stephen C. Davis. Generalized Israel junction conditions for a Gauss-Bonnet brane world. *Phys.Rev.*, D67:024030, 2003.

[32] Jan de Boer and Sergey N. Solodukhin. A Holographic reduction of Minkowski spacetime. *Nucl.Phys.*, B665:545–593, 2003.

[33] Sebastian de Haro, Sergey N. Solodukhin, and Kostas Skenderis. Holographic reconstruction of space-time and renormalization in the AdS / CFT correspondence. *Commun.Math.Phys.*, 217:595–622, 2001.

[34] M.H. Dehghani and Robert B. Mann. Lovelock-Lifshitz Black Holes. *JHEP*, 1007:019, 2010.

[35] Oscar J.C. Dias, Gary T. Horowitz, and Jorge E. Santos. Black holes with only one Killing field. *JHEP*, 1107:115, 2011.

[36] Roberto Emparan, Clifford V. Johnson, and Robert C. Myers. Surface terms as counterterms in the AdS / CFT correspondence. *Phys.Rev.*, D60:104001, 1999.

[37] C. Fefferman and R Graham. Conformal invariants. *in lie Cartan et les Mathmatiques d'Aujourdui,Asterisque*, 95:116, 1985.

[38] Hilmar Forkel, Michael Beyer, and Tobias Frederico. Linear square-mass trajectories of radially and orbitally excited hadrons in holographic QCD. *JHEP*, 0707:077, 2007.

[39] Mitsutoshi Fujita, Wei Li, Shinsei Ryu, and Tadashi Takayanagi. Fractional Quantum Hall Effect via Holography: Chern-Simons, Edge States, and Hierarchy. *JHEP*, 0906:066, 2009.

[40] Robert P. Geroch. Structure of the gravitational field at spatial infinity. *J.Math.Phys.*, 13:956–968, 1972.

[41] Ruth Gregory, Sugumi Kanno, and Jiro Soda. Holographic Superconductors with Higher Curvature Corrections. *JHEP*, 0910:010, 2009.

[42] Steven S. Gubser and Silviu S. Pufu. The Gravity dual of a p-wave superconductor. *JHEP*, 0811:033, 2008.

[43] U. Gursoy and E. Kiritsis. Exploring improved holographic theories for QCD: Part I. *JHEP*, 0802:032, 2008.

[44] Rudolf Haag, Jan T. Lopuszanski, and Martin Sohnius. All Possible Generators of Supersymmetries of the s Matrix. *Nucl.Phys.*, B88:257, 1975.

[45] Sarah Harrison, Shamit Kachru, and Huajia Wang. Resolving Lifshitz Horizons. 2012.

[46] Sean A. Hartnoll. Lectures on holographic methods for condensed matter physics. *Class.Quant.Grav.*, 26:224002, 2009.

[47] Sean A. Hartnoll, Christopher P. Herzog, and Gary T. Horowitz. Holographic Superconductors. *JHEP*, 0812:015, 2008.

[48] S.W. Hawking and Gary T. Horowitz. The Gravitational Hamiltonian, action, entropy and surface terms. *Class.Quant.Grav.*, 13:1487–1498, 1996.

[49] Christopher P. Herzog. Lectures on Holographic Superfluidity and Superconductivity. *J.Phys.*, A42:343001, 2009.

[50] Stefan Hollands, Akihiro Ishibashi, and Donald Marolf. Counter-term charges generate bulk symmetries. *Phys.Rev.*, D72:104025, 2005.

[51] Gary T. Horowitz. Theory of Superconductivity. *Lect.Notes Phys.*, 828:313–347, 2011.

[52] Gary T. Horowitz and Benson Way. Lifshitz Singularities. *Phys.Rev.*, D85:046008, 2012.

[53] Carlos Hoyos-Badajoz, Karl Landsteiner, and Sergio Montero. Holographic meson melting. *JHEP*, 0704:031, 2007.

[54] Ted Jacobson and Robert C. Myers. Black hole entropy and higher curvature interactions. *Phys.Rev.Lett.*, 70:3684–3687, 1993.

[55] Romuald A. Janik and Robert B. Peschanski. Asymptotic perfect fluid dynamics as a consequence of Ads/CFT. *Phys.Rev.*, D73:045013, 2006.

[56] Shamit Kachru, Xiao Liu, and Michael Mulligan. Gravity Duals of Lifshitz-like Fixed Points. *Phys.Rev.*, D78:106005, 2008.

[57] Sugumi Kanno. A Note on Gauss-Bonnet Holographic Superconductors. *Class.Quant.Grav.*, 28:127001, 2011.

[58] Peter Kopietz, Lorenz Bartosch, and F. Schtz. *Introduction to the functional renormalization group*. Berlin: Springer, 2010.

[59] Ben M. Leith and Ishwaree P. Neupane. Gauss-Bonnet cosmologies: Crossing the phantom divide and the transition from matter dominance to dark energy. *JCAP*, 0705:019, 2007.

[60] Juan Martin Maldacena. The Large N limit of superconformal field theories and supergravity. *Adv.Theor.Math.Phys.*, 2:231–252, 1998.

[61] Robert B. Mann. Misner string entropy. *Phys.Rev.*, D60:104047, 1999.

[62] Robert B. Mann. Lifshitz Topological Black Holes. *JHEP*, 0906:075, 2009.

[63] Robert B. Mann and Donald Marolf. Holographic renormalization of asymptotically flat spacetimes. *Class.Quant.Grav.*, 23:2927–2950, 2006.

[64] Robert B. Mann, Donald Marolf, Robert McNees, and Amitabh Virmani. On the Stress Tensor for Asymptotically Flat Gravity. *Class.Quant.Grav.*, 25:225019, 2008.

[65] Robert B. Mann and Robert McNees. Holographic Renormalization for Asymptotically Lifshitz Spacetimes. *JHEP*, 1110:129, 2011.

[66] Robert B. Mann and Simon F. Ross. Cosmological production of charged black hole pairs. *Phys.Rev.*, D52:2254–2265, 1995.

[67] Donald Marolf. Asymptotic flatness, little string theory, and holography. *JHEP*, 0703:122, 2007.

[68] W. D. McComb. *Renormalization methods : a guide for beginners* . Oxford : Clarendon Press ; New York : Oxford University Pr, 2004.

[69] V. Moretti. Quantum ground states holographically induced by asymptotic flatness: Invariance under spacetime symmetries, energy positivity and Hadamard property. *Commun.Math.Phys.*, 279:31–75, 2008.

[70] Valter Moretti. Uniqueness theorem for BMS-invariant states of scalar QFT on the null boundary of asymptotically flat spacetimes and bulk-boundary observable algebra correspondence. *Commun.Math.Phys.*, 268:727–756, 2006.

[71] Robert C. Myers and M.J. Perry. Black Holes in Higher Dimensional Space-Times. *Annals Phys.*, 172:304, 1986.

[72] Ishwaree P. Neupane. Black hole entropy in string generated gravity models. *Phys.Rev.*, D67:061501, 2003.

[73] Shin'ichi Nojiri and Sergei D. Odintsov. Modified Gauss-Bonnet theory as gravitational alternative for dark energy. *Phys.Lett.*, B631:1–6, 2005.

[74] Andy O'Bannon. Hall Conductivity of Flavor Fields from AdS/CFT. *Phys.Rev.*, D76:086007, 2007.

[75] Miok Park and Robert B. Mann. Holographic Renormalization of Asymptotically Flat Gravity. *JHEP*, 1212:098, 2012.

[76] Roger Penrose. Asymptotic properties of fields and space-times. *Phys.Rev.Lett.*, 10:66–68, 1963.

[77] Mukund Rangamani. Gravity and Hydrodynamics: Lectures on the fluid-gravity correspondence. *Class.Quant.Grav.*, 26:224003, 2009.

[78] Simon F. Ross. Holography for asymptotically locally Lifshitz spacetimes. *Class.Quant.Grav.*, 28:215019, 2011.

[79] Simon F. Ross and Omid Saremi. Holographic stress tensor for non-relativistic theories. *JHEP*, 0909:009, 2009.

[80] Subir Sachdev. *Quantum Phase Transitions.* Cambridge University Press, 2 edition edition, 2011.

[81] Kostas Skenderis. Lecture notes on holographic renormalization. *Class.Quant.Grav.*, 19:5849–5876, 2002.

[82] Sergey N. Solodukhin. Reconstructing Minkowski space-time. pages 123–163, 2004.

[83] D.T. Son. Toward an AdS/cold atoms correspondence: A Geometric realization of the Schrodinger symmetry. *Phys.Rev.*, D78:046003, 2008.

[84] Sean Stotyn, Miok Park, Paul McGrath, and Robert B. Mann. Black Holes and Boson Stars with One Killing Field in Arbitrary Odd Dimensions. *Phys.Rev.*, D85:044036, 2012.

[85] Leonard Susskind and Edward Witten. The Holographic bound in anti-de Sitter space. 1998.

[86] Marika Taylor. Non-relativistic holography. 2008.

[87] Takashi Torii and Hideki Maeda. Spacetime structure of static solutions in Gauss-Bonnet gravity: Neutral case. *Phys.Rev.*, D71:124002, 2005.

[88] Robert M. Wald. *General Relativity*. University Of Chicago Press, 1984 edition edition, 1984.

[89] James T. Wheeler. Symmetric Solutions to the Gauss-Bonnet Extended Einstein Equations. *Nucl.Phys.*, B268:737, 1986.

[90] Edward Witten. Anti-de Sitter space and holography. *Adv.Theor.Math.Phys.*, 2:253–291, 1998.

[91] Barton Zwiebach. Curvature Squared Terms and String Theories. *Phys.Lett.*, B156:315, 1985.